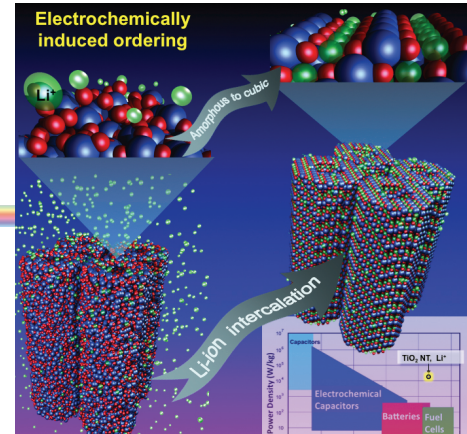
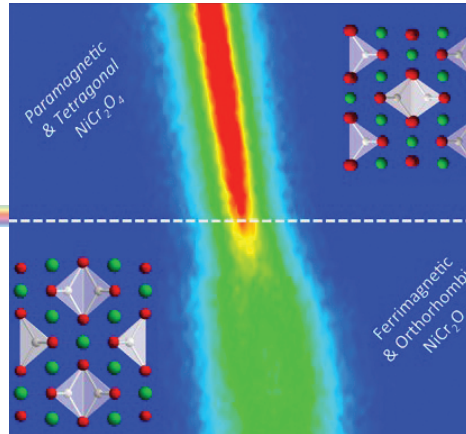
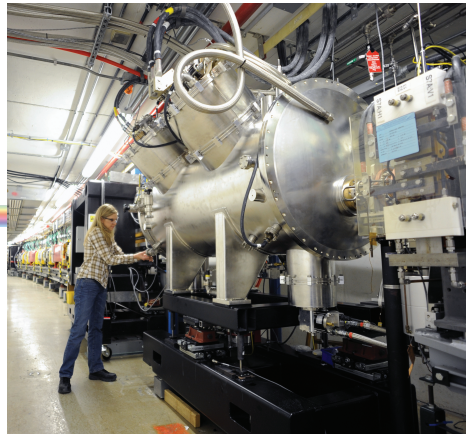


Advanced Photon Source

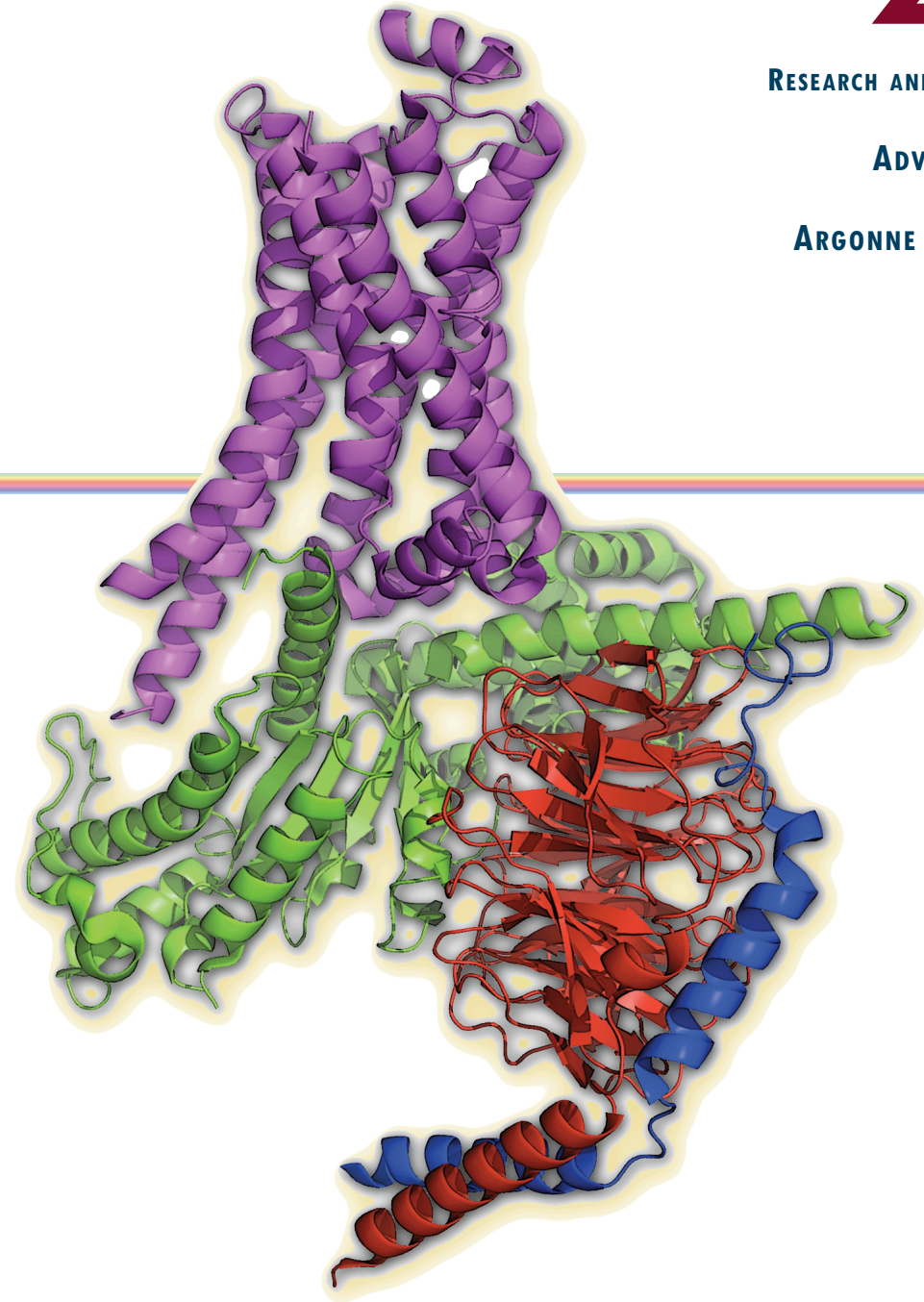
Argonne National Laboratory
9700 S. Cass Ave.
Argonne, IL 60439 USA

www.anl.gov
www.aps.anl.gov



APS SCIENCE 2012

RESEARCH AND ENGINEERING HIGHLIGHTS
FROM THE
ADVANCED PHOTON SOURCE
AT
ARGONNE NATIONAL LABORATORY



APS SCIENCE 2012

May 2013

Argonne National Laboratory

ANL-13/07

ANL-13/07
ISSN 1931-5007
May 2013

ANL-13/07
ISSN 1931-5007
May 2013

The Advanced Photon Source at Argonne National Laboratory is supported by the U.S. Department of Energy, Office of Science, Office of Basic Energy Sciences, under Contract No. DE-ACO2-06CH11357.

About Argonne National Laboratory

Argonne is a U.S. Department of Energy laboratory managed by UChicago Argonne, LLC under contract DE-ACO2-06CH11357. The Laboratory's main facility is outside Chicago, at 9700 South Cass Avenue, Argonne, Illinois 60439. For information about Argonne and its pioneering science and technology programs, see www.anl.gov.

Availability of This Report

This report is available, at no cost, at <http://www.osti.gov/bridge>. It is also available on paper to the U.S. Department of Energy and its contractors, for a processing fee, from: U.S. Department of Energy Office of Scientific and Technical Information
P.O. Box 62
Oak Ridge, TN 37831-0062
phone (865) 576-8401
fax (865) 576-5728
reports@adonis.osti.gov

ON THE FRONT COVER: An image of a G-protein-coupled receptor signaling complex whose structure was identified in 2011. The receptor is in magenta while the different G protein subunits are colored green, red, and blue. This structure was part of the research, carried out in large part at the National Institute of General Medical Sciences and National Cancer Institute Structural Biology Facility at the Advanced Photon Source, that received the Nobel Prize for Chemistry in 2012.

“Over the decades [Robert Lefkowitz and Brian Kobilka] learned in the finest molecular detail how [beta-adrenergic] receptors are built, how they transmit signals over the membrane and how they are regulated...Their discoveries are molecular masterpieces in many respects. One of nature's wonders is now revealed in all its beauty.”

From the 2012 Nobel Prize for Chemistry Presentation Speech by Professor Sara Snogerup Linse, Member of the Royal Swedish Academy of Sciences; Member of the Nobel Committee for Chemistry, 10 December 2012.

http://www.nobelprize.org/nobel_prizes/chemistry/laureates/2012/presentation-speech.html

Disclaimer

This report was prepared as an account of work sponsored by an agency of the United States Government. Neither the United States Government nor any agency thereof, nor UChicago Argonne, LLC, nor any of their employees or officers, makes any warranty, express or implied, or assumes any legal liability or responsibility for the accuracy, completeness, or usefulness of any information, apparatus, product, or process disclosed, or represents that its use would not infringe privately owned rights. Reference herein to any specific commercial product, process, or service by trade name, trademark, manufacturer, or otherwise, does not necessarily constitute or imply its endorsement, recommendation, or favoring by the United States Government or any agency thereof. The views and opinions of document authors expressed herein do not necessarily state or reflect those of the United States Government or any agency thereof, Argonne National Laboratory, or UChicago Argonne, LLC.

ANL-13/07
ISSN 1931-5007
May 2013

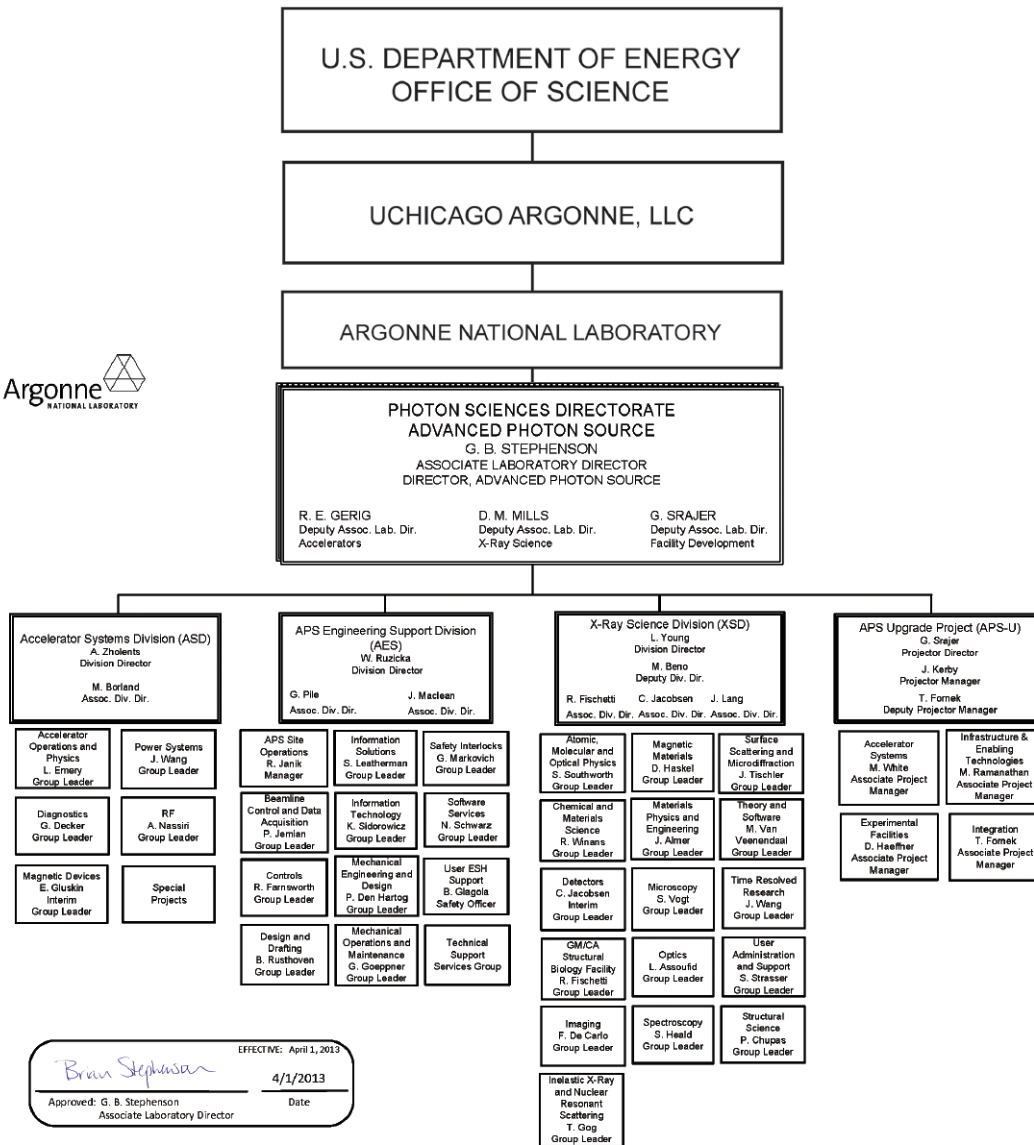
APS SCIENCE

**RESEARCH AND ENGINEERING HIGHLIGHTS
FROM THE ADVANCED PHOTON SOURCE
AT ARGONNE NATIONAL LABORATORY**

2012

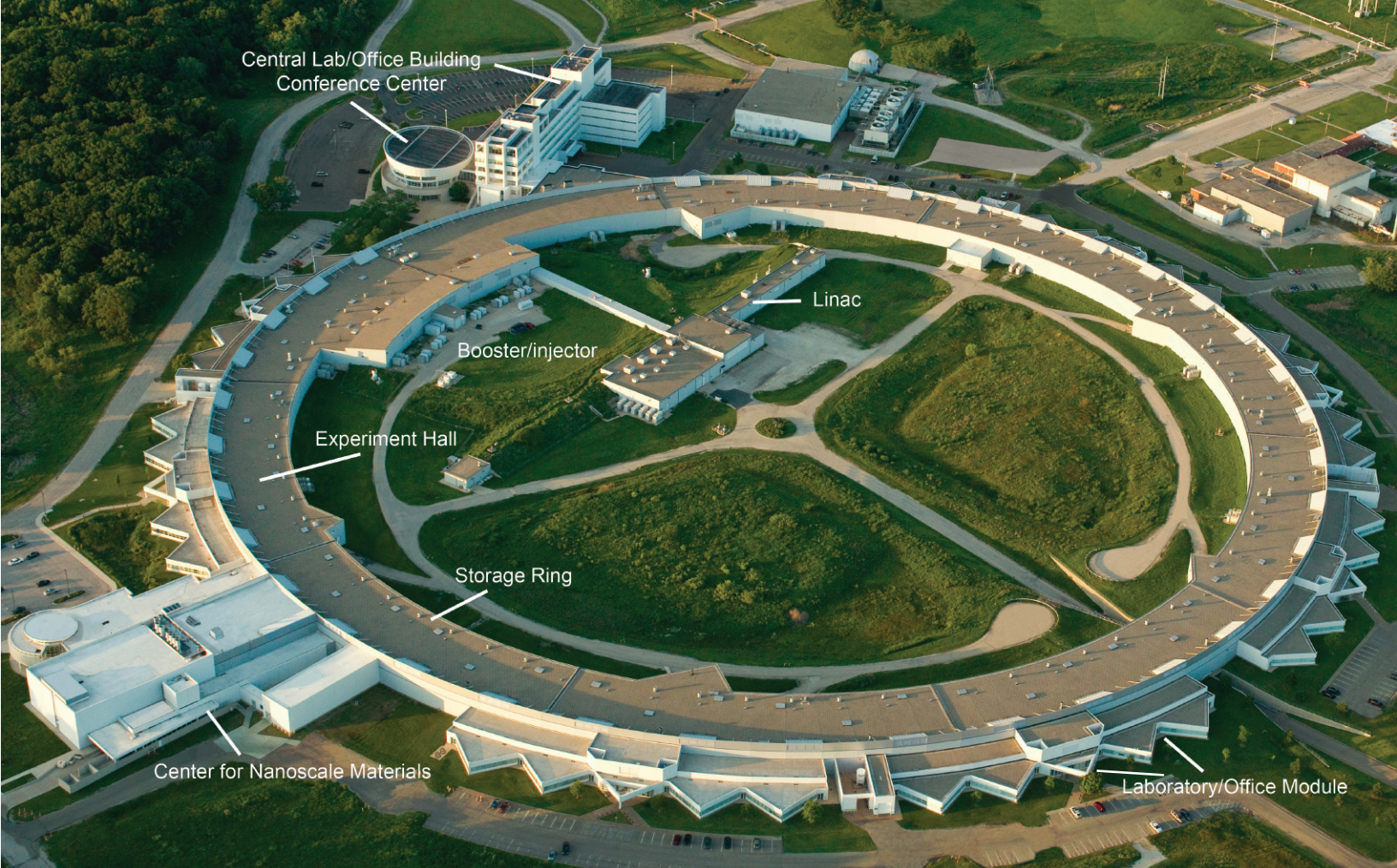


APS ORGANIZATION CHART



Acronyms for Argonne division and APS group names in this report

AES	APS Engineering Support Division	MD	Magnetic Devices Group (ASD)
AMO	Atomic, Molecular & Optical Physics Group (XSD)	MED	Mechanical Engineering & Design Group (AES)
AOP	Accelerator Operation & Physics Group (ASD)	MIC	Microscopy Group (XSD)
ASD	Argonne Accelerator Systems Division	MM	Magnetic Materials Group (XSD)
CNM	Center for Nanoscale Materials	MOM	Mechanical Operations & Maintenance (AES)
CMS	Chemical and Materials Science Group (XSD)	MPE	Materials Physics & Engineering (XSD)
CSE	Argonne Chemical Sciences and Engineering Division	MSD	Argonne Materials Science Division
CTL	Controls Group (AES)	OPT	Optics Group (XSD)
DD	Design & Drafting Group (AES)	PS	Power Systems Group (AES)
DET	Detectors Group (XSD)	PSC	Argonne Photon Sciences
DIA	Diagnostics Group (ASD)	SO	Site Operations Group (AES)
FMS	Argonne Facilities Management and Services Group	SRS	Structural Science Group (XSD)
IT	Information Technology Group (AES)	SSM	Surface Scattering & Microdiffraction Group (XSD)
IXN	Inelastic X-ray & Nuclear Resonant Scattering Group (XSD)	XSD	Argonne X-ray Science Division



THE ADVANCED PHOTON SOURCE FACILITY AT ARGONNE NATIONAL LABORATORY

The Advanced Photon Source (APS) occupies an 80-acre site on the Argonne National Laboratory campus, about 25 miles from downtown Chicago, Illinois.

For directions to Argonne, see <http://www.anl.gov/directions-and-visitor-information>.

The APS, a national synchrotron radiation research facility operated by Argonne for the U.S. Department of Energy (DOE) Office of Science, provides this nation's brightest high-energy x-ray beams for science. Research by APS users extends from the center of the Earth to outer space, from new information on combustion engines and microcircuits to new drugs and nanotechnologies whose scale is measured in billionths of a meter. The APS helps researchers illuminate answers to the challenges of our high-tech world, from developing new forms of energy, to sustaining our nation's technological and economic competitiveness, to pushing back against the ravages of disease. Research at the APS promises to have far-reaching impact on our technology, our economy, our health, and fundamental knowledge of the materials that make up our world.

CONTACT US

For more information about the APS or to order additional copies of this, or previous, issues of *APS Science*, send an e-mail to apsinfo@aps.anl.gov, or write to APS Info, Bldg. 401, Rm. A4115, Argonne National Laboratory, 9700 S. Cass Ave., Argonne, IL 60439, or go to <http://www.aps.anl.gov/Science/Reports/> to download PDF versions.

Visit the APS on the Web at www.aps.anl.gov

For links to online content including animations, videos, etc., look for URLs or (for readers of the print version of this book) QR codes (as below). QR codes quickly link smartphone users to the content.

A code reader can be downloaded from, for instance, <http://www.quickmark.com.tw/En/basic/download.asp>
Adobe Flash may be required for some films.



WELCOME



Brian Stephenson

May 2013

Those of us in science have an affinity for numbers. But numbers seem to occupy even more of our thoughts these days. As we here at the APS keep a watchful eye on the budget numbers coming out of Washington, we are also acutely aware of the impressive statistics being compiled by our

(from a strictly numerical standpoint and not for the moment considering the economic, sociological, and intellectual impact of our users' science) resulted in more than 1500 publications* and nearly 1400 deposits of biological protein structures in the Protein Data Bank – more than any other light source in the world.

Our users came from all 50 U.S. states, Washington D.C., Puerto Rico, and numerous foreign countries; they represented (just in FY12) 526 academic institutions, medical schools, industries, national labs and other federal research entities, and private research institutions.

All of the preceding depends on reliable delivery of x-rays from our source to our users. In FY12, our source performed at a record-setting pace. X-ray beams from our storage ring were available 99.4% of the scheduled 5,000 hours (4969.4 hours to be precise). During that time our accelerators (linac, booster, and storage ring) operated an average of 198.8 hours without an interruption. (For graphs that place these numbers and more in context, see pages xxx through xxx of this book).

their work on G-protein-coupled receptors, as described in the article on page xx by Janet Smith and Bob Fischetti, the Scientific Director and Group Leader, respectively, of the General Medical Sciences and Cancer Institutes (GM/CA-XSD) beamlines at Sector at the APS, where Prof. Kobilka carried out much of the experimentation that led to the Nobel. Prof. Kobilka and his group were able to understand these critically important membrane proteins in part because of the microfocusing capabilities available at the GM/CA beamlines, which allowed detailed atomic structures to be obtained from the tiny crystals. The hard work and perseverance of Prof. Kobilka was complemented by the dedication of the staff of GM/CA and of APS, who can deservedly feel proud of their contributions to this outstanding body of work.

This Nobel Prize is an illustration of how technical developments driven by the needs of one field can have widespread scientific impact across diverse areas. The continually improving ability to focus hard x-rays that has become so important in macromolecular crystallography also enables many other fields of science at the APS,



Left: Brian Kobilka; right: Robert Lefkowitz.

maturing facility and the active and growing user community we serve.

For instance: We now have 65 simultaneously operating x-ray beamlines delivering approximately 5000 hours of x-rays per year to over 4000 unique on-side users plus 1600 remote users in fiscal year (FY)12 who carried out more than 4900 experiments, which

But these remarkable numbers are simply a reflection of the dedication, intelligence, and hard work shown every day by our users and by the personnel of the APS.

Prof. Brian Kobilka, from Stanford University, along with Prof. Robert Lefkowitz from Duke University, won the 2012 Nobel Prize in Chemistry for

advancing the forefront of materials science, high-pressure research, high-resolution spectroscopy, nanoscience, and cell biology, to name a few. Imaging and *in situ* studies with hard x-rays, the two overarching strategic themes identified for the future of APS and the central science drivers of the APS Upgrade

"Welcome" cont'd. on page XX

THE ADVANCED PHOTON SOURCE UPGRADE PROJECT

May 2013

I am happy to report that it has been a busy and productive year for the Advanced Photon Source Upgrade (APS-U) Project. Significant advances were made in Project design as well as in R&D activities. Since the last APS-U Upgrade report in *APS Science 2011*, (<http://www.aps.anl.gov/Science/Reports/>) we have been the subject of several informative and successful reviews.

Even though we do not anticipate a Department of Energy (DOE) Critical Decision (CD)-3 review (which could grant construction approval) until at least the end of 2013, we were able to jump start work on two new beamlines by gaining early procurement approval in August 2012 following a successful CD-3A review. In mid-August of 2012, subsequent to a positive DOE Office of Science (SC) "Lehman review" of our long-lead procurement (LLP) plans for the new Resonant Inelastic X-ray Scattering (RIXS) and Advanced Spectroscopy/Low-Energy-Resolution Inelastic X-ray Scattering (ASL) beamlines, the DOE-SC Energy Systems Acquisition Advisory Board reviewed and, on August 30, approved CD-3A for the initial LLP. The CD-3A approval was an important step for the Project because it accelerates the project schedule, and at the same time reduces schedule risk by spreading installation of front-end and accelerator components over a greater number of shutdown periods.

For the RIXS beamline, the approval enabled us to begin procuring front-end components, undulators, vacuum chambers, and radiation enclosures immediately after the approval and continuing into fiscal year (FY) 2013. As of February 2013, contracts for radiation enclosures, an assortment of vacuum components, and the monochromator for this beamline were awarded. Construction of radiation enclosures at Sector 27, the new home for the RIXS program, starts in September 2013. As for the ASL beamline, the approval scope includes radiation enclosures, mono-

chromators, and mirrors. But additional funds will be required in FY13 in order to proceed.

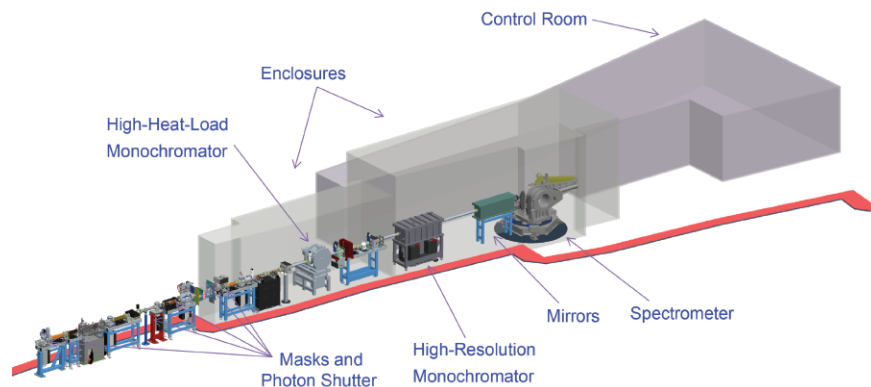
We have moved equipment to free-up space at Sector 35 for the new Dynamic Compression Sector (DCS), where DCS will use hard x-rays to study dynamically shocked materials. The construction of this sector is supported by DOE's National Nuclear Security Administration Office of Defense Programs. We expect construction of enclosures in the DCS sector to start in May 2013, and then in the RIXS sector in September 2013. Staggering construction of new and upgraded beamlines will enable us to generate scientific results well before the expected 2020 completion of the APS-U.

Another important review, the Argonne Director's CD-2 Review, took place in September 2012. The review committee, chaired by Ed



George Srajer

December 6, 2012, 26 reviewers delved into every aspect of project readiness on behalf of DOE, culminating in a successful CD-2 review, which is a precursor to the all-important CD-2 approval. However, due to budget uncertainties at the time of this writing, CD-2



A computer-aided design rendering of the RIXS beamline major components.

Temple (Argonne Office of the Director and APS-U Project Advisor), was charged by Argonne Director Eric Isaacs to assess the readiness of the APS-U in a broad range of categories, including management; scope; cost and schedule; environment, safety and health; quality assurance; and documentation preparation. The reviewers were uniformly positive in stating that the Upgrade Project was on track for achieving a successful DOE CD-2 review in December 2012.

From December 4 through

approval is not expected before late spring of 2013.

Three areas of research that were previously considered, but had not been included in the Project scope were integrated into the plan as part of the CD-2 review. These are the development of nanofocusing optics in the range of 20 nm at 25 keV, a two-year study of options for high-speed detectors, and development of RIXS optics.

Successful reviews were not the only milestones last year. The accelerator complex was a hive of activity with
"Upgrade" cont'd. on page XX

“Welcome” cont’d. from page XX

(APS-U), our way forward to a greatly improved APS, are both blossoming, helped by the revolution in focusing capabilities.

Progress of the APS Upgrade in FY12 is spelled out by George Srajer, the APS-U Project Director, on page xx. As you will see, the APS-U has successfully steered through a course of useful and productive reviews held by our sponsor, the U.S. Department of Energy Office of Science (DOE-SC) Basic Energy Science Program, and by Argonne management. The DOE-SC has been steady in their encouragement and support of the Upgrade, as they have always been of the APS. Argonne, led by Director Eric Isaacs, continues to provide the backing that is essential to the Upgrade success.

The Upgrade will bring many new research capabilities to our facility. A taste of those exciting new possibilities is the Dynamic Compression Sector (DCS) at Sector 35, which formalized its ties with the APS in a Memorandum of Understanding signed on September 6. The DCS results from the efforts of Prof. Yogendra Gupta, Director of the Institute for Shock Physics at Washington State University, and is being funded by the DOE National Nuclear Security Administration. See page xx for more details on this most recent addition to the family of APS beamlines.

In addition, in FY12 X-ray Science Division (XSD) beamline 34-ID was reconfigured to use the canted undulator scheme that increases the beams available from a single point in the storage ring lattice. Canting was also brought to the High-Pressure

Collaborative Access Team (CAT) 16-ID beamline, and GeoSoilEnviroCARS 13-ID. The Bionanoprobe at the Life Sciences CAT (21-ID) hosted its first users. XSD beamline 1-BM was reconfigured to host optics and detectors testing programs (see page xx), 1-D received was re-instrumented to begin a new era in high-energy in situ diffraction tomography, xsd 7-BM was officially inaugurated for the study of high-speed fuel sprays via micro-radiography page xx), and 17-BM was converted for the study of powder diffraction.

The team constructing the new intermediate energy x-ray (IEX) beamline at Sector 29 installed and commissioned the IEX undulator insertion device, an electromagnetic variable polarizing undulator that is the first of its kind.

APS expertise continued to foster a tradition of collaboration. Our scientists and engineers and their counterparts at the Linac Coherent Light Source (LCLS) at the SLAC National Accelerator Laboratory proved the feasibility of producing laser pulses of light that focus to the much narrower wavelengths of x-rays. This long-held goal for developers of an x-ray free-electron laser promises to open entirely new vistas in x-ray science.

Our people earned recognition from various quarters of the scientific world; a rundown begins on page xx.

As of June 1, the staff of the GM/CA-XSD beamlines mentioned above moved organizationally from the Argonne Biosciences Division to the Argonne X-ray Science Division within the APS (see page xx). GM/CA-XSD is a national user facility funded by two

National Institutes of Health institutes. For many years GM/CA-XSD has provided world-leading structural biology capabilities at APS. The GM/CA group received a 2010 R&D 100 Award for the development of the Hard X-ray Mini-beam Quad Collimator for Structural Biology, and led the recent effort to understand the mechanism for reduced radiation damage in crystals with micron-sized beams.

We are serious about the safety of all of our people at the APS, employees and users alike. Fiscal year 2012 was the best year yet for injury statistics, with 1 injury that required medical attention; 4 first-aid incidents; and 0 days away, restricted, or transferred (DART) injuries. Numbers are not the whole story here; the fact that no one suffered a serious injury is. Our goal for the future is to zero-out all of these numbers.

Finally, it is important that we communicate the value of scientific research in general, and the value of DOE-SC user facilities such as APS in particular. These are excellent investments to address the major challenges facing our society in energy, the environment, and health, which will provide ample returns for future generations. The research highlighted this book is just a fraction of the discoveries made by our users and staff in 2012. I hope it inspires you to join us in exploring our world.

Brian Stephenson

*Associate Laboratory Director,
Photon Sciences;
and Director, Advanced Photon Source*

“Upgrade” cont’d. from page xx

the construction and testing of prototype components.

Prototypes of two revolver-undulator engineering designs (previous page) were selected and subjected to rigorous testing. The revolver undulator is a single device with two different periods that will economize space in the straight section and, at the same time, provide users with greater flexibility to tune and optimize x-ray energy to their experimental needs.

The upgraded APS will be the first third-generation synchrotron to use super-conducting undulators. This will revolutionize the production of high-energy photons from a synchrotron and will give the upgraded APS the brightest x-rays by a factor of six above 25 keV. The short (0.32-m) prototype super-conducting undulator, or SCU0, was installed and tested in the APS accelerator tunnel in December 2012-January 2013 (see the article on page XX). Subsequently, x-ray measurements were performed and initial commissioning tests confirmed that SCU0 met design specifications. We will con-



The SPX0 team with the horizontal cavity tuner test set-up at the Argonne Tandem Linear Accelerator System. From left to right: Joe Matalевич (JLAB), Mike McCrea (JLAB), Tom Mann (APS-U), Joel Fuerst (APS-U), John Mammosser (seated, JLAB), Ali Nassiri (APS-U), Genfa Wu (APS-U), and Ned Arnold (APS-U). Inset: Jeremiah Holzbauer (Argonne).

high-repetition rate (MHz) pulsed x-rays at a synchrotron for the study of action occurring on the time scale of a few picoseconds. This will make the APS capable of studying the complex, ultrafast behavior of biological, material, and chemical systems at the molecular level and at a high-repetition rate of up to 6.5 MHz. The SPX sys-

grated and tested in the laboratory for the first time. This was a significant achievement and the initial results have been encouraging.

Building 400, which will house the cryogenics system for the SPX and is located in the storage ring infield adjacent to sectors 5 through 7, was finished in September 2012.

Our project management team has benefited greatly from new additions in 2012. Among these new hires are Jim Kerby (Project Manager), Thomas Fornek (Deputy Project Manager and Integration Associate Project Manager), and Thomas Burt (Financial Analyst). Their wealth of experience and expertise were critical to the successful reviews in 2012 and they will continue to play central roles in our successes going forward. An organization chart for the APS-U can be found on our web site at <http://www.aps.anl.gov/Upgrade/>.

In the coming year, we expect just as much, if not more activity. To make sure that the APS-U Project continues to receive the attention and expertise that it deserves as it ramps into high gear, we are in the process of hiring key personnel so we can be ready for the next major goal, CD-3, the approval to start construction!

We all look forward to these new challenges.

George Srajer

*Deputy Associate Laboratory Director,
Facility Development, Photon Sciences;
and Director,
Advanced Photon Source Upgrade Project*



The core members of the revolver-undulator team, in the APS Magnetic Measurement Facility. Left to right: Joe Gagliano, Jr.; John TerHAAR; Mike Merritt; and Sue Bettenhausen (all ASD Magnetic Devices Group) with the two APS prototype revolver undulators. At left is the “non-revolving strongback” design, which only revolves the magnet arrays and a fairly small structure that ties them together. Right: The “revolving strongback” design, where the entire beam (that provides bending stiffness for the magnet arrays) revolves. This is essentially an APS-specific adaptation of the design utilized at the European Synchrotron Radiation Facility.

tinue testing the device and use the results to fine-tune development toward building the 1.2-m-long “production” superconducting undulator.

As to the Short-Pulse X-ray (SPX) system, it will provide the world’s first

tem will make the APS the only light source where users can control the pulse rate between 2 and 100 psec for hard x-rays at individual beamlines. Earlier this year, the prototype short-pulse x-ray system, or SPX0, was inte-

THE 2012 NOBEL PRIZE IN CHEMISTRY: SHINING A BRIGHT LIGHT ON G-PROTEIN-COUPLED RECEPTORS

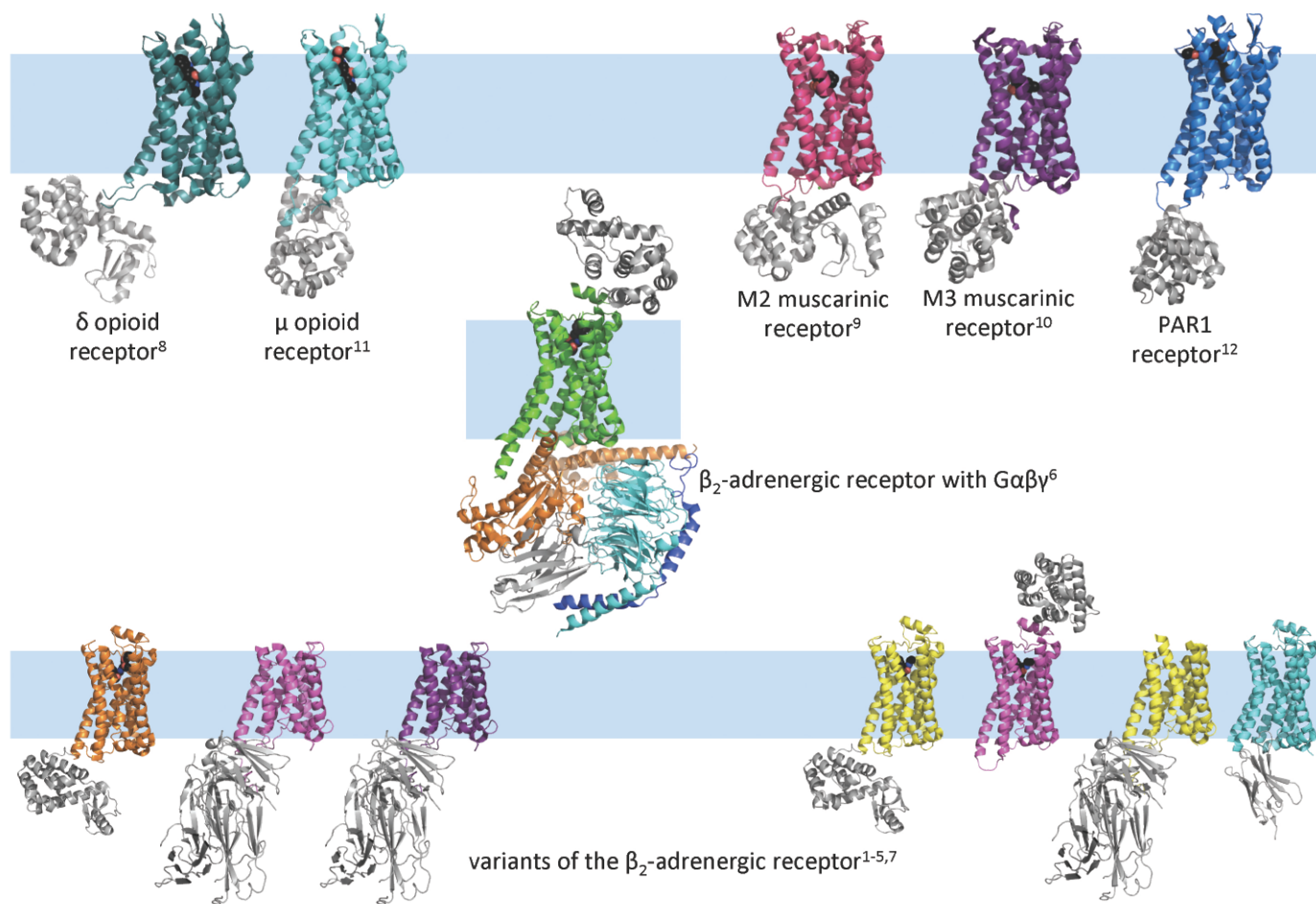


Fig. 1. Gallery of Brian Kobilka et al.'s GPCR structures from data collected at GM/CA-XSD. The receptors are shown in ribbon form. In the center, the β_2 AR is in green, and the three-part G protein is in orange ($G\alpha$), cyan ($G\beta$) and blue ($G\gamma$). Small signaling molecules are bound in some receptors (carbon atoms as black spheres, red oxygen, blue nitrogen). The light blue stripes represent the position of the cell membrane with the outside of the cell above the stripe and the cell interior below. Extra proteins to aid crystallization are in gray. Numbers refer to literature citations in the list on the next page.



© The Nobel Foundation.
Photo: Lovisa Engblom

A nearly 40-year journey of scientific discovery culminated in the awarding of the 2012 Nobel Prize in Chemistry to Robert Lefkowitz of Duke University and Brian Kobilka of Stanford University for their studies of G-protein-coupled receptors, or GPCRs. The award in part recognized the several receptor crystal structures solved by Brian Kobilka and co-workers from x-ray diffraction data recorded at the APS.

G-protein-coupled receptors are protein molecules embedded in the surface of a cell where they transmit information from the outside to the inside of the cell. The transmitted information starts a cascade of molecular events inside the cell, leading to a physiological response that can be quite dramatic, such as a rapid change of heart rate; constriction of

blood vessels; or a sensation of light, smell, or taste. Lefkowitz and Kobilka focused on a GPCR called the β_2 adrenergic receptor (β_2 AR). The β_2 AR is the receptor for adrenaline and is the target of many drugs for treatment of conditions as diverse as hypertension and asthma. The G proteins inside the cell are the first molecular recipients of GPCR signals. They carry the signal to other parts of the cell and initiate the physiological response.

Lefkowitz discovered GPCRs in the 1970s, and he and Kobilka characterized the behavior of the β_2 AR in the 1980s at Duke. Since the 1990s, Kobilka and his group at Stanford have studied the molecular details of the β_2 AR, with the goal of “seeing” the receptor in three dimensions by solving its crystal structure. This was a massive undertaking that required a deep understanding of receptor behavior and rigorous attention to experimental detail.

They obtained the first crystals in 1997, but these crystals were small, extremely fragile, and radiation sensitive. It took ten more years and the application of several experimental techniques to grow crystals of sufficient quality for structure determination. In 2007, Kobilka and his group determined the first human GPCR structures in atomic detail using diffraction data obtained at the General Medical



2012 Chemistry Laureate, Brian K. Kobilka (left) receiving his Nobel Prize from His Majesty King Carl XVI Gustaf of Sweden at the Stockholm Concert Hall, 10 December 2012. © Nobel Media AB 2012. Photo: Alex Ljungdahl

Sciences and National Cancer Institute (GM/CA-XSD) beamlines at the APS.

The high-brightness, high-energy synchrotron x-ray beams from undulator sources at the APS and the micro-crystallography beamlines at GM/CA-XSD were essential to solving the GPCR structures. The GM/CA-XSD end station for micro-crystallography exploits the APS x-ray beam properties of stability, brightness, and the ability to be focused on an extremely small spot. Critical features of the micro-crystallography end station include a rapidly changeable beam size and powerful software for micro-scale manipulation of beam and sample. These were exactly the right tools for the tiny, weakly diffracting crystals of the challenging GPCR projects.

Since determining the first β_2 AR structures in 2007, Kobilka’s group contributed structures of five other GPCRs as well as several variants of the β_2 AR (Fig. 1). Seeing the receptor in partnership with its G protein is the group’s most remarkable accomplishment to date. Removing the receptor from the cell membrane, stabilizing the isolated receptor in an active form, making a stable complex of the receptor and G protein, and capturing the receptor-G protein at a single step in the intricate signaling dance was a technical tour de force that required many experimental

methods and many collaborators.

About half of all medications are targeted directly or indirectly to one of the nearly 800 GPCRs. Kobilka’s GPCR structures give a clear picture of the receptors and where drugs bind within them. Thus, it has enormous implications for creating and improving pharmaceuticals and for understanding and controlling the effects of drugs of choice

such as caffeine, opium, and cocaine.

Janet L. Smith, JanetSmith@umich.edu, Robert F. Fischetti, rfischetti@anl.gov

PUBLICATIONS AND PROTEIN DATA BANK CODES FOR GPCR STRUCTURES FROM THE KOBILKA GROUP:

- ¹ Rasmussen et al., *Nature* **450**, 383 (2007). 2R4R, 2R4S
- ² Cherezov et al., *Science* **318**, 1258 (2007). 2RH1
- ³ Bokoch et al., *Nature* **463**, 108 (2010). 3KJ6
- ⁴ Rasmussen et al., *Nature* **469**, 175 (2011). 3POG
- ⁵ Rosenbaum et al., *Nature* **469**, 236 (2011). 3PDS
- ⁶ Rasmussen et al., *Nature* **477**, 549 (2011). 3SN6
- ⁷ Zou et al., *PLoS One* **7**, e46039 (2012). 4GBR
- ⁸ Granier et al. *Nature* **485**, 400 (2012). 4EJ4
- ⁹ Haga et al., *Nature* **482**, 547 (2012). 3UON
- ¹⁰ Kruse et al., *Nature* **482**, 552 (2012). 4DAJ
- ¹¹ Manglik et al., *Nature* **485**, 321 (2012). 4DKL
- ¹² Zhang et al., *Nature* **492**, 387 (2012). 3VW7

GM/CA-XSD has been funded in whole or in part with Federal funds from the National Cancer Institute (Y1-CO-1020) and the National Institute of General Medical Sciences (Y1-GM-1104). Use of the Advanced Photon Source at Argonne National Laboratory was supported by the U.S. Department of Energy Office of Science under Contract No. DE-AC02-06CH11357.

ACCESS TO BEAM TIME AT THE APS

All beam time at the APS must be requested each cycle through the web-based Beam Time Request System. Five types of requests are possible: General User (a researcher not associated with a particular beamline), Partner User (a member of a collaborative access team [CAT], a partner user proposer, or a member of a collaborative development team), CAT member, CAT staff, and APS staff. Each beam time request (BTR) must be associated with a proposal, but the requirements for each proposal type differ.

The new APS User Portal (http://www.aps.anl.gov/Users/aps_userPortal.html) provides access to comprehensive information for prospective and current APS users.

GENERAL USER PROPOSALS AND BTRs

Proposals are peer reviewed and scored by a General User Proposal Review Panel, and time is allocated on the basis of scores and feasibility. A new BTR must be submitted each cycle, and for each cycle, allocation is competitive. Proposals expire in two years or when the number of shifts recommended in the peer review have been utilized, whichever comes first.

PARTNER USER PROPOSALS AND BTRs

Proposals are peer reviewed by a General User Proposal Review Panel and reviewed further by a subcommittee of the APS Scientific Advisory Committee; the final decision on acceptance is made by the APS Deputy Director. Although a new BTR must be submitted each cycle, a specific amount of beam time is guaranteed for up to three years.

CAT MEMBER PROPOSALS AND BTRs

Proposals from CAT members are much shorter, do not expire, and are reviewed by processes developed by individual CATs. A new BTR must be submitted against these proposals for each cycle during which the proposal needs beam time, and allocation/scheduling is determined by the CAT.

CAT AND APS STAFF MEMBER PROPOSALS AND BTRs

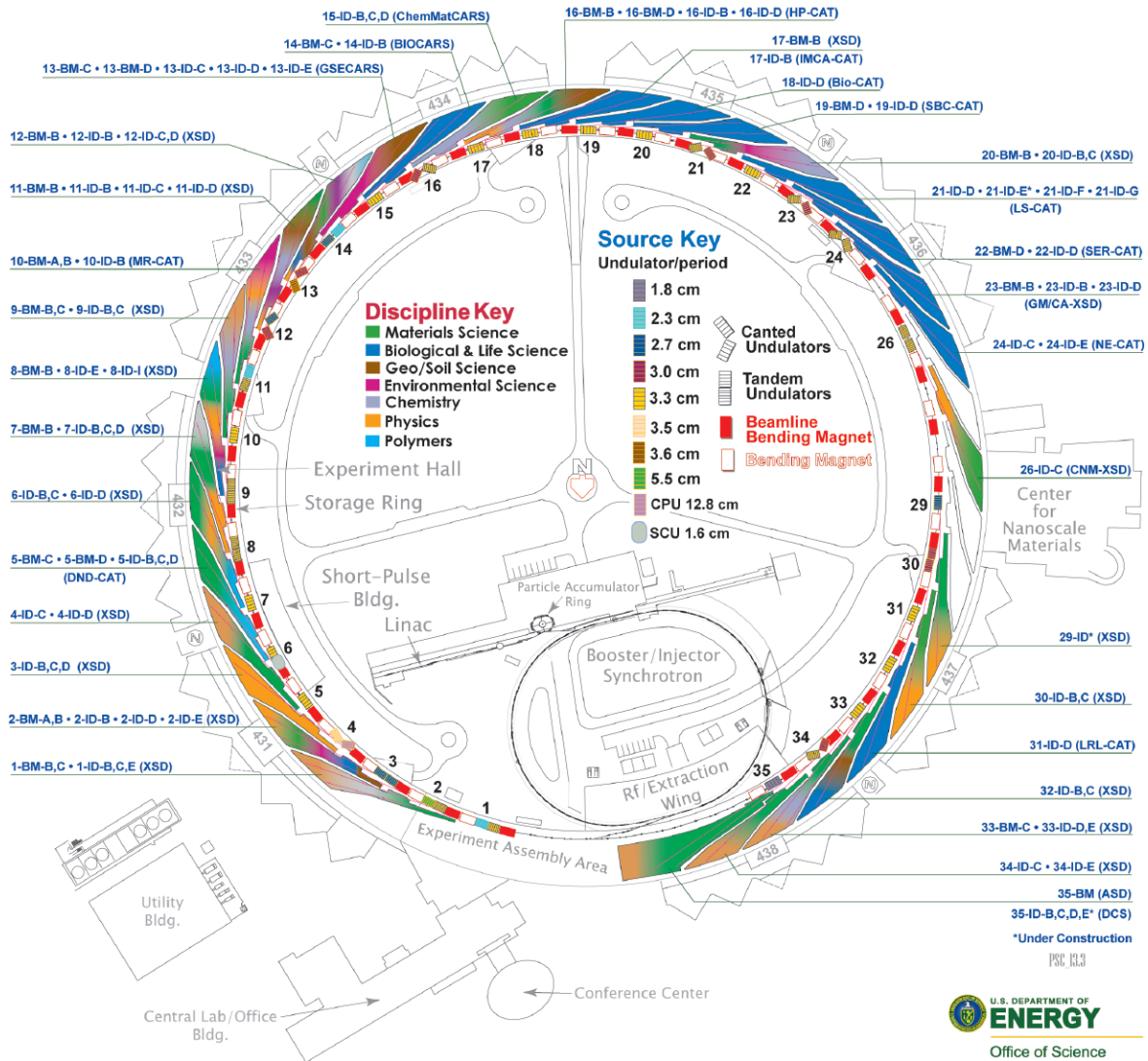
Proposals of this type are also very short, do not expire, and are reviewed through processes developed by either the CAT or the APS. A new BTR must be submitted against such proposals for each cycle during which the proposal needs beam time. Each CAT/beamline determines how these BTRs are allocated/scheduled.

INDUSTRIAL USERS

Improving industrial-user access to beam time is the focus of an APS pilot plan under the rubric "Measurement Access Mode" (MAM). Initially, several sectors agreed to participate in the MAM pilot. This involved setting aside three rapid-access beam-time shifts, at approximately two-week intervals (some 5% of the beam time). Qualifying MAM projects are then scheduled during each running cycle into the next available rapid-access period on the appropriate beamline. Concurrently, a web site (<http://www.aps.anl.gov/industry/>) was begun in order to make the whole access process easier for potential industrial users. An electronic contact information form filled out by the principal investigator (PI) is emailed to the APS Industrial Liaison Office for follow-up. This follow-up comprises an acknowledgement e-mail and contact with the PI for a verbal/e-mail discussion to obtain further information. If the consensus is that the proposed work meets three criteria (Can it be done here? Can it be done safely? Is there a reasonable chance that useful information can be obtained?), the office arranges contact between the PI and the beamline scientist for the APS sector where the work will be done. In addition, work on the appropriate administrative issues (user registration, user agreements, user accounts) is begun. The web site is currently being upgraded to include much more information for industrial users. For more information, contact Dennis Mills (DMM@aps.anl.gov) or the Industrial Liaison Office (aps-i@aps.anl.gov).

THE ADVANCED PHOTON SOURCE

Beamlines, Disciplines, and Source Configuration



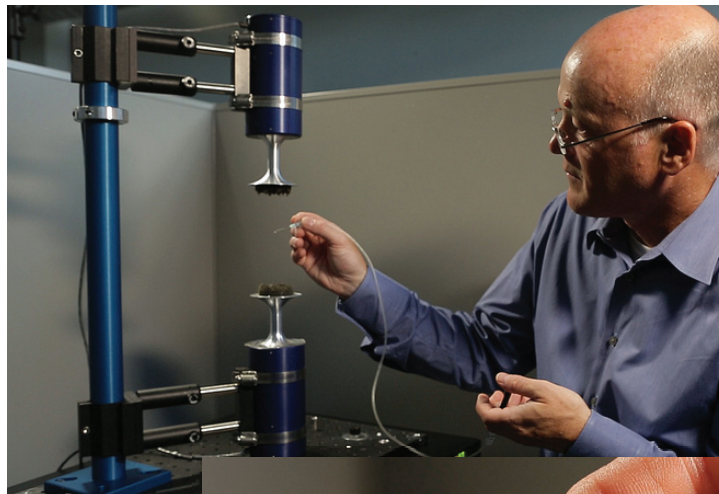
APS SECTORS: At the APS, a “sector” comprises the radiation sources (one bending magnet and one insertion device, although the number of insertion devices in the straight sections of the storage ring can vary), and the beamlines, enclosures, and instrumentation that are associated with a particular storage ring sector. The APS has 35 sectors dedicated to user science and experimental apparatus. **X-ray Science Division (XSD)** sectors comprise those beamlines operated by the APS. **Collaborative access team (CAT)** sectors comprise beamlines operated by independent groups made up of scientists from universities, industry, and/or research laboratories. **Key to the beamline descriptions that accompany each science highlight:** Beamline designation • Sector operator • Disciplines • Techniques • Radiation source energy • User access mode(s) • General user status •

Sectors not operated (or co-operated) by the APS:

- Sector 10: Materials Research CAT (MR-CAT)**
- Sector 13: GeoSoilEnviro(GSE)CARS-CAT**
- Sector 14: BioCARS-CAT**
- Sector 15: ChemMatCARS-CAT**
- Sector 16: High Pressure CAT (HP-CAT)**
- Sector 17: Industrial Macromolecular Crystallography Association CAT (IMCA-CAT)**
- Sector 18: Biophysics CAT (Bio-CAT)**
- Sector 19: Structural Biology Center CAT (SBC-CAT)**

- Sector 21: Life Sciences CAT (LS-CAT)**
- Sector 22: Southeast Regional CAT (SER-CAT)**
- Sector 23: General Medicine and Cancer Institutes (GM/CA)**
- Sector 24: Northeastern CAT (NE-CAT)**
- Sector 26: Center for Nanoscale Materials/X-ray Science Division (CNM/XSD)**
- Sector 31: Lilly Research Laboratories CAT (LRL-CAT)**
- Sector 35: Dynamic Compression Sector (DCS)**

APS ACOUSTIC LEVITATION VIDEO GOES VIRAL



Chris Benmore demonstrates his acoustic levitator, which could help to improve the efficiency and quality of pharmaceutical development.



More than 41,000 Google hits for “acoustic levitation Argonne” and 1,300,000 YouTube views and climbing as of April 2013; those numbers qualify the Argonne National Laboratory video entitled “Acoustic levitation” as a worldwide Web sensation:

<http://www.youtube.com/watch?v=669AcEBpdsY>.

The video shows Argonne physicist Chris Benmore, who is with the APS X-ray Science Division, suspending droplets of liquid between two speakers that “generate sound waves at frequencies slightly above the audible range – roughly 22 kilohertz,” according to in the online Argonne story on the development.

“When the top and bottom speakers are precisely aligned, they create two sets of sound waves that perfectly interfere with each other, setting up a phenomenon known as a standing wave.

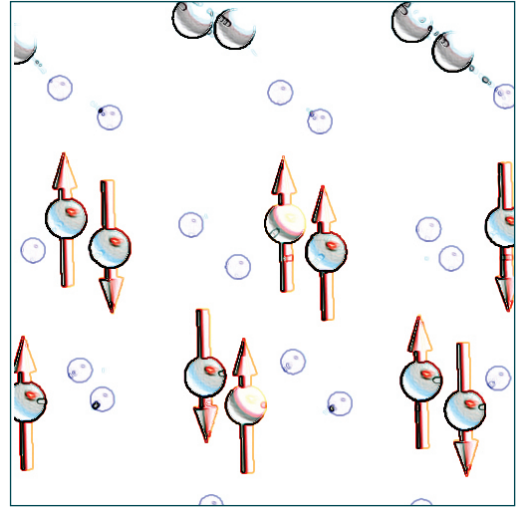
“It’s not a magic trick and it’s not sleight of hand,” the article notes, “scientists really are using levitation to improve the drug development process, eventually yielding more effective pharmaceuticals with fewer side effects.”

Thanks to the video, the Benmore team’s work has been featured on a list of web sites that includes (to name

but a scant few) *Mythbusters* (“Acoustic Levitation Used to Test Pharmaceuticals”) where it was Video of the Week, the CBS News (“‘Glitch in the matrix’ becomes a scientific reality with acoustic levitation”), Wired UK (“Acoustic levitation’ used to develop more efficient drugs”), *Scientific American* (where it was Video of the Week for September 20), CNET Australia (“...science wizardry at its best”), *Chicago Magazine* (“Argonne Scientists Float Drugs in Sound”), NBC News Future Tech (“See sound waves levitate drops of liquid”), *New Scientist* (“Wingardium leviosa! Wand used to make water levitate!” for you Harry Potter fans), *Discover Magazine* (“Watch This: Water Droplets Held Aloft by Sound Waves”), *Popular Science* (“Government Wizards Levitate Drugs with Ultrasonic Sound”), and MSN New Zealand (“Scientists find way to make liquid levitate”), as well as an array of televised newscasts.

For a complete rundown of the technique and its potential application, see the Argonne feature story, “No magic show: Real-world levitation to inspire better pharmaceuticals,” which can be read at:

<http://www.anl.gov/articles/no-magic-show-real-world-levitation-inspire-better-pharmaceuticals>



ELECTRONIC & MAGNETIC MATERIALS

AN UNLIKELY ROUTE TO FERROELECTRICITY

Multiferroics have attracted increased interest due to their potential use in technologies such as improved electronic memory chips and highly sensitive magnetic field sensors. Researchers utilized the XSD 4-ID-C and 6-ID-D beamlines at the APS and other techniques to unmask the exact source of the purported ferroelectric behavior in a multiferroic material of great technological interest, overturning the conventional wisdom.

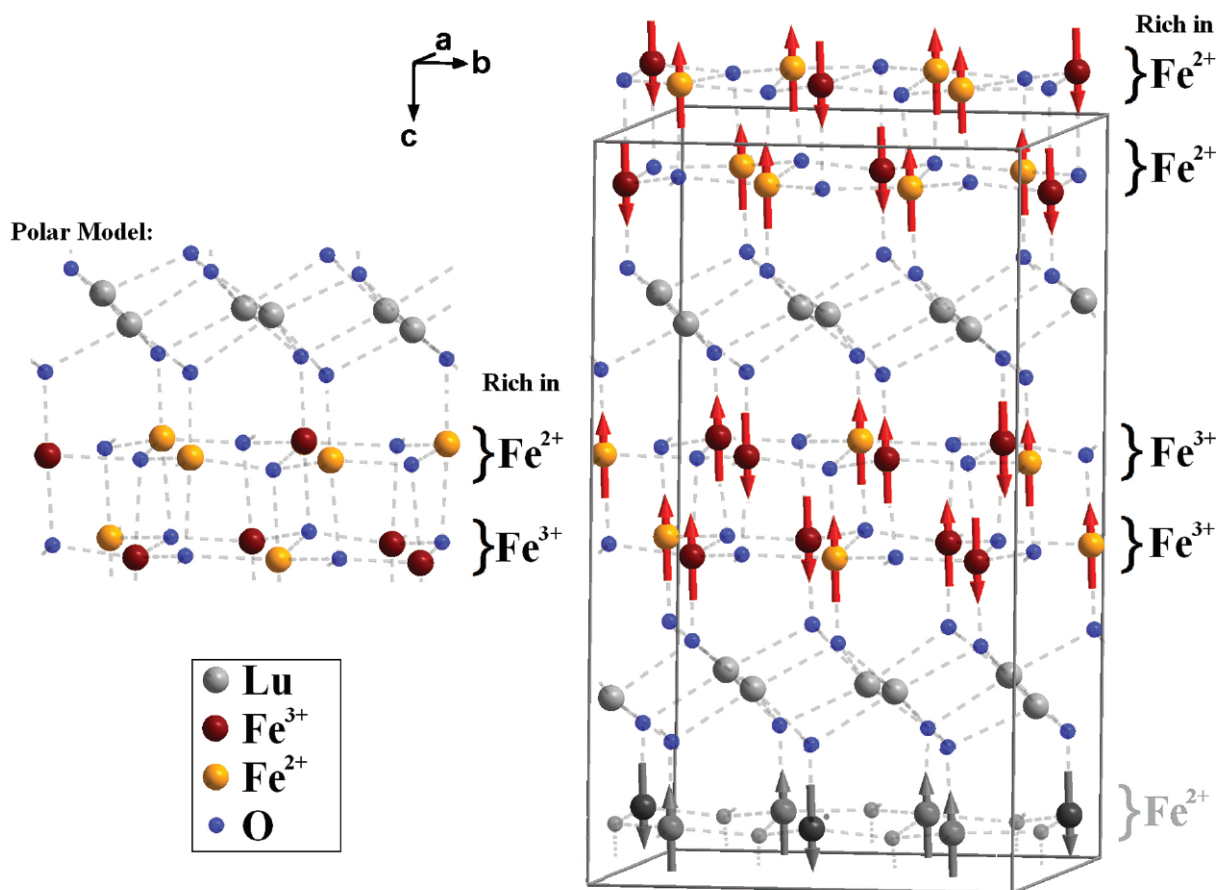


Fig. 1. Left side: The charge order configuration [after “N. Ikeda et al., *Nature* **436**, 1136 (2005)”] with polar bilayers previously assumed for LuFe₂O₄. Right side: The refined LuFe₂O₄ monoclinic crystal structure containing charged bilayers. For both configurations, the Fe atoms are arranged in Fe/O bilayers separated by Lu single layers. The different Fe valences are indicated by different colors. The brackets beside (each) indicate the majority charge configuration for each single layer. Here, for the polar model (left side), from the charge imbalance a net electric polarization is present; in contrast the model on the right side contains non-polar bilayers. The red arrows indicate the spin structure.

Ferroelectricity, first observed in the 1940s, involves the spontaneous (non-induced) formation of charge polarization (separation of charge) in certain materials. This is analogous to the spontaneous formation of magnetic fields in iron and other elements via ferromagnetism. Multiferroics (materials exhibiting both ferroelectricity and ferromagnetism) have attracted increased interest of late due to their potential use in various technologies, such as improved electronic memory chips and highly sensitive magnetic field sensors. The crystalline material lutetium-iron-oxide (LuFe₂O₄) has, in turn, garnered much attention due to its purported multiferroic properties.

A team of researchers from the Jülich Centre for Neutron Science (Germany) and Argonne National Laboratory utilized several techniques, including studies at the APS, bond-valence-sum analysis, and the charge-spin coupling of valence electrons to unmask the actual charge ordering within LuFe₂O₄, determining the source of its purported ferroelectric behavior.

Previous laboratory measurements and theoretical considerations had indicated the most likely charge ordering (the microscopic localization of electric charges) within LuFe_2O_4 was due to polarized iron/oxygen (Fe/O) bilayers.

Using an “assumption-free” approach, the research team’s application of multiple techniques unmasked the actual charge ordering within LuFe_2O_4 . Against all expectations, charge ordering does not arise from polar bilayers, but rather is due to charge separation on neighboring Fe/O bilayers. This finding means that the reported ferroelectric behavior of LuFe_2O_4 is highly unlikely.

Crystalline LuFe_2O_4 consists of alternating stacks of one lutetium oxide (Lu/O) and two ferrous oxide (Fe/O) planes or layers (Fig. 1). According to the conventional model depicted in the left half of the figure, charge ordering in Fe/O bilayers (a pair of adjacent Fe/O planes) leads to an electric dipole moment perpendicular to the Fe/O planes.

The iron-oxygen bonds within the bilayer are predominately ionic, featuring iron atoms in the Fe^{+2} and Fe^{+3} valence states. The superscripts refer to the number of electrons “donated” by individual iron atoms to the Fe/O molecular bonding.

Note that the top Fe/O layer in the figure (left side) has more Fe^{+2} than Fe^{+3} valence states, while the reverse is true for the bottom Fe/O layer. The different valence predominance in the two ferrous oxide layers (one rich in Fe^{+2} , the other rich in Fe^{+3}) produces the polarization (separation) of charges giving rise to an electric field. This pattern repeats multiple times in the crystal, producing large-scale (macroscopic) ferroelectricity.

This conventional model, however, was never proven directly by any previous research. To pin down the exact distribution of iron valence states within the Fe/O bilayers and settle the question of whether or not they are polar, the researchers used bond-valance-sum analysis linked to x-ray diffraction data of single LuFe_2O_4 crystals.

The XSD 6-ID-D high-energy station at the APS was utilized for the x-ray diffraction study. The picture that emerged showed two possible, but dia-

metrically opposed charge-ordering structures: one featuring polarity within the Fe/O bilayers, the other with non-polar Fe/O bilayers featuring net charges on distinct bilayers.

The structure of Fe valence states within the Fe/O bilayers was further refined via x-ray magnetic circular dichroism (XMCD) carried out at the XSD 4-ID-C beamline. XMCD uses right- and left-circularly polarized x-rays to determine electron spin states in a material immersed in a magnetic field. X-ray absorption is carried out at the iron atoms’ L-edge, which is the energy value at which electrons residing in the L orbital of the Fe atoms are just capable of absorbing photons.

LuFe_2O_4 crystals were subjected to a 4-T magnetic field. The XMCD data revealed that all spins of the Fe^{+2} ions were oriented in the direction of the magnetic field, as were one-third of the Fe^{+3} spins. Two-thirds of the Fe^{+3} spins were aligned opposite to the magnetic field.

Combining this result with the spin-structure determined earlier, only 28 charge configurations were possible, and only one was consistent with x-ray diffraction. The result is the charge ordering structure depicted in the right side of the figure.

Conventional wisdom held that LuFe_2O_4 provided a clear (and only known) example of an oxide compound exhibiting ferroelectricity via charge ordering. But the detailed picture of charge ordering revealed by this research is incompatible with a polar structure within the Fe/O bilayers. Instead, a more complex charge ordering structure has emerged, one that is non-polar and unaffected by external electric fields, and incompatible with any ferroelectric behavior in LuFe_2O_4 .

The apparent lack of multiferrocity in LuFe_2O_4 comes as a disappointment to those looking to exploit the potential of such materials. Charge-order-based multiferrocity is very attractive from the point of view of applications, but as these results show, an actual example has yet to be found.

Nevertheless, the unexpected structure elucidated for this rare-earth iron oxide is interesting in its own right. For one thing, the way in which bilayers rich in Fe^{+2} and Fe^{+3} produce

charge ordering is quite unexpected, suggesting that similar mechanisms for charge ordering in other crystalline materials await discovery. And theorists must now attempt to answer how charge transfer occurs between the Fe/O bilayers of this material, across a distance of some 6 Å (0.6 nm)

— *William A. Atkins and Philip E. Koth*

See: J. de Groot¹, T. Mueller¹, R.A. Rosenberg², D.J. Keavney², Z. Islam², J.-W. Kim², and M. Angst^{1*}, “Charge order in LuFe_2O_4 : an unlikely route to ferroelectricity,” *Phys. Rev. Lett.* **108**, 187601 (2012).

DOI:10.1103/PhysRevLett.108.187601
Author affiliations: ¹Jülich Centre for Neutron Science, ²Argonne National Laboratory

Correspondence:

*M.Angst@fz-juelich.de

See also:

M. Angst, R.P. Hermann, A.D. Christianson, M.D. Lumsden, C. Lee, M.-H. Whangbo, J.-W. Kim, P.J. Ryan, S.E. Nagler, W. Tian, R. Jin, B.C. Sales, and D. Mandrus, *Phys. Rev. Lett.* **101**, 227601 (2008).

X.S. Xu, M. Angst, T.V. Brinzari, R.P. Hermann, J.L. Musfeldt, A.D. Christianson, D. Mandrus, B.C. Sales, S. McGill, J.-W. Kim, and Z. Islam, *Phys. Rev. Lett.* **101**, 227602 (2008).

J. de Groot, K. Marty, M.D. Lumsden, A.D. Christianson, S.E. Nagler, S. Adiga, W.J.H. Borghols, K. Schmalzl, Z. Yamani, S.R. Bland, R. de Souza, U. Staub, W. Schweika, Y. Su, and M. Angst, *Phys. Rev. Lett.* **108**, 037206 (2012).

Support from the initiative and networking fund of the Helmholtz Association of German Research Centers by funding the Helmholtz-University Young Investigator Group “Complex Ordering Phenomena in Multifunctional Oxides” is gratefully acknowledged. Use of the Advanced Photon Source at Argonne National Laboratory was supported by the DOE Office of Science under Contract No. DE-AC02-06CH11357.

4-ID-C • XSD • Physics, materials science • Magnetic circular dichroism (x-ray magnetic circular dichroism, soft x-ray), x-ray magnetic linear dichroism, x-ray photoemission spectroscopy, x-ray photoemission electron microscopy, anomalous and resonant scattering (soft x-ray) • 500-2800 eV • On-site • Accepting general users •

6-ID-D • XSD • Physics, materials science • Magnetic x-ray scattering, high-energy x-ray diffraction, powder diffraction, pair distribution function • 27-52 keV, 50-100 keV, 67-130 keV • On-site • Accepting general users •

TUNING THE SPIN-ORBIT COUPLED ELECTRONIC GROUND STATE OF STRONTIUM IRIDATE VIA APPLIED PRESSURE

Experiments at elevated pressure present a remarkable opportunity to shed light on questions about the interactions that lead to novel electronic states in materials, such as: What is the relative importance of Coulomb interactions and magnetic ordering in driving electronic gap formation? How do exchange interactions as a result of sizable spin and orbital local moments depend on lattice structure (crystal electric fields)? Can superconductivity be induced at very high pressures where these complex $5d$ oxides would more closely resemble their first-row $3d$ (cuprates) and $4d$ (ruthenates) analogs, and where spin-orbital (SO) physics would become less relevant? To address these questions, researchers carried out studies at three APS x-ray beamlines to see if structural changes accompanied magnetic changes at high pressure. Their results found no discontinuities in lattice parameters or evidence of a structural phase transition, indicating that the sharp magnetic transition is not driven by a concomitant structural transition. Their work may also provide the first experimental observation of a spin-orbital liquid state in an iridate oxide.

Over the last three decades, artificial transition metal oxides synthesized using $3d$ transition metal ions have enabled groundbreaking discoveries that are bound to revolutionize the ways we harness energy and process information. Chief among these are the discovery of high-temperature superconductivity in copper-based oxides (cuprates) and colossal magnetoresistance and multiferroicity in manganese-based oxides (manganites), bringing us closer to the previously unimaginable dream of transporting electricity without energy loss and achieving several-fold increases in the density of information storage. Recent discoveries involving new families of third-row ($5d$) transition metal oxides, especially those based on iridium atoms (iridates), show that transition metal oxides will continue to surprise us for some time to come. Novel electronic ground states with exotic properties, including topological band insulators, spin-orbital liquids, Mott insulators driven by weak electron correlations, and possibly high-temperature superconductors have been predicted and in some cases observed. The key driver of these novel properties is the sizable SO interaction in the heavy $5d$ ions.

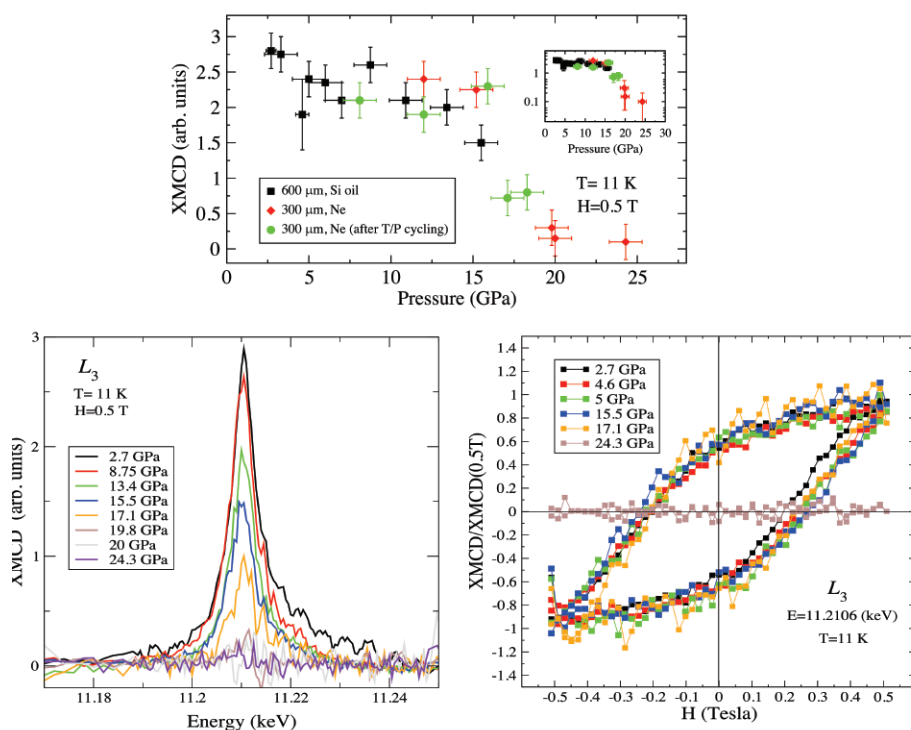


Fig. 1. Pressure dependence of iridium's L_3 edge XMCD signal (top, bottom left) and its field dependence normalized to its 0.5 T value (bottom right).

The researchers in this study, from Argonne, Washington University, the Chinese Academy of Sciences, the University of Kentucky, and Northern Illinois University studied the effects of pressure on the SO-coupled electronic ground state of strontium iridate (Sr_2IrO_4). X-ray absorption near edge structure (XANES) and magnetic circular dichroism (XMCD) measurements were made on powder samples at XSD beamlines 4-ID-D and 20-BM-B at the APS. X-ray diffraction measurements were done at HP-CAT beamline 16-BM-D to check whether structural changes accompanied magnetic changes at high pressure.

In its ground state, Sr_2IrO_4 is an insulating weak ferromagnet (WFM)

with an ordering temperature of $T_N = 240$ K. Although a strong SO limit $J_{\text{eff}} = 1/2$ state is usually assumed for the magnetic-insulating ground state of Sr_2IrO_4 at ambient pressure, the researchers found that exchange interactions between local moments and a small tetragonal crystal field reduce the “purity” of the $J_{\text{eff}} = 1/2$ state by mixing SO-split $J_{\text{eff}} = 1/2, 3/2$ states. This is clearly seen in the x-ray spectroscopy data where a non-zero XMCD signal at the Ir L_2 edge was seen. Configuration interaction calculations predict pure $J_{\text{eff}} = 1/2$ state would have resulted in a zero XMCD signal.

Application of hydrostatic pressure was found to induce a sharp magnetic phase transition at ~ 17 GPa with the weak ferromagnetic component vanishing at 20 GPa and the material retaining insulating behavior to at least 40 GPa (Fig. 1). Using x-ray diffraction to probe for structural changes at pressures up to 25 GPa, the researchers found no discontinuities in lattice parameters or evidence of a structural phase transition, indicating that the sharp magnetic transition is not driven by a concomitant structural transition. Since the XANES data show that iridium’s local spin and orbital moments remain present at ~ 20 GPa, the disappearance of WFM (canted antiferromagnetism) at this pressure could be a result of either loss of long-range magnetic order (paramagnetic phase) or a transition into a collinear antiferromagnetic state, the latter being predicted by theory to arise under the action of an increasing tetragonal crystal electric field. While the XMCD experiment could not distinguish between these two possibilities, a paramagnetic-insulating phase at high pressures would indicate that the electronic gap is driven mainly by on-site Coulomb interactions (Mott-Hubbard gap), with long-range magnetic order playing a secondary role (i.e., not a Slater gap). The results may also provide the first experimental observation of a spin-orbital liquid state in an iridate oxide.

Generally speaking, heightened pressure increases bandwidth (inter-site hopping) relative to Coulomb and SO interactions, so it may be expected that extreme pressures would lead to strong mixing of SO-split $J_{\text{eff}} = 1/2, 3/2$

bands and bring Sr_2IrO_4 closer to the “normal metal” regime where SO interactions and electron correlations no longer dominate. Support for this comes from XANES branching ratio (BR) measurements at $T = 300$ K. While the BR is nearly constant to 25 GPa, it decreases rapidly above this pressure (Fig. 2). The researchers conclude that the fast reduction in BR must originate in bandwidth-driven mixing of $J_{\text{eff}} = 1/2, 3/2$ states and related quenching of the orbital angular momentum in the 5d states. Since the separation between J_{eff} states is much larger than the insulating gap, a bandwidth-driven insulator-metal transition would take place before J_{eff} states are fully mixed by band effects at about 100 GPa (1 Mbar). This high-pressure regime above 1 Mbar could provide fertile ground for searching for emerging superconductivity. — *Vic Comello*

See: D. Haskel^{1*}, G. Fabbris^{1,2}, Mikhail Zhernenkov¹, P.P. Kong³, C.Q. Jin³, G. Cao⁴, and M. van Veenendaal^{1,5}, “Pressure Tuning of the Spin-Orbit Coupled Ground State in Sr_2IrO_4 ,” *Phys. Rev. Lett.* **109**, 027204 (13 July 2012).

DOI:10.1103/PhysRevLett.109.027204

Author affiliations: ¹Argonne National Laboratory, ²Washington University, ³Chinese Academy of Sciences, ⁴University of Kentucky, ⁵Northern Illinois University

Correspondence: *haskel@aps.anl.gov

Work at the APS and Northern Illinois University was supported by the U.S. Department of Energy Office of Science (DOE-SC) under Contracts No. DE-AC02-06CH11357 and No. DE-FG02-03ER46097, respectively. The beamlines at APS Sector 20 are supported by the U.S. DOE-SC, a Major Resources Support grant from the Natural Sciences and Engineering Research Council of Canada, the University of Washington, the Canadian Light Source, and the APS.

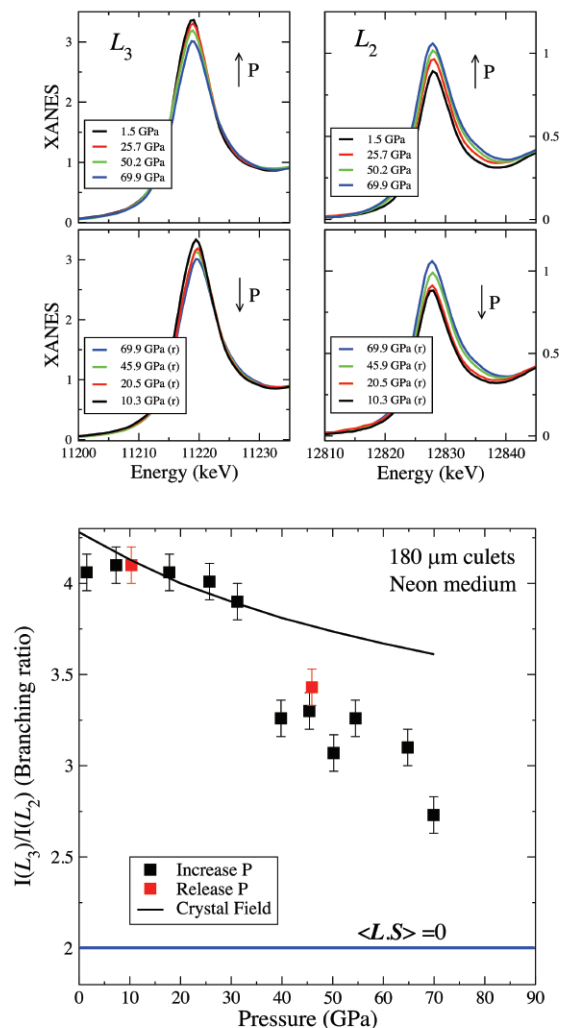


Fig. 2. Pressure dependence of iridium’s $L_{2,3}$ XANES data (top) and the derived branching ratio (bottom).

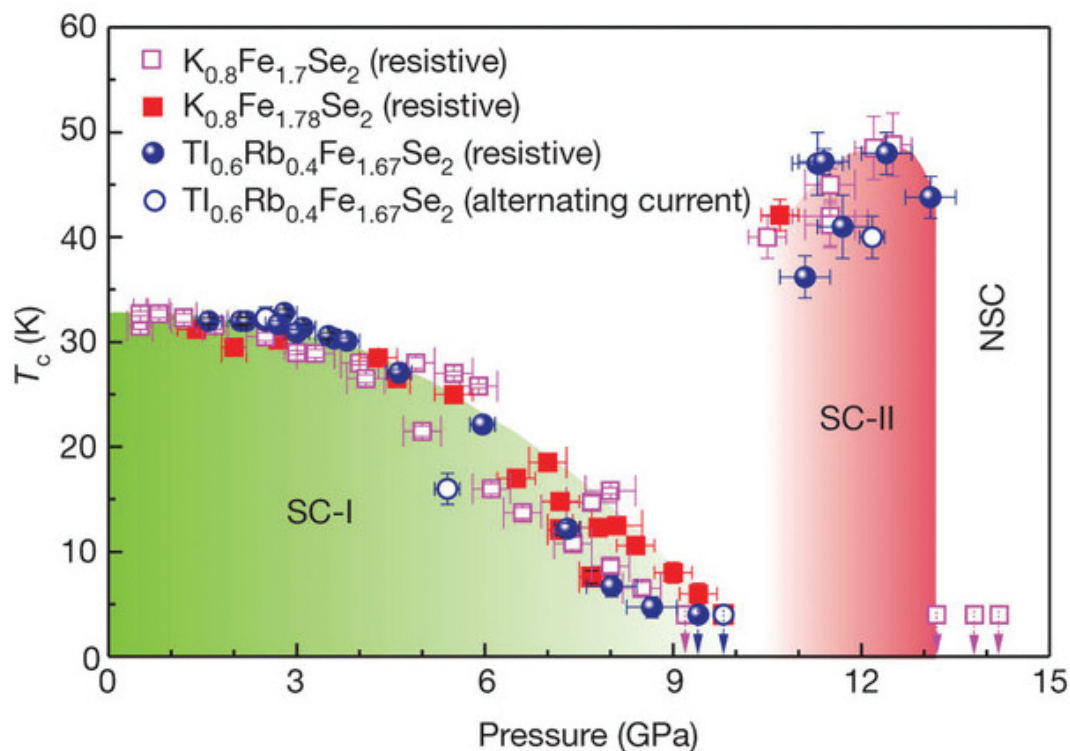
4-ID-D • XSD • Physics, materials science • Anomalous and resonant scattering (hard x-ray), magnetic x-ray scattering, magnetic circular dichroism (x-ray magnetic circular dichroism, hard x-ray) • 2.7-40 keV • On-site • Accepting general users •

16-BM-D • HP-CAT • Materials science, geoscience, chemistry, physics • Powder angular dispersive x-ray diffraction, x-ray absorption near-edge structure, single-crystal diffraction, high-pressure diamond anvil cell • 6-70 keV • On-site • Accepting general users •

20-BM-B • XSD • Materials science, environmental science, chemistry • X-ray absorption fine structure, microfluorescence (hard x-ray), micro x-ray absorption fine structure, diffraction anomalous fine structure • 2.7-25 keV, 2.7-30 keV, 2.7-35 keV • On-site • Accepting general users •

SUPERCONDUCTIVITY'S REAPPEARING ACT IN IRON CHALCOGENIDES

Sometimes it's good to put the pressure on. In iron-based superconducting materials such as the iron chalcogenides, pressure can be used to manipulate the superconducting transition temperature (T_C), a trick that could be important for utilizing these materials in practical applications. With an assist from an HP-CAT beamline at the APS and a beamline at the Shanghai Synchrotron Radiation Facilities (China), a group of researchers has discovered a new wrinkle on this phenomenon, observing the emergence of a new high-temperature superconductivity regime in a number of iron chalcogenides under increasing pressures.



Mills says hold off on this one

The experimental team, hailing from the Chinese Academy of Sciences, the Carnegie Institution of Washington, South China University of Technology, the National Institute of Standards and Technology, and Zhejiang University (China) studied crystals of $\text{Tl}_{0.6}\text{Rb}_{0.4}\text{Fe}_{1.67}\text{Se}_2$, $\text{K}_{0.8}\text{Fe}_{1.7}\text{Se}_2$, and $\text{K}_{0.8}\text{Fe}_{1.78}\text{Se}_2$ using high-pressure x-ray diffraction at the 16-BM-D and the BL15U beamline at Shanghai Synchrotron Radiation Facilities.

The researchers initially examined the samples through resistance and susceptibility measurements. They studied chalcogenides, compounds containing an element from group 16 of the periodic table with another element such as iron, were recently found to display superconductivity beginning at a T_C around 30 K, and as expected, the crystals examined in the present work displayed similar behavior. The $\text{Tl}_{0.6}\text{Rb}_{0.4}\text{Fe}_{1.67}\text{Se}_2$, for example, became superconducting at 33 K and a pressure of 1.6 GPa. The T_C shifted to lower temperatures as the pressure was increased, until superconductivity disappeared completely at ~ 9 GPa.

But when the experimenters decided to investigate even higher pressure regimes, things became interesting. At 12.4 GPa, a second superconducting phase emerged at around 48 K, an increase in temperature of

< Fig. 1. Pressure dependence of the T_C for $\text{Tl}_{0.6}\text{Rb}_{0.4}\text{Fe}_{1.67}\text{Se}_2$, $\text{K}_{0.8}\text{Fe}_{1.7}\text{Se}_2$, and $\text{K}_{0.8}\text{Fe}_{1.78}\text{Se}_2$. Two superconducting regions (SC-I and SC-II) are separated by a critical pressure at around 10 GPa. "NSC" refers to the non-superconducting region above 13.2 GPa. The maximum T_C is found to be 48.7 K in $\text{K}_{0.8}\text{Fe}_{1.7}\text{Se}_2$ at a pressure of 12.5 GPa. At higher pressures above 13.2 GPa, the samples are non-superconducting.

18°. Magnetic susceptibility measurements also showed two distinct superconducting phases. Repeated experiments with fresh crystal samples proved that the results were reproducible and consistent.

To determine whether this highly unusual behavior was unique to this particular compound or could be seen in other iron chalcogenides, the research team repeated the experiments on $\text{K}_{0.8}\text{Fe}_{1.7}\text{Se}_2$ crystals. The results were nearly identical. Again, the critical temperature of 32 K decreased with increasing pressure until superconductivity vanished at ~ 9.2 GPa, and a new superconductivity phase re-emerged at a T_C of 48.7 K and pressure of 12.5 GPa. Further tests with $\text{K}_{0.8}\text{Fe}_{1.7}\text{Se}_2$, a slightly different compound, showed similar behavior.

X-ray diffraction studies probed for structural clues to the mechanism behind this re-emerging superconductivity behavior. Interestingly, the basic tetragonal crystal structure of all the materials studied is preserved throughout the entire range of pressures, indicating that the key to the re-emergence of superconductivity in these compounds lies deeper within the basic unit cell. The experimenters speculate that quantum criticalities may play a role, and that the two distinct superconducting phases may indicate that different charge carriers are involved. The characteristic presence of Fe-vacancies in the crystal lattice of these iron chalcogenides may also be important.

For now, the origins of the re-emerging superconductivity phase in these new materials remains a mystery to be further explored and investigated through intensive research. But even before that mystery is solved, it hints at tantalizing possibilities for the discovery or development of true high-tempera-

ture, ambient pressure superconductors, perhaps through structural alterations of the right compounds. The present work is a vital step toward that ultimate goal. — [Mark Wolverton](#)

See: Liling Sun¹, Xiao-Jia Chen^{2,3}, Jing Guo¹, Peiwen Gao¹, Qing-Zhen Huang⁴, Hangdong Wang⁵, Minghu Fang⁵, Xiaolong Chen¹, Genfu Chen¹, Qi Wu¹, Chao Zhang¹, Dachun Gu¹, Xiaoli Dong¹, Lin Wang², Ke Yang¹, Aiguo Li¹, Xi Dai¹, Ho-kwang Mao^{2*}, and Zhongxian Zhao^{1**}, "Re-emerging superconductivity at 48 kelvin in iron chalcogenides," *Nature* **483**, 67 (1 March 2012).

DOI:10.1038/nature10813

Author affiliations: ¹Chinese Academy of Sciences, ²Carnegie Institution of Washington, ³South China University of Technology, ⁴National Institute of Standards and Technology, ⁵Zhejiang University

Correspondence:

**zhxzhao@iphy.ac.cn,
*hmao@gl.ciw.edu

This work was supported by the National Natural Science Foundation of China, 973 projects, and the Chinese Academy of Sciences; EFree, an Energy Frontier Research Center funded by the US Department of Energy Office of Science, Basic Energy Sciences Program (DOE-BES). HP-CAT is supported by CIW, CDAC, University of Nevada Las Vegas and Lawrence Livermore National Laboratory through funding from the DOE-National Nuclear Security Administration, the DOE-BES and the U.S. National Science Foundation.

16-BM-D • HP-CAT • Materials science, geoscience, chemistry, physics • Powder angular dispersive x-ray diffraction, x-ray absorption near-edge structure, single-crystal diffraction, high-pressure diamond anvil cell • 6-70 keV • On-site • Accepting general users

DOPING STRONTIUM IRIDATE MAY MAKE IT SUPERCONDUCTIVE

Transition metal oxides (TMOs) exhibit a uniquely wide range of electronic and magnetic properties. The discovery of high-temperature superconductivity (HTSC) in cuprates (e.g., La_2CuO_4) has sparked an intense search for other TMOs that may be superconductive. Prime candidates are $5d$ TMOs because of their strong relativistic spin-orbit coupling (SOC), which can drastically modify magnetic interactions, giving rise to a rich spectrum of magnetic systems. Researchers carrying out studies at two APS beamlines focused on magnetic interactions in Sr_2IrO_4 , a $5d$ TMO with a spin-orbit entangled ground state and effective total angular momentum $J_{\text{eff}} = 1/2$ magnetic moments, using resonant inelastic x-ray scattering (RIXS). They found evidence suggesting that a doped hole or electron in Sr_2IrO_4 may display the same dynamics as that observed for a doped hole or electron in the cuprates, opening the door to the possibility of HTSC.

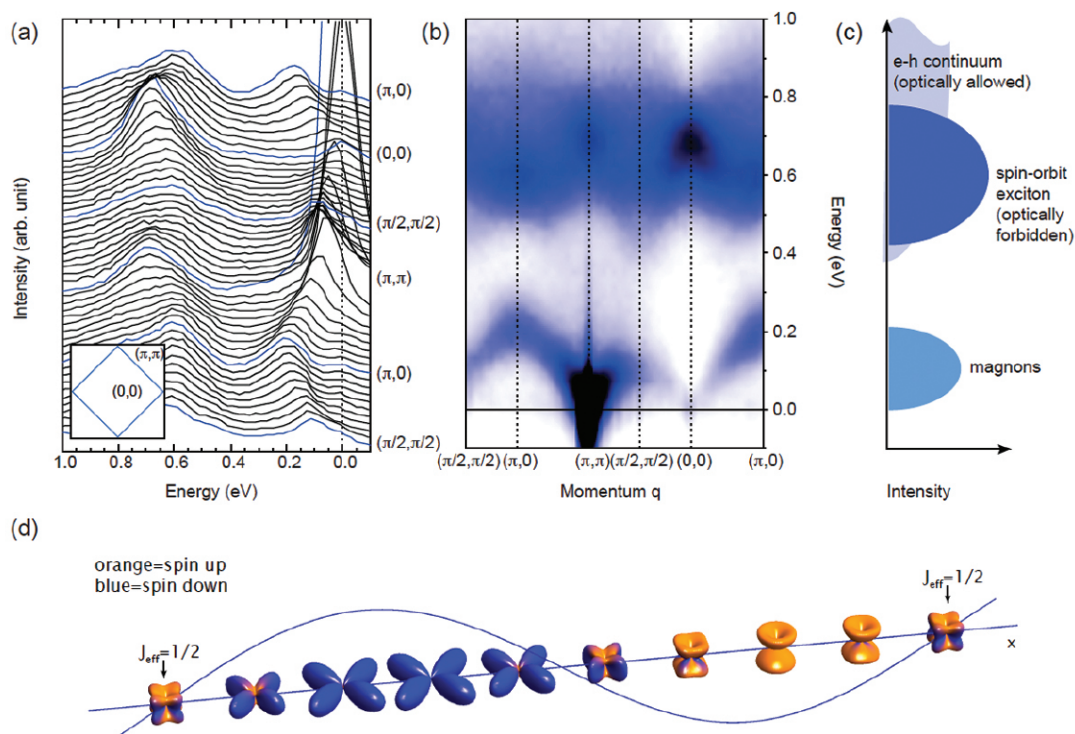


Fig. 1. (a) and (b): RIXS energy loss spectra recorded at $T = 15$ K, well below $T_N = 240$ K. (c) Schematic of three representative features in the RIXS data. (d) A real-space interpretation of the high-energy spin-orbit exciton mode; orange and blue colors represent up and down spins, respectively.

Sr_2IrO_4 is a layered perovskite whose Ir^{4+} ($5d^5$) ions are situated inside corner-shared oxygen octahedral cages, which are arranged in a square lattice, resulting in a canted antiferromagnetic (AF) structure. Although the structure of a single magnetic moment in Sr_2IrO_4 , which is composed of orbital and spin moments, is drastically different from that of the pure spins in La_2CuO_4 —a parent insulator for cuprate superconductors—the two compounds share a similar magnetic structure as revealed by dispersion and intensity measurements of a single magnon. The dispersion and the momentum dependence of the intensity show striking similarities to those observed in the cuprates (e.g., La_2CuO_4) by inelastic neutron scattering. This provides confidence that the observed mode is indeed a single magnon excitation.

The magnon mode strongly affects the dispersion of a doped hole or electron and is believed to provide a pairing mechanism for HTSC. In addition to the low-energy magnon branch (≤ 0.2 eV), the researchers from Argonne National Laboratory, the University of Toronto (Canada), Northern Illinois University, the Leibniz Institute for Solid State and Materials Research Dresden (Germany), and the Max Planck Institute for Solid State Research (Germany) working at the XSD 9-ID-B,C and 30-ID-B,C beamlines at the APS, observed high-energy excitations with strong momentum dependence in the energy range of 0.4-0.8 eV (Fig. 1). The energy scale of these excitations coincides with the known energy scale of spin-orbit coupling in Sr_2IrO_4 , permitting it to be seen as an intra-site excitation of a hole across the spin-orbit split levels from the $J_{\text{eff}} = 1/2$ level to one of $J_{\text{eff}} = 3/2$ quartet levels. The dispersion of the spin-orbit exciton has a bandwidth of at least 0.3 eV, implying that this local excitation can propagate coherently through the lattice.

Despite important differences in the high-energy scale, the measurement of the magnon spectrum high-

lights the similarities with cuprates in the low-energy effective physics. Further, from the observed spin-orbit exciton dispersion, it may be expected that a doped hole or electron in Sr_2IrO_4 will display the same dynamics as that observed for a doped hole or electron in the cuprates. Although superconductivity has not yet been reported, the phase diagram of lightly doped Sr_2IrO_4 has just begun to be revealed experimentally. Only further study will tell if doping can drive Sr_2IrO_4 to a superconducting state. — *Vic Comello*

See: Jungho Kim¹, D. Casa¹, M.H. Upton¹, T. Gog¹, Young-June Kim², J.F. Mitchell¹, M. van Veenendaal^{1,3}, M. Daghofer⁴, J. van den Brink⁴, G. Khaliullin⁵, and B. J. Kim^{1*}, "Magnetic Excitation Spectra of Sr_2IrO_4 Probed by Resonant Inelastic X-Ray Scattering: Establishing Links to Cuprate Superconductors," *Phys. Rev. Lett.* **108**, 177003 (27 April 2012). DOI:10.1103/PhysRevLett.108.177003

Author affiliations: ¹Argonne National Laboratory, ²University of Toronto, ³Northern Illinois University, ⁴Leibniz Institute for Solid State and Materials

Research Dresden, ⁵Max Planck Institute for Solid State Research
Correspondence: *bjkim@anl.gov

Work in the Materials Science Division and the use of the Advanced Photon Source at Argonne National Laboratory were supported by the U.S. Department of Energy (DOE) Office of Science under Contract No. DE-AC02-06CH11357. Y.K. was supported by the Canada Foundation for Innovation, Ontario Research Fund, and Natural Sciences and Engineering Research Council of Canada. M.v.V. was supported by the DOE Basic Energy Science (BES) Program under Award No. DE-FG02-03ER46097. M.D. acknowledges support by the Emmy-Noether program of the Deutsche Forschungsgemeinschaft. This work benefited from the RIXS collaboration supported by the Computational Materials Science Network program of U.S. DOE under Grant No. DE-FG02-08ER46540.

9-ID-B,C • XSD • Physics, materials science • Resonant inelastic x-ray scattering, inelastic x-ray scattering, liquid scattering • 4.5-24 keV • On-site • Accepting general users

30-ID-B,C • XSD • Physics, materials science • Inelastic x-ray scattering, resonant inelastic x-ray scattering • 5-14 keV, 5-30 keV, 23.7-23.9 keV • On-site • Accepting general users •



Then-Argonne Director Alan Schriesheim demonstrates high-temperature superconductivity to U.S. President Ronald Reagan in 1987.

Photo: Argonne National Laboratory.

X-RAYS AND MAGNETS TEAM UP TO PROBE SUPERCONDUCTORS

Aside from their fundamental importance and interest as physical phenomena, magnetic fields can also be quite handy for practical experimentation. In materials science, the application of just the right sort of magnetic field can create effects and reveal changes in a material that provide key insights into its properties and structure, all without any direct physical contact. Researchers from Argonne, Stanford University, the SLAC National Accelerator Laboratory, and Tohoku University (Japan) combined a pulsed magnetic field with x-ray diffraction (XRD) studies at XSD beamline 6-ID-B at the APS to investigate anisotropic magnetic susceptibility behavior in an iron arsenide superconductor. This work opens the door to greater characterization of iron arsenide superconductors.

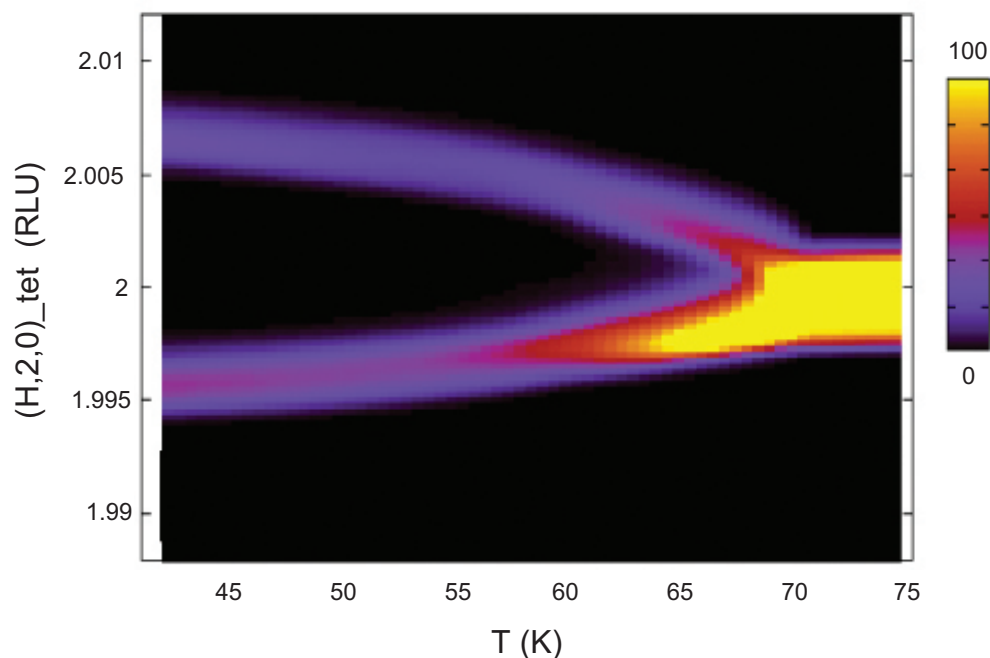


Fig. 1. High-resolution x-ray diffraction shows the $(2, 2, 0)$ Bragg peak splitting at the structural phase transition ($T_s \sim 70$ K). From J. P.C. Ruff et al., *Phys. Rev. Lett.* **109** (2012). © 2012 American Physical Society

Previous experiments have demonstrated a strong electronic anisotropy within the $a - b$ plane in these materials. While it has been speculated that this anisotropy may be the impetus for the tetragonal-to-orthorhombic phase transition, transformational twinning effects mask detection of the anisotropy by resistivity and susceptibility measurements, unless they are performed under significant applied uniaxial stress.

The current work illuminates a new way to probe the iron arsenide phase transition without any kind of physical contact, thus avoiding secondary symmetry-breaking effects. Through the application of pulsed magnetic fields under XRD, magnetic detwinning measurements can provide unique information about the evolution of susceptibility anisotropy.

Studying a sample crystal of underdoped $\text{Ba}(\text{Fe}_{1-x}\text{Co}_x)_2\text{As}_2$ at the 6-ID-B beamline, the experimenters first observed the tetragonal-to-orthorhombic phase transition at 70 K (Fig. 1). The evolution of Bragg scattering from structural twins during the application of pulsed magnetic fields up to 27.5 T show complete detwinning in the orthorhombic phase, which the authors ascribe to anisotropy in magnetic susceptibility between the a and b axes (Fig. 2). The detwinning effects set in immediately as the temperature drops below the critical temperature of the structural phase transition, as a precursor to magnetic order. The detwinning effects also accompany the anisotropy down to the superconducting transition temperature and then, surprisingly, disappear, signifying either kinetic inhibition or a return of susceptibility isotropy.

After application of magnetic field pulses to 27.5 T at low temperatures, a residually detwinned state remains that is quite similar to the detwinning induced under uniaxial strain and seems quite stable, lasting for at least several hours. Improved crystal quality is also seen in this remnant phase. This opens the possibility that the use of magnetic fields might provide a new “hands-off” treatment for the creation of superior detwinned iron arsenides

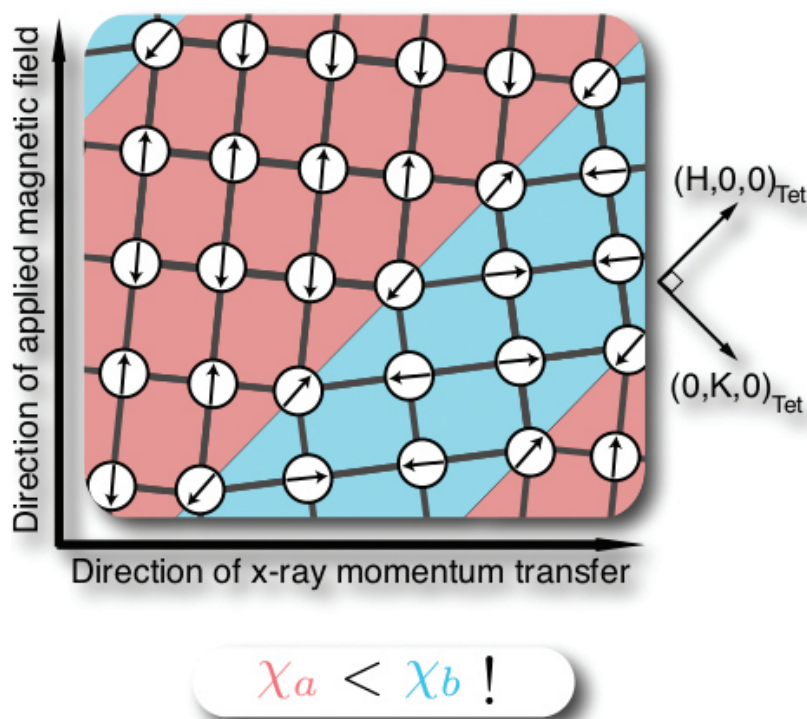


Fig. 2. Schematic of twin domains within the $a - b$ plane. Orthorhombic strain and the density of twinning are exaggerated for effect. The highly anisotropic magnetic ordering pattern of Fe spins is also illustrated. From J.P.C. Ruff et al., *Phys. Rev. Lett.* **109** (2012).

without the use of uniaxial pressure treatment.

The pulsed-magnet x-ray diffraction technique demonstrated here offers numerous experimental possibilities for the investigation and characterization of iron arsenide superconductors. Because it can be applied over a wide range of temperatures and magnetic field strengths, it provides a valuable window into the magnetic anisotropy of iron arsenides throughout their various phase transitions.

The next step will be to develop more-accurate models of how twin domains behave in magnetic fields, which will lead to more accurate measurements of magnetic susceptibility. Further development and refinement of pulsed-magnetic XRD techniques will make possible exciting new inroads in both experiment and theory.

— Mark Wolverton

See: J.P.C. Ruff^{1*}, J.-H. Chu^{2,3}, H.-H. Kuo^{3,2}, R.K. Das¹, H. Nojiri⁴, I.R. Fisher^{2,3}, and Z. Islam¹, “Susceptibility Anisotropy in an Iron Arsenide Superconductor Revealed by X-Ray

Diffraction in Pulsed Magnetic Fields,” *Phys. Rev. Lett.* **109**, 027004 (2012). DOI:10.1103/PhysRevLett.109.027004
 Author affiliations: ¹Argonne National Laboratory, ²Stanford University, ³SLAC National Accelerator Laboratory, ⁴Tohoku University
 Correspondence: *jpcruff@aps.anl.gov

A part of this work was enabled by the International Collaboration Center at the Institute for Materials Research at Tohoku University. H.N. acknowledges KAKENHI Grant No. 23224009 from the Ministry of Education, Culture, Sports, Science & Technology (Japan). J.P.C.R. acknowledges the support of the Argonne Director’s Fellowship and of the Natural Sciences and Engineering Research Council of Canada. Use of the Advanced Photon Source at Argonne National Laboratory was supported by the U.S. Department of Energy Office of Science under Contract No. DE-AC02-06CH11357.

6-ID-B,C • XSD • Physics, materials science • Magnetic x-ray scattering, anomalous and resonant scattering (hard x-ray), general diffraction, grazing incidence diffraction, surface diffraction (UHV) • 3.2-38 keV • On-site • Accepting general users •

REVEALING THE INTERPLAY BETWEEN ATOMIC STRUCTURE AND MAGNETISM

Many factors can alter the magnetic properties of a material. Temperature is perhaps the best-known example: permanent magnets will lose their intrinsic magnetic field if they become too hot. A particularly interesting phenomenon observed in some substances is a link between magnetism and atomic crystalline structure. In such cases, a change in the ordering of atomic structure produces a change in the material's magnetic phase — for instance, a change from ferrimagnetism to paramagnetism. The details of these coupling phenomena are not completely understood, and sometimes they appear unexpectedly in substances with simple structures. A good example is the coupling between magnetism and the ruby-type crystalline structure of nickel chromite (NiCr_2O_4) and copper chromate (CuCr_2O_4). The “magnetostructural” couplings observed in these materials are highly temperature-dependent. Utilizing the intense synchrotron radiation at the APS, temperature-controlled x-ray powder diffraction experiments were performed on these two materials to better understand correlations between coincident changes in their structure and magnetic properties. This research will help unlock the complex relationships between magnetism and atomic structure observed in many materials.

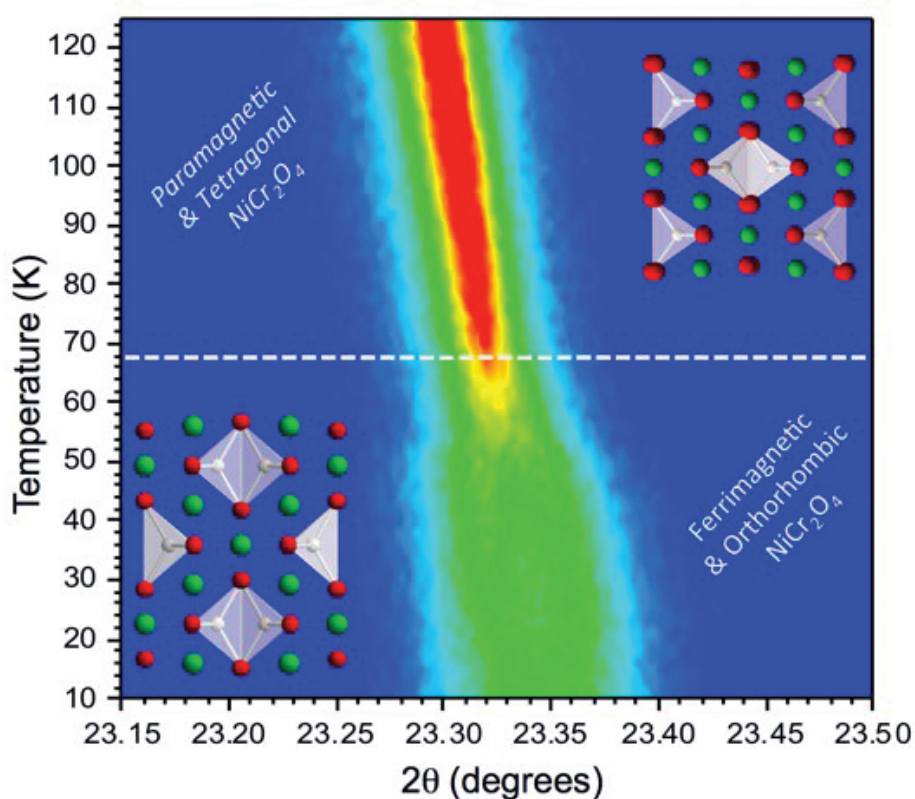
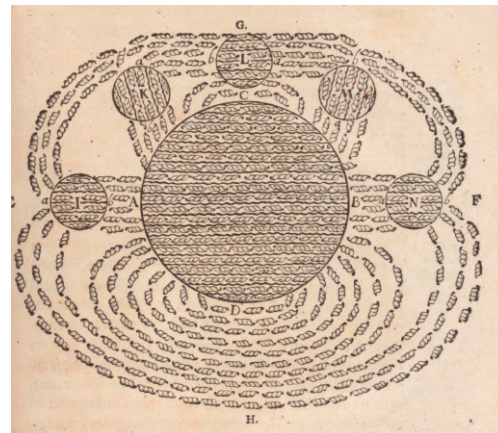


Fig. 1. Broadening in high-resolution x-ray powder diffraction peaks with decreasing temperature in data measured at APS beamline 11-BM-B reveals concurrent magnetostructural transitions in the spinel NiCr_2O_4 .

> Drawing of a magnetic field by French philosopher René Descartes, from his *Principia Philosophiae*, 1644. This was one of the first drawings of the concept of a magnetic field. It shows the magnetic field of the Earth (D) attracting several round lodestones (I, K, L, M, N) and illustrates his theory of magnetism. From René Descartes (1644) *Principia Philosophiae*, Ludovicum, Amsterdam, p. 271 (Wikicommons).



At normal room temperatures, NiCr_2O_4 and CuCr_2O_4 (both classified as spinels, a type of mineral) possess tetragonally distorted lattice structures due to the so-called “Jahn-Teller effect.” This occurs in response to the degeneracy of electronic states associated with these materials’ structure and chemical composition. Quantum mechanical rules determine how electrons are arranged within the orbitals of atoms and molecules. A system of atoms or molecules tends toward the lowest energy level. However, when two or more states in a system have electrons that are at the same (lowest) energy level, then the system is said to be degenerate and it is generally unstable. In response to electron degeneracy, the ions composing a crystal may rearrange to lower the overall energy of the system. The lattice undergoes a Jahn-Teller distortion that yields a single lowest-energy electron configuration. Such distortions can also affect the material’s magnetic behavior.

Previous studies have investigated the lattice distortions and magnetic phase changes of NiCr_2O_4 and CuCr_2O_4 . The x-ray diffraction (XRD) measurements performed in this research by scientists from Argonne National Laboratory and the University of California, Santa Barbara, revealed previously unresolved details of the structural and magnetic changes occurring within the two materials, especially at lower temperatures. The XRD measurements were performed on carefully prepared samples of powdered NiCr_2O_4 and CuCr_2O_4 , using equipment that allowed fine temperature control. The experiments were carried out at XSD beamline 11-BM-B at the APS, which provides one of the highest resolution

probes available in the world for this technique.

These x-ray measurements showed three lattice transitions in NiCr_2O_4 at three disparate temperatures. Each lattice change was coupled to a change in the material’s magnetic phase. At 310 K the lattice structure of NiCr_2O_4 transitions from tetrahedral — which predominates just below 310 K — to a cubic unit cell above 310 K. (Tetrahedral unit cells are basically three-sided pyramids of equal-length sides.)

Above 310 K, the cubic lattice structure of NiCr_2O_4 produces paramagnetism (in this state, a magnetic field within the material only arises from an applied external field). In the 310 K to 65 K temperature range, a weakened paramagnetic state exists. At 65 K, NiCr_2O_4 again undergoes a structural change, with lattice geometry shifting from tetrahedral to orthorhombic (basically a stretched cube with sides a , b , and c unequal). The magnetic phase also transitions at 65 K, shifting from paramagnetism to ferrimagnetism (Fig. 1).

A third, but subtle, structural change occurs at 30 K, which is reported for the first time in this research. This low-temperature structural change is associated with an additional antiferromagnetic component. Besides the magnetostructural changes, the researchers also measured significant changes in the heat capacity of NiCr_2O_4 at 65 and 30 K.

For the CuCr_2O_4 sample, a pronounced magnetostructural change was observed to occur around 130 K, with its lattice structure shifting from tetragonal below ~ 130 K to orthorhombic above it. This lattice shift was

accompanied by a transition from paramagnetism below ~ 130 K to ferrimagnetism above it. This research produced the first observation of the tetragonal-to-orthorhombic structural shift concurrent with the appearance of ferrimagnetism via x-ray powder diffraction.

The powerful synchrotron radiation of the APS, combined with the high-resolution x-ray powder diffraction probe at beamline 11-BM-B revealed fresh details of the coupled magnetostructural changes in NiCr_2O_4 and CuCr_2O_4 that will help scientists better understand the delicate interplay between the properties of magnetism and structure in an array of materials, with the hope of harnessing these properties for new technological applications.

— Philip Koth and William A. Atkins

See: Matthew R. Suchome1*, Daniel P. Shoemaker1, Lynn Ribaud1, Moureen C. Kermei2, and Ram Seshadri2, “Spin-induced symmetry breaking in orbitally ordered NiCr_2O_4 and CuCr_2O_4 ,” *Phys. Rev. B* **86**, 054406 (2012).

Author affiliations: 1Argonne National Laboratory, 2University of California, Santa Barbara

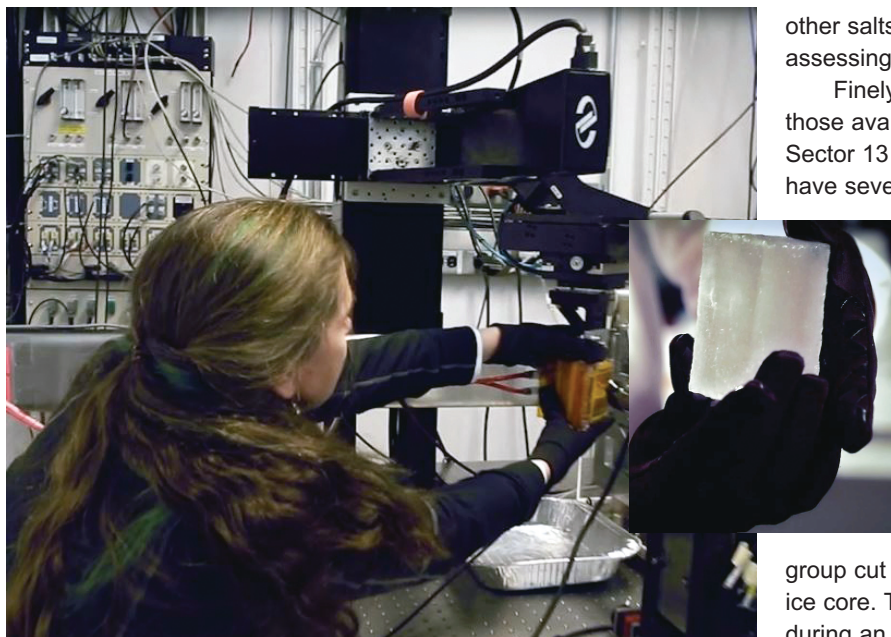
Correspondence:

*suchome1@aps.anl.gov

M.C.K. is supported by the Schlumberger Foundation Faculty for the Future Fellowship, and the research (M.C.K. and R.S.) is supported by the National Science Foundation through a Materials World Network grant (DMR0909180).

11-BM-B • XSD • Chemistry, materials science, physics • Powder diffraction • 15-35 keV • On-site, mail-in • Accepting general users •

UNLOCKING A SEA ICE SECRET: BROMIDE AND OTHER IMPURITIES IN SNOW AND SEA ICE



Rachel Obbard mounting the sea ice core sample (inset) in the GSECARS 13-ID-E research station. Pictures are frames from the Argonne video about this research, which can be seen at <http://www.youtube.com/watch?v=NUES118GR7M&feature=youtu.be>

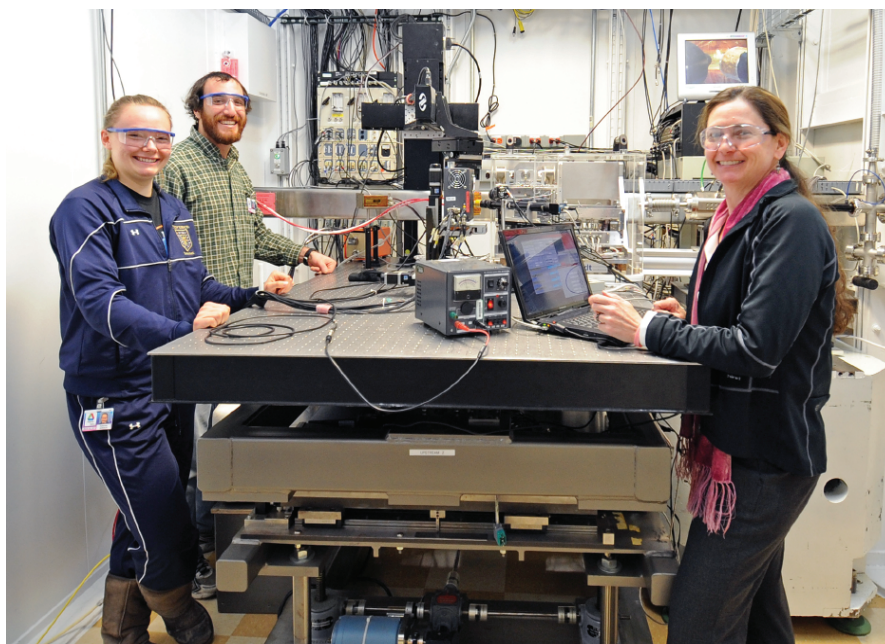
In October and November 2012, Assistant Professor Rachel Obbard and her research group from The Thayer School of Engineering at Dartmouth College traveled to the Antarctic to collect sea ice cores and snow from different locations on the Ross Sea, Antarctica. Next stop: the GSECAR x-ray beamlines at the APS, which gave the Obbard team the frontier scientific tools they needed to study the path bromide takes as it travels from the polar ocean through the sea ice and snow.

Polar tropospheric ozone depletion events are strongly correlated with increased tropospheric concentrations of reactive bromine gases (BrO and Br). But, while scientists know that sea ice plays a critical role in mediating the exchange of heat, gases, and chemical species across the ocean-atmosphere interface, the exact mechanism by which bromide enters the lower atmosphere is not well understood. This research focuses on the transport of bromide, which originates in sea water, is present in brine channels in the sea ice, and is thought to be lofted into the boundary layer atmosphere by snow blowing across the ice. By identifying the microstructural and stratigraphic location of bromide and

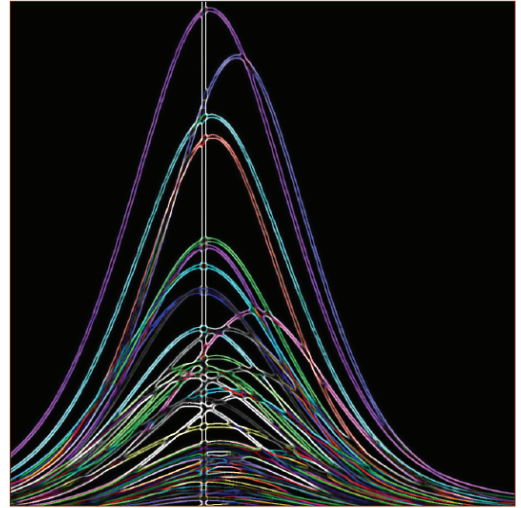
other salts in sea ice and snow, the researchers are assessing the validity of this hypothesis.

Finely-focused synchrotron x-ray beams such as those available at GeoSoilEnviroCARS (GSECARS) Sector 13 of the APS where the studies were carried out, have several benefits over other techniques the researchers will use. First, the high intensity beam cuts data acquisition time and the potential for thermal drift. Second, synchrotron techniques provide higher spatial resolution than other spectroscopic techniques and can be used to map impurities within the ice and snow microstructure. Third, detection limits of a few parts per million permit the soluble impurities without the need for preconcentration of impurities through sublimation.

Prior to visiting APS, the Dartmouth group cut small samples at intervals of 10 cm in each sea ice core. They utilized the GSECARS 13-ID-E beamline during an initial visit in 2013 to study the sea ice samples from their expedition. This six-day experiment established their technique and identify impurities at the grain boundaries and brine channels in sea ice. They will return to the APS for a new round of studies of surface and blowing snow samples. With XRF, they expect that analysis of their new data will allow them to assess the potential that snow blowing across sea ice lofts bromide into the atmosphere, ultimately leading to ozone depletion events.



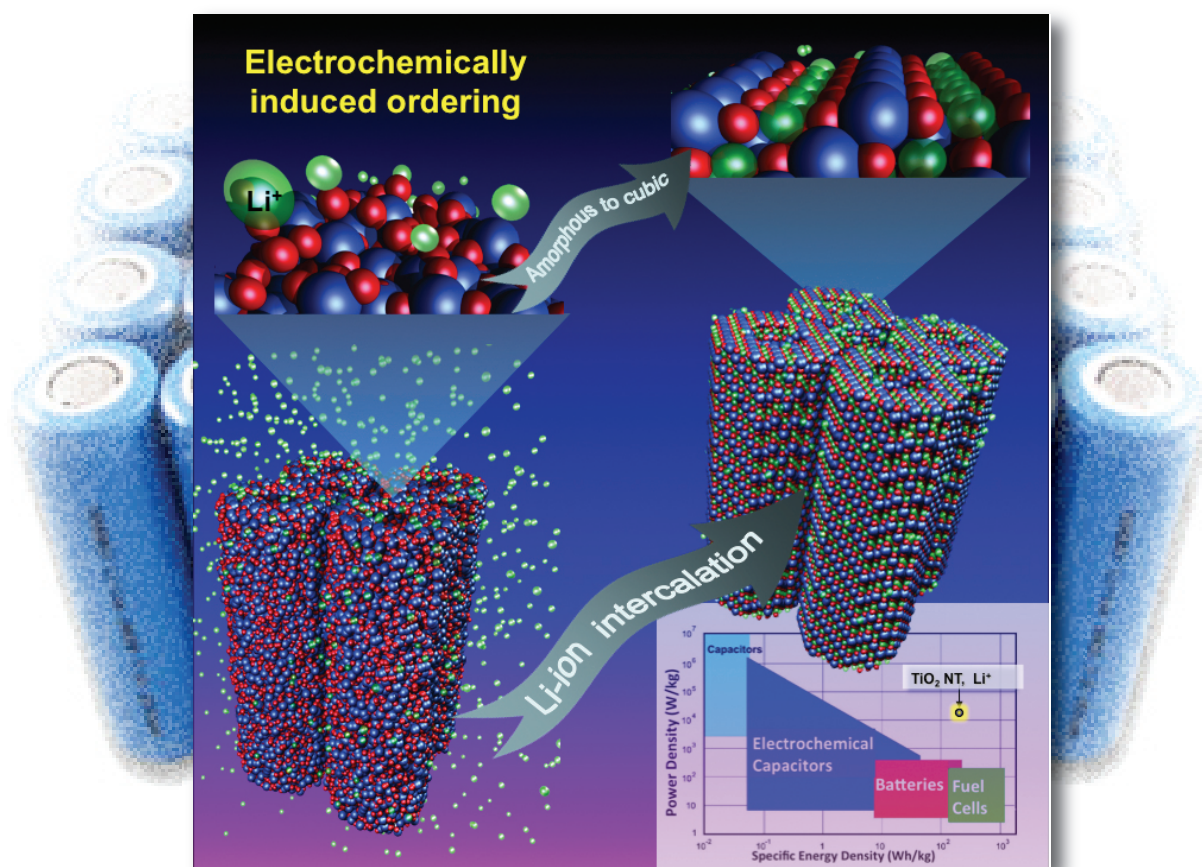
The Dartmouth group in the GSECARS 13-ID-E research station at the APS. Left to right: undergraduate student Katherine Nordick, graduate student Ross Lieb-Lappen, and Rachel W. Obbard.



ENGINEERING MATERIALS & APPLICATIONS

SELF-IMPROVEMENT OF LITHIUM-ION BATTERIES

The search for clean and green energy in the 21st century requires a better and more efficient battery technology. The key to attaining that goal may lie in designing and building batteries not from the top down, but from the bottom up — beginning at the nanoscale. A team of researchers from Argonne National Laboratory and The University of Chicago working at two APS beamlines took such an approach by developing titanium dioxide (TiO_2) electrodes that can actually improve their own electrochemical performance as they are used.



The experimenters synthesized TiO₂ nanotubes and assembled them into Li-ion coin cells, then cycled them galvanostatically between 0.8 V and 2.0 V. Electrode samples from the cells were then examined using x-ray diffraction (XRD) at the GSECARS 13-ID-C,D beamline and x-ray absorption spectroscopy (XAS) at the XSD 20-BM-B beamline, both at the APS.

In addition to the synthesis of the TiO₂ nanotubes, scanning electron microscopy imaging and molecular dynamics simulations also were performed at the Argonne Center for Nanoscale Materials. All these techniques provided a window into the inclusion and removal of ions (intercalation/deintercalation process) occurring within the TiO₂ nanotubes.

Using the amorphous nanoscale TiO₂ nanotubes as an anode in lithium half-cells, the researchers noted a consistently linear decreasing voltage during the first discharge, followed by a “hump” at ~1.1 V vs Li/Li⁺. This indicated an irreversible phase transition in the nanotube material.

On subsequent cycles, Li⁺ ions reversibly intercalated/deintercalated into the TiO₂ nanotubes with capacities far beyond those observed in other TiO₂ varieties such as anatase.

The team concluded that this is due to a different structure or intercalation mechanism occurring as a result of the phase transition. Compared to anatase, the phase-transformed TiO₂ nanotube anode displayed greatly improved Li-ion diffusion, especially at high cycling rates. The TiO₂ nanotube anode demonstrated both much higher energy and higher power compared to its structural TiO₂ cousins, which displayed a decrease in capacity in similar experiments using fast cycling.

The XRD and XAS studies, along with computational simulations, displayed how the anode structure

< Amorphous titanium oxide nanotubes, upon lithium insertion in a Li-ion battery, self-create the highest capacity cubic lithium titanium oxide structure.

changed upon cycling. Above ~1.1 V, no changes were observed with cycling, but below 1.1 V, a highly-symmetric, closely-packed cubic oxygen crystalline structure formed, with Ti and Li randomly distributed among octahedral sites.

Interestingly, the type of short-range order that would be expected in such a fully-ordered octahedral system apparently does not develop in this case. However, this does not affect thermodynamic stability, and the cubic structure remained both highly stable and reversible following the phase transition.

It appears that the intercalation/deintercalation of Li⁺ ions initiates a new structure that allows even better intercalation of Li⁺ ions. Because all layers of the new structure retain metal atoms even in the charged state, the cubic phase of the material is preserved. Molecular dynamics simulations of Li-ion diffusion in other types of TiO₂ structures showed that the most efficient diffusion and the lowest activation barrier (0.257 eV) occurs in the amorphous cubic Li₂Ti₂O₄ form, compared to other TiO₂ varieties such as, again, anatase.

The amorphous-to-cubic TiO₂ nanotube anode was tested in a full cell configuration with a 5-V spinel cathode (LiNi_{0.5}Mn_{1.5}O₄). On repeated cycling, the cell displayed an average voltage of 2.8 V and improving capacity.

Another distinct advantage of the TiO₂ nanotube anode is that because it does not suffer capacity degradation, it avoids Li plating at the graphite anode and electrode over-potentials that create possible safety hazards in other types of Li-ion batteries.

By creating a nanoscale electrode material that can actually order itself into a more efficient and powerful electrochemical structure as it is subjected to repeated discharging and charging, the research team forged a new pathway for the design and development of higher capacity, higher power, safer batteries. In our world of smart-phones technology and electric cars, the impor-

ance of such an advance can hardly be overestimated.

— Mark Wolverton

See: Hui Xiong¹, Handan Yildirim¹, Elena V. Shevchenko¹, Vitali B. Prakapenka², Bonil Koo¹, Michael D. Slater¹, Mahalingam Balasubramanian¹, Subramanian K.R.S. Sankaranarayanan¹, Jeffrey P. Greeley¹, Sanja Tepavcevic¹, Nada M. Dimitrijevic¹, Paul Podsiadlo¹, Christopher S. Johnson^{1*}, and Tijana Rajh^{1**}, “Self-Improving Anode for Lithium-Ion Batteries Based on Amorphous to Cubic Phase Transition in TiO₂ Nanotubes,” *J. Phys. Chem. C* **116**, 3181 (2012). DOI:10.1021/jp210793u
Author affiliations: ¹Argonne National Laboratory, ²The University of Chicago
Correspondence: *cjohnson@anl.gov; **rajh@anl.gov

This work, use of the Argonne Center for Nanoscale Materials, and use of the Argonne Advanced Photon Source were supported by the U.S. Department of Energy Office of Science (DOE-SC) under Contract DE-AC02-06CH11357. The beamlines at APS Sector 20 are supported by the U.S. DOE-SC, a Major Resources Support grant from the Natural Sciences and Engineering Research Council of Canada, the University of Washington, the Canadian Light Source, and the Advanced Photon Source. GeoSoilEnviroCARS is supported by the National Science Foundation Earth Sciences (EAR-1128799) and DOE Geosciences (DE-FG02-94ER14466).

13-ID-C,D • GSECARS • Geoscience, environmental science • Inelastic x-ray scattering, small x-ray absorption fine structure, microdiffraction, x-ray absorption fine structure, microfluorescence (hard x-ray), high-pressure diamond anvil cell, high-pressure multi-anvil press • 4-45 keV • On-site • Accepting general users •

20-BM-B • XSD • Chemistry, environmental science, geoscience, materials science • Micro x-ray absorption fine structure, microfluorescence (hard x-ray), x-ray absorption fine structure • 2.7-25 keV, 2.7-30 keV, 2.7-35 keV • On-site • Accepting general users •

HOW LEAD-FREE SOLDER (MIS) BEHAVES UNDER STRESS

The reliability and longevity of electronics is critical to our interconnected world that is dependent upon internet and telecommunications technology. The computers, routers and switches, phones, and all the devices that link us together must be dependable down to the solder joints that connect integrated circuits to circuit boards, which can be an Achilles heel in an otherwise failure-free device. New synchrotron x-ray techniques and two x-ray beamlines at the APS enabled studies of the beginnings of the thermal fatigue process in environmentally friendly, lead-free solder joints, as well as what happens toward the end of that process. These insights bring scientists a step closer to developing useful models for making physically based reliability predictions about solder-joint failure in this new material.

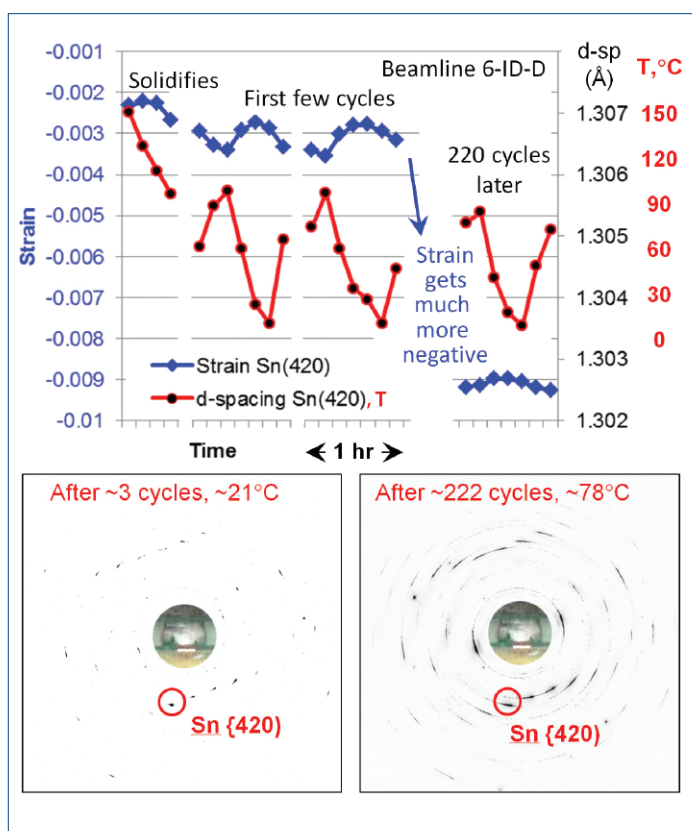


Fig. 1. Lead-free SAC305 solder joints are often a single crystal upon solidification. Thermal strain in the corner joint of a WLCSP package was measured *in situ* by the peak shift in diffraction patterns during a thermal cycle: Unstrained (420) plane spacing in the unit cell (black) varies with temperature. Strain $\sim \frac{\Delta d}{d}$ to joint on (420) plane varies with temperature (blue). Elastic strain is much more negative after 220 thermal cycles, and the diffraction patterns (bottom) develop streaks, indicating increased dislocation density and subgrain development. This shows how the microstructural evolution mechanism begins. Image courtesy of T.R. Bieler, F. Pourboghrat, and T.-K. Lee.

The first century of electronics used lead-based solder because it has desired material properties for manufacturing and reliability. Engineers thoroughly understood the electrical, thermal, and structural behavior of these solders and were able to accurately predict reliability. In 2006, the European Union Restriction of Hazardous Substances Directive came into effect, banning lead-containing solders from all consumer electronics devices, manufacturers looked for alternative solder materials. But the ban created a new problem: How reliable were lead-free solders?

Especially in the telecommunications industry, the expected lifetime of many products is long, and also a very low failure rate is needed.

The researchers in this study, from Cisco Systems, Inc.; Michigan State University; and the Max-Planck-Institut für Eisenforschung GmbH developed new techniques and employed them at the APS to track the development of the failure mechanism of lead-free solder joints *in situ* for the first time. Working at the XSD 6-ID-D and 34-ID-E beamlines at the APS, they conducted experiments to demonstrate how synchrotron x-ray diffraction could reveal the evolution of crystal orientation and strain patterns during thermal cycling in tin-containing, lead-free solder joints, specifically in the commonly

used tin-silver-copper alloy SAC 305 (Sn-3%Ag-0.5% Cu).

Older lead-tin solders tend to solidify as a polycrystal, delivering a solder joint that has a uniform microstructure, with reproducible properties. But lead-free solders usually solidify either as a randomly oriented single crystal or a tricrystal. "With the lead-free solders, the properties of solder joints vary depending on both crystal orientation and position in the package, so it is important to identify worst-case scenarios to insure that lifetimes can be more accurately predicted" Bieler said.

Failures in lead-free solders don't always occur in areas where shear strains from thermal expansion mismatches are highest. This is a consequence of the non-cubic structure of tin and its highly anisotropic thermal expansion and stiffness. It is difficult to predict the strains that develop in an individual joint, given the random crystal orientation, so the prediction of damage is even more challenging. Furthermore, the crystal orientations evolve with thermal cycling. The experimenters examined SAC 305 joints both in a plastic ball grid array (PBGA) package sample and a wafer-level chip-scale package (WLCSPP). Both types have been examined under thermal cycling, and the latter was studied *in situ* during melting, resolidification, and thermal cycling.

The advantages of the x-ray approach over the cross-sectional electron microscopy generally used to study solder joints were immediately apparent. In a two-dimensional cross section, one does not necessarily know what has been removed or what is underneath the surface. With three-dimensional full illumination of the joint, we were able to prove that we did indeed primarily have single crystals in some joints and tricrystals in others.

To clearly predict the lifetime of a certain joint requires understanding of the failure mechanism. This study afforded a look inside the joint while imposing thermal cycles *in situ*. Most of the earlier studies used destructive analysis to see the microstructure development after things happened. But the APS synchrotron let the group see the microstructure evolution during the event.

The x-ray diffraction measurements also provide a more dynamic picture of what happens inside the solder joint as it passes through different phases over time. For example, although there are only a few different tin crystal orientations in a given SAC lead-free solder joint, different orientations are always observed after melting and resolidification. Recrystallization behavior under thermal cycling also results in evolution of the tin crystal orientation.

The researchers were intrigued by the overall tin material response to the external factors. Tin has been considered a "dead" material with a certain crystal structure. But upon closer examination, it seems to react like a living thing.

The APS data revealed a comprehensive picture of the very beginning of the thermal fatigue process (studied on beamline 6-ID-D) and connected it with what happens toward the end (beamline 34-ID-E).

Observing how the x-ray diffraction peaks changed from initial solidification and proceeded to spread out over repeated thermal cycles helped the team arrive at the point where they could describe the sequential mechanism from the moment of solidification up to the first crack that forms. They were then able to explain everything that happened and why it happened.

These fresh insights into the failure mechanism of lead-free solder joints guide scientists in their development of models for making reliability predictions. Although it is too early to proclaim any definite remedy for improving reliability in lead-free solder joints, the work provides some important clues.

Finding the right mitigation requires determination of the right failure mechanism. Based on the study so far, the team identified that the grain refinement in tin interconnects reduce thermal cycling performance. But at the same time it is beneficial for resistance to mechanical shock. So there are no golden rules, but they are at least beginning to understand why.

As next steps, finding a reliable automated way to index diffraction patterns from multi-crystal joints would greatly speed up the ability to mine the data more effectively. Analysis strate-

gies to obtain stress and strain would naturally follow using established methods. Continuing *in situ* measurements in thermomechanical cycling specimens, and looking toward comparing the microstructure before and after shock conditions (or possibly *in situ*), could also be effective. Microbeam diffraction in solder bumps is also a desirable thing to do, as the volumes are small, and this method is well suited for exploring tiny places.

— Mark Wolverton

See: Bite Zhou¹, Thomas R. Bieler^{1*}, Guilin Wu², Stefan Zaeferrer², Tae-Kyu Lee³, and Kuo-Chuan Liu³, "*In Situ* Synchrotron Characterization of Melting, Dissolution, and Resolidification in Lead-Free Solders," J. Electron. Mater. **41**(2), 262 (2012). DOI: 10.1007/s11664-011-1785-8
Author affiliations: ¹Michigan State University; ²Max-Planck-Institut für Eisenforschung GmbH; ³Cisco Systems, Inc.

And: Thomas R. Bieler^{1*}, Bite Zhou¹, Lauren Blair¹, Amir Zamiri¹, Payam Darbandi¹, Farhang Pournoghraht¹, Tae-Kyu Lee², and Kuo-Chuan Liu², "The Role of Elastic and Plastic Anisotropy of Sn in Recrystallization and Damage Evolution During Thermal Cycling in SAC305 Solder Joints," J. Electron. Mater. **41**(2), 283 (2012). DOI: 10.1007/s11664-011-1811-x
Author affiliations: ¹Michigan State University; ²Cisco Systems, Inc.
Correspondence: *bieler@egr.msu.edu

This research was supported by National Science Foundation-Grant Opportunities for Academic Liaison with Industry Contract 1006656; and Cisco Systems, Inc., San Jose, CA. Use of the Advanced Photon Source at Argonne National Laboratory was supported by the U.S. Department of Energy Office of Science under Contract No. DE-AC02-06CH11357.

6-ID-D • XSD • Physics, materials science • Magnetic x-ray scattering, high-energy x-ray diffraction, powder diffraction, pair distribution function • 27-52 keV, 50-100 keV, 67-130 keV • On-site • Accepting general users •

34-ID-E • XSD • Materials science, physics • Microdiffraction, Laue crystallography, microbeam • 7-30 keV • On site • Accepting general users •

BUILDING BETTER BATTERIES BY OBSERVING NANOCRYSTAL FORMATION

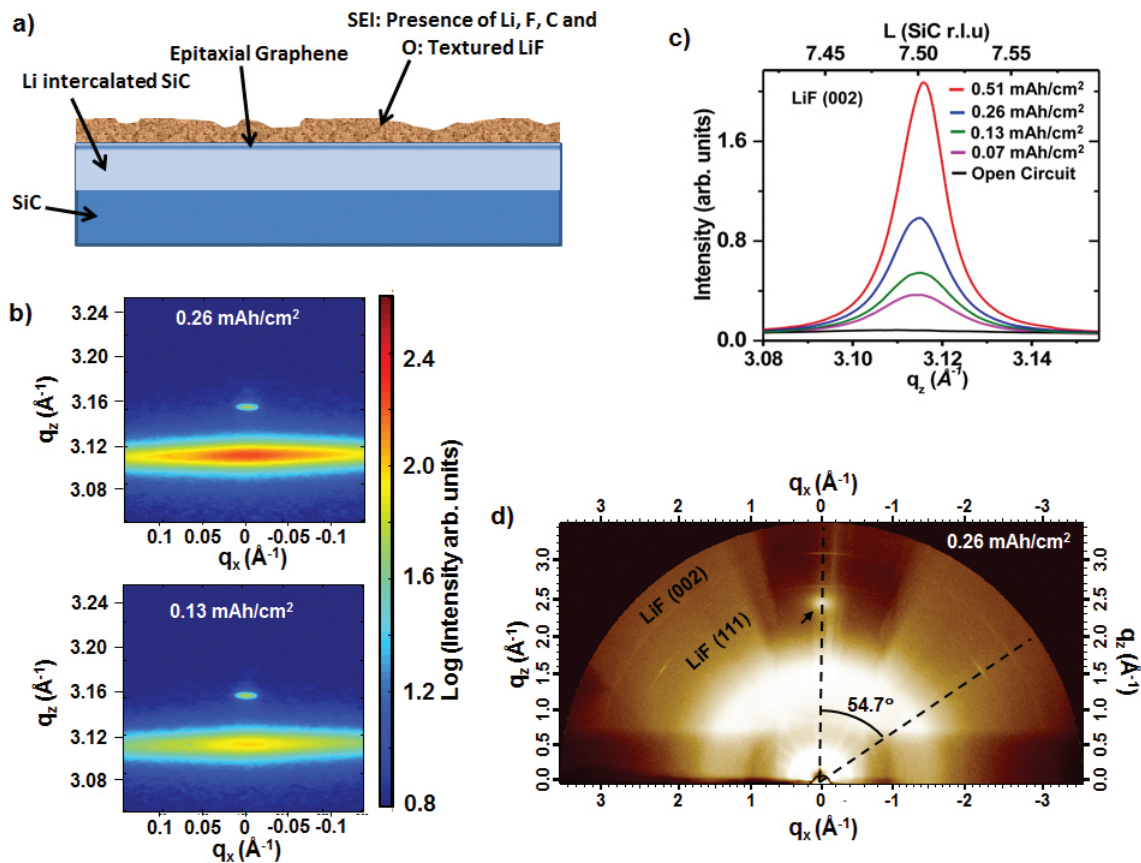


Fig. 1. Wide-angle x-ray scattering shows that lithiation of a graphitized SiC(0001) anode causes the formation and growth of textured LiF crystallites inside the solid electrolyte interphase (SEI). a) Schematic layered diagram of the lithiated EG/SiC system indicating the solid electrolyte interphase (SEI) on top of the epitaxial graphene layer on top of a Li intercalated region of SiC. b) Charge-coupled device (CCD) image of the x-ray diffraction pattern around the LiF (002) peak (incidence angle of 10.6°) at different states of lithiation. The central spot (at $q_z=3.16$ Å⁻¹) in the image is scattering from the EG/SiC surface rod; while the feature at $q_z=3.11$ Å⁻¹ is the LiF (002) Bragg reflection. c) The LiF (002) Bragg peak at different lithiation states showing that LiF crystallites are growing in both crystal size (peak narrowing) and quantity (increased peak intensity) with increasing lithiation. d) *In situ* diffraction pattern of 0.26 mAh/cm² lithiated EG/SiC, taken using a large area CCD (MAR CCD) at an incidence angle of 5°, showing rings from the LiF (111) and LiF (002) Bragg peaks. The arrow indicates diffuse scattering from the SiC (0006) Bragg peak.

Lithium-ion (Li-ion) batteries are powering devices ranging from cell phones to the electric vehicles now arriving in the market. All these devices depend on lithium-ion chemistry, but some aspects of these batteries are still mysterious. For example, when the battery discharges, some of the electrolyte decomposes, forming a so-called solid electrolyte interphase (SEI) on Li-ion electrodes. What, exactly, is in this SEI, how does it effect the performance of the battery, and (in the long run) can this understanding be used to improve battery properties? Right now, we know that SEI is undesirable because it reduces the capacity of the battery and may shorten its lifetime. On the other hand, it can prevent damage from uncontrolled reactions, such as highly publicized fires that result from overheated batteries. Researchers carrying out studies at an APS beamline observed the anode end of a lithium ion battery to study the evolution of texture and crystals in the SEI. They uncovered some heretofore unknown information about the way nanocrystals form, knowledge that could help in the design of better Li-ion batteries.

Commercial Li-ion battery anodes are made of graphite. Previous research suggests that SEI growth is different for different crystal planes. For the purposes of this study, the researchers used graphene to provide a well-defined graphitic-like surface. The researchers from Northwestern University and Argonne National Laboratory grew a sample of SEI more than 100-nm thick. Utilizing 17-keV photons from the DuPont-Northwestern-Dow Collaborative Access Team (DND-CAT) 5-ID-C beamline at the U.S. Department of Energy Office of Science's Advanced Photon Source at Argonne, they performed *in situ* x-ray scattering experiments.

By employing *in situ* x-ray reflectivity, the researchers can "see" the different interfaces with resolution of individual atoms. This method has been used before in Li-ion battery research, but never for studying the SEI.

They found that the crystals growing in the SEI were made of lithium fluoride, and that most grow in a very specific orientation parallel to the graphene crystal structure. Crystal orientation is important because it can modify the rate of lithium-diffusion to the electrode surface – and this could change the rate at which the battery provides charge.

Additional x-ray experiments revealed more about the SEI. Using x-ray photoelectron spectroscopy (XPS) to study the SEI atomic composition they found organic compounds as well as LiF, but only LiF-formed crystals, while the rest of the SEI components were amorphous. If other crystals had formed, they would have provided diffraction peaks.

The number of LiF crystals and their size depended on the amount of lithium available. Crystals grew with increasing lithiation, and got as large as about 50 nm on average.

Ex situ high-resolution transmission electron microscopy revealed another surprise. These images showed that the LiF nanometer-sized crystallites were located about 3 nm away from the graphene surface, and mostly oriented parallel to it, but did not actually grow epitaxially on the graphene.

Taken together, this new information will result in more accurate modeling and engineering of the SEI growing on graphitic surfaces, which should allow Li-ion battery designers to create devices that can safely provide more power with longer lifetimes.

— Yvonne Carts-Powell

See: Sudeshna Chattopadhyay¹, Albert L. Lipson¹, Hunter J. Karmel¹ Jonathan

D. Emery¹, Timothy T. Fister², Paul A. Fenter², Mark C. Hersam^{1*}, and Michael J. Bedzyk^{1**}, "In Situ X-ray Study of the Solid Electrolyte Interphase (SEI) Formation on Graphene as a Model Li-ion Battery Anode," *Chem. Mater.* **24**(15), 3038 (2012). DOI:10.1021/cm301584r
Author affiliations: ¹Northwestern University, ²Argonne National Laboratory

Correspondence: **bedzyk@northwestern.edu, *m-hersam@northwestern.edu

This research was supported by the Center for Electrical Energy Storage, an Energy Frontier Research Center funded by the U.S. Department of Energy (DOE) Office of Science Basic Energy Sciences Program (Award Number DE-AC02-06CH11357). DND-CAT is supported by E.I. DuPont de Nemours & Co., The Dow Chemical Company, and Northwestern University. Use of the Advanced Photon Source at Argonne National Laboratory was supported by the U.S. DOE Office of Science under Contract No. DE-AC02-06CH11357.06CH11357.

5-ID-B,C,D • DND-CAT • Materials science, polymer science • Powder diffraction, x-ray standing waves, x-ray optics development/techniques, small-angle x-ray scattering, surface diffraction, x-ray reflectivity, wide-angle x-ray scattering • 5-20 keV • On-site • Accepting general users

THE RETURN OF ORDER: WATCHING ANNEALING AS IT HAPPENS

Annealing, the process of subjecting a metal (or other solid substance) to strictly controlled temperature conditions in order to change its crystalline structure and thus improve its material properties, is nothing new. It is a procedure that is utilized every day in the production of everything from steel girders to silicon microchips. But while the mathematical theory and physical stages of the annealing process have been well-understood and thoroughly analyzed for many years, our ability to actually observe — and therefore understand — the phenomenon directly *in situ* on the microscale has been limited. Among other factors, the high temperatures and special atmospheres used in annealing rule out many characterization techniques. But researchers have finally managed to transcend those limitations, thanks to the high-energy x-rays and x-ray beamlines at the APS, characterizing the evolution of defected crystalline microstructure under annealing via the near-field high-energy x-ray diffraction microscopy (nf-HEDM) technique.

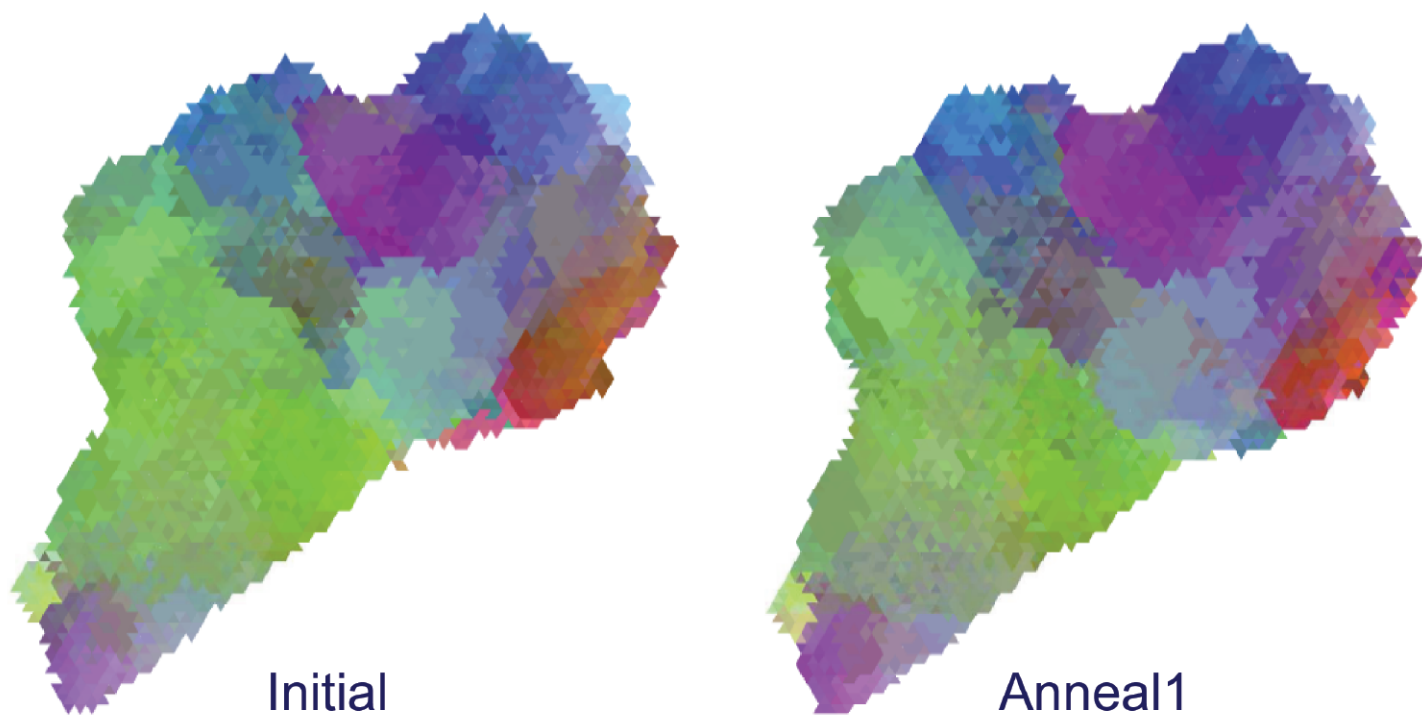


Fig. 1. The same grain (a single cross-section) in three different annealing states (this page and next). Colors correspond to deviations of the crystal lattice orientation from the average orientation of this grain (the three parameters that specify the misorientation are mapped to RGB colors). Subtle changes in the arrangement and distribution of misorientations indicate annealing of lattice defects and motions of low angle grain boundaries. All orientations displayed here are within two degrees of each other.

1-ID-B,C,E • XSD • Materials science, physics, chemistry • High-energy x-ray diffraction, radiography, small-angle x-ray scattering, fluorescence spectroscopy, pair distribution function • 50-90 keV, 50-150 keV • On-site • Accepting general users •

X-rays are non-destructive and allow for repeated observations of the same sample volume. While synchrotron x-ray techniques have been employed to study ordering responses to annealing, they have either reported statistical quantities or have observed isolated events without resolving surrounding structure. Through repeated measurements after successive annealing cycles, the nf-HEDM measurements are able to watch an entire volume of material evolve.

Working at the XSD 1-ID beamline at the APS, the experimenters from Carnegie Mellon University and Argonne accomplished detailed crystallographic mapping in a sample of high-purity aluminum, observing both the recovery and recrystallization phases of annealing (Fig. 1). The former showed the recovery of order among existing grains, and the latter displayed new crystal orientations emerging from disordered regions.

The investigators used a cylindrical Al wire that had been formed by drawing, to ensure that a high level of deformed structure would be present within the sample. After an initial nf-HEDM examination, the sample was further studied during annealing treatments at ~50 and ~70 °C. The x-ray diffraction data was reconstructed using the forward modeling method, through which detailed orientation maps can be created showing the complex intragranular structure of each scanned layer.

In this study, existing grain boundaries as displayed by the forward modeling reconstructions show only very subtle motion during the recovery stage of annealing, indicating little growth or reorganization. As annealing proceeds, highly disordered regions become more ordered, as shown by stronger and sharper Bragg peaks that allow more accurate orientation data. Orientation appears more uniform in the voxel-by-voxel reconstruction afforded by forward modeling, so that the rearrangement of particular areas into greater order can be followed from the initial state throughout the ~50 and ~70 °C annealing treatments.

The recrystallization stage is marked by more dramatic and obvious changes in the microstructure of the

sample, as new grains form, grow, and fill in originally disordered regions. The experimenters were able to identify the formation of new grains by comparing reconstruction images among the different sample states. A large amount of nucleation was seen in the sample, especially near the surface.

The researchers devoted particular attention to one internal grain, observing how it nucleated from a previously highly disorganized region to finally replace most of the disordered area. The approximately 5- μm spatial resolution permitted by the forward modeling reconstructions made it feasible to search for the mechanisms controlling the emergence of specific orientations, although in this case they were unable to identify the orientation origin of this new grain because of insufficient intensity peaks and resolution at that individual region.

The work provides an elegant example of the ability of the nf-HEDM technique combined with forward modeling to reveal and characterize the evolution of defected crystalline microstructure under annealing. The emergence of new ordered grains from disordered regions can be seen throughout the sample both internally and at the surface, derived from the great number of Bragg peaks collected in the data sets. Because the method demonstrated in this work is nondestructive, it allows the examination of regions before, during, and after the various stages of the annealing process, and observations could be extended to microstructural evolution throughout the application of other external environmental forces.

The research team notes that substantial improvements in the APS beamline facilities that will result from the APS Upgrade promise new observations of even greater refinement and resolution, not only during recovery and recrystallization but also the grain growth stage of annealing.

— Mark Wolverton

See: Christopher M. Hefferan¹, Jonathan Lind¹, Shiu Fai Li¹, Ulrich Lienert², Anthony D. Rollett¹, Robert M. Suter^{1*}, “Observation of recovery and recrystallization in high-purity aluminum measured with forward modeling analysis of high-energy diffraction microscopy,” *Acta Mater.* **60**, 4311 (2012).

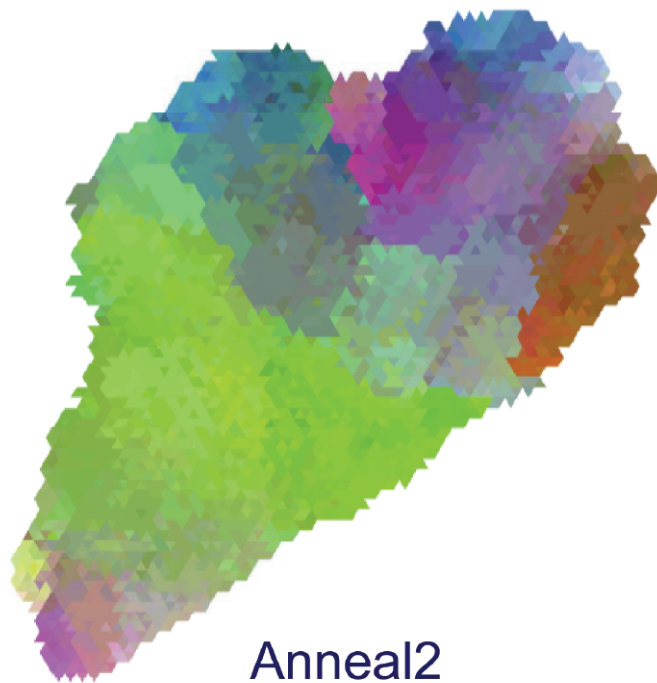
DOI:10.1016/j.actamat.2012.04.020

Author affiliations: ¹Carnegie Mellon University, ²Argonne National Laboratory

Correspondence:

*suter@andrew.cmu.edu

This work was supported primarily by the Metals and Nanostructures and the Materials Research Science and Engineering Center programs of the National Science Foundation under Award Numbers DMR-1105173 and DMR-0520425, respectively. The research was also supported in part by the National Science Foundation through TeraGrid resources pro-



vided by the Texas Advanced Computing Center under Grant No. DMR080072. Use of the Advanced Photon Source at Argonne National Laboratory was supported by the U.S. Department of Energy Office of Science under Contract No. DE-AC02-06CH11357.

ENGINEERING THIN-FILM OXIDE INTERFACES

Research at the APS provides new insights about a material that might form the basis for an alternative to conventional silicon-based semiconductor technology. The study utilized high-energy x-rays from the APS to observe intriguing electrical conductivity at the interface between two oxide insulators and helped resolve the heretofore mysterious origin of conductivity in epitaxially-grown lanthanum aluminate (LaAlO_3) and strontium titanate (SrTiO_3) thin films. The unexpected presence of a two-dimensional (2-D) electron gas (2DEG) at the interface between two insulators for epitaxial thin films of LaAlO_3 (LAO) grown on SrTiO_3 (STO) substrates was first reported some eight years ago. Both LAO and STO belong to the perovskite class of minerals, which exhibit a multitude of dielectric and physical properties of interest to materials science, including superconductivity, magnetoresistance, ionic conductivity, and applications in microelectronics and telecommunications.

The discovery of electrical conductivity at the LAO/STO interface stimulated intense research that revealed other fascinating properties, including magnetism and superconductivity. In a broader context, the discovery has created great excitement and opened up the possibility of oxide electronics becoming an alternative to conventional semiconductor technology based on silicon.

The unusual behavior of the LAO/STO interface was first reported for thin films grown by pulsed laser deposition (PLD), which utilizes intense laser pulses to create a plume of plasma by ablating a solid LAO target. The species in the PLD plume (such as atomic and molecular ions) travel from the target to the STO substrate where they arrange into an epitaxial LAO layer. Epitaxial growth compels the crystalline structure of the deposited film to match the crystalline structure of the substrate. In addition to the structure imposed by the STO lattice, the ordering perfection of the deposited LAO film depends upon the interaction between the growing film and the plasma plume; in turn, plume dynamics are affected by the oxygen pressure in the vacuum chamber.

In the research discussed here, investigators from the Oak Ridge and Argonne national laboratories systematically explored the effects of high and low oxygen pressures on the physical properties of thin-film LAO/STO systems produced using PLD.

Both real-time and post-experimental methods were used to construct

Cont'd next page

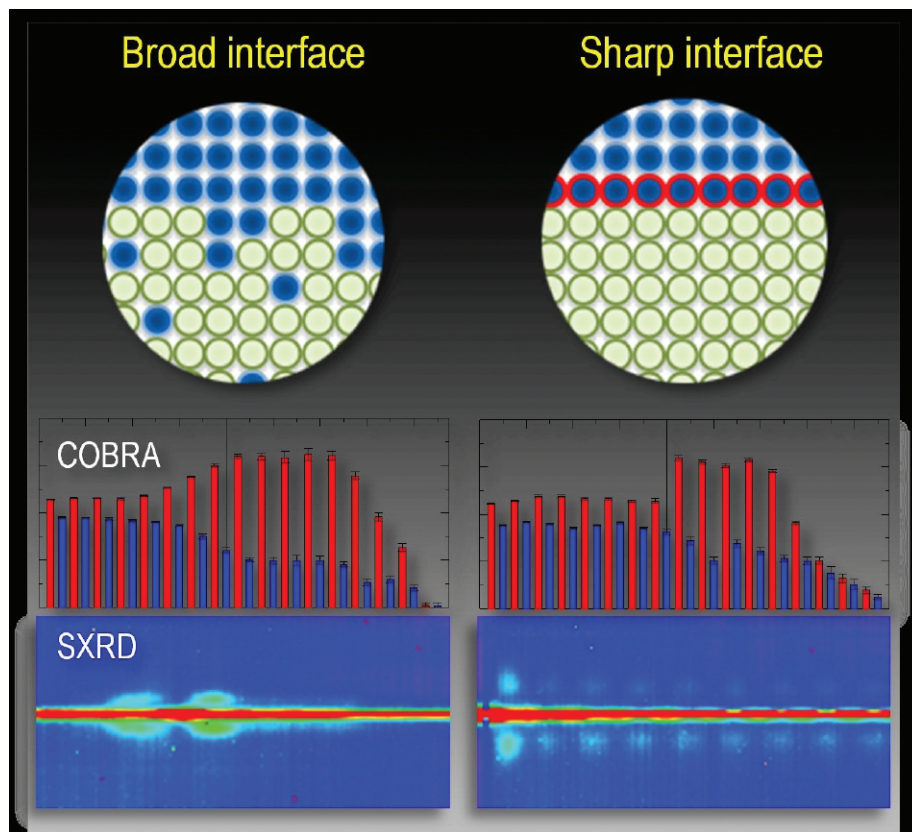


Fig. 1. LAO thin films on STO substrates are depicted in the top schematics (LAO indicated by blue spheres, STO by green spheres). The top left-hand panel demonstrates a chemically broad interface resulting from conventional growth in a low pressure oxygen environment. In contrast, the top right-hand panel shows a chemically abrupt interface produced by inserting a monolayer-thick buffer (blue spheres circled red) grown in high pressure with the rest of the thin-film structure grown at low pressure. The middle two panels indicate electron densities obtained by COBRA associated with the SrO and LaO layers (red bars), and the TiO and AlO_2 layers (blue bars): while the electron densities corresponding to a sharp interface (right panel) abruptly change at the boundary, the left middle panel indicates chemical mixing (the LAO/STO boundary is marked by a vertical line). The bottom two panels represent the results from real-time surface x-ray diffraction (SXR) during the growth of LAO films. The regularly spaced intensity oscillations of the diffuse scattering peaks in the right panel indicate a 2-D layer-by-layer growth, whereas in the left panel no pronounced 2-D growth and a delayed appearance of the first oscillation peak are observed when grown in low pressure due to chemical broadening of the interface.

a profile of thin-film properties resulting from different oxygen pressure conditions. The highly sensitive diffraction techniques enabled by the extreme brightness of the APS synchrotron x-rays allowed the study of the structure and composition of the LAO/STO near-interface region with unprecedented detail.

Two different APS beamlines were involved in these measurements. The formation and evolution of the LAO epitaxial layers were visualized in real time at XSD beamline 33-ID using time resolved surface x-ray diffraction. After the growth, the chemical composition of the interface region was examined using coherent Bragg rod analysis (COBRA) from one-dimensional electron density profile measurements performed at XSD beamline 12-ID-D.

These two x-ray diffraction techniques combined with other data reveal the surprising result that even a single unit-cell-thick layer of LAO (approximately 0.4 nm) grown at high oxygen background pressure effectively promotes the formation of atomically sharp interfaces.

In a series of experiments, LAO films deposited on STO substrates were produced under oxygen pressures of 10^{-6} Torr or 10^{-2} Torr. The experimental measurements demonstrated that LAO/STO thin films grown at the lower pressure of 10^{-6} Torr exhibit substantial mixing of elements across the LAO/STO interface. The top left panel of the accompanying figure illustrates the intermixing of elements and the appearance of a chemically broad interface.

In contrast, thin films grown at the considerably higher oxygen pressure of 10^{-2} Torr were largely free of intermixing between LAO and STO. However, epitaxial growth at high oxygen pressure builds up strain in the film causing it to crack and delaminate (i.e., layer separation) from the STO substrate. The researchers demonstrated that forming a “shielding layer” of LAO grown at high oxygen pressure (10^{-2} Torr), followed by continued growth at the lower pressure of 10^{-6} Torr, results in a highly ordered inter-

face while avoiding delamination, as indicated in the figure's top right panel. Even a single unit-cell-thick layer of LAO (about 0.4 nm) grown at high oxygen pressure effectively promotes the formation of atomically sharp interfaces.

The ability to suppress interface broadening is an extremely noteworthy achievement because it is known that interface broadening adversely affects the manifestation of intrinsic interface behavior, including electrical conductivity. The fact that the oxygen background pressure alters the properties of epitaxial oxide films grown by PLD is not surprising since collisions of oxygen molecules with the plume species are known to be the main mechanism that mediates the incident kinetic energy (speed) of the growth species. In turn, the average kinetic energy of the growth species directly affects the rate and quality of epitaxial growth of the deposited LAO layer.

The researchers were surprised to learn that even a one-atomic-layer-thick buffer could drastically improve the quality of the interface. This unexpected observation opens a door to new strategies for custom tailoring oxide heterostructures needed for discovering novel functionalities originating from the atomically well-defined oxide interface.

Identifying and separating the growth related phenomena to enable the study of the intrinsic interface properties in their pure form represents the main challenge of film growth kinetics studies. The sophisticated surface x-ray diffraction methods available at the APS were instrumental for determining the origin of the LAO/STO interface behavior.

This research unequivocally demonstrates that even a single unit-cell-thick shielding layer effectively prevents both elemental intermixing and strain relaxation at the interface. The oxygen pressure used in fabricating the thin films is a controlling factor that determines the blocking ability of such single unit-cell-thick LAO layers. In particular, the pressure of oxygen at the beginning of epitaxial growth is critical:

while low initial oxygen pressure leads to intermixing of LAO and STO materials and subsequent strain relaxation, employing higher oxygen pressure at the beginning of LAO growth results in a highly ordered shielding layer.

By precisely controlling conditions at the LAO/STO boundary, the system's physical properties can be fine-tuned. Most importantly, the researchers note that these findings are not limited to fine-tuning only LAO/STO thin-films, but are applicable generally to a host of other epitaxially-grown oxide heterostructures.

— Philip Koth

See: Woo Seok Choi¹, Christopher M. Rouleau¹, Sung Seok A. Seo^{1,2}, Zhenlin Luo^{3,4}, Hua Zhou³, Tim T. Fister³, Jeffrey A. Eastman³, Paul H. Fuoss³, Dillon D. Fong³, Jonathan Z. Tischler³, Gyula Eres¹, Matthew F. Chisholm¹, and Ho Nyung Lee^{1*}, “Atomic Layer Engineering of Perovskite Oxides for Chemically Sharper Heterointerfaces,” *Adv. Mater.* **24**, 6423 (2012).

DOI:10.1002/adma.201202691.

Author affiliations: ¹Oak Ridge National Laboratory, ²University of Kentucky, ³Argonne National Laboratory, ⁴University of Science and Technology of China

Correspondence: *hnlee@ornl.gov

This work was supported by the U.S. Department of Energy (DOE) Materials Sciences and Engineering Division. Use of the Advanced Photon Source at Argonne National Laboratory was supported by the U.S. DOE Office of Science under Contract No. DE-AC02-06CH11357.

12-ID-C,D • XSD • Chemistry, physics, materials science • Small-angle x-ray scattering, grazing incidence small-angle scattering, wide-angle x-ray scattering, surface diffraction • 4.5-36 keV • On-site • Accepting general users •

33-ID-D,E • XSD • Materials science, physics, chemistry • Anomalous and resonant scattering (hard x-ray), diffuse x-ray scattering, general diffraction, surface diffraction, x-ray reflectivity, x-ray standing waves • 4-40 keV, 6-21 keV • On-site • Accepting general users •

TESTING ASSUMPTIONS ABOUT LINE PROFILE ANALYSIS

Sometimes assumptions must suffice because the available tools are not quite able to produce final answers. That has been the case when using x-ray diffraction (XRD) to probe deformed metal microstructures. Because the unpredictable irregularities of the deformities tend to broaden XRD profiles and make them “fuzzy,” it is notoriously difficult to put together a truly accurate x-ray line profile of such microstructures. Crystallographers had to interpret their data using modeling techniques based on assumptions about the behavior of dislocations that, while still quite useful, only yielded a partial and somewhat approximate picture of a material's true microstructural qualities. But new developments in synchrotron x-ray techniques have made it possible to sharpen our view and refine some long-held models. Researchers employed some of the newest capabilities of the APS to test the fundamental assumptions upon which the most common model is based, helping to verify some important aspects of XRD line profile interpretation.

The microstructure of deforming metals breaks down into irregular dislocation cells with fuzzy walls that move and change configuration under stress. The differences in stress between these dislocation cell walls and their interiors lead to differences in the XRD line profiles, which are broadened into distinctive asymmetric shapes. These diffraction line profiles are then analyzed. The Mughrabi model, first defined in 1983 and refined somewhat since then, is the typical tool used to interpret the line profiles and piece together the microstructure by considering the macroscopic asymmetric line profile of a sample to be the sum of the subprofiles of the dislocation cell walls and interiors.

The problem is that a single measured asymmetric line profile could consist of an infinite number of possible sub-profiles. How to know which sub-profiles were the correct ones? To answer that question, scientists typically make three basic assumptions: the subprofiles of the cell walls and cell interiors are approximately symmetric; the areas under the subprofiles are proportional to the cell wall and interior

volumes visible under transmission electron microscopy; and the shapes of the subprofiles can be extracted from the asymmetric line profile.

Working at the XSD 33-BM-C and 34-ID-E beamlines of the APS, investigators from the National Institute of Standards and Technology, the University of Southern California, Oak Ridge National Laboratory, and Argonne conducted conventional large-sample volume diffraction line profile measurements on both a nearly perfect, unstressed Cu single crystal and a heavily deformed (under compression) sample. They followed this with spatially resolved energy-wire scans of eight separate locations in the deformed sample to obtain detailed line profiles from numerous dislocation cell walls and interiors.

With the benefit of this data, the team was able to test each of the above assumptions. While previous work had demonstrated that the stresses within the dislocation cell walls were quite different from stresses in cell interiors, the wall and interior subprofiles still showed very high symmetry. The second assumption was also

found to be valid, as the researchers found that the general volume fraction of 55% to 45% respectively for cell walls and interiors, as seen on transmission electron microscopy (TEM) imaging micrographs, was within about 10% of the volumes measured from the line subprofiles.

Confirming the third proposition for the classical analysis, however, was considerably more problematic. The experimenters tried a number of different techniques in order to extract accurate cell wall and cell interior subprofiles from an asymmetric line profile. But because different constraints produce wildly differing solutions, and an infinite number of other subprofiles could be added to produce the measured profile, it was not possible to settle on a particular method. Although the experimenters found that the closest matches required that the volume fractions obtained from TEM micrographs be included, it was still necessary to greatly overestimate the long-range dislocation stresses to make the subprofiles fit the measured line profile.

The research team also investigated the assumption that the

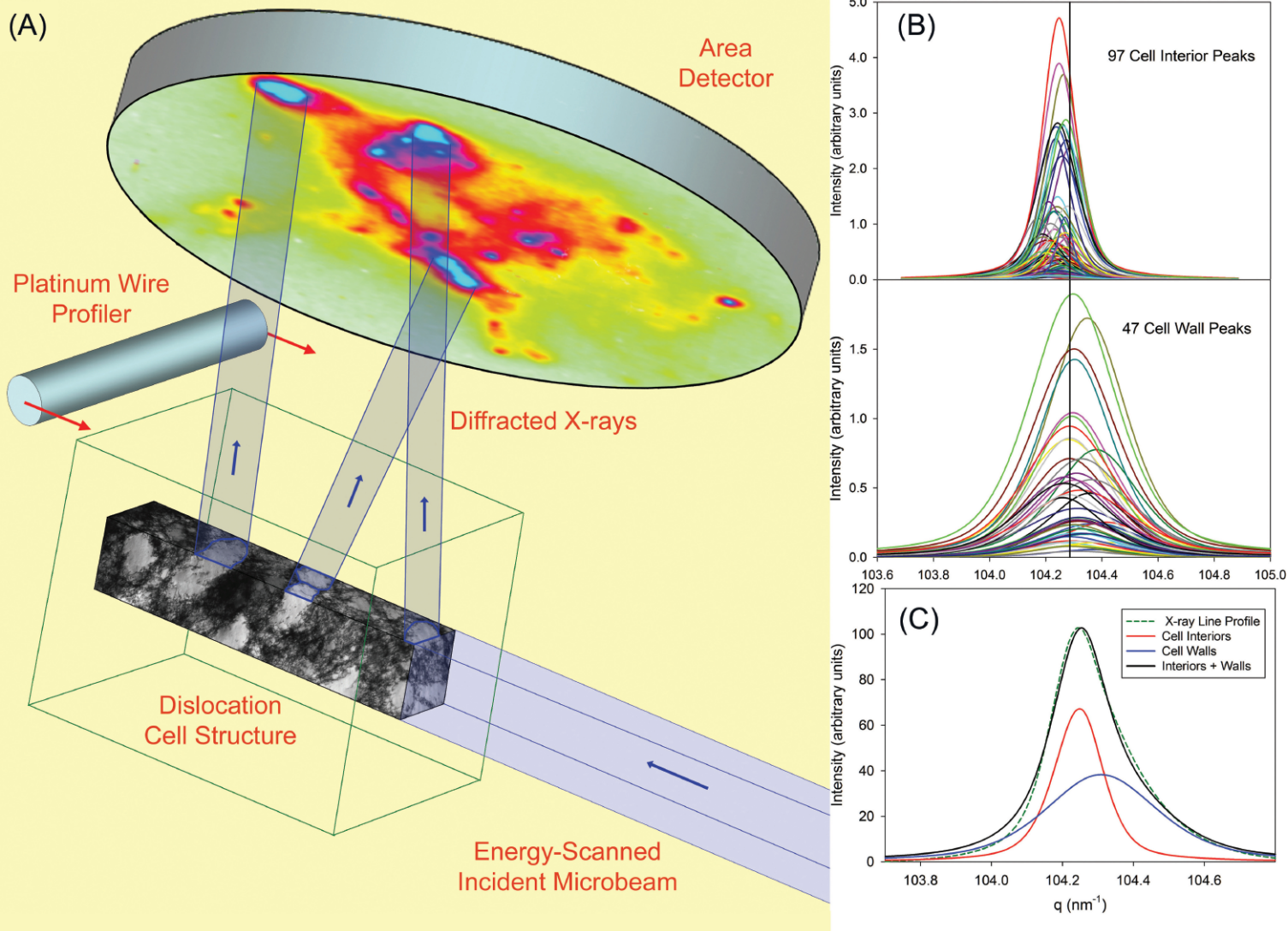


Fig. 1. (A) the microbeam instrument; (b) the measured line profiles from individual dislocation cell interiors (top) and dislocation cell walls (bottom); (C) the summed measurements from (B) (red and blue curves), their sum (black), and a classical measurement of the diffraction line profile (dashed green).

observed widening of subprofiles is due mostly to dislocation broadening instead of other factors such as local cell wall and/or interior strains. They concluded that this was essentially correct, and that local stress variations are generally a minor factor in the cell wall and interior subprofile broadening.

While the investigators note that the present work examined only one particular experimental circumstance (the axial 006 reflection from a pure single Cu crystal compressed by 30% along the [001] axis), and that differences in the sample composition, orientation, and applied strain could show quite different microstructures and thus subprofiles, this study helps to verify some important aspects of XRD line profile interpretation. Further testing of other analysis methods and sample configurations will continue to refine

and improve our tools for the interpretation of x-ray diffraction data on microstructures. — *Mark Wolverton*

See: Lyle E. Levine^{1*}, Peter Geantil², Bennett C. Larson³, Jonathan Z. Tischler^{3†}, Michael E. Kassner², and Wenjun Liu⁴, “Validating classical line profile analyses using microbeam diffraction from individual dislocation cell walls and cell interiors,” *J. Appl. Cryst.* **45**, 157 (2012).

DOI:10.1107/S0021889812001616

Author affiliations: ¹National Institute of Standards and Technology, ²University of Southern California, ³Oak Ridge National Laboratory, ⁴Argonne National Laboratory. [†]Present address: Argonne National Laboratory

Correspondence: *lyle.levine@nist.gov
M.E.K. acknowledges support from the National Science Foundation through grant No. DMR-901838. Use of the Advanced Photon Source at Argonne National Laboratory was supported by the U.S. Department of Energy Office of Science under Contract No. DE-AC02-06CH11357.

33-BM-C • XSD • Materials science, physics, chemistry • Diffuse x-ray scattering, general diffraction, powder diffraction, x-ray reflectivity, grazing incidence diffraction, anomalous and resonant scattering (hard x-ray) • 5-35 keV • On-site • Accepting general users •

34-ID-E • XSD • Materials science, physics • Microdiffraction, Laue crystallography, microbeam • 7-30 keV • On site • Accepting general users •

BAKING A BETTER BATTERY

Rechargeable lithium-ion batteries are essential to the electronics we use every day, from mobile phones and digital cameras to increasingly common electric vehicles. But their portable power supplies can run out of charge at the most inopportune moment, and access to an electric outlet is not always available. Additionally, such rechargeable batteries have only a limited recharge lifespan. Their intrinsic chemistry and structure will, after 18 months (or at best a couple of years) of daily use fail to recharge to full capacity. Battery health gradually worsens over the subsequent months until much more frequent access to a power outlet is needed, defeating the object of having a portable device. But new scientific insights into the nature of the phase changes that take place near the surface of battery anodes might allow development of the next generation of batteries that would not only hold more charge for longer periods, but would maintain overall battery health for a several years, even in everyday use. Researchers working at XSD beamline 33-BM-C at the APS have made real-time observations of the lithiation, or impregnation by lithium ions, of a thin film of metal silicide. Their results could pave the way to better rechargeable lithium-ion batteries.

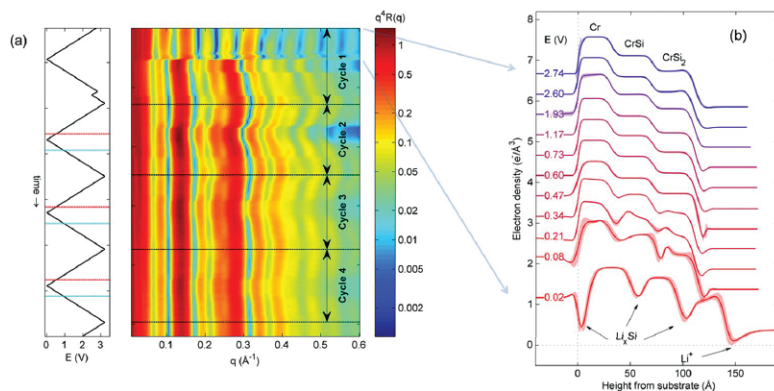


Fig. 1. (a) X-ray reflectivity was measured for four charge cycles using cyclic voltammetry. (b) The most dramatic changes occurred during the first lithiation, where the metal silicide phase separated into nanometer-thick, lithium-rich layers.

The researchers from Argonne and the University of Illinois at Urbana-Champaign utilized x-ray reflectivity with a 20-keV photon energy on a four-circle diffractometer at the 33-BM-C beamline to map the structural changes of a lithium silicide thin film standing in for a lithium-ion battery electrode. The researchers point out that the next generation of rechargeable batteries could most likely use silicon, tin, or other intermetallic compounds rather than traditional carbon-based electrodes for the battery anode, hence the rationale for studying such thin films. The alloying of these materials with lithium has the potential to

make rechargeable batteries able to hold a much greater electric charge.

The greater charge capacity of such a development comes at a price as silicides can expand up to 400% during lithiation. These large volume changes can stress the internal structure of the electrode, leading to delamination from the battery over repeated charge cycling. Researchers have adopted various strategies to reduce the impact of this volume change such as using compacted particles in the anode, ball milling and nanofabrication with some degree of success.

One aspect of the experimental work that remains unclear is precisely

how a non-crystalline material rearranges itself to accommodate so much lithium during its first discharge and during subsequent cycling. By employing the x-ray reflectivity technique, the team probed the lithiation and de-lithiation processes in a model anode material made from chromium silicide. The x-ray data revealed an accumulation of lithium near the surface of the electrode that grows as the film reaches a potential where the silicon will alloy with lithium. At that point, the film abruptly expands and phase-separates into what might be referred to as a “layer cake” of distinct lithium-rich and chromium-rich layers. Over repeated cycles, the researchers found that this layered structure was able to persist and showed more reversible expansion and contraction during lithiation and de-lithiation.

This could be a critical design consideration in making more efficient and longer-lasting rechargeable lithium ion batteries and keep many of our electronic gadgets powered up for much longer while on the move. The layering phenomenon could also have implications for metal silicides used in nanoelectronics and thermoelectric, the researchers suggest. — *David Bradley*

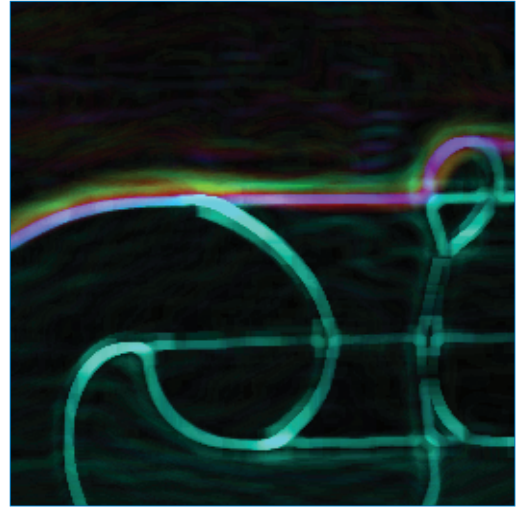
See: Tim T. Fister^{1*}, Brandon R. Long², Andrew A. Gewirth², Bing Shi¹, Lahsen Assoufid¹, Sang Soo Lee¹, and Paul Fenter¹, “Real-Time Observations of Interfacial Lithiation in a Metal Silicide Thin Film,” *J. Phys. Chem. C* **116**, 22341 (2012). DOI/10.1021/jp305465j

Author affiliations: ¹Argonne National Laboratory, ²University of Illinois at Urbana-Champaign

Correspondence: *fister@anl.gov

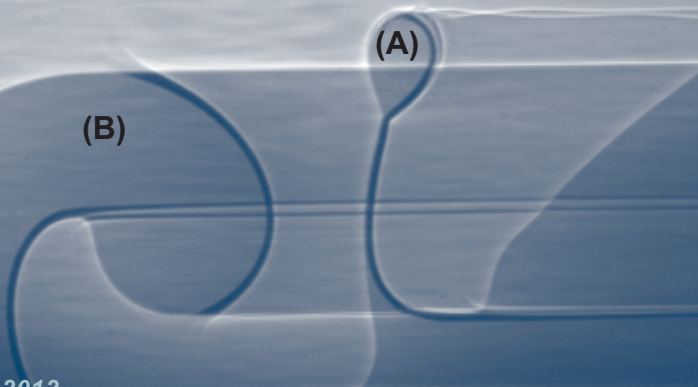
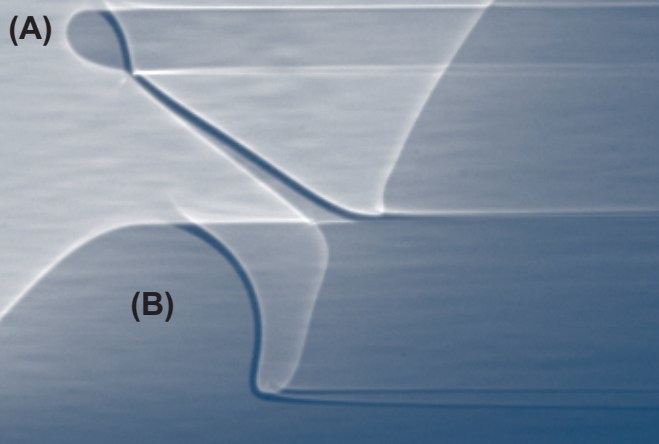
This research was supported as a part of the Center for Electrical Energy Storage: Tailored Interfaces, an Energy Frontier Research Center funded by the U.S. Department of Energy (DOE) Office of Science under Award DE-AC02-06CH11. Use of the Advanced Photon Source at Argonne National Laboratory was supported by the U.S. DOE Office of Science under Contract No. DE-AC02-06CH11357.

33-BM-C • XSD • Materials science, physics, chemistry • Diffuse x-ray scattering, general diffraction, powder diffraction, x-ray reflectivity, grazing incidence diffraction, anomalous and resonant scattering (hard x-ray) • 5-35 keV • On-site • Accepting general users •



SOFT MATERIALS & LIQUIDS

HOW TO MAKE A SPLASH



A team of physicists employed optical and phase-contrast x-ray imaging at the XSD 32-ID-B,C beamline at the APS to capture images of the impact of a drop of silicone oil falling into a deep pool of the same liquid. Their work penetrated the everyday mystery of a splash, revealing previously hidden structures and dynamics.

< Fig.1. X-ray images of a splash formed by the impact of a drop on a deep pool of the same liquid, illustrating the formation of two jets. The round structure visible in the upper panel (A) is the rim of the first jet, which sometimes breaks into droplets. The second jet (B) is a thicker lamella that folds on itself and forms a vortex. The black band at the bottom of each image is the pool in which the x-rays are completely absorbed. The images are at 270, 440, and 620 μm after impact.



Sometimes, the simplest and most common things are also the most complicated. Consider a raindrop falling into a lake or the ocean — a gentle, elemental event that has occurred innumerable times every day since liquid water has existed on Earth. Yet the precise nature of a splash remains largely unknown, even after more than a century of careful experiment and observation. It's a question of more than simply fundamental interest, because the manner in which splashes create and disperse miniscule droplets in their surroundings holds critical implications in many industrial applications and natural processes dependent upon the control of liquids. The major obstacle in understanding the physics of droplet splashing has been the difficulty of directly observing and recording the phenomenon in detail, because it happens so quickly and at an extremely small scale. In recent years, high-speed video imaging has largely resolved the problems of time and scale, but the internal structure of the droplet and splash eluded observation.

Working with x-rays from the high-speed imaging facility at the 32-ID-B,C beamline at the APS, researchers from the University of Michigan and Argonne used both optical and phase-contrast x-ray imaging to capture images of the impact of a drop of silicone oil falling into a deep pool of the same liquid. Different viscosities and drop velocities were used to examine their effects on splash behavior.

The rough outlines of the inner structure of the splash were known for some time. When a drop impacts the surface of a liquid pool, a sheet-like jet called the lamella spreads outward immediately, followed by the break-up of its leading edge into a secondary halo of droplets. But recent work, including mathematical modeling by Weiss and Yarin in 1999 showed that the splash is even more complex. The lamella is actually preceded by an ejecta sheet of even finer droplets that emerges from the "neck" area between the drop and the

pool surface, as verified experimentally by Thoroddsen in 2002.

One of the main objectives of the current experiment was to identify the role of this ejecta sheet and determine how to distinguish it from the lamella. Previous thought on the phenomenon held that a single jet (the lamella) forms. But this work reveals that there are really two distinct jets, and that they merge.

The experimenters found that the dynamic behavior of the splash is largely dependent upon the Reynolds number (involving fluid viscosity) and the Weber number (surface tension), dimensionless numbers that express ratios rather than exact units.

After observing splashes over a wide range of Reynolds and Weber numbers, the group developed a phase diagram showing four basic regimes: (1) the drop simply merges with the fluid and forms capillary waves; (2) a single jet appears; (3) the ejecta sheet forms, followed by a thicker lamella; and (4) the ejecta sheet and lamella form, but the ejecta sheet disintegrates into microdroplets. As the impact speed and properties of the liquid are varied, a switch occurs from one regime, in which they are clearly separated, to the other regime, in which they are combined. As the liquid properties change, the interval of time between when the ejecta sheet comes out and when the lamella comes out gets smaller and smaller until they are essentially comingling.

This work confirms definitively that the splash consists of two distinct jets, but that the structural dynamics are strongly dependent upon the various parameters involved, with a continuous jet at low Reynolds numbers and two distinct jets at higher Reynolds values.

The way the two jets merge came as a surprise to the team. A minor 1% change to the parameters results in a sudden change in the qualitative character of the splash.

The next experimental vista for the team involves considering how additional parameters affect the splash

behavior, such as the surrounding air pressure, which, as a group at the University of Chicago showed, affected splashing from drop impact on a dry surface. It can qualitatively change the splash, which is surprising, because the air is a thousand times less dense and its viscosity is a hundred times less than the liquid, so one would expect that these effects would be minor. But they can be significant.

The team also wants to understand how the size and number of the liquid jets are determined. They can measure empirically the number of jets and state the thickness and speed of the jets, but they do not yet have a deep understanding of that behavior.

Already, the researchers have used the x-ray phase-contrast technique to break through a long-standing barrier that obscured understanding of this common mystery.

— Mark Wolverton

See: L.V. Zhang¹, J. Toole^{1†}, K. Fezzaa², and R.D. Deegan^{1*}, "Evolution of the ejecta sheet from the impact of a drop with a deep pool," *J. Fluid Mech.* **690**, 5 (2012).

DOI:10.1017/jfm.2011.396

Author affiliations: ¹University of Michigan, ²Argonne National Laboratory. [†]Present address: MIT

Correspondence:

*rddeegan@umich.edu

R.D.D. acknowledges support from the James S. McDonnell Foundation 21st Century Science Initiative in Studying Complex Systems – Research Award. Use of the Advanced Photon Source at Argonne National Laboratory was supported by the U.S. Department of Energy Office of Science under Contract No. DE-AC02-06CH11357.

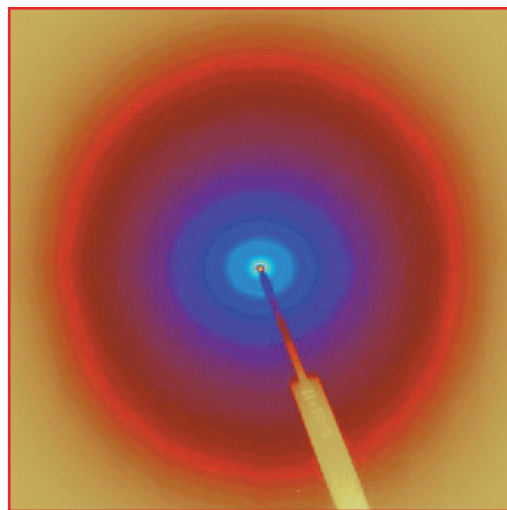
Splash photo on preceding page by Pro2, from Wikimedia Commons, http://commons.wikimedia.org/wiki/File:Splash_2_color.jpg

32-ID-B,C • XSD • Materials science, life sciences, geoscience • Phase contrast imaging, radiography, transmission x-ray microscopy, tomography • 7-40 keV • On-site • Accepting general users

THE APS AND THE 2012 ARGONNE ENERGY SHOWCASE

The APS was a popular tour stop for the 2012 Argonne Energy Showcase, that took place on Saturday, September 15. More than 12,500 members of the public came to Argonne for an informative day highlighting energy-related research. A team of 134 APS personnel guided visitors through the facility, answered a seemingly endless stream of questions about APS science and engineering, and delighted visitors (especially the kids) with 30 exhibits and demonstrations including three-dimensional tomography of new materials for lighter cars and airplanes, a nanometer-scale look into green energy materials using hard x-ray fluorescence microscopy, a "virtual linac," a miniature beamline, robotics, rapid computer-aided design prototyping of APS beamline components, and acoustic levitation. These and other photos from the APS Energy Showcase can be seen here: <http://www.flickr.com/photos/advancedphotonsource/sets/72157631569259958/>





CHEMICAL SCIENCE

SHEDDING LIGHT ON CHEMISTRY WITH A BIOLOGICAL TWIST

Many of life's processes rely on light to trigger a chemical change. Photosynthesis, vision, the movement of light-seeking or light-avoiding bacteria, for instance, all exploit photochemistry. Discovering exactly how living things absorb and convert light energy into a form that can change the molecules involved in such processes would not only help scientists understand them, but could lead to ways to mimic such processes to produce more efficient solar energy conversion, for instance. A clearer understanding of how light can drive biological processes has emerged from x-ray diffraction studies carried out on beamlines at the APS and the European Synchrotron Radiation Facility (ESRF). This work will help science shed a brighter light on some of life's most critical processes.



At the heart of these processes are photoactive protein molecules. Under the right conditions, when light shines on them, specific chemical bonds within the light-absorbing part of the protein can undergo a chemical change called isomerization. For example, photoactive yellow protein (PYP) is a light receptor in the bacterium *Halorhodospira halophila*. When PYP is activated by light it triggers a cascade of biochemical reactions that allow the bacterium to move away from the light, a process known as negative phototaxis. At the heart of PYP is a color center, or chromophore, that absorbs the required photons of light and in so doing undergoes a chemical transformation — a *trans* to *cis* isomerization (Fig. 1). This chemical flip in turn changes the behavior of PYP itself and signals the start of that cascade.

The use of the word “flip” belies a much more complicated process than a straightforward transformation of the chromophore, as the researchers from the Institute for Basic Science (Republic of Korea), KAIST (Republic of Korea), The University of Wisconsin–Milwaukee, and The University of Chicago discovered. They point out that the complexity of any protein discounts the simplistic one-bond flip of the kind that might take place in simple laboratory chemicals. Instead, they suggest that a sophisticated chemical choreography must take place to allow the flip to occur without disrupting the overall shape and volume of the protein.

The team utilized time-resolved Laue diffraction x-ray crystallography at the BioCARS 14-ID-B beamline at the APS and the ESRF ID09B beamline to build up a frame-by-frame picture of the changes occurring every 100 ps, at

< Fig. 1. The isomerization of a small molecule caged inside a photoactive protein recorded by time-resolved x-ray crystallography reveals a detailed sequence of events (represented by dominos) composed of a short-lived intermediate (red) whose reaction trajectory bifurcates along bicycle-pedal (left) and hula-twist (right) pathways.

1.6-Å resolution, as the chromophore absorbs light and the photochemical reactions in PYP begin.

The PYP chromophore is *p*-coumaric acid, a molecule widespread in nature and present in several edible plants including tomatoes and garlic, as well as the bacterium on which the research team has focused. This molecule contains a double bond between two central carbon atoms in its structure. Such bonds are usually amenable to the kind of transformation that involves a flip from a *trans* to a *cis* state where chemical groups linked by the double bond shift from both being on opposite sides to both being on the same side. In the *trans* state, *p*-coumaric acid gives rise to the yellow color of PYP, but when it changes to *cis*, having absorbed a photon, its color is lost and the light energy is transformed into the required physical change in the protein.

Whereas in the laboratory the *trans*-to-*cis* flip can occur in a straightforward manner, the team’s crystallographic studies of the transformation as it occurred within the protein revealed that an intermediate is involved. This intermediate is a highly strained molecule in which the chemical groups on either side of the double bond in *p*-coumaric acid are forced to align from their original positions on either side before the molecule releases its pent-up energy to generate the *cis* form with both groups on the same side.

Even this apparently simple release is complicated by the existence of two reaction paths: the “hula-twist” and the “bicycle-pedal.” These distinct reaction routes allow the groups adjacent to the double bond either to squirm into the *cis* position, in the former case, or to rotate around the bond like rotating bicycle pedals. The team has used a mutant version of the protein to control which of these two pathways is taken. A mutation in PYP known as E46Q weakens the connection between *p*-coumaric acid and the protein itself and this seems to preclude the process from taking the bicycle pedal route.

These findings will help scientists better interpret spectroscopic data from this and similar systems as well as improved their computational models all shedding more light on some of life’s most critical processes.

— David Bradley

See: Yang Ouk Jung^{1,2}, Jae Hyuk Lee², Joonghan Kim², Marius Schmidt³, Keith Moffat⁴, Vukica Šrajer⁴, and Hyotcherl Ihee^{1,2*}, “Volume-conserving *trans*–*cis* isomerization pathways in photoactive yellow protein visualized by picosecond X-ray crystallography,” *Nat. Chem.* **5**, 212 (March 2013).

DOI:10.1038/NCHEM.1565

Author affiliations: ¹Institute for Basic Science, ²KAIST, ³University of Wisconsin–Milwaukee, ⁴The University of Chicago

Correspondence:

*hyotcherl.ihee@kaist.ac.kr

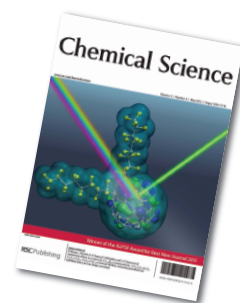
This work was supported by the Research Center Program (CA1201) of the Institute for Basic Science (Korea) and by Creative Research Initiatives (Center for Time-Resolved Diffraction) of the Ministry of Education, Science, and Technology/ National Research Foundation of Korea. M.S. is supported by National Science Foundation grants 0952643 (Career) and 0843459. K.M. is supported by National Institutes of Health (NIH) grant GM036452. Use of the BioCARS Sector 14 at the APS was supported by NIH National Institute of General Medical Sciences grant P41GM103543. The time-resolved set-up at Sector 14 was funded in part through collaboration with P. Anfinrud (NIH/ National Institute of Diabetes and Digestive and Kidney Diseases) through the Intramural Research Program of the Research Program of the National Institute of Diabetes and Digestive and Kidney Diseases.

See also: F. Schotte et al., *Proc. Natl. Acad. Sci. USA* **109**(47), 19256 (November 20, 2012).

14-ID-B • BioCARS • Life sciences • Time-resolved crystallography, time-resolved x-ray scattering, Laue crystallography, wide-angle x-ray scattering, biohazards at the BSL2/3 level, macromolecular crystallography • 7-20 keV • On-site • Accepting general users •

REWRITING THE ORGANOFLUORINE PLAYBOOK

Sometimes it is easy to overgeneralize, to conclude that simply because a group of things are pretty much all the same, they are identical in all respects, even interchangeable. But such assumptions can cause a lot of problems, not just in everyday life but also in science. One example is the findings of a research team whose experiments at the ChemMatCARS x-ray facility at the APS have shaken up the field of organofluorine chemistry by challenging some long-held theoretical assumptions, and because of their implications for the practical application of materials based on certain important molecules. Their published study was the cover article for the May 2012 issue of the journal *Chemical Science*.

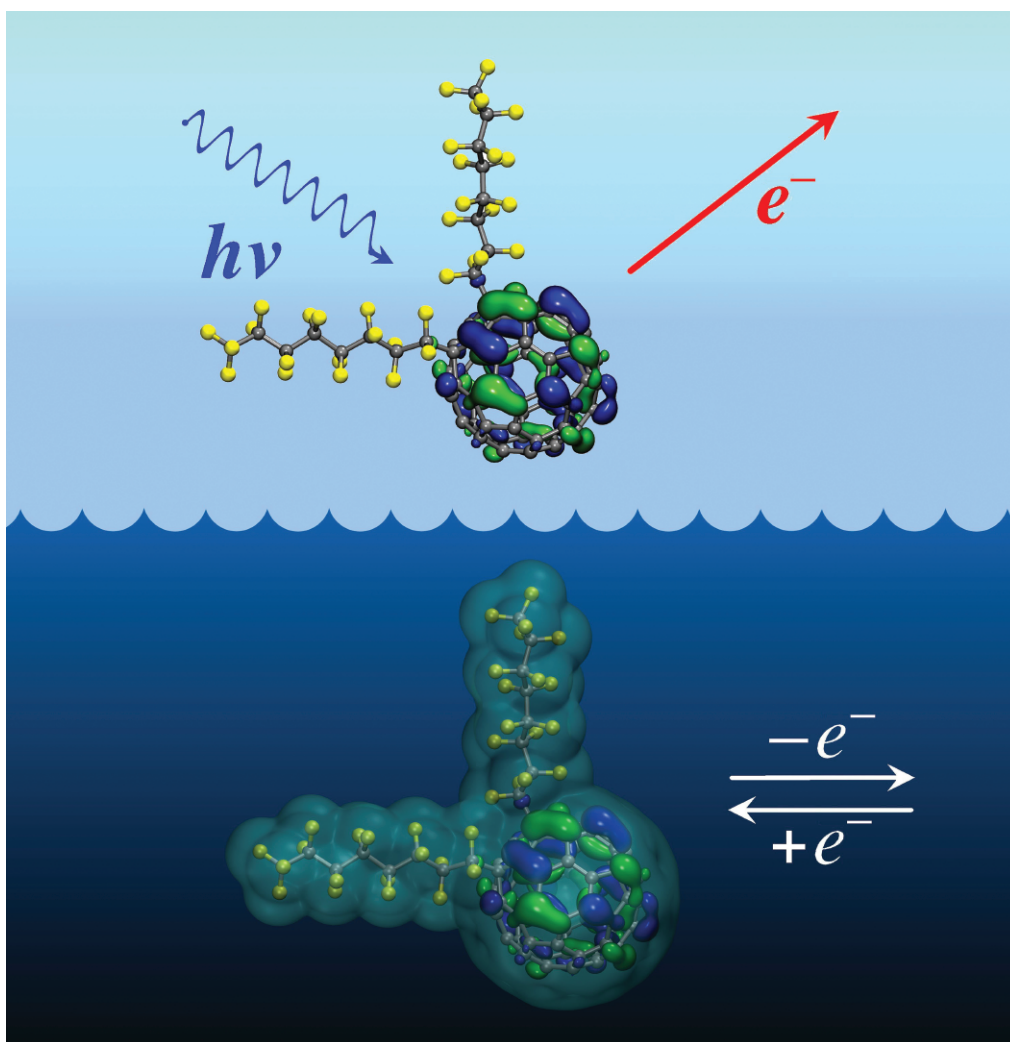


The highly complex and specialized realm of organofluorine chemistry involves the study and application of organic compounds based on the carbon-fluorine bond. Organofluorines are used in a dizzying array of applications, including solvents and nonstick coatings, blood substitutes, anesthetics and various other drugs, lubricants, and even organic photovoltaic (OPV) devices such as highly efficient solar cells.

Because the electronic properties of a particular compound are crucial to understanding and controlling its application, chemists have devised some handy mathematical shortcuts for determining and comparing the properties of related organofluorines.

Basically, the idea is that by experimentally determining the value of one of these properties, the others could be derived simply by using a set of simple linear equations.

But the team of researchers in this study, from Colorado State University, The University of Chicago, the Dresden University of Technology (Germany), Washington State University, the Leibniz Institute for Solid State and Materials Research (Germany), Argonne, and Pacific Northwest National Laboratory demonstrated that it is not that simple.



The processes of removing an electron from the negatively-charged radical anion of 1,7-C60(C8F17)2, in the gas-phase by low-temperature photoelectron spectroscopy and in solution by cyclic voltammetry. Image by Alexey A. Popov.

After preparing a series of seven 1,7- $C_{60}(R_F)_2$ organofluorine compounds and carefully studying the electron affinities, first-order reduction potentials ($E_{1/2}(0/-)$), and DFT-predicted $E(LUMO)$ values of each, the team found that the convenient and generally assumed correlations among these properties were not present.

The research team, led by some expert organofluorine chemists, conducted advanced x-ray crystallography at beamline 15-ID-B,C,D. The seven compounds studied ($R_F = C_{F_3}, C_2F_5, n-C_3F_7, i-C_3F_7, n-C_4F_9, s-C_4F_9,$ and $n-C_8F_{17}$) were chosen because of their potential use as electron acceptors in organic photovoltaic materials.

In previous work the researchers had studied how different numbers of a single type of perfluoroalkyl (PFA) group, CF_3 (trifluoromethyl), in different relative positions on the fullerene cage will change the electron accepting properties. They wanted to know whether, given the same structure and the same relative positions, what happens if the PFA group is changed from a short group like trifluoromethyl CF_3 to a long group like $n-C_8F_{17}$. Is there a difference in the electron withdrawing properties?

The common wisdom that has guided the design and development of most organofluorines is that such similar compounds will also share more or less the same electrochemical properties. For example, determining the first reduction potential ($E_{1/2}(0/-)$) of a particular molecule will also allow its electron affinity to be estimated. But here is an example of a series of compounds where the correlations do not work, where the solution electrochemistry would lead one to believe that these compounds are virtually the same, and yet they are not.

At first, the seven PFA compounds displayed virtually identical first reduction potentials at the ± 10 -mV level of uncertainty. The researchers confirmed the molecular structures and PFA positions with low-temperature anion photoelectron spectroscopy carried out at the Environmental Molecular Sciences Laboratory (EMSL) at the U.S. Department of Energy's Pacific

Northwest National Laboratory, and very precise x-ray crystallographic studies at the ChemMatCARS beamline. (The collaboration with ChemMatCARS is important for the team because the facilities that Yu-Sheng Chen has developed can handle the smallest crystals of the fullerenes.)

But when the experimenters measured electron affinities of the compounds in the gas phase, they found them to be quite different. The researchers were also surprised by a significant lack of correlation between the measured ($E_{1/2}(0/-)$) and $E(LUMO)$ values predicted with DFT calculations.

The team's findings have shaken up the field of organofluorine chemistry not only because they have overturned some long-held theoretical assumptions, but also because of their implications for the practical application of materials based on such molecules, such as OPVs. This came as a surprise to the team and, they suspect, to the community. It points out the risk inherent in taking results from experiments in one phase (e.g., solution, gas phase) and using them to draw conclusions about the molecules in another phase (e.g., solid thin films).

The work demonstrates that greater precision and accuracy in measurement are necessary to create fullerene materials with the desired electrochemical properties. When trying to design a system, a number of different electrochemical properties or electron acceptor properties must be measured to get a real idea of how a particular compound might result in a particular efficiency in a solar cell.

The next step for the team will likely involve studying the solid state electronic signature of these materials in order get into all three phases. With solid state measurements, they can correlate them with the gas phase and solution phase. Armed with that information, the team will be able to collaborate with those who are actually making devices, provide them with compounds, and see how well they work or do not work. Either way, new information will emerge about what is important in making better devices.

— Mark Wolverton

See: Igor V. Kuvychko¹, James B. Whitaker¹, Bryon W. Larson¹, Travis C. Folsom¹, Natalia B. Shustova¹, Stanislav M. Avdoshenko², Yu-Sheng Chen³, Hui Wen^{4,5}, Xue-Bin Wang^{4,5}, Lothar Dunsch⁶, Alexey A. Popov⁶, Olga V. Boltalina^{1**}, and Steven H. Strauss^{1*}, "Substituent effects in a series of 1,7- $C_{60}(R_F)_2$ compounds ($R_F = CF_3, C_2F_5, n-C_3F_7, i-C_3F_7, n-C_4F_9, s-C_4F_9, n-C_8F_{17}$): electron affinities, reduction potentials and $E(LUMO)$ values are not always correlated," Chem. Sci. **3**, 1399 (2012).

DOI:10.1039/c2sc01133f

Author affiliations: ¹Colorado State University, ²Dresden University of Technology, ³The University of Chicago, ⁴Pacific Northwest National Laboratory, ⁵Washington State University, ⁶Liebniz Institute for Solid State and Materials Research

Correspondence:

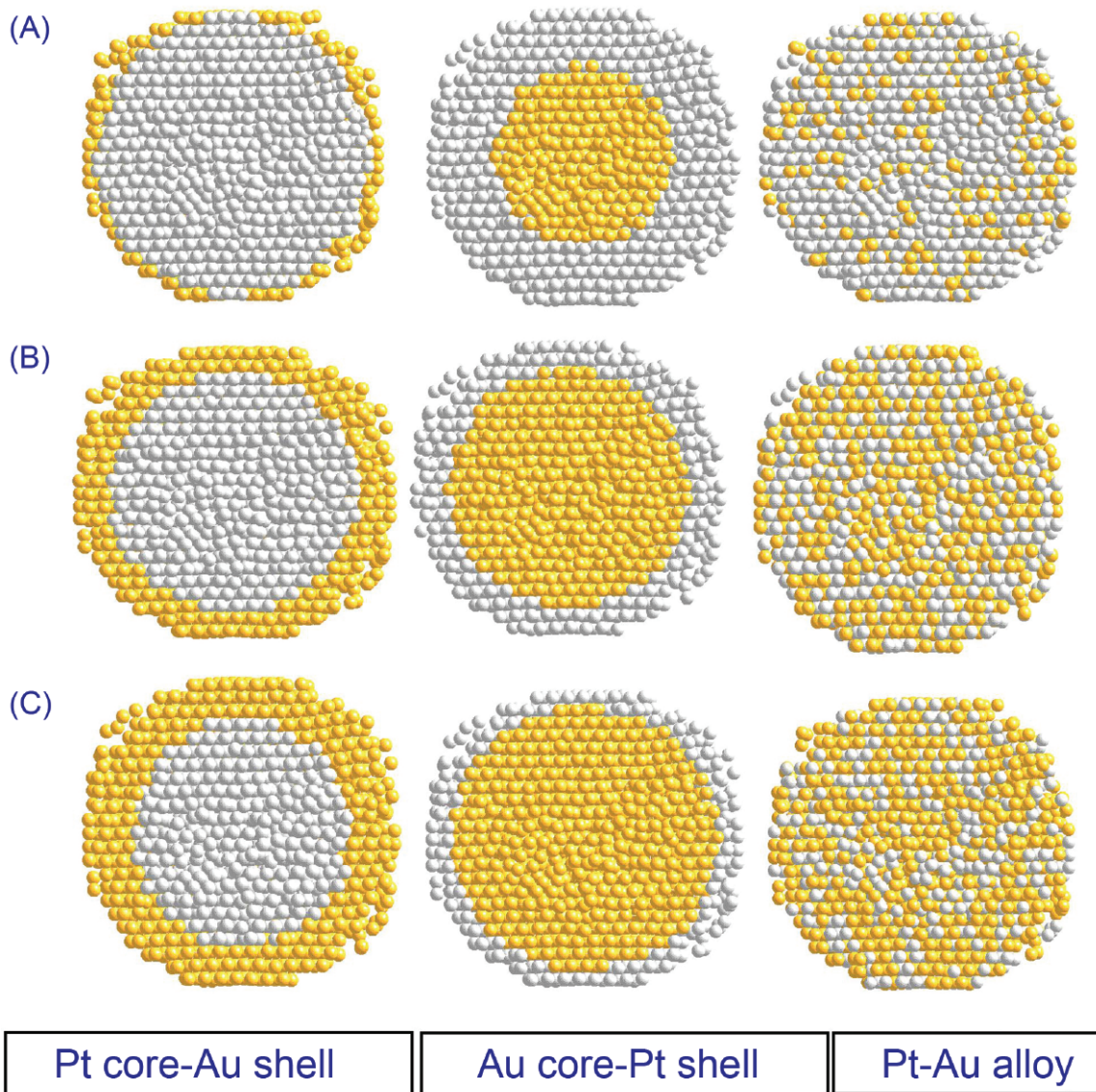
*steven.strauss@colostate.edu,

**olga.boltalina@colostate.edu

This work supported by the U.S. National Science Foundation (NSF) (CHE-0707223, CHE-1012468) and the Colorado State University Research Foundation. H.W. acknowledges a Pacific Northwest National Laboratory alternate sponsored fellowship. The AvH Foundation is acknowledged for financial support to A.A.P., J.B.W., and O.V.B. The Erasmus Mundus Program External Co-operation (EM ECW-L04 TUD 08–11) is acknowledged for financial support to S.M.A.; J.B.W. thanks The Electrochemical Society for an F.M. Beckett Summer Fellowship. ChemMatCARS is principally supported by the U.S. NSF under grant number CHE-0822838. The EMSL is sponsored by the U.S. Department of Energy (DOE) Biological and Environmental Research Program. Use of the Advanced Photon Source at Argonne National Laboratory was supported by the U.S. DOE Office of Science under Contract No. DE-AC02-06CH11357.

15-ID-B,C,D • ChemMatCARS • Materials science, chemistry • Single-crystal diffraction, anomalous and resonant scattering (hard x-ray), wide-angle x-ray scattering, microdiffraction, liquid surface diffraction, small-angle x-ray scattering, ultra-small-angle x-ray scattering, high-pressure diamond anvil cell • 6-32 keV, 10-6 keV • On-site • Accepting general users •

PLATINUM AND GOLD TOGETHER AT THE NANOSCALE TO MAKE A BETTER CATALYST



Platinum is a versatile chemical catalyst. It is also scarce and expensive. Chemists have made great efforts to combine platinum with other elements in order to make cheaper catalysts, but platinum is not always eager to enter into such combinations. Gold and platinum, for example, do not form an alloy in bulk. However, experiments at XSD beamline 1-ID-B,C,E at the APS show that platinum and gold join together in nanoparticles less than 10 nm in size, forming true alloys in which atoms of the two elements are randomly interspersed. The finding offers clues to the surprising catalytic activity of these alloy nanoparticles, in comparison to pure platinum.

Researchers from Central Michigan University, the State University of New York at Binghamton, and Argonne grew spherical platinum-gold nanoparticles with diameters of 5.1 nm and 8 nm. The team made the nanoparticles with a range of compositions, from pure platinum (Pt) at one extreme to pure gold (Au) at the other, and annealed them at temperatures of 400° C and 800° C.

X-ray diffraction studies of the nanoparticles at beamline 1-ID-B,C,E produced patterns with very broad peaks that were not amenable to conventional Bragg analysis and therefore could not be used to generate detailed, atomic-scale structure models. Instead, the team utilized the diffraction data to generate pair distribution functions (PDFs), which have peaks corresponding to all distances between atom pairs in the nanoparticles.

For nanoparticles of mixed composition, the first PDF peak represented an average over Pt-Pt, Au-Au, and Pt-Au bond lengths. As the composition varied, this peak moved smoothly from 27.7 nm to 28.6 nm, those values being close to the bond length in pure platinum and pure gold, respectively. The PDFs also showed distinct peaks at greater distances, corresponding to second, third, and higher neighbor distances between atoms in the nanoparti-

< Fig. 1. Simulations of possible atomic arrangements in 5.1-nm Pt–Au nanoparticles: (A) $\text{Pt}_{0.77}\text{Au}_{0.23}$; (b) $\text{Pt}_{0.51}\text{Au}_{0.49}$; and (c) $\text{Pt}_{0.40}\text{Au}_{0.60}$. Pt atoms are in gray, Au in yellow. Contrary to theoretical predictions, the models in the right-most column, in which platinum and gold form stable alloys, give the best fit to x-ray diffraction data.

cles. The team was able to reproduce these PDFs using models based on a face-centered cubic (fcc) structure, the structure of the pure metals, but found that they needed to include extra structural distortion that increased toward the surface of the nanoparticles.

To reveal how the two elements are arranged within the nanoparticles, the team conducted further diffraction experiments at two wavelengths close to the K absorption edge of platinum. By taking the difference between the data sets collected at these two wavelengths, the researchers were able to separate the scattering due to Pt-Pt and Pt-Au atom pairs from that due to Au-Au pairs. This result is not trivial because Pt and Au are neighbors in the Periodic Table and scatter x-rays in a very similar way.

The resulting Pt differential and Au-Au partial PDFs revealed that the bond length between atoms of the same species remained almost constant regardless of the composition of the nanoparticles, indicating that the structural distortions come not only from surface relaxation effects, but also from the need to accommodate atomic species of two different sizes.

Finally, the team used Monte Carlo simulations to construct models in which platinum and gold atoms populated the nanoparticles in a variety of ways (Fig. 1). Models in which the two kinds of atoms were segregated — a core of platinum encased in a shell of gold, or vice versa — gave a poor fit to the experimental Au-Au partial PDFs. The best fit came from distributing gold and platinum atoms randomly within the nanoparticles, so that the composi-

tion was a genuine alloy. Surprisingly, this was true even for the nanoparticles that had been annealed at higher temperature, a process that according to conventional theory should have caused the gold and platinum components to separate out, as they do in bulk.

These findings help explain the effectiveness of the nanoparticles in catalyzing a methanol oxidation reaction. Per unit mass of platinum, nanoparticles with a $\text{Pt}_{0.2}\text{Au}_{0.8}$ composition had more than four times the catalytic activity of pure platinum. This comes about, the group suggests, because of changes in the charge balance between platinum and gold atoms bonded to each other, an effect that happens to a greater extent in a true alloy than if the nanoparticles had a segregated composition.

By revealing not only atomic but also chemical ordering in nanoparticles, the team says, structural analysis of the type reported in this study can speed the development of more effective as well as cheaper catalysts.

— David Lindley

See: Valeri Petkov^{1*}, Bridgid N. Wanjala², Rameshwori Loukrakpam², Jin Luo², Lefu Yang², Chuan-Jian Zhong², and Sarvit Shastri³, “Pt-Au Alloying at the Nanoscale,” *Nanolett.* **12**, 4289 (2012).

DOI:/10.1021/nl302329n

Author affiliations: ¹Central Michigan University, ²Binghamton University, ³Argonne National Laboratory

Correspondence:

*petko1vg@cmich.edu

This work was supported by the U.S. Department of Energy Office of Science (DOE-SC), Basic Energy Science Program Grant DESC0006877. Use of the Advanced Photon Source at Argonne National Laboratory was supported by the DOE-SC under Contract No. DE-AC02-06CH11357.

1-ID-B,C,E • XSD • Materials science, physics, chemistry • High-energy x-ray diffraction, radiography, small-angle x-ray scattering, fluorescence spectroscopy, pair distribution function • 50-90 keV, 50-150 keV • On-site • Accepting general users •

AN INTRIGUING TWIST IN THE STRUCTURE OF A COBALT OXIDE CATALYST

Hydrogen is a clean fuel, producing only water vapor when it burns. But generating hydrogen in large quantities and in a “green” fashion is not straightforward. Biological photosynthesis includes an efficient reaction step that splits water into hydrogen and oxygen with the help of catalysts that have been used as models for synthetic catalysts. Working at the XSD 11-ID-B beamline at the APS, a team of Argonne scientists determined the structure of one such catalyst, a complex cobalt oxide. The material is composed of crystalline domains containing just 13 or 14 cobalt atoms, with distortions at their boundaries that may be important for its catalytic properties.

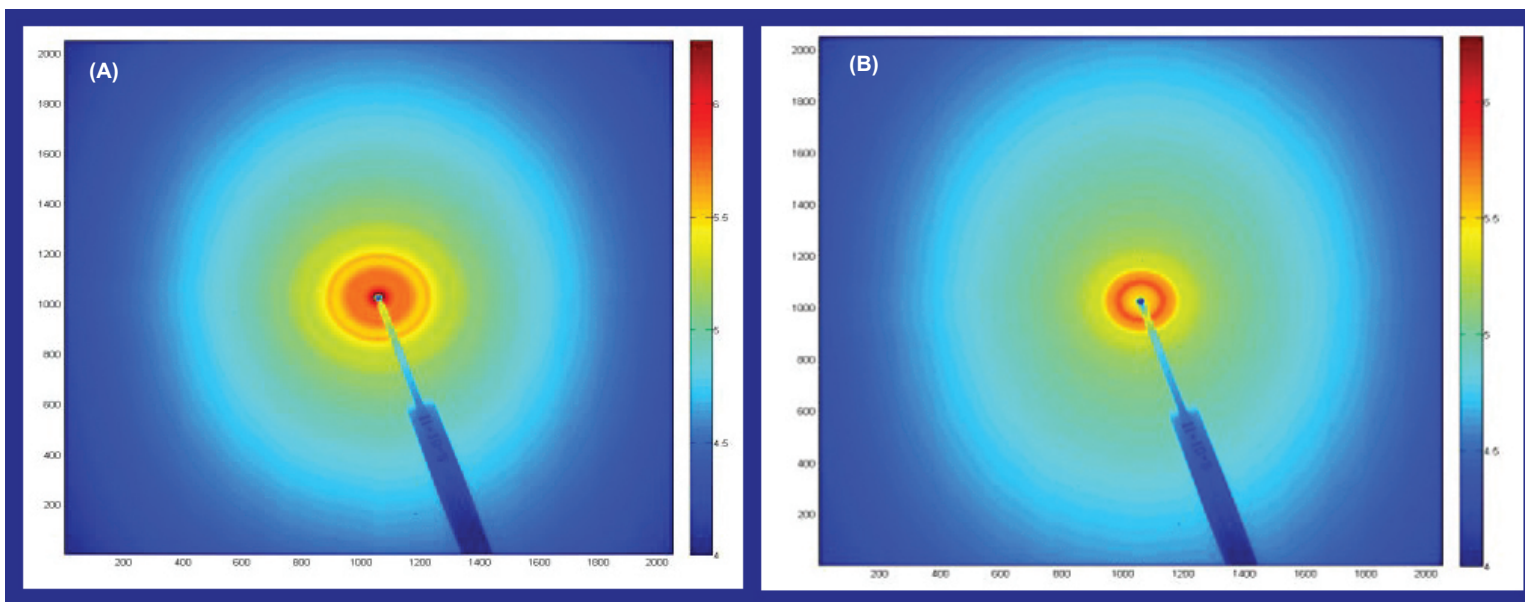


Fig. 1. Experimental two-dimensional scattering images. Part (A): the cobalt oxide catalyst film sample in an aqueous slurry in a kapton capillary. Part (B): water background; Part (C): the difference pattern. Scattering intensity is represented by a log color scale in Parts A and B, and by a linear color scale in Part C. From P. Du et al., *J. Am. Chem. Soc.* **134** (2012), Supp. Info.

The water-splitting cobalt oxide catalyst was discovered serendipitously about three years ago in experiments where an electric current ran through a solution containing dissolved cobalt salts. Because of the amorphous nature of the catalyst film, the details of its structure have remained unclear.

Previous x-ray and other spectroscopy studies showed that cobalt in the catalyst exists in an octahedral coordination environment, CoO_6 , with Co at the center and O at the vertices. This conformation is analogous to the lattice sheet domains of the non-catalytic crystalline cobalt oxides, but is present here in domains of undetermined molecular-scale dimensions.

However, some earlier publications suggested that the x-ray spectroscopy

data could also be interpreted in terms of cobalt oxide cubane structures, Co_4O_4 , that are analogous to the structure and spectroscopy of the water-splitting catalyst that occurs in biological photosynthesis systems.

lyst's composition makes it impossible to infer definitive crystallographic structure from standard diffraction measurements. Instead, the researchers used a straightforward mathematical technique – essentially a Fourier transform – to turn the observed x-ray scattering data into the electron pair density distribution function, which appears as a series of peaks corresponding to a set of distances between the atoms in the structure.

Interpreting the results was then a matter of modeling the expected pair distribution function (PDF) from a supposed structure and seeing how well it fit the experimental data.

The researchers found that the best fit came from structures with domains consisting of CoO_6 octahedra with shared edges, and careful analysis allowed them to deduce the most likely number of cobalt atoms in the domains. Domains with 12 cobalt atoms or fewer didn't fit the PDF for interatomic distances greater than about 10 Å, while domains with 15 or more cobalt atoms failed to match the PDF at smaller distances.

The team thus concluded that

each domain in the amorphous material must have 13 or 14 cobalt oxide octahedra.

The model-fitting exercise also revealed some characteristic differences between the PDFs observed experimentally and those calculated using crystalline lattice models for the domains, demonstrating that the structure for the lattice domains in the catalyst differs from those of non-catalytic crystalline cobalt oxides.

Their analysis showed that slight alterations to the coordination geome-

tries for the oxygen atoms bound to the cobalt atoms at the edges of the domains (for example a 4° shift from their normal positions) could account for most of the discrepancy between the experimental and model structures.

Cubane-type inclusions were also found to be possible additional sparse defects that could bring experiment and model into better alignment. Also significant was the finding that phosphate anions, which are required for catalytic activity, were detected as disordered constituents of the film.

Ongoing work is directed at investigating the correlation between structure and catalytic function of the cobalt oxide catalysts, and developing more highly refined models. The researchers suggest that the distorted cobalt coordination geometries in the catalyst may be a distinguishing feature that confers the ability to catalyze the water-splitting reaction compared to the non-catalytic crystalline cobalt oxides, although the team acknowledges that this suggestion is somewhat speculative.

It will take a while to figure out the catalytic mechanism, but it is crucial to know the structure of the material and this is the best structure out there at the moment — *David Lindley*

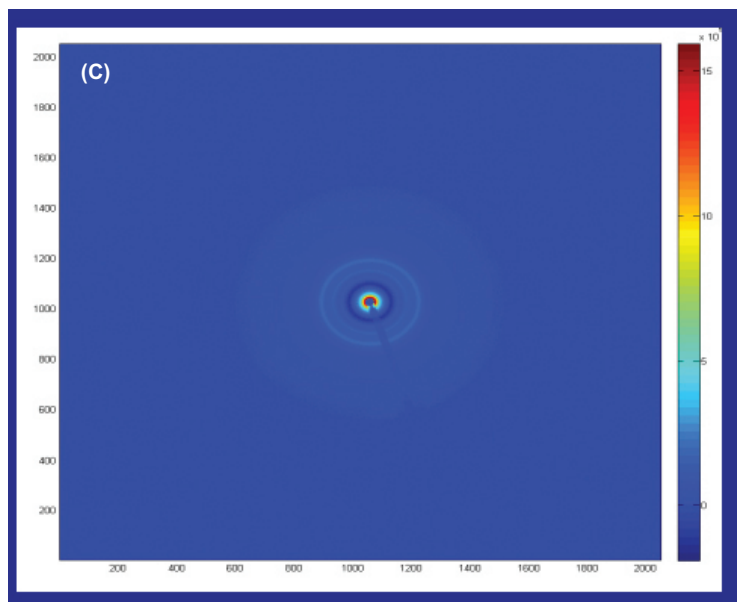
See: Pingwu Du, Oleksandr Kokhan, Karena W. Chapman, Peter J. Chupas, and David M. Tiede*, "Elucidating the Domain Structure of the Cobalt Oxide Water Splitting Catalyst by X-ray Pair Distribution Function Analysis," *J. Am. Chem. Soc.* **134**, 11096 (2012). DOI:10.1021/ja303826a

Author affiliation: Argonne National Laboratory

Correspondence: *tiede@anl.gov

Use of the Advanced Photon Source at Argonne National Laboratory was supported by the U.S. Department of Energy Office of Science under Contract No. DE-AC02-06CH11357.

11-ID-B • XSD • Chemistry, environmental science, materials science • Pair distribution function • 58-60 keV, 90-91 keV • On-site • Accepting general users •

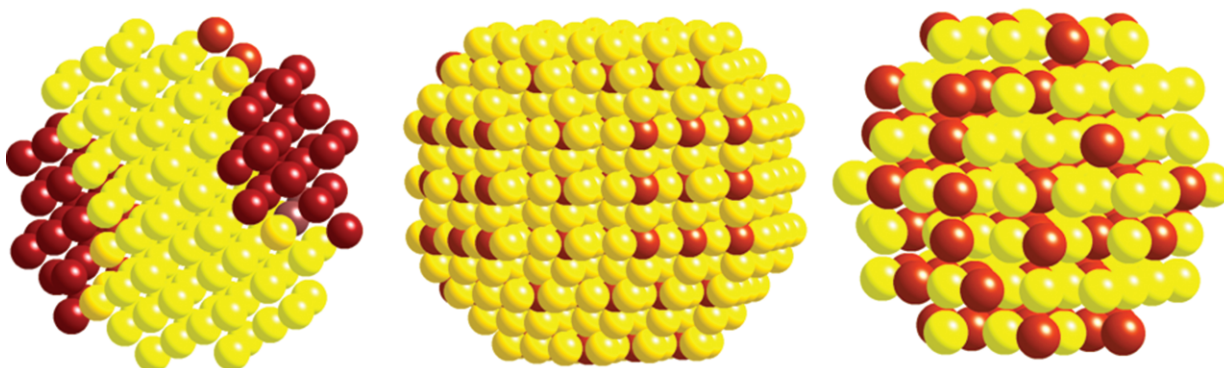


The researchers prepared the cobalt oxide material by electrodeposition from a solution buffered with potassium phosphate. Working at 11-ID-B, they conducted x-ray diffraction studies on samples either of dry powder or aqueous slurry (Fig. 1).

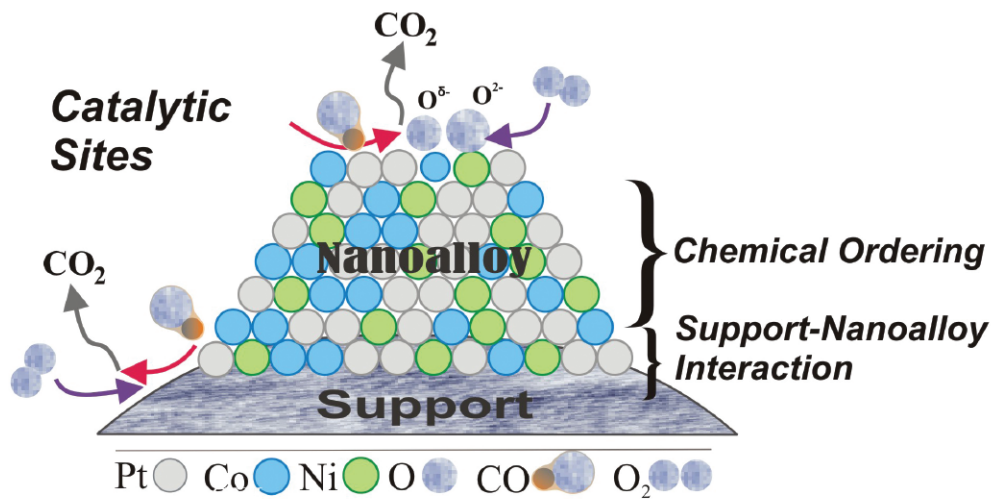
The amorphous nature of the cata-

TUNING NANOALLOY CATALYSTS WITH CHEMICAL ORDER

A clear understanding of how catalytic sites in nanoalloys can be tuned through chemical ordering at the atomic scale has emerged from research carried out using synchrotron radiation at three APS beamlines. This work hints at the possibility of developing designer nanoalloy catalysts for preferential oxidation reactions and other catalytic reactions in energy conversion/storage.



Chemical order-disorder effects in supported $\text{Pt}_{39}\text{Ni}_{22}\text{Co}_{39}$ catalysts. From left to right: phase segregated, chemically ordered and chemically disordered structures in, respectively, silica, carbon, and titania supported $\text{Pt}_{39}\text{Ni}_{22}\text{Co}_{39}$ catalysts as revealed by synchrotron radiation-based techniques coupled to computer simulations. Pt atoms are in yellow, transition metal atoms in red.



Schematic illustration of the catalytic oxidation of carbon monoxide by oxygen at the active sites on a supported nanoalloy catalyst.

Understanding the structural arrangement of atoms in a catalyst is vital to improving the efficiency of these important industrial materials and for designing new, improved catalysts to speed up a wide range of chemical reactions.

Researchers from the State University of New York at Binghamton, Central Michigan University, the Pacific Northwest National Laboratory, Argonne, and The Pennsylvania State University utilized APS high-energy synchrotron radiation and x-ray diffraction in *ex situ* and *in situ* modes at the XSD beamlines 11-ID-C and 11-ID-B to investigate the role of interactions between nanoalloys and the supporting material in catalytic site tuning (Fig. 1). They relied upon three main techniques in combination: x-ray photoelectron spectroscopy, high-energy x-ray crystallography, and synchrotron x-ray fine structure absorption spectroscopy at XSD beamline 9-BM. They investigated the structure of ternary nanoalloy particles made from platinum-nickel-cobalt on three different support materials: carbon, silicon dioxide (silica), and titanium dioxide (titania). This research team had previously shown that ternary alloys might have benefits over bimetallic catalysts, as evidenced by electrochemical studies of the catalysts in fuel cell reactions and supported by theoretical modeling of the reactions. The team has employed the catalyzed oxidation of carbon monoxide by oxygen to carbon dioxide as a model reaction to help them probe the behavior of the different supported catalytic materials.

Much of the research into catalysts for speeding up the conversion of one chemical to another has been on increasing activity, and so efficiency, but at the same time reducing the amount of costly precious metals, such as platinum and palladium, needed in high-performance catalysts. A promising route has been the formation of nanoparticles just a few billionths of a meter in diameter. Researchers hope that such species will have novel properties compared to the bulk and powdered forms of a metal catalyst. Moreover, the ability to form composites, or alloys, from more than one metal in a nanoparticle opens the possibility of creating tunable catalysts by

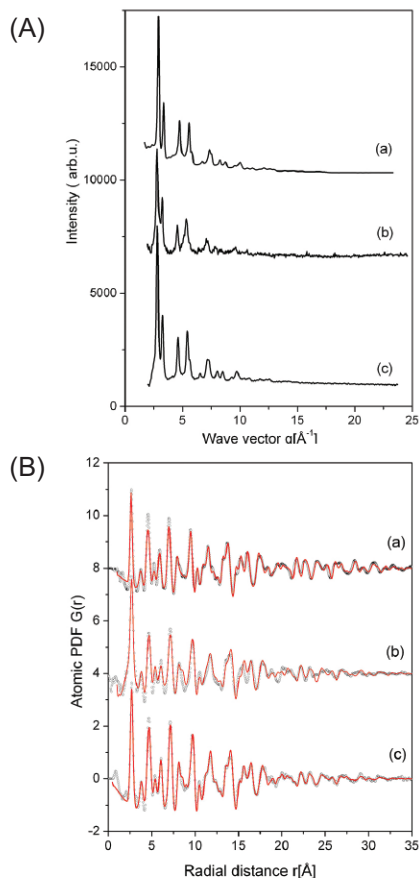


Fig. 1. High-energy XRD patterns (A), and atomic PDFs (B) for $\text{Pt}_{39}\text{Ni}_{22}\text{Co}_{39}$ nanoalloys supported on (a) carbon, (b) SiO_2 , and (c) TiO_2 . From L. Yang et al., *J. Am. Chem. Soc.* **134** (2012). ©2012 American Chemical Society.

varying the ratio of each metal in the particle as well as changing the nature of the material on which the particles are supported in the reaction.

Alloys of platinum and cobalt, and platinum and nickel — bimetallic alloys — have been investigated previously and have been shown to be efficient. However, adding a third metal to give a ternary alloy could open new avenues for catalysis.

The research team's work has revealed much about the structure of such ternary nanoalloys on three different supports. The results show that the interaction between nanoalloy and support material can influence how the catalytic reaction proceeds, which the team says implies they could tune the catalyst for specific reactions based on their insights into the catalytic centers involved.

For instance, they found a particular site involving nickel and cobalt on the nanoalloy that activates oxygen

ready for reaction but is different than previously observed activated oxygen sites in conventional noble metal catalysis that are supported on metal oxides. In terms of catalytic rate, the ternary nanoalloys supported on carbon far outstripped the reactions in which a bimetallic catalyst was utilized on the same support.

Fundamentally, the presence of cobalt in the nanoparticles is revealed to promote catalytic efficiency while the nickel stabilizes the chemical system. This hints at the possibility of developing designer nanoalloy catalysts for preferential oxidation reactions and other catalytic reactions in energy conversion/storage. — *David Bradley*

See: Lefu Yang¹, Shiyao Shan¹, Rameshwori Loukrakpam¹, Valeri Petkov^{2*}, Yang Ren⁴, Bridgid N. Wanjala¹, Mark H. Engelhard³, Jin Luo¹, Jun Yin¹, Yongsheng Chen⁵, and Chuan-Jian Zhong^{1**}, "Role of Support–Nanoalloy Interactions in the Atomic-Scale Structural and Chemical Ordering for Tuning Catalytic Sites," *J. Am. Chem. Soc.* **134**, 15048 (2012). DOI:10.1021/ja3060035

Author affiliations: ¹Binghamton University, ²Central Michigan University, ³Pacific Northwest National Laboratory, ⁴Argonne National Laboratory, ⁵The Pennsylvania State University

Correspondence:

**cjzhong@binghamton.edu;
*petko1vg@cmich.edu

This work was supported by the U.S. Department of Energy Office of Science (DOE-SC) Grant DE-SC-0006877, and in part by the National Science Foundation (CBET-0709113). Use of the Advanced Photon Source at Argonne National Laboratory was supported by the DOE-SC under Contract No. DE-AC02-06CH11357.

9-BM-B,C • XSD • Materials science, chemistry • X-ray absorption fine structure • 2.1-23 keV • On-site • Accepting general users •

11-ID-B • XSD • Chemistry, environmental science, materials science • Pair distribution function • 58-60 keV, 90-91 keV • On-site • Accepting general users •

11-ID-C • XSD • Materials science • High-energy x-ray diffraction, diffuse x-ray scattering, Pair distribution function • 115 keV • On-site • Accepting general users •

NEW STRUCTURAL DETAILS IN BLUE RD CATALYSIS FOR HYDROGEN GENERATION

Photosynthetic water oxidation is a fundamental process in the biosphere that results in the sunlight-driven formation of O_2 from water. Biological photosynthesis encompasses a series of complicated processes involving several transition states and intermediates that scientists continue to investigate. Mimicking this reaction in a man-made device will allow for sunlight-to-chemical energy conversion, with water providing electrons and protons for the formation of oxygen and reduced chemicals. Such processes are best suited for sustainable and clean generation of H_2 . The first synthetic catalyst designed to mimic the portion of biological photosynthesis involved in water oxidation, i.e., the catalyzed evolution of O_2 from H_2O , was the ruthenium (Ru)-based compound commonly referred to as “blue dimer” (BD). Although the water-oxidizing capabilities of blue dimer were first reported some three decades ago, several aspects of this catalytic process remained hidden. Recently, scientists utilizing a variety of spectroscopic techniques to probe the catalysis process, including x-ray absorption spectroscopy performed at XSD beamline 20-BM-B at the APS, reported progress in revealing previously unknown mechanistic details about blue dimer’s water oxidation reaction, which may in the not-too-distant future result in cost-effective, practical, and sustainable alternative energy sources.

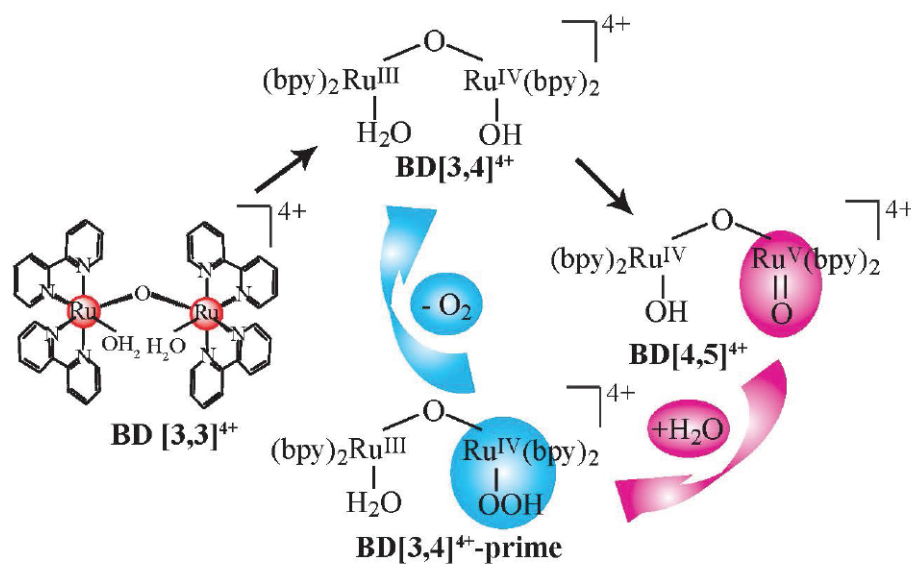


Fig 1. Key intermediates in the water oxidation catalytic cycle of the blue dimer characterized by x-ray spectroscopy. Optimization of the reactivity toward water (purple arrow) and oxidation of the resulting peroxo-intermediate (blue arrow) are needed for improved catalytic activity.

Blue dimer contains two ruthenium atoms bound together by a single oxygen atom. Each Ru atom also forms bonds with a ligand (Fig. 1). The ligands are composed of linked pyridine rings, structurally very similar to the simple benzene ring (C_6H_6). The two ruthenium atoms can exhibit different oxidation states. The chemical formula of blue dimer, *cis,cis*- $[(bpy)_2(H_2O)Ru^{III}ORu^{III}(OH_2)(bpy)_2]^{4+}$ (where “bpy” is 2,2-bipyridine), indicates that the two ruthenium atoms are in the [3,3] oxidation state. A water molecule is attached to each Ru atom in the [3,3] state.

The researchers from Purdue University, the University of North Carolina at Chapel Hill, and Southern Federal University (Russia) monitored the catalytic cycle of BD via stopped-flow ultraviolet visible spectroscopy with millisecond precision, electron paramagnetic resonance (EPR), resonance Raman spectroscopy, and x-ray absorption spectroscopy (XAS). Use of techniques with high sensitivity to the electronic states of molecules, namely EPR and XAS, was crucial in determining the electronic requirements of the water oxidation process. Extended x-ray

absorption fine structure (EXAFS) measurements allowed determination of bond distances. This research identified for the first time structural details of two short-lived intermediates involved in the blue dimer catalytic cycle, one reactive towards the formation of the O-O bond and the other the product of this reaction (peroxo-intermediate), see Fig. 1.

All intermediates in the blue dimer water oxidation cycle were generated chemically by addition of the powerful oxidant cerium ammonium(IV) nitrate CeIV. In the future, sunlight will be utilized to produce the oxidant via the process of charge separation. Upon one electron oxidation, BD in the [3,3] oxidation state was converted to [3,4] form (Fig. 1). The addition of excess of oxidant to initiate the catalytic process (water oxidation requires removal of at least four electrons) resulted in the detection of two highly reactive intermediates: BD[4,5] and BD[3,4]' (Fig. 1). BD[4,5] can be prepared in 0.1-M HNO₃ by oxidation of BD[3,4] with an excess of Ce(IV) and fast (less than 10-15 sec) freezing utilizing a freeze-quench technique. The BD[4,5] intermediate was characterized by Ru K-edge XANES (x-ray absorption near-edge structure) and showed a pronounced shift to high energy in comparison to stable compounds BD[3,3] and BD[3,4] (Fig. 2A). Extended x-ray absorption fine structure (EXAFS) analysis, on the other hand, demonstrated a short (1.7-Å) Ru=O bond (Fig. 2B).

X-band EPR analysis of the reaction mixtures was carried out in parallel with the XAS measurements. It allowed observation of the reactivity of the short-lived transient intermediate [4,5] with the formation of the new intermediate [3,4]'. This intermediate slowly decayed to BD[3,4] within around 20 min, as found from EPR analysis, to complete the catalytic cycle. The new intermediate [3,4]' is denoted as such because it demonstrates the same oxidation state as BD[3,4] from XANES analysis. But [3,4]' possesses a very unique EPR signal and shows different EXAFS results with a different Ru-O-Ru

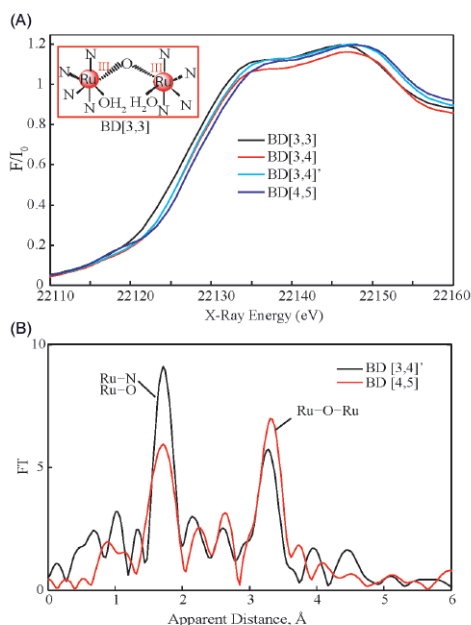


Fig. 2. (A) Normalized Ru K-edge XANES of the blue dimer in oxidation states [3,3], [3,4] and its reactive intermediates [4,5] and [3,4]' (Inset represents the blue dimer structure in oxidation state [3,3]). (B) Fourier transforms of k^3 -weighted Ru EXAFS of oxidized blue dimer intermediates [3,4]' and [4,5].

coordination angle (Fig. 2B). Upon adding four equivalents of Ce(IV) to induce a single turnover of the catalytic cycle, oxygen evolution was observed on the same time scale as the formation of the BD[3,4]' intermediate. Resonance Raman experiments detected a 683-cm⁻¹ band, which underwent a 46-cm⁻¹ shift upon substitution of one oxygen isotope with another (i.e., ¹⁶O/¹⁸O) within the blue dimer.

These experimental results have revealed new aspects about the intermediates and time frames utilized by the BD catalyst to oxidize water. Research shows that under studied conditions, and in spite of fast reaction with water, evolution of oxygen lagged behind. This was attributed to stabilization of the peroxo species. This new information should help the development of next-generation synthetic catalysts from the water oxidation reaction. These should form a highly oxidized state analogous to the RuV = O species with good reactivity toward water, and aid in the conversion of per-

oxo species resulting from this reaction. The researchers hope that their findings will ultimately lead to practical solutions in the quest to find a cost effective, practical, and sustainable alternative energy source in the not-too-distant future — Philip Koth

See: Dooshaye Moonshiram¹, Jonah W. Jurss², Javier J. Concepcion², Taisiya Zakharova¹, Igor Alperovich^{2,3}, Thomas J. Meyer², and Yulia Pushkar^{1*}, "Structure and Electronic Configurations of the Intermediates of Water Oxidation in Blue Ruthenium Dimer Catalysis," *J. Am. Chem. Soc.* **134**, 4625 (2012).

DOI:10.1021/ja208636f

Author affiliations: ¹Purdue University, ²University of North Carolina at Chapel Hill, ³Southern Federal University

Correspondence:

*ypushkar@purdue.edu

D.M. was partially supported by a Purdue Research Foundation grant. We thank the U.S. Department of Energy (DOE) Office of Science Basic Energy Sciences Program for financial support of this work under grants DE-FG02-10ER16184 (Y.P.) and DE-FG02-06ER15788 (T.M.). Synthesis and characterization (J.J.C.) were supported by the UNC EFRC: Solar Fuels and Next Generation Photovoltaics, an Energy Frontier Research Center funded by the U.S. DOE Office of Science, Basic Energy Sciences, under Award Number DE-SC0001011. Utilization of 20-BM-B supported by DOE Basic Energy Sciences, a Major Resources Support grant from the Natural Sciences and Engineering Research Council of Canada, the University of Washington, the Canadian Light Source, and the APS. Use of the Advanced Photon Source at Argonne National Laboratory was supported by the DOE Office of Science under Contract No. DE-AC02-06CH11357.

20-BM-B • XSD • Chemistry, environmental science, geoscience, materials science • Micro x-ray absorption fine structure, micro-fluorescence (hard x-ray), x-ray absorption fine structure • 2.7-25 keV, 2.7-30 keV, 2.7-35 keV • On-site • Accepting general users •

PROFILING BORDER IONS

The way ions arrange themselves on either side of a polarized interface is crucial to the functioning of a variety of systems, from biological membranes to supercapacitors. But both theoretical analysis and experimental investigation of such ion distributions have proved difficult. Researchers performed x-ray reflectivity measurements at ChemMatCARS beamline 15-ID-B,C,D in order to map the ion distribution across the interface between two immiscible solutions. Modeling the results showed that both ion-solvent interactions and ion-ion correlations — two factors not fully taken into account in previous analyses — play a role in determining how ions line up across the interface, information that is of significant importance for nanotechnology applications. For example, the charge-holding ability of a supercapacitor depends on precisely how ions stack up at internal interfaces in a nanodevice.

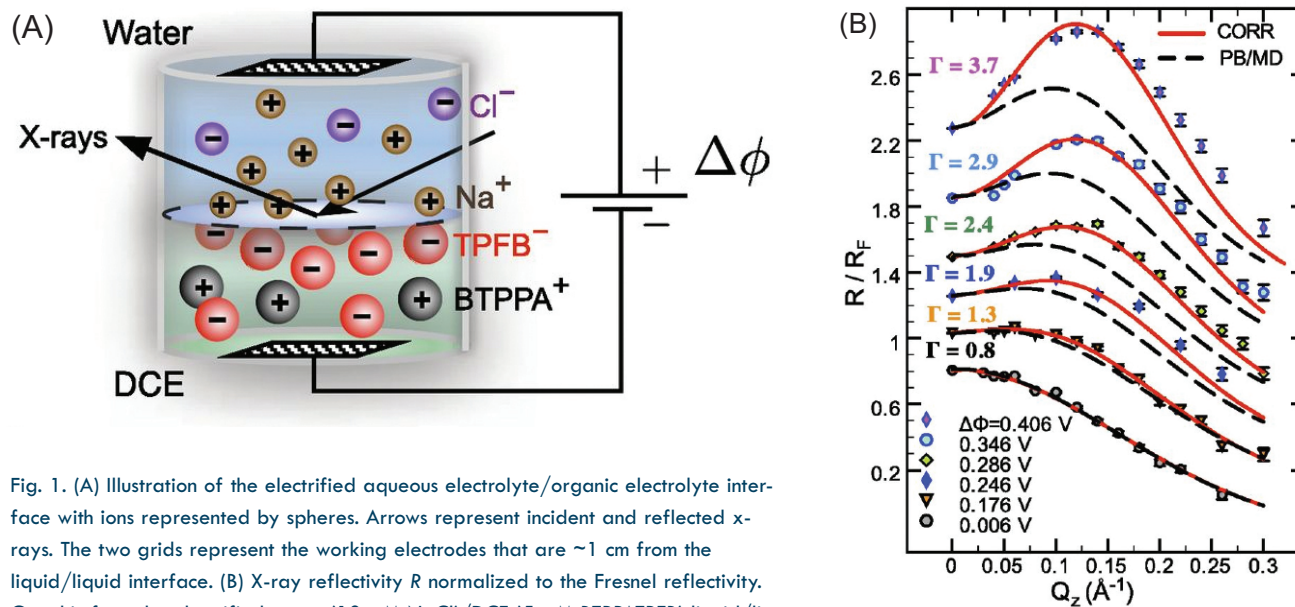


Fig. 1. (A) Illustration of the electrified aqueous electrolyte/organic electrolyte interface with ions represented by spheres. Arrows represent incident and reflected x-rays. The two grids represent the working electrodes that are ~ 1 cm from the liquid/liquid interface. (B) X-ray reflectivity R normalized to the Fresnel reflectivity. Graphic from the electrified water (10 mM NaCl)/DCE (5 mM BTPPATPFB) liquid/liquid interface as a function of wave vector transfer. From N. Laanait et al., Proc. Natl Acad. Sci USA **109** (2012). © 2012 National Academy of Sciences

Classical theory dating back a century treats ions in an electrolyte solution adjacent to a flat electrode as independent particles finding an equilibrium position in the local electric field, which in turn depends on the ion distribution. For many years, experiments have shown that this treatment is often inadequate. In particular, when the ion density is high enough that the average electrostatic energy between pairs of ions exceeds their thermal energy, ion-ion correlations arise for which that the old theory does not account.

Researchers from the University of Illinois at Chicago; Northern Illinois University; the University of Chicago; and the University of California, Santa Cruz set up a model system of two immiscible liquids to investigate ion distribution across the boundary between them. On one side was common salt, NaCl, in water. On the other was an ionic organic molecule, bis(triphenylphosphoranylidene) ammonium tetrakis(pentafluorophenyl)borate (BTPPA TPFB), in 1,2-dichloroethane. Applying a voltage across the liquid interface caused Na⁺ ions to gather on the aqueous side against TPFB⁻ ions on the other. By varying the applied potential, the researchers could alter the ion density at the interface and thereby fine-tune the balance between electrostatic and thermal ion energies.

Utilizing the high-brightness x-ray beams from beamline 15-ID-B,C,D the team measured the reflectivity of 30-keV x-rays, with a footprint of about 1 by 5 mm, across the boundary. Dividing the results by the theoretical Fresnel reflectivity for a simple plane boundary revealed a peak at a fixed

value of momentum transfer whose amplitude increases with applied potential. This signature of a layer of ions condensed at the interface suggested that ion-ion correlations might be present.

To determine the ion density profile, the researchers developed a theoretical model of the interface, based on the classic theory for ion distribution but adding ion-solvent interactions and

Ion-solvent interactions and ion-ion correlations — two factors not fully taken into account in previous analyses — play a role in determining how ions line up across the interface, information that is of significant importance for nanotechnology applications.

ion-ion correlations. Ion-solvent interactions were calculated using numerical molecular models, including molecular interactions among the various ionic and solvent chemical species and excluded-volume effects; TPFB⁻ is a large ion, approximately 1 nm in diameter. Ion-ion correlations came from a thermodynamic model that yielded the most energetically favorable configurations for the ions, given their electrostatic influence on each other.

Ion-solvent interactions tended to reduce ion density close to the boundary: Na⁺ ions tried to stay away from the organic solvent, while the TPFB⁻ ions steered clear of the aqueous layer, so that both ion types pushed back from the interface. Ion-ion interactions mainly affect the TPFB⁻ layer, making it thinner and denser because the preferred distribution is for these negative ions to huddle tighter in a sea of positive BTPPA⁺ ions.

Previous studies looked at ion-solvent interactions, but the experiments in this study explain the observed ion distribution only when the interfacial ion density was relatively small, so that

electrostatic correlations between ions could be neglected. In all other cases, both ion-solvent and ion-ion effects were important in correctly modeling the observed ion density profiles.

— David Lindley

See: Nouamane Laanait^{1*}, Miroslav Mihaylov¹, Binyang Hou¹, Hao Yu¹, Petr Vanýsek², Mati Meron³, Binhua Lin³, Ilan Benjamin⁴, and Mark L.

Schlossman^{1**}, "Tuning ion correlations at an electrified soft interface," Proc. Natl. Acad. Sci. USA **109**, 20326 (2012)

DOI:10.1073/pnas.1214204109

Author affiliations: ¹University of Illinois at Chicago; ²Northern Illinois University; ³The University of Chicago;

⁴University of California, Santa Cruz

Correspondence: **schloss@uic.edu,

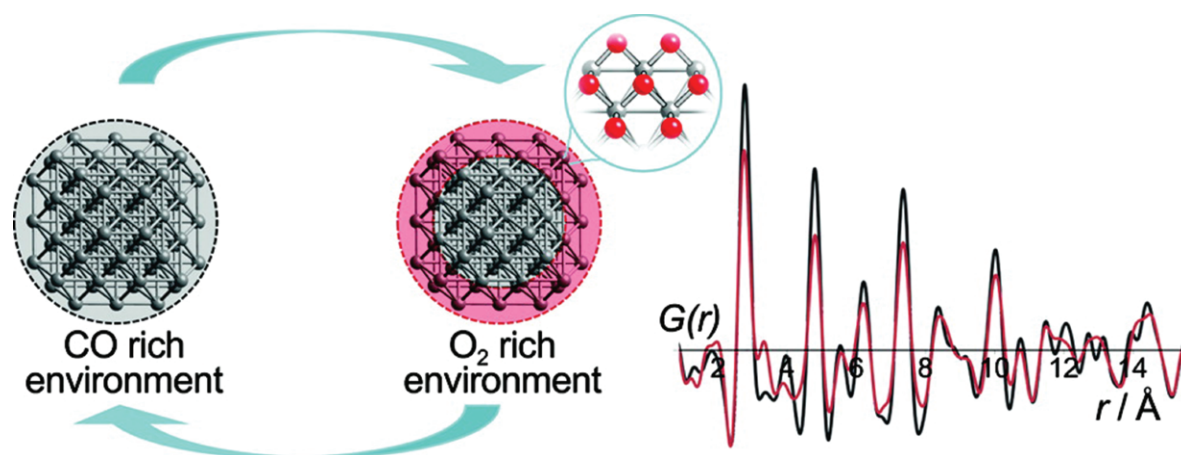
*nlaanait@anl.gov

This work was supported by a University of Illinois at Chicago Graduate Fellowship and the Graduate Assistance in Areas of National Need program (to N.L.), and National Science Foundation (NSF) Grants CHE-0910825 (to P.V. and M.L.S.) and CHE-0809164 (to I.B.). ChemMatCARS is principally supported by the NSF/Department of Energy (DOE) under grant number NSF/CHE-0822838. Use of the Advanced Photon Source at Argonne National Laboratory was supported by the DOE Office of Science under Contract No. DE-AC02-06CH11357.

15-ID-B,C,D • ChemMatCARS • Materials science, chemistry • Single-crystal diffraction, anomalous and resonant scattering (hard x-ray), wide-angle x-ray scattering, microdiffraction, liquid surface diffraction, small-angle x-ray scattering, ultra-small-angle x-ray scattering, high-pressure diamond anvil cell • 6-32 keV, 10-60 keV • On-site • Accepting general users •

OPENING A NEW WINDOW ON MATERIAL PERFORMANCE

Nanoparticles of materials, with diameters a few billionths of a meter in size, can have properties not displayed by the bulk material and certainly differing in their behavior from the individual atoms or compounds from which they are composed. This difference is exploited technologically in a wide range of applications, which includes the use of nanoparticles in catalysts for accelerating industrial reactions to commercially viable speeds, in environmental and medical sensors, for energy conversion and in remediating some forms of pollution. An international team of researchers working at XSD beamline 11-ID-B at the APS has demonstrated how analysis of high-energy x-ray total scattering data from supported platinum nanoparticles could improve our understanding of the surface catalytic properties of new materials and has implications for studying other related nanoparticles and developing new, even more powerful catalysts.



When materials are reduced to the nanoscale, their structure and reactivity can deviate greatly from the bulk or extended surface case. Utilizing the archetypal example of supported Pt nanoparticles (ca. 2-nm diameter, 1 wt % Pt on Al₂O₃) catalyzing CO oxidation to CO₂ during cyclic redox operation, high-energy x-ray total scattering, utilized with subsecond time resolution, can yield detailed, valuable insights into the dynamic behavior of nanoscale systems. This approach reveals how these nanoparticles respond to their environment and the nature of active sites being formed and consumed within the catalytic process. Specific insight is gained into the structure of the highly active Pt surface oxide that formed on the nanoparticles during catalysis. From M.A. Newton et al., *J. Am. Chem. Soc.* **134** (2012). ©2012 American Chemical Society.

The team members from the European Synchrotron Radiation Facility (France), Argonne National Laboratory, and the Johnson Matthey Technology Centre (England) carried out the total x-ray scattering measurements at 11-ID-B utilizing approximately 58-keV x-rays. They then applied pair distribution function (PDF) methods to analyze the data and extract important clues about the catalytic processes taking place on the particle surface (Fig. 1).

The team points out that such nanoparticles are not passive entities; they adapt dynamically to the changing chemical and physical conditions in which they find themselves and so it is critical for understanding and future development to observe their behavior on a suitable time scale. The group has now utilized what they refer to as an “archetypal reaction” involving alumina-supported platinum nanoparticles (with an average diameter of approximately 2 nm) involved in the oxidation of carbon monoxide to carbon dioxide. The x-ray experiments provided access to the nanoparticle dynamics on a sub-second timescale. The work not only reveals details of the changes but shows how a highly active oxide forms on the surface of the nanoparticles, which seems to be critical to catalysis of the reaction.

The superficially simple catalytic oxidation of CO to CO₂ has been studied for decades: an extra oxygen atom is added to CO with catalytic assistance. This description belies the complexity of the catalyst’s involvement in somehow cleaving an oxygen molecule, O₂, freeing up the active oxygen atoms thus released, and then attaching them individually to the CO. Revelations about the structure of the catalyst would provide important clues

as to how the reaction proceeds.

The team notes that third-generation synchrotron sources such as the APS allow them to exploit time-resolved PDF in order to reach the heart of the process and bridge the gap between the resolution of extended x-ray absorption fine structure studies and conventional x-ray crystallography on the approximate scale of 0.5 nm to 2 nm.

The researchers studied the catalysis by periodically switching between two different sets of reaction condi-

oxidizing conditions is shown to be considerably more active for the catalytic oxidation of CO than that formed under the stoichiometric gas feed.

The manner in which the experiment was conducted, along with analysis and modeling of the PDF data obtained, permits the evolution and structure of a surface oxide to be derived, *in operando* and in a significantly more precise manner than has previously been possible with more conventional measurements. This reveals details invisible to conventional

techniques and hints at how other industrially important catalytic reactions might be studied.

— David Bradley

See: Mark A. Newton^{1*}, Karena W. Chapman^{2**}, David Thompsett³, and Peter J. Chupas^{2***}, “Chasing Changing Nanoparticles with Time-Resolved Pair Distribution Function Methods,” *J. Am. Chem. Soc.* **134**, 5036 (2012).

DOI:10.1021/ja2114163

Author affiliations:

¹European Synchrotron Radiation Facility, ²Argonne National Laboratory, ³Johnson Matthey Technology Centre

Correspondence:

*mark.newton@esrf.fr,
**chapmank@aps.anl.gov,
***chupas@aps.anl.gov

The work done at Argonne and use of the Advanced Photon Source was supported by the U.S. Department of Energy Office of Science under Contract No. DE-AC02-06CH11357. M.A.N. thanks the Royal Society of Chemistry for a Journals grant (09 01 639) funding travel to participate in these measurements.

11-ID-B • XSD • Chemistry, environmental science, materials science • Pair distribution function • 58-60 keV, 90-91 keV • On-site • Accepting general users •

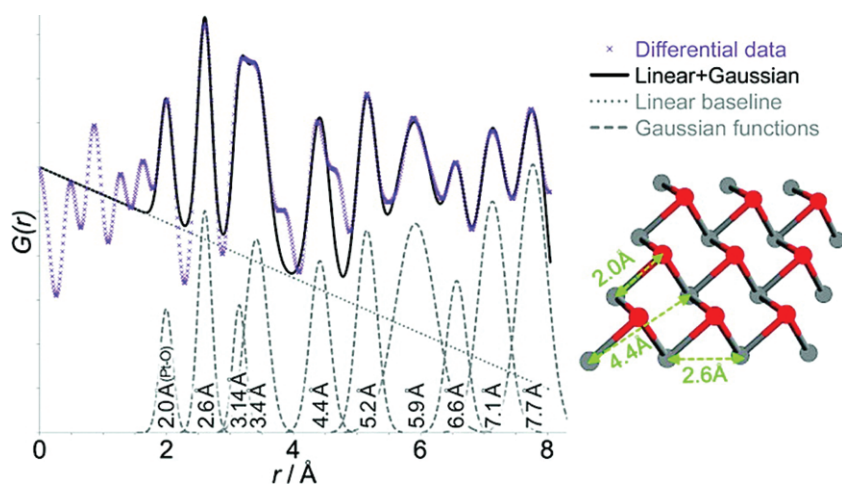


Fig. 1. A surface differential PDF ($G(r)_{ox} - G(r)_{stoich}$) corresponding to the structure generated in oxidizing conditions. Gaussian functions fit to correlations in the data suggest that it is consistent with a two-dimensional PtO₂ layer over an fcc lattice. From M.A. Newton et al., *J. Am. Chem. Soc.* **134** (2012). ©2012 American Chemical Society.

tions: oxidizing, in which there is a high concentration of oxygen gas relative to the carbon monoxide, and stoichiometric, in which there are two CO molecules for every O₂. This approach allowed them to model the behavior of the platinum-on-alumina catalyst in two distinct settings and so examine how oxygen flow affects catalytic activity.

In the stoichiometric setting, the CO molecules occupy most of the catalyst sites, slowing the rate at which oxygen can attach, be split, and reduce the rate of CO₂ formation. In contrast, higher oxygen concentration forces CO off the catalyst surface, increases the rate of oxygen splitting, and leads to a surge in CO₂ production. In both cases, the reaction comes to an equilibrium state.

Critically, the state formed under

THE KEY TO POWER FADE IN POLYMER ELECTROLYTE FUEL CELLS

Polymer electrolyte fuel cells (PEFCs) show promise as high-efficiency energy sources for stationary and mobile power applications, particularly for powering automobiles. A major challenge to cost-effective implementation of PEFC technology in many applications is sustaining power output over practical lifetimes (e.g., 5000 operating hours for automobiles). The chief contributing factor to diminished output is the loss of electrochemically active surface area (ECA) of platinum/carbon (Pt/C) electrocatalysts (Pt or Pt alloy nanoparticles on high surface area carbon supports) at the cathode as a PEFC is operated. While numerous studies using *ex situ* post-mortem techniques have provided insight into the effect of operating conditions on ECA loss, the governing mechanisms remain unspecified. To more clearly understand the electrocatalyst degradation mechanisms, researchers working at XSD beamline 12-BM-B at the APS followed Pt nanoparticle growth and oxide formation as the electrical potential of the Pt/C electrocatalyst was cycled in an aqueous acidic environment, mimicking the conditions of the PEFC. Their results illustrate the importance of limiting oxide formation and reduction to extend the life of Pt-based PEFC cathode catalysts.

The high-energy efficiency of PEFCs is due to the direct conversion of chemical energy to electrical energy. In a PEFC, hydrogen fuel flows across the anode of the fuel cell while oxygen from the air flows across the cathode. At each electrode, chemical reactions become greatly enhanced by the Pt/C electrocatalysts. The enhanced reactions ultimately give rise to electrical power across the cell and the release of water at the cathode.

The researchers from the University of Wisconsin–Madison and Argonne employed *in situ* anomalous small-angle x-ray scattering (ASAXS) at 12-BM-B to obtain particle size distributions (PSDs) of the Pt particles at periodic intervals during cycling. This *in situ* characterization permitted the researchers to correlate ASAXS-determined particle growth with oxide coverages (determined through electrochemical techniques) and the concentration of dissolved Pt lost to the electrolyte (determined by high-resolution induc-

tively coupled plasma-mass spectrometry). This multi-technique correlation demonstrated that oxide coverage plays a key role in the loss of ECA, the dissolution of Pt from smaller particles, and the increase in mean Pt particle size through redeposition of the soluble Pt species onto larger Pt particles. This outcome potentially reduces the complex changes in particle size distributions and ECA resulting from operating PEFCs using various voltage profiles to a single variable — the peak oxide coverage reached during each potential cycle.

The experiments show that holding the anodic potential constant at 1.0 V and 1.1 V results in minimal change in Pt nanoparticle mean diameter and surface area at the cathode, whereas cycling up to these potentials results in significant particle growth and surface area loss.

Over the first 80 potential cycles, the ASAXS results indicate that the dominant mechanism of particle growth

is preferential dissolution or loss of small particles, with secondary particle growth due to reprecipitation of the dissolved Pt onto existing larger particles (Fig. 1). For all three potential cycling profiles utilized in this study (triangular, trapezoidal, and square), the researchers observed a loss in the number of particles with diameters of <2.8–3.6 nm. This “critical particle diameter” of about 3 nm was found to depend on the upper potential limit of cycling and the potential profile. This type of growth is driven by the lower stability of the smaller particles and the corresponding greater tendency for dissolution.

The rapid loss of particles less than the critical diameter is responsible for the initial rapid increase in mean diameter and ECA loss of Pt/C electrocatalysts. The mean particle size then plateaus as these smallest and thermodynamically least stable particles diminish in number and the distribution is increasingly dominated by larger,

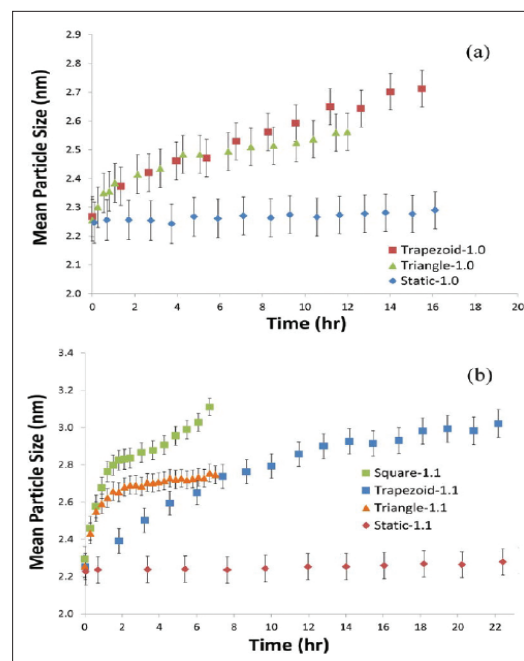
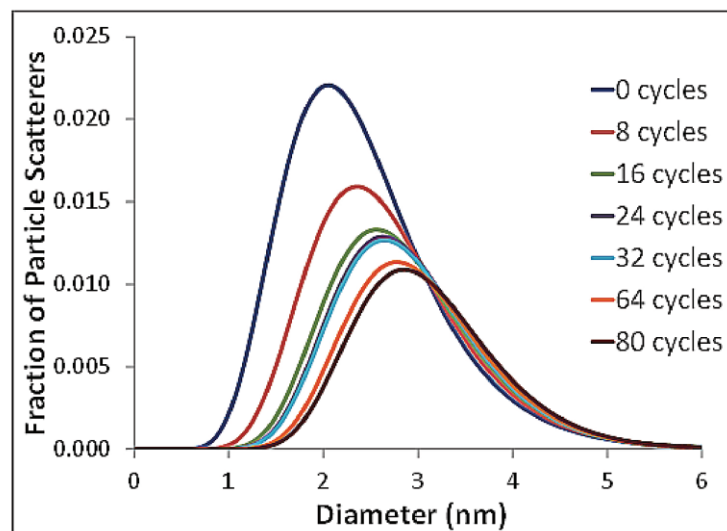


Fig. 1. Left: Results of the evolution of the particle size distribution over the first 80 potential cycles. Right: Mean particle size growth of Pt/C electrocatalysts over the duration of the experiments for experiments with anodic potential limits of (a) 1.0 V and (b) 1.1 V. From J.A. Gilbert et al., *J. Am. Chem. Soc.* 134 (August 2, 2012). © 2012 American Chemical Society

more stable particles, which are more difficult to dissolve. Beyond this plateau, further growth in mean particle size is caused by a more evenly distributed dissolution/reprecipitation mechanism, which is more prevalent for cycles with extended holds at reducing potentials. The growth mechanism thus transitions from one dominated by dissolution to one given over to dissolution/reprecipitation as the potential of the system is cycled.

The correlation of the oxide coverage, solution concentration of dissolved Pt, and ASAXS-derived PSD evolution showed that the dominant particle growth mechanism is enhanced or controlled by the same factors as oxide formation and/or oxide reduction. The anodic potential limit and the type of potential profile have direct effects on the maximum oxide coverage per cycle. This suggests that the oxide coverage reached during a cycle plays a key role in the dissolution process and in the corre-

sponding growth of the mean Pt nanoparticle size and loss of ECA.

While further work is required to establish the exact mechanism by which oxide formation is enhancing Pt dissolution, these results illustrate the importance of limiting oxide formation and reduction to extend the life of Pt-based PEFC cathode catalysts.

ASAXS proved to be a suitable technique for the *in situ* determination of the evolution of PSDs and geometric surface area distributions of Pt/C electrocatalysts with time and as a result of changing electrochemical conditions (e.g., potential cycling). This technique should also prove suitable for more complex systems (such as metal alloys, core-shell catalysts) and for studying Pt/C electrocatalysts in operating PEFCs. — *Vic Comello*

See: James A. Gilbert^{1*}, Nancy N. Kariuki², Ram Subbaraman², A. Jeremy Kropf², Matt C. Smith², Edward F. Holby^{1,‡}, Dane Morgan¹, and Deborah

J. Myers², “*In Situ* Anomalous Small-Angle X-ray Scattering Studies of Platinum Nanoparticle Fuel Cell Electrocatalyst Degradation,” *J. Am. Chem. Soc.* **134**, 14823 (August 2, 2012). DOI:10.1021/ja3038257
Author affiliations: ¹University of Wisconsin-Madison, ²Argonne National Laboratory. [‡]Present address: Los Alamos National Laboratory
Correspondence: *jagilbert@wisc.edu

This work was funded by the U.S. Department of Energy (DOE) Office of Energy Efficiency and Renewable Energy, Fuel Cell Technologies Program. Use of the Advanced Photon Source and the Electron Microscopy Center at Argonne National Laboratory were supported by the DOE Office of Science under Contract No. DE-AC02-06CH11357.

12-BM-B • XSD • Materials science • X-ray absorption fine structure, powder diffraction, general diffraction, x-ray reflectivity, fluorescence spectroscopy, small-angle x-ray scattering • 5-23 keV • On-site • Accepting general users •

THE DYNAMIC COMPRESSION SECTOR JOINS THE APS



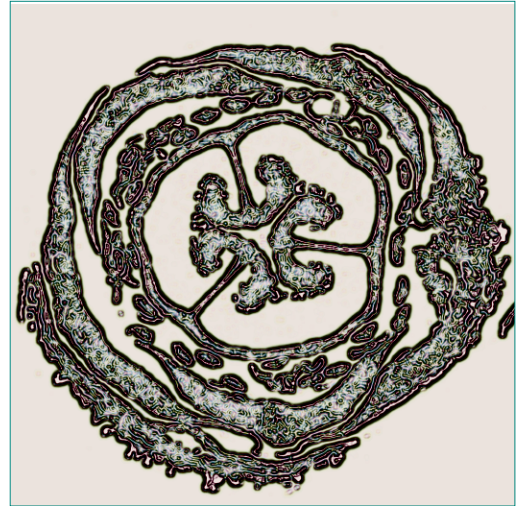
Left to right: Yogendra Gupta PI, Director, Institute of Shock Physics, WSU; Brian Stephenson, APS Director; Eric Isaacs, Argonne National Laboratory Director; Chris Deeney, Assistant Deputy Administrator for Stockpile Stewardship, NNSA; Daryll DeWald, Dean of the College of Arts and Sciences, WSU; and Keith LeChien, Federal Program Manager in the Defense Science Division, NNSA.

In the most recent addition to the family of APS beamlines, the Dynamic Compression Sector (DCS) formalized its ties with the APS in a Memorandum of Understanding (MOU) signed on September 6, 2012.

The DCS, which will reside on APS Sector 35, brings an exciting new research capability to the user program. As noted in the report from the DCS User Workshop held at Argonne in January 2012, "...*in situ*, time-resolved measurements at microscopic length scales constitute the overarching science need for achieving a fundamental understanding of the mechanisms governing time-dependent condensed matter phenomena (structural transformations, inelastic deformation and fracture, and chemical reactions) under dynamic loading."

The DCS is funded by the Department of Energy National Nuclear Security Administration (NNSA) and is managed as a partnership between Washington State University (WSU) and the APS.

Signing the MOU were Yogendra Gupta, Director of the Institute for Shock Physics at WSU; Daryll DeWald, Dean of the WSU College of Arts and Sciences; Argonne Director Eric Isaacs; and APS Director Brian Stephenson. Among the distinguished guests attending the ceremony were Chris Deeney, NNSA Assistant Deputy Administrator for Stockpile Stewardship; and Keith LeChien, NNSA Federal Program Manager in the Defense Science Division.



LIFE SCIENCE

CLUES ABOUT RHEUMATOID ARTHRITIS DAMAGE

Rheumatoid arthritis (RA) is a progressively incapacitating and devastating disease that involves destruction of many tissues within the body, but especially the joint tissues. Joints contain cartilage, which consists of collagen fibers, and synovial tissue, which produces a fluid that helps lubricate the joints. Both the cartilage and synovial tissue are damaged by RA. The exact cause(s) of the destruction of joint tissues by RA have been unclear. But with the use of x-ray crystallography at an APS beamline, researchers with the Illinois Institute of Technology were able to view the actions of an antibody targeted toward the proteoglycan biglycan — one of a group of polysaccharide-protein conjugates present in connective tissue and cartilage — that may help illustrate the underlying pathology of RA and help develop therapies and treatments.

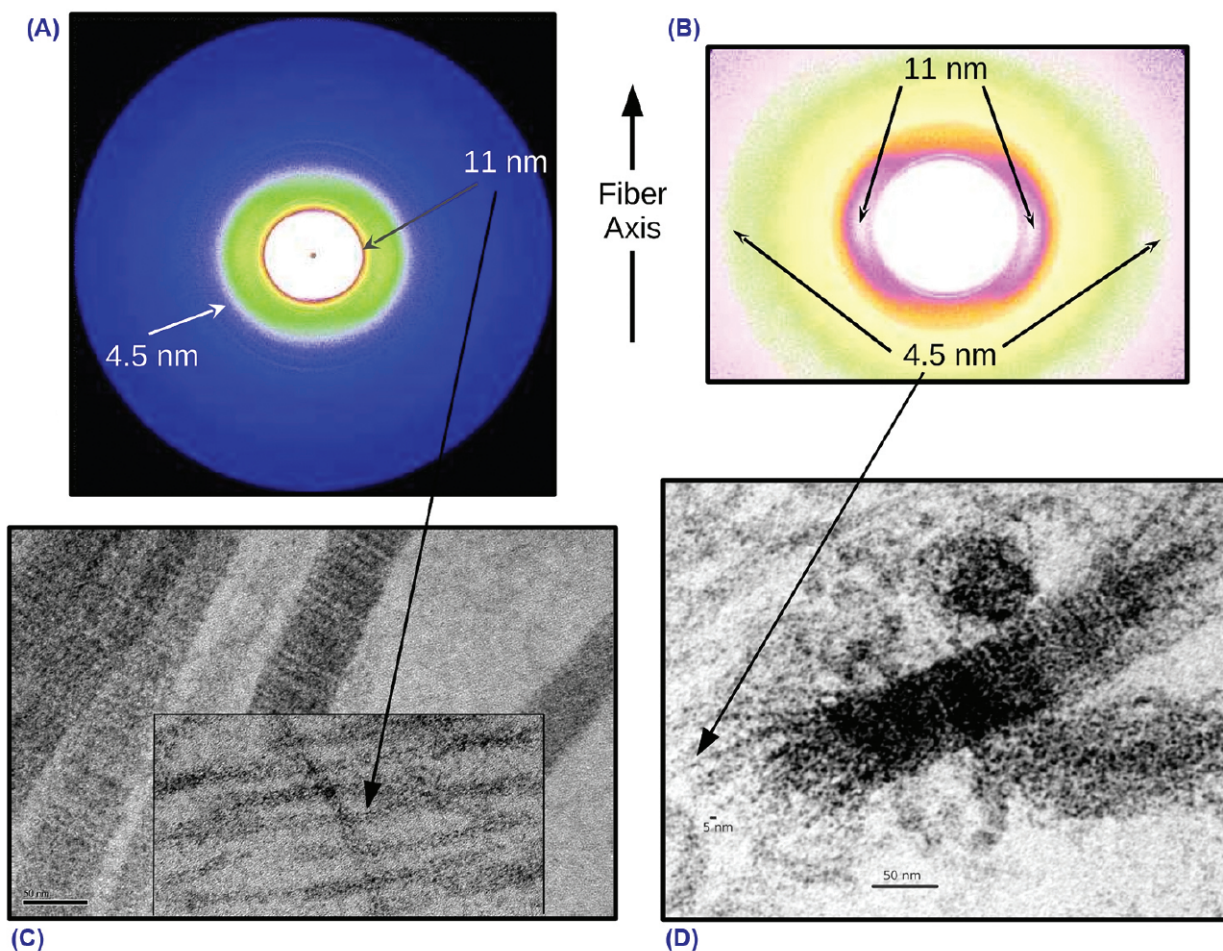
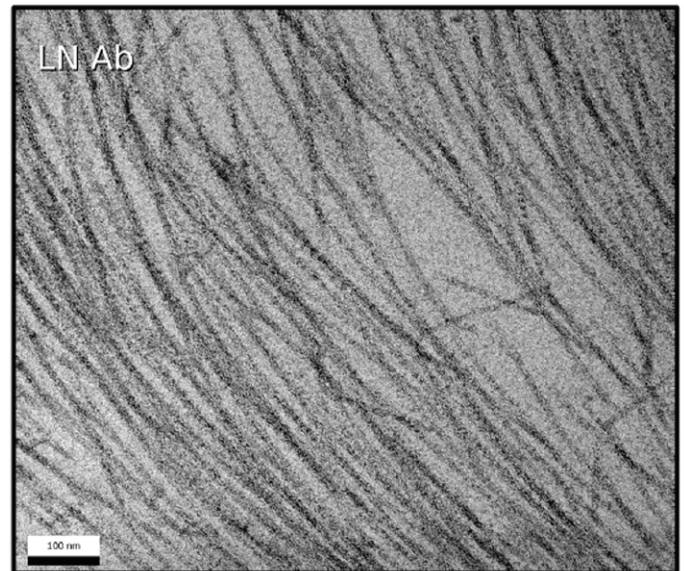
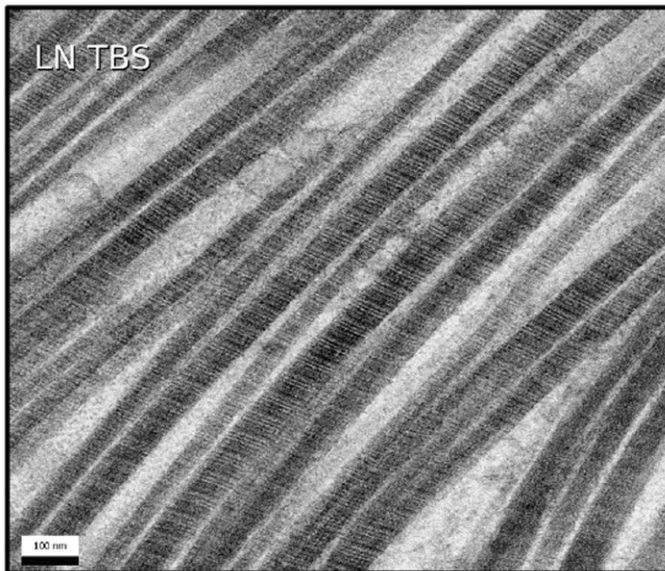


Fig. 1. Type II collagen fibrils decomposed into their basic aggregates (viewed via x-ray diffraction and TEM). Some parts of the antibody-treated samples maintain a loose alignment of the thin-fibrils allowing them to be analyzed with small-angle x-ray diffraction (A) and insert (B). An 11- and 4.5-nm packing function are apparent, which appear to correspond to the approximate diameter of the thin-fibrils [insert of (C)] and microfibrils (D). Native thick fibrils are shown in (C) as a comparison to the decomposition product (thin-fibrils). Both figures from O. Antipova and J.P.R.O. Orgel, PLoS ONE 7(3), e32241 (March 2012).



Left: Native (prior to fixing) type II collagen fibrils, incubated in TBS as control. Average fibril size is around 35 nm. Right: Collagen type II fibrils following short incubation with anti-biglycan antibody. Fibril diameter is 10-15 nm.

The findings in part are based on x-ray diffraction data collected at the Bio-CAT 18-ID-D beamline at the APS (Fig. 1). The role of x-ray crystallography was central to the work because the researchers could view the structure of antibody disrupted tissue without concern that sample preparation had introduced artifacts.

About 1% of the U.S. population is affected by RA, and the disease strikes women up to three times as often as men. RA is characterized by a highly variable disease course. Some of the afflicted have mild and transient symptoms, but most will experience ongoing disease for the rest of their lives. Many different types of treatments can alleviate symptoms and/or modify the disease process; however, there is no known cure for rheumatoid arthritis and a need exists for therapies that will halt the underlying disease processes.

The current study speculates as to what happens to the joint cartilage collagen fibrils during RA. Proteins called proteoglycans bind to collagen and help to stabilize the collagen bundles and keep it healthy. In this study, utilizing x-ray crystallography and transmission electron microscopy (TEM), the researchers demonstrated that an antibody against a proteoglycan called biglycan resulted in tissue destruction that may be comparable to what actually happens in RA-affected tissues.

According to the researchers, ele-

vated levels of anti-biglycan antibodies are detected in the body fluids of arthritis patients and are considered an early warning sign of the disease, but their specific role has not previously been clarified. To test their theory about the antibody levels as early-warning signs, the researchers incubated thin pieces of cartilage with antibody for various time points and then visualized the extent of tissue disruption with TEM and with x-ray diffraction experiments carried out at 18-ID-D.

The x-ray diffraction data produced what has been described by these researchers as a plausible molecular mechanism for RA. According to the team, the destructive effect of the antibody was more potent than that of chemicals and other treatments often used to mimic RA tissue damage. The researchers suggest that the initiation of RA-associated tissue destruction during the actual disease process may involve a similar antibody-mediated breakdown of collagen fibrils that they observed in their study.

This proposed model highlights the crucial position of the biglycan antibody in the development of rheumatoid arthritis and the associated observations provide the first indication of what its role is beyond being a marker of this common and widespread disease. These findings pave the way for further studies; a greater understanding of the destructive process in RA may help in

developing therapies to ultimately prevent or delay joint disruption and help treat millions of patients with RA.

— Emma Hitt

See: Olga Antipova** and Joseph P.R.O. Orgel*, “Non-Enzymatic Decomposition of Collagen Fibers by a Biglycan Antibody and a Plausible Mechanism for Rheumatoid Arthritis,” *PLoS ONE* 7(3), e32241 (March 2012). DOI:10.1371/journal.pone.0032241

Author affiliation:

Illinois Institute of Technology

Correspondence: *orgel@iit.edu

**olga.antipova@gmail.com

This work supported by the National Science Foundation (Grant #MCB-0644015 CAREER). Material is based on the work supported by, or in part by, the U.S. Army Research Laboratory and the U.S. Army Research Office under contract/grant number W911NF 09-1-0378. Bio-CAT is supported by grants from the National Institute of General Medical Sciences (9 P41 GM103 622-18) from the National Institutes of Health. Use of the Advanced Photon Source at Argonne National Laboratory supported by the U.S. Department of Energy Office of Science under Contract No. DE-AC02-06CH11357.

18-ID-D • Bio-CAT • Life sciences • Fiber diffraction, microdiffraction, microfluorescence (hard x-ray), small-angle x-ray scattering, time-resolved x-ray scattering, micro x-ray absorption fine structure • 3.5-35 keV • On-site • Accepting general users •

MODERN IMAGING TECHNIQUES REVEAL STRUCTURES OF ANCIENT FLOWERS

The first known appearance of flowering plants (angiosperms) dates to over 130 million years ago (Ma), near the beginning of the geologic Cretaceous Period. Over the last few decades, new fossil finds coupled with genetic information gleaned from extant representatives of angiosperms have helped provide new details of their astonishing diversification through time. An international team of paleobotanists recently added to our knowledge of angiosperm evolution a description of the extinct species *Glandulocalyx upatoiensis*. This scientific classification represents a new (proposed) species and genus. Fossilized remains of *G. upatoiensis*, carbonized under high heat, were found in the U.S. state of Georgia, within strata dating to the Santonian age (86.3-83.6 Ma). The fossil specimens studied consisted of floral buds in various stages of development. Several imaging methods were utilized to probe their intricate structures. Fully three-dimensional, high-resolution images of several fossilized specimens were obtained using synchrotron radiation x-ray tomographic microscopy (SRXTM) at the APS and the SPring-8 light source in Japan.

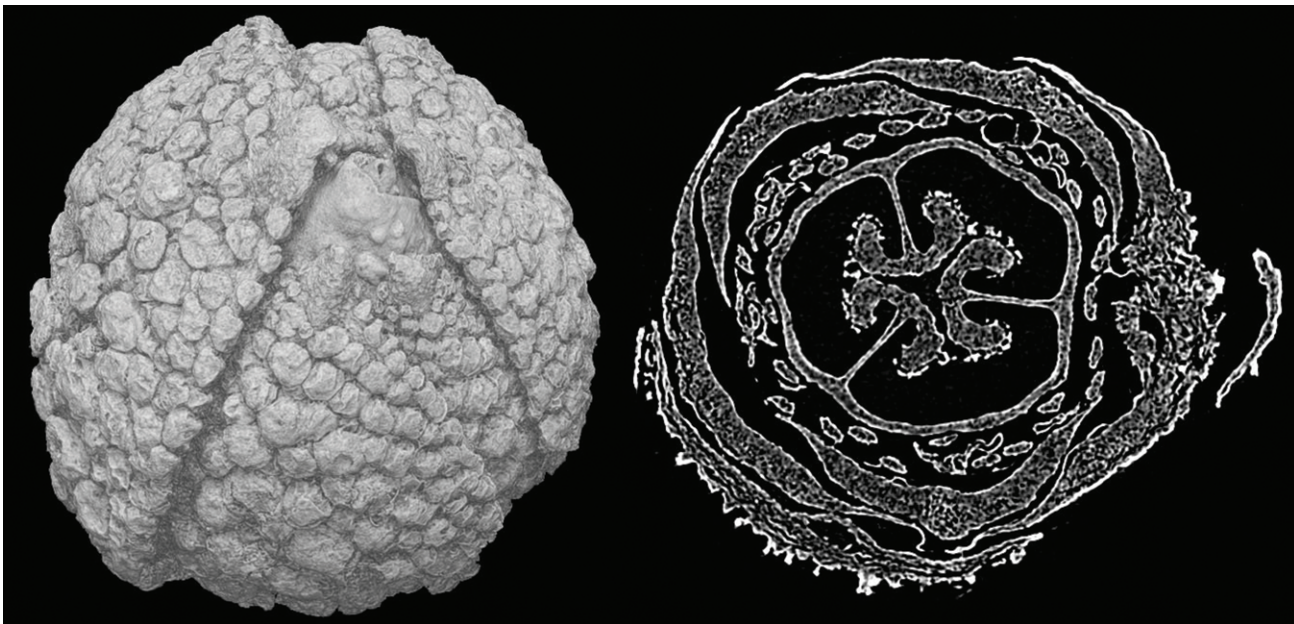


Fig. 1. Synchrotron radiation x-ray tomography reconstructions of floral buds of *Glandulocalyx upatoiensis*. Left: top-view of a floral bud with five imbricate (i.e., overlapping) sepals with conspicuous, multicellular trichomes (appearing as multiple surface bumps). The bud is 2.5 mm in diameter. Right: transverse section through a second specimen, 2.1 mm in diameter, showing details of floral organization, including five imbricate petals, numerous stamens (the tiny, mostly oval-shaped spots forming a ring halfway from the center), and a trimerous, syncarpous pistil (i.e., the flower's female reproductive structure composed of three fused carpels) in the center. The sepals are only partially preserved in this second specimen.

Angiosperms are among the most successful and diverse group of plants on Earth, encompassing well over a quarter million species. To place the fossil specimens examined for this study within the evolutionary framework of flowering plants, the researchers from the University of Vienna (Austria), Niigata University (Japan), Argonne, Yale University, and the Chicago Botanic Garden needed to determine the plants' particular structural characteristics and compare them to the characteristics of various known groups of angiosperms.

The 13 fossil buds examined in this study constituted a small portion of the total number collected from the banks of Upatoi Creek (from which the species name *upatoiensis* is derived) located in central-western Georgia. The fossils buds were quite small, having maximum lengths around 5 mm, and were exquisitely preserved within the sediments encasing them.

The intricate fossil structures were probed with the SRXTM technique, scanning electron microscopy (SEM), and visible light microscopy. The SEM method entailed first sputter-coating specimens with gold or gold-palladium. The coated samples were then scanned by an electron microscope to create images. Visible light microscopy was used to examine very thin slices of specimens. Obviously, this later technique is destructive, since fossil specimens must be cut.

The SRXTM method employed at XSD beamline 2-BM-A,B at the APS, and at the BL20B2 beamline at SPring-8, on the other hand, is non-destructive. SRXTM utilizes principles similar to those of a medical computer-aided tomography scan: three-dimensional images of an object's volume are generated via x-rays passing through incremental sections of the object. The individual x-ray data sets are then utilized to produce high-resolution, cross-sectional images that reveal the internal structure of the object. Figure 1 shows a cross-section of a *G. upa-*

toiensis bud produced using SRXTM.

Several features of the fossil specimens led the researchers to recognize them as members of the asterid clade of flowering plants (a clade represents all organisms descended from a common ancestor). The asterids arose around 90 Ma during the Late Cretaceous (spanning approximately 100-66 Ma). Within the asterid clade, the researchers were further able to assign their fossil flowers to the group (or order) Ericales.

Ericales encompasses a large number of diverse angiosperm families. Just a few of the living species within Ericales are blueberry, persimmon, and azalea. The high-resolution images produced with the SRXTM and SEM techniques revealed structural details that helped identify the families of Ericales to which the fossil specimens are most closely related. These structural details included the quantities and orientations of the flower's organs including the sepals (sepals are the outermost and protective organs in a flower); the petals; stamens (the male reproductive organs incorporating pollen); and carpels (the female reproductive organs containing the ovules), as well as other floral features.

Images of the fossil buds revealed key attributes, such as pentamerous characteristics (penta meaning five), appearing as five overlapping petals and five overlapping sepals. Trimerous characteristics (tri meaning three) were present in the female part of the flower, which was composed of three united carpels. Of particular interest was the male part of flower buds that contained between 20 and 28 extrorse (outward-facing) stamens.

Noting these and many other characteristics exhibited by the fossil buds, the researchers determined that *G. upatoiensis* is best placed within the family Actinidiaceae (the Kiwi-fruit family) of the Ericales group of asterids. The ability to place *G. upatoiensis* in the asterid evolutionary tree is a testament to the power of the sophisticated

imaging techniques used in the study, most notably synchrotron-based SRXTM.

The researchers caution that in spite of the strong evidence they have gathered, the correct phylogeny (evolutionary position) for *G. upatoiensis*, as well as for other Ericales specimens from the Late Cretaceous, cannot be determined with total certainty until additional knowledge is gained concerning angiosperm diversity and structure.

— William A. Atkins and Philip Koth

See: Jürg Schönenberger^{1*}, Maria von Balthazar¹ Masamichi Takahashi², Xianghui Xiao³, Peter R. Crane⁴, and Patrick S. Herendeen⁵, "*Glandulocalyx upatoiensis*, a fossil flower of Ericales (Actinidiaceae/Clethraceae) from the Late Cretaceous (Santonian) of Georgia, USA," *Ann. Bot. London* **109**, 921 (2012). DOI:10.1093/aob/mcs009
Author affiliations: ¹University of Vienna, ²Niigata University, ³Argonne National Laboratory, ⁴Yale University, ⁵Chicago Botanic Garden

Correspondence:

*juerg.schoenenberger@univie.ac.at

This work was supported by a grant-in-aid (18570083) from the Ministry of Education, Science, and Culture of Japan to M.T. This work was initiated with support from the Japan Society for the Promotion of Science (S-97128, S-98106) and the National Science Foundation (EAR-9614672) to P.R.C., and completed, in part, with financial support from the World Class University program of the National Research Foundation of Korea (R33-10089). Use of the Advanced Photon Source, an Office of Science User Facility operated for the U.S. DOE Office of Science by Argonne National Laboratory, was supported by the U.S. DOE under Contract No. DE-AC02-06CH11357.

2-BM-A,B • XSD • Physics, life sciences, geoscience, materials science • Tomography, phase contrast imaging • 5-30 keV, 10-30 keV • On-site • Accepting general users •

A NEW PHASE IN CELLULAR COMMUNICATION

In many physical processes, substances undergo phase transitions where they are transformed from one state (solid, liquid, or gas) to another. Wiskott-Aldrich Syndrome Proteins (WASP) function as intracellular signaling molecules, and one member of the family, N-WASP, interacts with two other proteins, forming a complex that plays an integral role in the regulation of the cell's internal scaffold. This interaction provides a system for investigation of phase transitions that result from multivalent protein-protein interactions. Utilizing the Bio-CAT synchrotron x-ray facility at the APS, researchers investigated interactions between engineered multivalent substances. Understanding this research will be important in guiding future studies to further evaluate the role of phase transitions in biological systems.

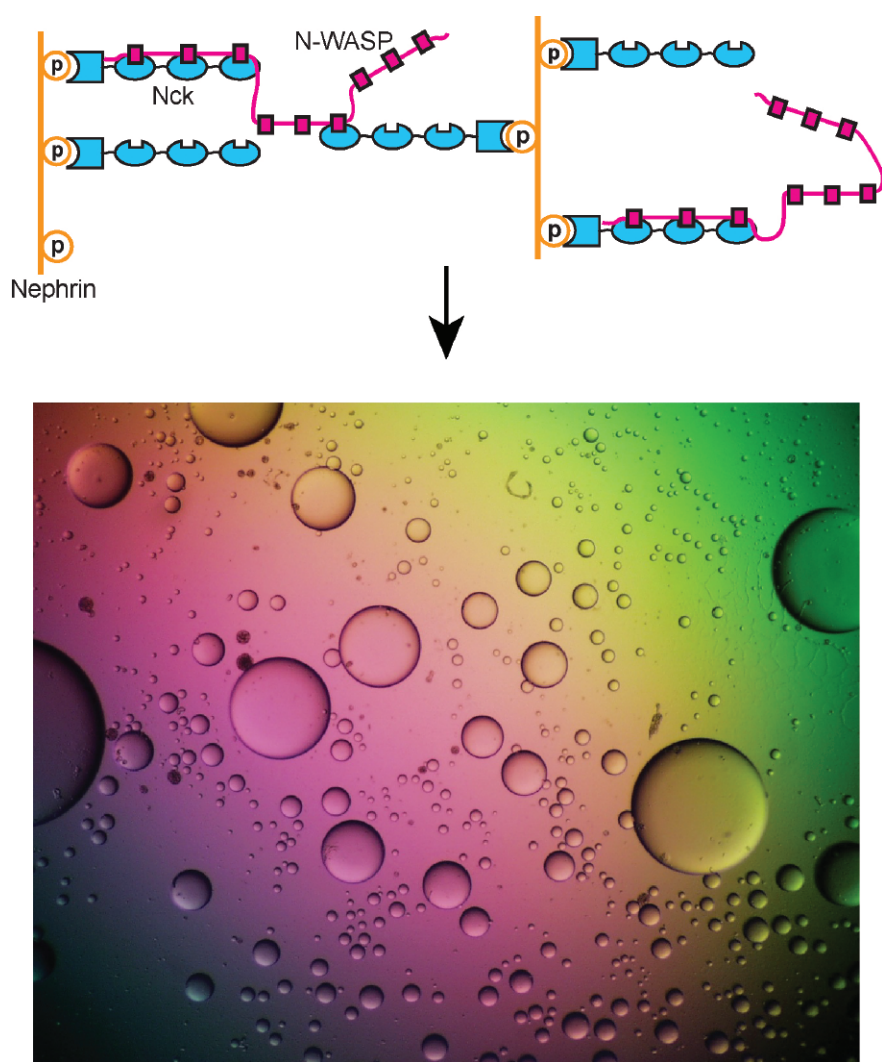


Fig.1. Interactions between N-WASP, phospho-Nephrin, and Nck produce large polymers (top panel) that phase separate to produce liquid droplets suspended in aqueous solution (bottom panel).

The researchers in this study, from the University of Texas Southwestern Medical Center; the Illinois Institute of Technology; Louisiana State University; the University of California, Berkeley; and The Pennsylvania State University described the occurrence of sharp liquid-liquid-demixing phase separations corresponding to transformation between small complexes and large polymers at the molecular level, leading to the production of micrometer-diameter liquid droplets in aqueous solution. This phenomenon was observed for several different protein systems, suggesting that it may be a general property of multivalent macromolecules. In the N-WASP system, phosphorylation of one of its interacting proteins by a kinase enzyme controls the phase separation, showing how this behavior could be regulated *in vivo*.

Phase transitions occur widely throughout nature, and involve transformation of a substance from one phase to another in response to changes in external conditions. One well-known example is that of evaporation, where liquid water is transformed to water vapor when temperature reaches a critical value (100° C at 1 atm pressure).

It has been known since the 1940s that interactions between multivalent (multiple unit) small molecules can lead to "sol-gel transitions," which involve sharp transformations between small assemblies and large polymer gels. In these processes, the sol-gel transition can occur when the concentration of the molecules reaches a critical value.

Just as differences in pressure can change the boiling point of water, differences in the physical properties of a multivalent molecule can change the critical concentration for a sol-gel transition. The polymer formed by these transitions can take on various physical forms, from liquid to solid, again depending on the properties of the molecules.

Multivalency has been investigated mostly in relation to extracellular substances binding to receptors on the cell surface. In this context, protein systems aggregate to form cross-linked networks, especially precipitates, but also liquid-like gels.

Many biological processes involve interactions between multivalent molecules, including intracellular signaling. Members of the WASP family of proteins act as intracellular signaling molecules in the regulation of the cellular scaffolding, or cytoskeleton. They are involved in the transfer of signals from receptors on the cell surface to the inside of the cell, where they promote assembly of the cytoskeletal protein actin into long filaments. N-WASP is a member of this family with the highest levels in the nervous system, and, together with its two protein partners (Nck and phosphorylated nephrin), represents a system for investigation of phase transitions that result from multivalent interactions.

This study aimed to investigate multivalency in relation to intracellular molecules, and in particular to determine whether these systems also experience sharp transformations to polymers. Utilizing small-angle x-ray scattering at the Bio-CAT 18-ID-D beamline to evaluate reactions, the researchers showed that interactions

between synthetic, multivalent substances result in sharp liquid-liquid-demixing phase separations, in which two liquid substances separate to produce 1-50- μm -diameter liquid droplets in aqueous solution (analogous to oil droplets in water). At the molecular level, this correlates with a transformation between small complexes and large polymers.

When they investigated N-WASP in this way, the researchers discovered that when it interacts with its two protein partners, a phase transition also occurs (Fig. 1). This transformation is regulated by the degree of phosphorylation of nephrin, demonstrating how kinase enzymes could control this behavior of the system.

Further, the phase transition also increases the ability of N-WASP to promote formation of actin filaments, explaining why this behavior might be biologically important. This study has provided new insights into how macroscopic structures (phase separated liquid droplets) can be generated from individual protein molecules. The work has also suggested why this behavior may be important in biological processes, including intracellular signaling.

These results will help guide research in biophysics, biochemistry, and cell biology on the assembly of proteins into large structures in the cell. Since multivalent systems are very common in nature, it seems possible that phase transitions may be involved in many aspects of biology through their ability to control spatial organization within cells, and regulate biochemical information transfer.

— *Nicola Parry*

See: Pulong Li¹, Sudeep Banjade¹, Hui-Chun Cheng¹, Soyeon Kim¹, Baoyu Chen¹, Liang Guo², Marc Llaguno¹, Javoris V. Hollingsworth³, David S. King⁴, Salman F. Banani¹, Paul S. Russo³, Qiu-Xing Jiang¹, B. Tracy Nixon⁵, and Michael K. Rosen^{1*}, “Phase transitions in the assembly of multivalent signalling proteins,” *Nature* **483**, 336 (5 March 2012).

DOI:10.1038/nature10879

Author affiliations: ¹University of Texas Southwestern Medical Center; ²Illinois Institute of Technology; ³Louisiana State University; ⁴University of California, Berkeley; ⁵The Pennsylvania State University

Correspondence:

*Michael.Rosen@utsouthwestern.edu

This work was supported by the following: the Howard Hughes Medical Institute and grants from the National Institutes of Health (NIH) (R01-GM56322) and Welch Foundation (I-1544) to M.K.R., a Chilton Foundation Fellowship to H.-C.C., a NIH EUREKA award (R01-GM088745) to Q.-X.J., a NIH Cancer Biology T32 Training Grant to M.L., a National Science Foundation award (DMR-1005707) to P.S.R. and a Gates Millennium Fund award to J.V.H. Bio-CAT is supported by grants from the National Institute of General Medical Sciences (9 P41 GM103 622-18) from the National Institutes of Health. Use of the Advanced Photon Source at Argonne National Laboratory was supported by the U.S. Department of Energy Office of Science under Contract No. DE-AC02-06CH11357.

18-ID-D • Bio-CAT • Life sciences • Fiber diffraction, microdiffraction, microfluorescence (hard x-ray), small-angle x-ray scattering, time-resolved x-ray scattering, micro x-ray absorption fine structure • 3.5-35 keV • On-site • Accepting general users •

BREAKING RECORDS IN NEUROLOGICAL MICRORADIOLOGY

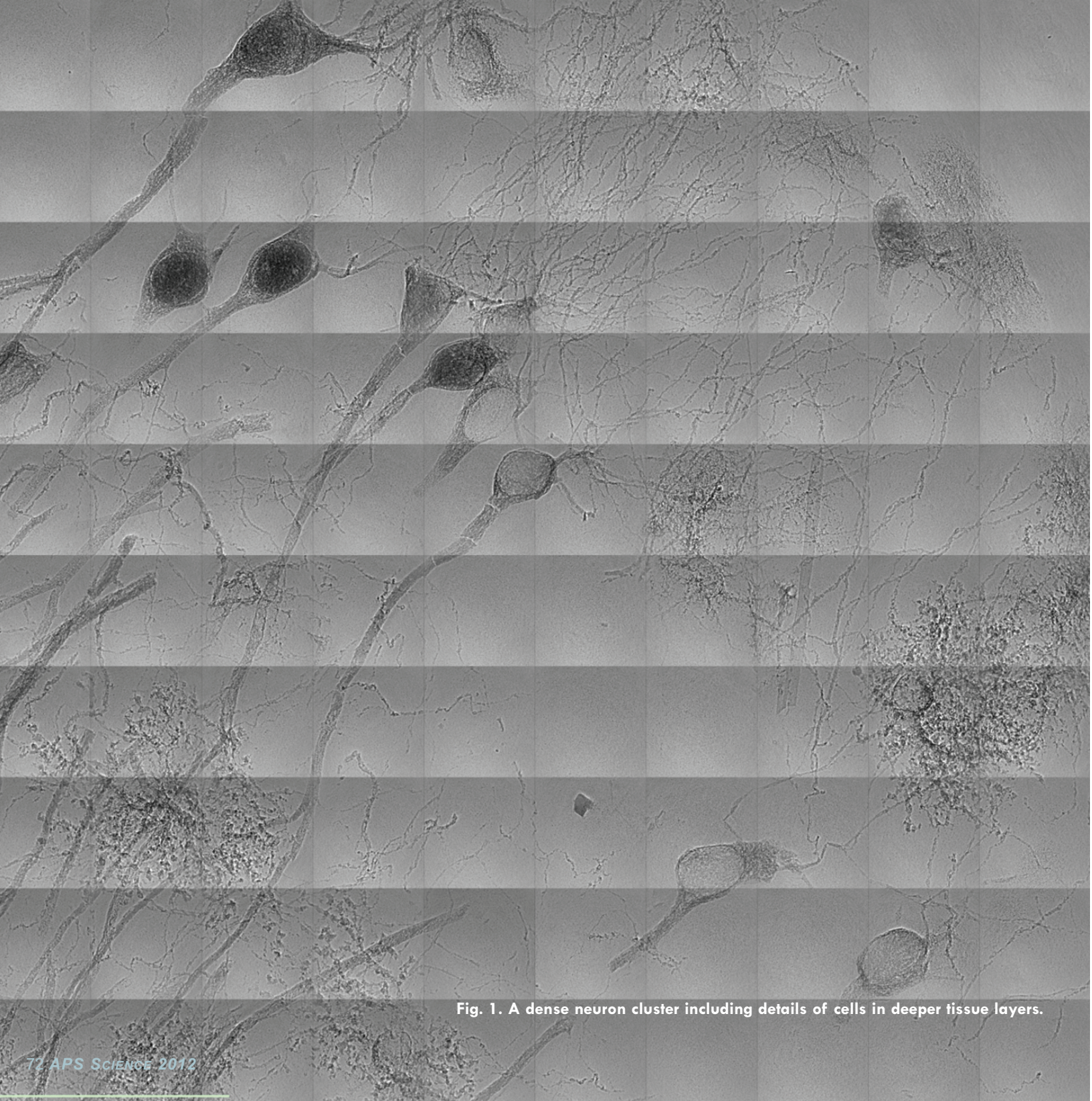


Fig. 1. A dense neuron cluster including details of cells in deeper tissue layers.

As neuroscientists probe ever deeper into the mysteries of the brain and nervous system, they need ever sharper vision. A group of researchers has developed some exciting new techniques for imaging neuronal and synaptic networks utilizing the APS. These techniques provide images with unprecedented detail and world-record resolution, and open the door to three-dimensional tomographic reconstructions, a vital tool for studying the complex, tree-like branching nature of neuronal networks.

Understanding intricate neuronal and synaptic networks, particularly in more complex mammalian brains, requires high-resolution mapping of large volumes of tissue, preferably in three dimensions in order to capture all the subtle structural details. Mapping neuron networks has been providing a very significant understanding of how the brain works. While such work has been quite successful in the study of small organisms such as *Caenorhabditis elegans* and *Drosophila*, the available optical and electron microscopy techniques are not quite up to all of the special challenges posed by neuroradiology, even though they are invaluable for startlingly clear imaging of other types of tissue.

Methods mainly based on fluorescence and optical microscopy face the problem of not being able to examine larger mammalian brains. The method employed in this study takes advantage of the high penetration of hard x-rays and new developments in nanoresolution.

Working at the XSD 32-ID-B,C x-ray beamline, the researchers from Brookhaven National Laboratory, EPFL (Switzerland), Pohang University of Korea, and National Cheng Kung University (Taiwan) achieved significant breakthroughs in neurological microradiology, including a Rayleigh contrast resolution of about 16.5 nm at 8 keV — a world record for resolution with hard x-rays. They examined sections of mouse cerebellum to demonstrate their approach.

The researchers pushed the neuroradiology envelope by using new nanofabrication techniques to create Fresnel zone plates that also acted as magnifying lenses. Their zone plate design achieved a delicate compromise between the narrow structure needed for high resolution and the thickness

required to focus the hard x-rays.

This proved to be the key to coupling the penetrating power of x-rays with the extreme resolution required to visualize extremely fine subcellular details.

Nanoscale x-ray microscopy is still only available with synchrotron x-rays. This new level of resolution performance was not possible with the previous state-of-the-art x-ray optics. The researchers noted that the high brightness of APS x-rays were another key factor allowing them to pursue very-high-resolution imaging of the fine details of neuron networks.

The team also developed a new staining technique specifically tailored to microradiology. Staining is essential for proper visualization of neurological structures.

But the long-established techniques used for optical microscopy are not workable in microradiology, where thicker specimen samples are the rule, meaning that fluorophores in the staining material can't provide sufficient x-ray enhancement.

After an extensive search for a suitable procedure, the experimenters finally settled on a modification of the mercury and silver-based Golgi-Cox protocol generally used for staining neurons. By simply extending the incubation period to a month or longer, they found that the stain was able to perfuse throughout the entire depth of the specimen, allowing visualization of cells in the deepest tissue layers.

These two new techniques not only provided images of unprecedented detail and resolution (Fig. 1), but also allowed the generation of three-dimensional tomographic reconstructions, which are a vital tool for studying the complex tree-like branching nature of neuronal networks.

The researchers are already look-

ing ahead to further refining these methods and developing newer techniques of ever greater sophistication. The team intends to fabricate higher resolution and higher efficiency zone plate optics and develop more stable mechanics. With collaborations they will continue the challenging work to obtain neuron images of as many neuron cells as possible in order to study their relation to neuronal diseases.

— Mark Wolverton

See: H.R. Wu^{1,2}, S.T. Chen¹, Y.S. Chu³, R. Conley³, N. Bouet³, C.C. Chien¹, H.H. Chen¹, C.H. Lin¹, H.T. Tung¹, Y.S. Chen¹, G. Margaritondo⁴, J.H. Je⁵, and Y Hwu^{1,2,6*}, "Nanoresolution radiology of neurons," *J. Phys. D* **45**, 242001 (2012).

DOI:10.1088/00223727/45/24/242001

Author affiliations: ¹Academia Sinica, ²National Tsing Hua University, ³Brookhaven National Laboratory, ⁴Ecole Polytechnique Fédérale de Lausanne, ⁵Pohang University of Science and Technology, ⁶National Cheng Kung University

Correspondence:

*phhwu@sinica.edu.tw

This research was supported by the National Science and Technology for Nanoscience and Nanotechnology; the Academia Sinica; the Fonds National Suisse pour la Recherche Scientifique; the Ecole Polytechnique Fédérale de Lausanne; the Center for Biomedical Imaging; and the Brookhaven Science Associates, LLC, under Contract No DE-AC02-98CH10886. Use of the Advanced Photon Source at Argonne National Laboratory is supported by the U.S. Department of Energy Office of Science under Contract No. DE-AC02-06CH11357.

32-ID-B,C • XSD • Materials science, life sciences, geoscience • Phase contrast imaging, radiography, transmission x-ray microscopy, tomography • 7-40 keV • On-site • Accepting general users

RNA FOLDING: A LITTLE COOPERATION GOES A LONG WAY

Synchrotron x-ray scattering experiments carried out at the Bio-CAT beamline at the APS allowed researchers to investigate the unique folding behavior of ribozyme using a particular RNA that acts as a catalyst. Their work provides a path for helping to predict the structures of newly discovered noncoding RNAs, and will ultimately further enhance understanding of important information about these biological functions.

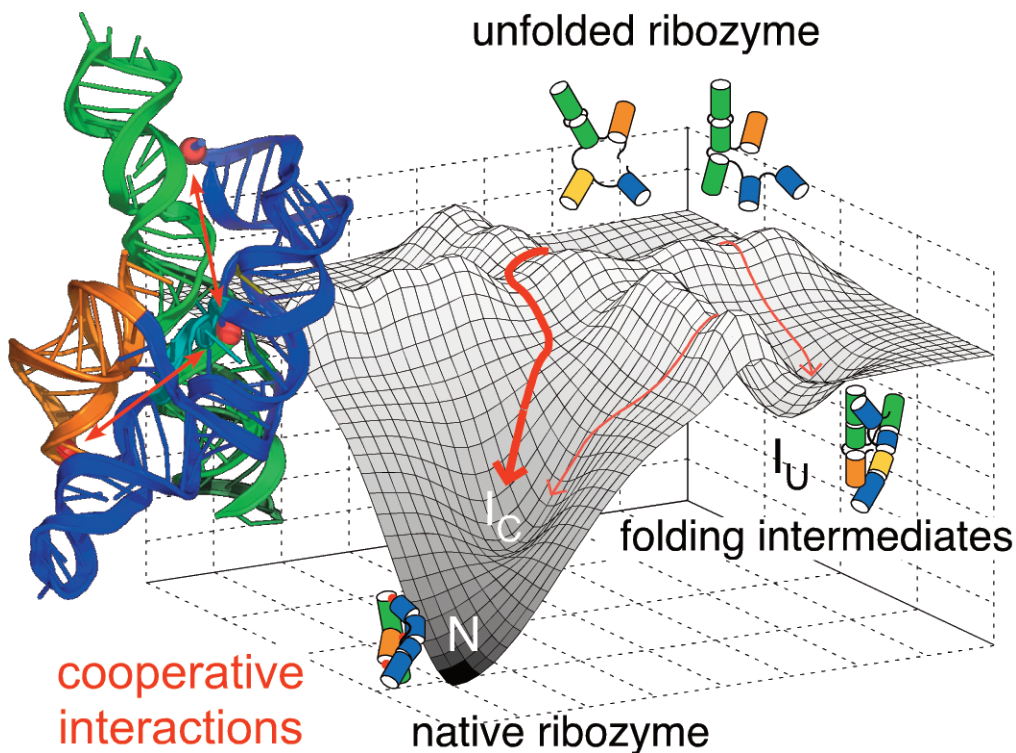


Fig.1. Shown here is the energy landscape for the folding of a ribozyme, and how cooperation between tertiary interactions at different parts of the structure (red dots) help the RNA reach its unique native structure and avoid non-native intermediates.

The nucleic acid RNA carries the instructions for the critical process by which cells in our bodies build or manufacture proteins. But non-coding RNAs also exist whose sequences, while not converted into proteins, play important roles in many biological processes.

RNA molecules aggregate into complex three-dimensional (3-D) or “tertiary” structures, producing globular forms stabilized by various interactions. Proteins, ligands, and other RNA molecules recognize these folded RNAs and result in the biochemical pathways that affect all aspects of cellular metabolism.

RNA is one of two types of nucleic acids found in all cells. Its main role is to carry instructions for protein synthesis from DNA, the second type of nucleic acid, which stores the genetic information in cells. While messenger RNA represents the RNA that codes for proteins, noncoding RNAs also exist that are not translated into proteins. Noncoding RNAs are found widely in biology, having roles in the process of protein translation or gene regulation, for example.

It is now thought that noncoding RNAs play a role in even more biochemical functions than originally suspected. To do this, noncoding RNAs must adopt unique, complex 3-D structures that are critical to their function, creating sites that allow for chemical reactions or control gene expression.

The tertiary structure of RNA refers to the 3-D arrangement of RNA building blocks that are held together via connections known as tertiary interactions. Although studies of noncoding RNAs have revealed the existence of structural themes called tertiary motifs, the exact mechanism by which these encode the self-assembly of unique 3-D RNA structures remains poorly understood. This study aimed to examine why RNAs fold so specifi-

cally in spite of the relatively small number of tertiary motifs.

Using small-angle x-ray scattering (as well as other techniques) at Bio-CAT beamline 18-ID-D to measure changes in the folding energy landscape, the researchers from Johns Hopkins University, the University of Maryland, and the National Institute of Standards and Technology (NIST) showed that these tertiary interactions are highly related to the folding intermediates of the ribozyme.

A key finding was that the formation of structural motifs is cooperatively linked in near-native folding intermediates, and this cooperativity depends on the native helix orientation. The research team demonstrated how this cooperativity occurs early in the RNA folding process.

Coupling between tertiary structures in different areas of the RNA inhibits nonnative structures, while favoring the active RNA structure by increasing the free energy gap between the native state and the next most stable structure, thus simplifying the search for the native fold (Fig 1).

The researchers determined how stabilizing tertiary interactions cooperate at an intermediate stage of folding, much earlier in the folding process than previously suspected. The native structure of ribozyme was found to be important for this cooperation, with small alterations in the ribozyme architecture determining the entire folding pattern.

The study shows that tertiary interactions are very important at early stages of folding, but have surprisingly little effect on the further stability of the ribozyme native state. While cooperation between tertiary interactions at different places in the RNA is important for getting from the unfolded to the intermediate state, it is less important for getting from the intermediate state to the native state.

This study provides new insights about the importance of these early interactions in the RNA folding process, and indicates that cooperativity in noncoding RNAs may have arisen as an evolutionary process due to natural selection of structures that favor formation of unique folds.

The results increase our understanding of tertiary interactions in RNA and how they promote cooperative self-assembly, and will guide further research into the components of tertiary RNA structure, helping to predict the structures of newly discovered noncoding RNAs, and ultimately enhancing our understanding of these important biological functions.

— Nicola Parry

See: Reza Behrouzi¹, Joon Ho Roh^{2,3}, Duncan Kilburn¹, R.M. Briber², and Sarah A. Woodson^{1*}, “Cooperative Tertiary Interaction Network Guides RNA Folding,” *Cell* **149**, 348 (April 13, 2012). DOI:10.1016/j.cell.2012.01.057

Author affiliations: ¹Johns Hopkins University, ²University of Maryland, ³National Institute of Standards and Technology

Correspondence: *swoodson@jhu.edu

This work supported by grants from the National Institutes of Health (NIH) (GM60819) and the NIST. Bio-CAT is supported by grants from the National Institute of General Medical Sciences (9 P41 GM103 622-18) from the National Institutes of Health.. Use of the Advanced Photon Source at Argonne National Laboratory was supported by the U.S. Department of Energy Office of Science under Contract No. DE-AC02-06CH11357.

18-ID-D • Bio-CAT • Life sciences • Fiber diffraction, microdiffraction, microfluorescence (hard x-ray), small-angle x-ray scattering, time-resolved x-ray scattering, micro x-ray absorption fine structure • 3.5-35 keV • On-site • Accepting general users •

GM/CA BEAMLINES JOIN THE APS

In June 2012, the General Medical Sciences and Cancer Institutes (GM/CA) beamlines and staff at Sector 23 of the APS joined the X-ray Science Division (XSD) in the Argonne Photon Sciences directorate. GM/CA is a national user facility for biological research funded by the National Institutes of Health's National Cancer Institute (NCI) and the National Institute of General Medical Sciences (NIGMS).

For 11 years after its inception at the APS as a collaborative access team, GM/CA resided organizationally in the Argonne Biosciences Division. As noted on the GM/CA web site (http://www.gmca.anl.gov/gmca_at_aps_2012.html): "The new administrative home [in the APS organization] will provide new opportunities for scientific and technical collaboration with world-leading synchrotron scientists." The move into the APS did not change GM/CA's relationship with the National Institutes of Health.

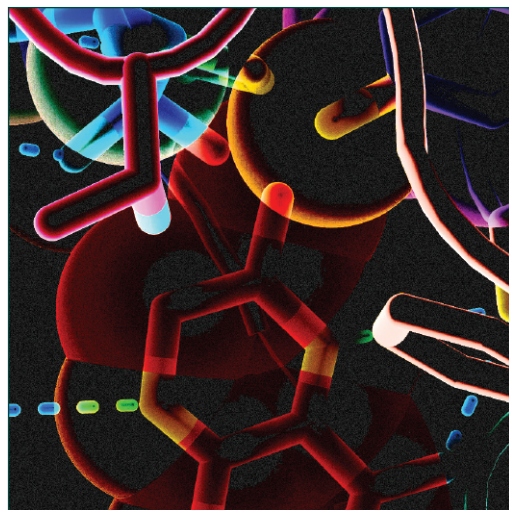
All members of the group continue with their former responsibilities, and the GM/CA management team remains in place. Robert Fischetti continues as GM/CA Group Leader and also serves as Associate Director for Structural Biology in XSD. Janet Smith (University of Michigan) is Scientific Director for GM/CA with responsibility to the sponsors at NIGMS and NCI.

According to the mission statement of GM/CA, "the project has been established by the National Institutes of Health's National Institute of General Medical Sciences and National Cancer Institute to build and operate a national user facility for crystallographic structure determination of biological macromolecules by X-ray diffraction... The scientific and technical goals of GM/CA emphasize streamlined, efficient throughput for a variety of sample types,

es and qualities, presenting the cutting edge of structural biology research."



The GM/CA staff in front of the 23-ID-B enclosure in the APS experiment hall. Left to right: Mark Hilgart, Craig Ogata, Robert Fischetti, Sergey Stepanov, Dale Ferguson, Janet Smith, Oleg Makarov, Shenglan Xu, Michael Becker, and Sudhir Babu Pothineni. Insets left to right: Sheila Trznadel, Ruslan Sanishvili (Nukri), Nagarajan Venugopalan, and Stephen Corcoran.



STRUCTURAL BIOLOGY

THE SECRETS OF OPIOID RECEPTORS

Long ago, humans discovered that opium, and its derivatives codeine and morphine, are excellent pain relievers. The opioids are so good at performing this function that addiction can easily ensue. Understanding the biochemical intricacy of how opioids bind to and activate receptors is therefore of critical economic and social importance for both creating better pain relievers and curing addiction. Although the identity of the four types of opioid receptors was already known, key structural details were missing. Now, thanks to studies involving two large research teams, with help from the Advanced Photon Source GM/CA-XSD beamlines 23-ID-B and 23-ID-D at the APS, exciting and much needed new details about opioid receptors are available for drug design and therapeutics.

One group of researchers, from the Stanford University Medical School, the University of Michigan School of Medicine, Universitat Autònoma de Barcelona (Spain), and Institut de Génomique Fonctionnelle (France) unveiled the crystal structures of the μ - and δ -opioid receptors. A second group, from The Scripps Research Institute, the University of North Carolina at Chapel Hill Medical School, the Research Triangle Institute, Virginia Commonwealth University, and the University of Ferrara (Italy) revealed the crystal structure of the κ -opioid receptor and the more recently discovered nociceptin/orphanin FQ receptor. So exciting were these findings on opioid receptors that *Nature* magazine published all four papers in one issue, which hailed the discoveries on the magazine's cover, and the American Chemical Society listed the structures as a 2012 research highlight.

Of the four opioid receptor structures published by the researchers, the data from the Stanford team, on the μ -opioid receptor, because of its association with both therapeutic and illegal drug use, will likely prove to be of significant economic importance. Opioids such as morphine and codeine — the main active opioid alkaloids in opium — produce pain relief, and undesirable side effects such as sedation and dependence, by binding and activating the G-protein-coupled μ -opioid receptor (μ -OR) in the central nervous system. That opioids can be highly addictive is well known from the example of heroin, an acetylated form of morphine. In activating the μ -OR, positive effects (such as pain relief) and negative effects (such as addiction) appear to be regulated by different pathways. One very promising line of research would be to find ways to decouple these processes so that the positive effects could be enhanced and the negative effects diminished or eliminated entirely.

Employing a mouse model system, the Stanford team obtained the crystal structure of μ -OR bound to a morphinan antagonist. The resulting structure

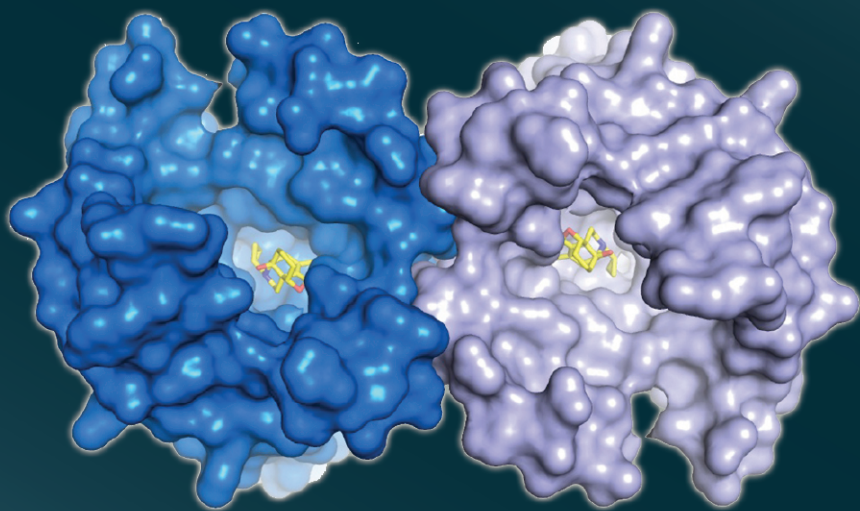


Fig. 1. The μ -opioid receptor, the target of opium, may partner with itself when bound to a morphine-like drug. Image courtesy of Kobilka Lab.

revealed some surprises. While in previously characterized G-protein-coupled receptors the binding pocket is buried, in μ -OR the morphinan binding is deep inside a large, exposed pocket. In the exquisite detail with which this structure is now known, the researchers found that the μ -OR in crystal form is a two-fold symmetrical dimer through a four-helix bundle motif (Fig. 1). The dimer structure is of particular interest in revealing the mechanism by which methadone reduces tolerance to morphine.

Like the μ -OR, the other two members of related opioid receptors (δ - and κ -opioid) are G-protein-coupled receptors, are closely related to the μ -receptor, and respond to morphine and heroin as well as to endogenous endorphins. The Stanford team obtained the crystal structure of the mouse δ -OR bound to the subtype-selective antagonist naltrindole. The Scripps group determined the crystal structure of the human κ -OR bound to the selective antagonist JDTC, a compound active in rodent models of depression and anxiety. By combining these results the teams provide important insights about conserved elements of opioid recognition by the receptors and make predictions about ligand-subtype selectivity. If the receptor pocket is divided into two parts, the lower part is highly conserved among opioid receptors while the upper part has varying components that confer subtype selectivity. This finding provides structural details to support previously proposed mechanisms for the inner workings of opioid receptor pharmacology and also suggests general principles that may extend to other G-protein-coupled receptors.

The Scripps group also reported the structure of the more recently discovered fourth opioid receptor nociceptin/orphanin FQ peptide receptor (NOP). Though NOP does show some sequence similarity with the μ -, δ -, and κ -opioid receptors, it behaves quite differently with respect to activation and selectivity. Comparison of the NOP pocket structure with that of the other three opioid receptors shows marked differences that seem to be caused by a small number of components, which is good news for drug designers.

Taken together, the detailed structural information provided by the research teams promises rapid progress on opioid-related therapeutics and addiction treatment. — *Mona Mort*

See:

Aashish Manglik¹, Andrew C. Kruse¹, Tong Sun Kobilka¹, Foon Sun Thian¹, Jesper M. Mathiesen¹, Roger K. Sunahara², Leonardo Pardo³, William I. Weis¹, Brian K. Kobilka^{1**}, and Sébastien Granier^{1,4*}, “Crystal structure of the μ -opioid receptor bound to a morphinan antagonist,” *Nature* **485**, 321 (17 May 2012). DOI:10.1038/nature10954

Author affiliations: ¹Stanford University School of Medicine, ²University of Michigan Medical School, ³Universitat Autònoma de Barcelona, ⁴Institut de Génomique Fonctionnelle

Correspondence:

*granier@stanford.edu,

**kobilka@stanford.edu

This research was supported by INSERM (S.G.), the Stanford Medical Scientist Training Program (A.M.), the U.S. National Science Foundation (A.C.K.), the Lundbeck Foundation (J.M.M.), the National Institutes of Health (NIH) Grants NS028471 (B.K.K.) and DA031418 (B.K.K. and R.K.S.), and the Mathers Foundation (B.K.K. and W.I.W.).

and

Huixian Wu¹, Daniel Wacker¹, Mauro Mileni¹, Vsevolod Katritch¹, Gye Won Han¹, Eyal Vardy², Wei Liu¹, Aaron A. Thompson¹, Xi-Ping Huang², F. Ivy Carroll³, S. Wayne Mascarella³, Richard B. Westkaemper⁴, Philip D. Mosier⁴, Bryan L. Roth², Vadim Cherezov¹, and Raymond C. Stevens^{1*}, “Structure of the human κ -opioid receptor in complex with JDTC,” *Nature* **485**, 327 (17 May). DOI:10.1038/nature10939

Author affiliations: ¹The Scripps Research Institute, ²University of North Carolina at Chapel Hill Medical School, ³Research Triangle Institute, ⁴Virginia Commonwealth University

Correspondence:

*stevens@scripps.edu

This work was supported by PSI:Biography grant U54 GM094618 (V.K., V.C., R.C.S.) for biological studies and structure production, NIH Roadmap grant P50 GM073197 (V.C., R.C.S.) for technology development and R01 DA017624 (B.L.R., E.V., R.B.M., P.D.M.), R01 DA027170 (B.L.R.), the National Institute of Mental Health (NIMH) Psychoactive Drug Screening Program Contract (B.L.R., X.-P.H.), the Michael Hooker Distinguished Chair of Pharmacology (B.L.R.), and NIH grant R01 DA009045 (F.I.C.). D.W. is supported by a Boehringer

Ingelheim Fonds Ph.D. Fellowship. *and*

Aaron A. Thompson¹, Wei Liu¹, Eugene Chun¹, Vsevolod Katritch¹, Huixian Wu¹, Eyal Vardy², Xi-Ping Huang², Claudio Trapella³, Remo Guerrini³, Girolamo Calo³, Bryan L. Roth², Vadim Cherezov¹, and Raymond C. Stevens^{1*}, “Structure of the nociceptin/orphanin FQ receptor in complex with a peptide mimetic,” *Nature* **485**, 395 (17 May 2012). DOI:10.1038/nature11085

Author affiliations: ¹The Scripps Research Institute, ²University of North Carolina at Chapel Hill Medical School, ³University of Ferrara

Correspondence:

*stevens@scripps.edu

This work was supported by PSI:Biography grant U54 GM094618 for biological studies and structure production, NIH Roadmap grant P50 GM073197 for technology development and R01 DA017204, R01 DA27170, and the NIMH Psychoactive Drug Screening Program (X.-P.H., E.V. and B.L.R.) and the Michael Hooker Chair of Pharmacology (B.L.R.), University of Ferrara (FAR grant to G.C.), Italian Ministry of University (FIRB Futuro in Ricerca 2010 grant to C.T.).

and

Sébastien Granier^{1,2*}, Aashish Manglik^{1*}, Andrew C. Kruse^{1*}, Tong Sun Kobilka¹, Foon Sun Thian¹, William I. Weis¹, and Brian K. Kobilka^{1**}, “Structure of the δ -opioid receptor bound to naltrindole,” *Nature* **485**, 400 (17 May 2012). DOI:10.1038/nature11111

Author affiliations: ¹Stanford University School of Medicine, ²Institut de Génomique Fonctionnelle

Correspondence:

*granier@stanford.edu,

**kobilka@stanford.edu

This research was supported by INSERM (S.G.), the Stanford Medical Scientist Training Program (A.M.), the U.S. National Science Foundation (A.C.K.), NIH grants NS028471 (B.K.K.) and DA031418 (B.K.K.), and the Mathers Foundation (B.K.K. and W.I.W.). GM/CA-XSD has been funded in whole or in part with Federal funds from the National Cancer Institute (Y1-CO-1020) and the National Institute of General Medical Sciences (Y1-GM-1104). Use of the Advanced Photon Source at Argonne National Laboratory was supported by the U.S. DOE Office of Science under Contract No. DE-AC02-06CH11357.

23-ID-B • GM/CA-XSD • Life sciences • Large unit cell crystallography, macromolecular crystallography, microbeam, multi-wavelength anomalous dispersion, single-wavelength anomalous dispersion, subatomic (<0.85 Å) resolution • 3.5-20 keV (23-ID-D: 5-20 keV) • On-site, remote • Accepting general users •

WATCHING A PROTEIN AS IT FUNCTIONS

When it comes to understanding how proteins perform their amazing cellular feats, it is often the case that the more one knows the less one realizes they know. For decades, biochemists and biophysicists have worked to reveal the relationship between protein structural complexity and function, only to discover more complexity. One challenging aspect of protein behavior has been the speed with which they change shape and interact with their neighboring biomolecules. Until recently, researchers have relied on a somewhat static approach, using freeze-trapping to capture protein intermediates at various steps along a biochemical pathway. But exciting breakthroughs now allow us to watch proteins changing in real time. A research group has developed the necessary infrastructure at the BioCARS 14-ID-B beamline at the APS to watch proteins function in real time on the picosecond time scale. Their work brings us many steps closer to knowing how proteins function, or malfunction when leading to disease.

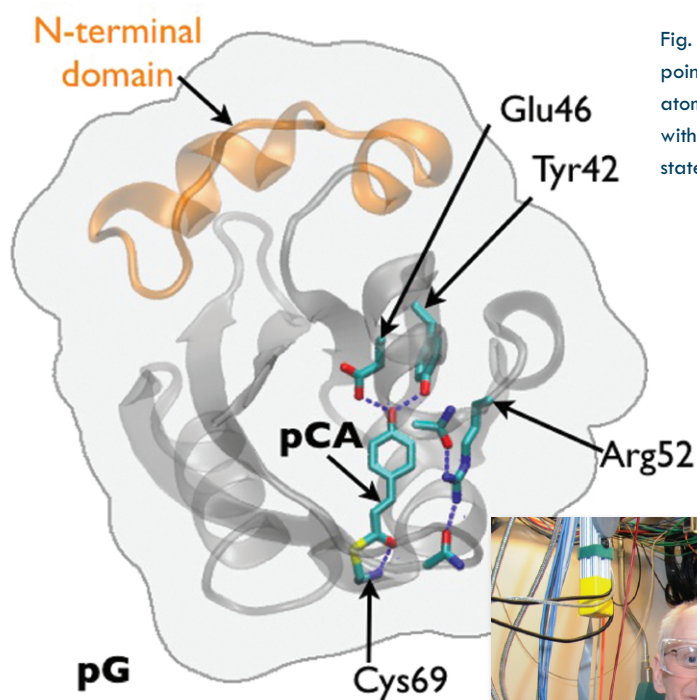
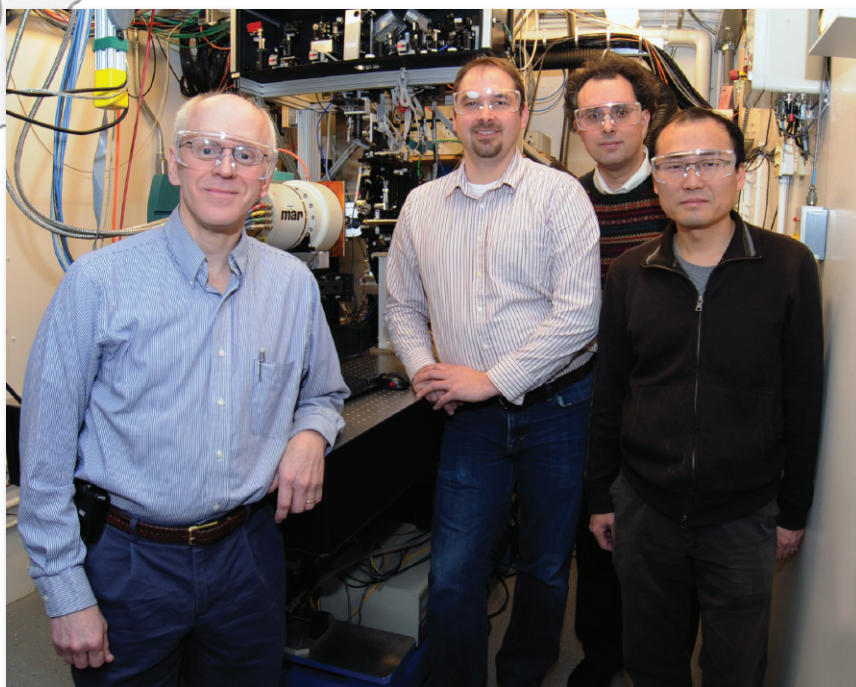


Fig. 1. The PYP structure in its ground (pG) state: Arrows point to the pCA C2=C3 double bond and the C α atoms of key residues. Hydrogen bonds are indicated with dashed blue lines. Arg52 is stabilized in its “closed” state via hydrogen bonds to the protein backbone.



Members of the team, in the BioCARS 14-ID-B research station. Left to right: Philip Anfinrud, Robert Henning, Friedrich Schotte, and Hyun Sun Cho.

14-ID-B • BioCARS • Life sciences • Time-resolved crystallography, time-resolved x-ray scattering, Laue crystallography, wide-angle x-ray scattering, biohazards at the BSL2/3 level, macromolecular crystallography • 7-20 keV • On-site • Accepting general users •

A signaling protein usually responds to a messenger or trigger, such as heat or light, by changing its shape, which initiates a regulatory response in the cell. Signaling proteins are all-important to the proper functioning of biological systems, yet the rapid sequence of events, occurring in picoseconds, had, until now, meant that only an approximate idea of what was actually occurring could be obtained.

The researchers from the National Institutes of Health, the Nara Institute of Science and Technology (Japan), The University of Chicago, and the European Synchrotron Radiation Facility (France) worked to remedy that situation by developing a time-resolved, 150-ps Laue crystallography technique that can be utilized to watch structural changes in the photocycle of a protein first discovered in the photosynthetic bacterium *Halorhodospira halophila*. The protein, called photoactive yellow protein (PYP), is implicated in causing the bacterium to swim away from blue light, which could be genetically harmful, and toward green light, which it needs for photosynthesis.

The team tracked the reversible photocycle of PYP over ten decades of time, from 100 ps to 1 sec (Fig. 1). The signaling reaction is triggered by absorption of a photon of light by *p*-coumaric acid (pCA) chromophore, the non-protein entity that actually absorbs the photon, and which undergoes *trans*-to-*cis* isomerization. The bacterium responds to this light signaling within about half a second, indicating how rapidly the biochemical changes that facilitate the response must occur in the cell. The team identified four major intermediates in the photoisomerization cycle (Fig. 2). The first *cis*

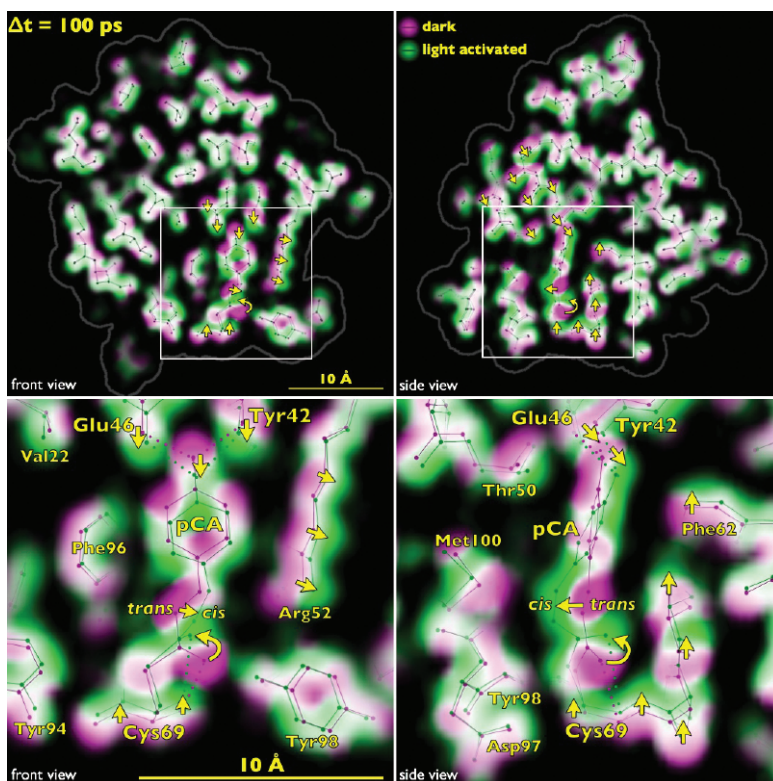


Fig. 2. Front and side views of time-resolved structural changes recorded 100 ps after photoexcitation of PYP. (Lower) Expanded, annotated view of upper insets. The ground-state electron density map is colored magenta, and the 100-ps map is colored green. Where magenta and green overlap, the electron density blends to white. The magenta-to-green color gradient unveils the direction of atomic motion; large-amplitude displacements are indicated with yellow arrows. The stick models correspond to refined structures for the ground state (pG) and the first intermediate (pR0).

intermediate, lasting for only 600 ps, is in an unusual, highly contorted form not previously observed in crystallography experiments and is the precursor to intermediates that had been observed on the time scale of nanoseconds. Additional intermediate steps in the process of structural transition include breaking and making of hydrogen bonds, formation and relaxation of strain, and gated water penetration into the protein's interior. The researchers cross-validated their structural data, utilizing density functional theory calculations to confirm the chemical plausibility of the intermediates.

By tracking structurally the PYP photocycle with near-atomic resolution, the team provided a foundation for understanding the general process of signal transduction in proteins at nearly the lightning speed in which they are actually happening. By extending these techniques to enzymes, it would be possible to perform real-time observations of enzymatic action. Thanks to

the team's groundbreaking work, the mechanistic and kinetic complexities with which proteins carry out their sophisticated functions are now much more clearly on view to those who have been eagerly waiting to see. — *Mona Mort*

See: Friedrich Schotte¹, Hyun Sun Cho¹, Ville R.I. Kaila¹, Hironari Kamikubo², Naranbaatar Dashdorj^{1†}, Eric R. Henry¹, Timothy J. Graber³, Robert Henning³, Michael Wulff⁴, Gerhard Hummer¹, Mikio Kataoka², and Philip A. Anfinrud^{1*}, "Watching a signaling protein function in real time via 100-ps time-resolved Laue crystallography," *Proc. Natl. Acad. Sci. USA* **109**(47), 19256 (November 20, 2012). DOI:10.1073/pnas.1210938109

Author affiliations:

¹National Institutes of Health, ²Nara Institute of Science and Technology, ³The University of Chicago, ⁴European Synchrotron Radiation Facility. [†]Present address: Argonne National Laboratory
Correspondence: *anfinrud@nih.gov

Use of the BioCARS Sector 14 was supported by National Center for Research Resources Grant 5P41RR007707 and National Institute of General Medical Sciences Grant 8P41GM103543 from the National Institutes of Health (NIH). The time-resolved setup at Sector 14 was funded in part through collaboration with P.A.A. This research was supported by the Intramural Research Program of the National Institute of Diabetes and Digestive and Kidney Diseases, NIH. V.R.I.K. is the recipient of a European Molecular Biology Organization Long-Term Fellowship. Use of the Advanced Photon Source at Argonne National Laboratory was supported by the U.S. DOE Office of Science under Contract No. DE-AC02-06CH11357.

See also: Y.O. Jung et al., *Nat. Chem.* **5**, 212 (March 2013).

IMPROVED PLANT GROWTH MAY HINGE ON ENZYME FLEXIBILITY

Hormone compounds such as jasmonates, auxins, and benzoates that act as signaling molecules are important to the regulation of growth, development, and defense responses in plants. Conjugation reactions that alter the cellular concentrations of these hormones represent an important mechanism for the regulation of the activity and stability of such compounds. Researchers working at the SBC-CAT 19-ID-D beamline at the APS and two beamlines at the European Synchrotron Radiation Facility (ESRF) examined the structure and function of two plant proteins and discovered new information that will be important in guiding future studies to help scientists develop more effective herbicides, and also to discover improved ways to breed plant species that are able to withstand difficult environmental conditions.

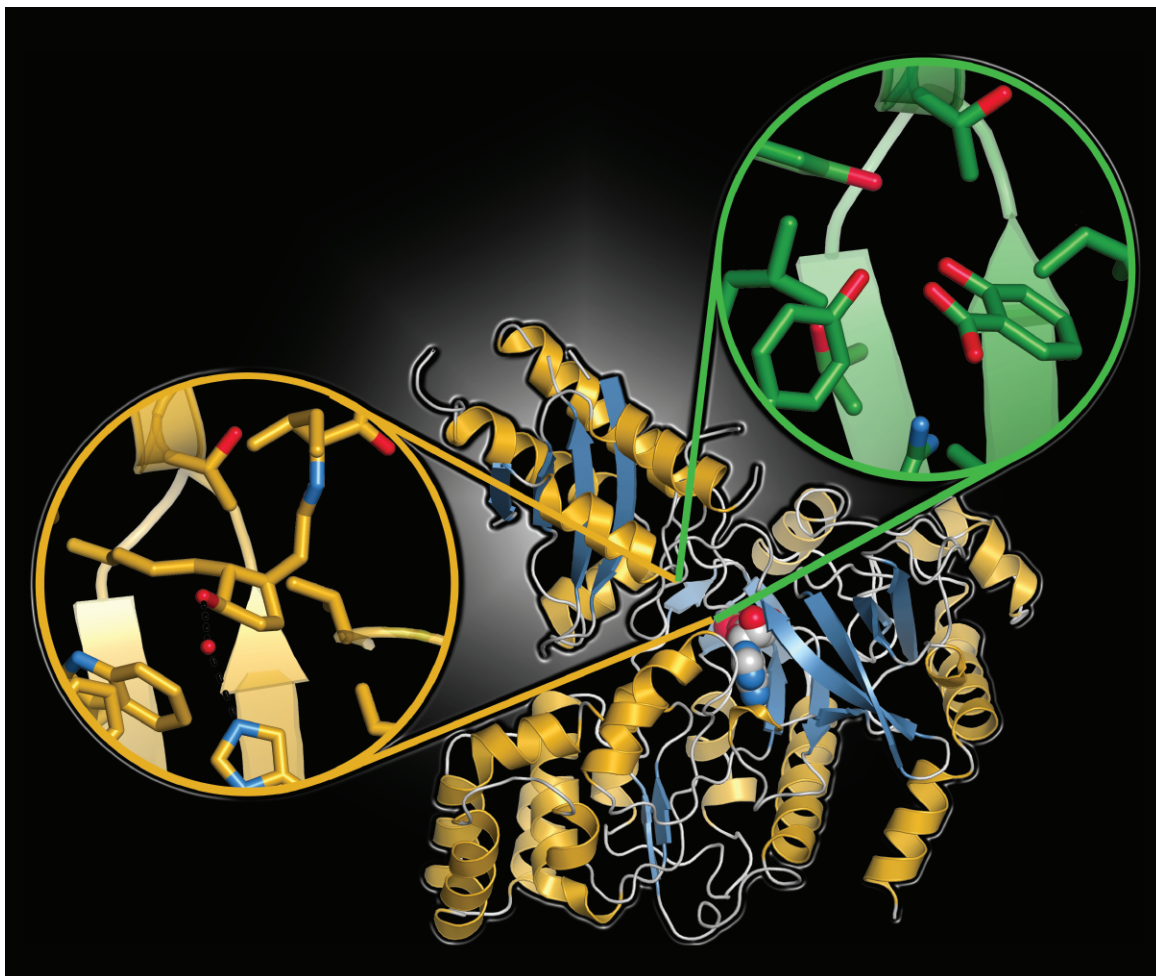


Fig. 1. In plants, GH3 proteins acts as molecular on/off switches that control formation of bioactive plant hormones by catalyzing the addition of specific amino acids to jasmonic acid, auxin, and benzoates. The x-ray structures of GH3 proteins reveal a common three-dimensional fold, but variability in the hormone binding site. This figure shows the variation in the jasmonic acid binding site of *Arabidopsis thaliana* GH3.11/JAR1 (gold) and the salicylic acid binding site of *A. thaliana* GH3.12/PBS3 (green).

Cellular signaling pathways are important for the diverse aspects of plant development and survival. Plants produce many bioactive hormone compounds, such as jasmonates, auxins, and benzoates with important regulatory roles in these pathways. Conjugation reactions that alter cellular concentrations of these hormones represent an important mechanism for the regulation of the activity and stability of hormone compounds and involve attachment of certain molecules to these compounds, leading to their activation, inactivation, or degradation.

For example, amino acid conjugation of jasmonic acid (JA), the auxin indole acetic acid (IAA), and the benzoate salicylic acid (SA) changes the concentrations of their active forms in cells, and therefore their potency, to help control plant growth, development, and defense responses. Conjugation of the amino acid isoleucine to JA produces jasmonyl-isoleucine (JA-Ile), an active form of the hormone that leads to activation of genes involved in plant growth and development.

Conjugation of IAA with the amino acids aspartate and glutamate produces IAA-Asp and IAA-Glu, respectively. These target IAA for breakdown and reduce auxin signaling. Similarly, modification of SA leads to changes in biological activity that affect plant defense responses.

GH3 proteins are widespread across the plant kingdom, and numerous mutant forms connect these enzymes to JA, auxin, and SA responses in various plant species, including *Arabidopsis* (a small, flowering plant that is widely used as a model organism in plant biology) and rice. The GH3 family of enzymes plays a key role in the conjugation reactions that control the activity of many hormones, using a basic two-step reaction.

This same reaction, however, can affect different hormones in different ways. For example, it can activate a jasmonate plant hormone compound by adding the amino acid isoleucine to it. In contrast, it can target an auxin plant hormone for destruction by adding the amino acid aspartate to it. In *Arabidopsis* the two best-studied GH3 proteins are AtGH3.11 and

AtGH3.12. The *Arabidopsis* jar1 mutant form is defective in AtGH3.11, which prevents formation of JA-Ile and inhibits JA-mediated responses. Similarly, the *Arabidopsis* SA-response mutant form pbs3 alters AtGH3.12, resulting in signaling problems that lead to increased susceptibility of the plant to infection with the bacterium *Pseudomonas syringae*.

Researchers from Washington University, the European Synchrotron Radiation Facility (France), and the Université Joseph Fourier (France) utilized beamline 19-ID-D at the APS and the BM-14 and ID23-2 beamlines at the ESRF to examine the structure and function of the two GH3 proteins to understand how GH3 proteins can affect plant signaling molecules so differently.

They discovered that the structure of both GH3 proteins was similar to what had been previously described for the adenylating-firefly-luciferase (ANL) enzyme superfamily. They also discovered a flexible hinge loop within the structure of both proteins that allows conformational changes after substrate binding. This has not been described in the ANL superfamily, and may represent an evolutionary change that allows the two-step reaction to occur.

Certain amino acids were required to be present at specific locations within the structure of the enzyme's active site for the two-step reaction to occur. For example, in AtGH3.12, the presence of threonine, leucine, and phenylalanine at positions 161, 217, and 218 are essential for correct active site function, and a serine at position 328 is for the transferase reaction.

When ATP, the cell's energy currency, binds to the enzyme, the hinge moves to open the active site. This allows binding of the plant hormone and amino acid, and the first step of adenylation occurs. The enzyme then removes phosphate groups from ATP, producing AMP, which is added to an activated form of the enzyme. This causes the enzyme to change conformation again, closing the hinge, ready for the second reaction. This second step, the transferase reaction, can now proceed and produce the hormone-amino acid conjugate.

These structural and functional

studies provide some explanation of how this enzyme family can adapt its scaffold (Fig. 1) to produce a range of effects on different signaling molecules involved in various aspects of plant development and survival.

The results of this study will help guide further research into the mechanisms by which enzymes interact with hormones that allow plants to control their growth and development, adapt to changes in environmental conditions, or even defend itself from bacterial attack. This represents a potential target for production of herbicides, as well as genetically-modified plants that can withstand extreme environmental conditions. — *Nicola Parry*

See: Corey S. Westfall¹, Chloe Zubieta², Jonathan Herrmann¹, Ulrike Kapp², Max H. Nanao^{3,4}, and Joseph M. Jez^{1*}, "Structural Basis for Pre-receptor Modulation of Plant Hormones by GH3 Proteins," *Science* **336**, 1708 (29 June 2012). DOI:10.1126/science.1221863

Author affiliations: ¹Washington University, ²European Synchrotron Radiation Facility, ³European Molecular Biology Laboratory, ⁴Université Joseph Fourier

Correspondence:

*jjez@biology2.wustl.edu

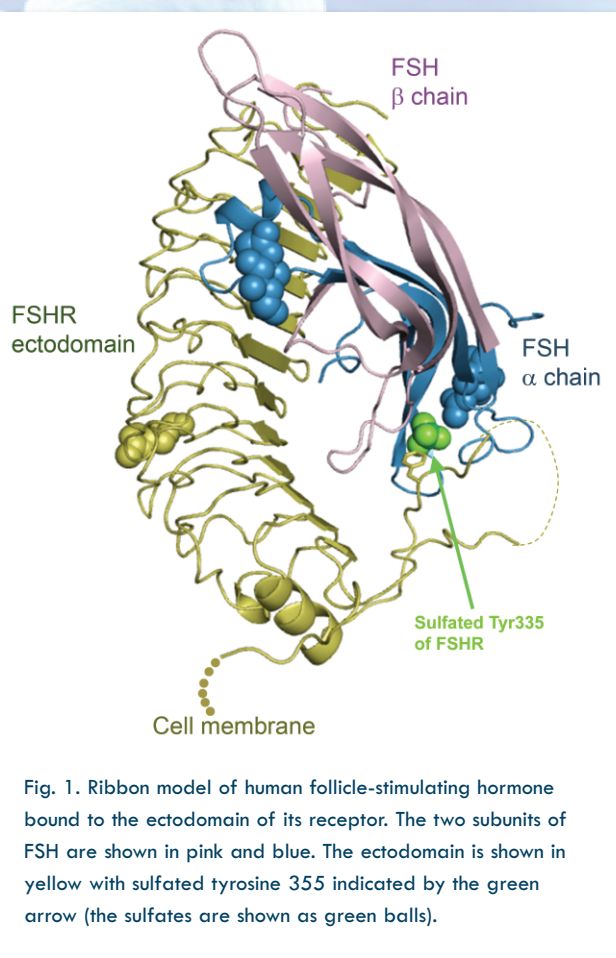
This work was supported by National Science Foundation grant MCB-1157771 to J.M.J. C.S.W. was supported by a U.S. Department of Agriculture–National Institute of Food and Agriculture predoctoral fellowship (MOW-2010-05240), and J.H. was supported by an American Society of Plant Biologists–Summer Undergraduate Research Fellowship award and the Howard Hughes Medical Institute–Washington University Summer Scholars Program in Biology and Biomedical Research. SBC-CAT is funded by the U.S. Department of Energy Office of Science (DOE-SC) Biological and Environmental Research Program under contract DE-AC02-06CH11357. Use of the Advanced Photon Source at Argonne National Laboratory was supported by the U.S. DOE-SC under 19-ID-D • SBC-CAT • Life sciences • Large unit cell crystallography, macromolecular crystallography, microbeam, multi-wavelength anomalous dispersion, single-wavelength anomalous dispersion, subatomic (<0.85 Å) resolution, ultra-low-temperature (15K) • 6.5-19.5 keV • On-site, remote, mail-in • Accepting general users •

TINKERING WITH FERTILITY

For people who want to have children but need a little medical assistance to make it a reality, research into how hormones such as the follicle stimulating hormone (FSH) work is of critical importance. FSH is important to the regulation of fertility in both men and women and is, therefore, a target for intervention. Now, data collected at the LS-CAT 21-ID-D beamline at the APS has determined the structure of FSH in complex with the entire extracellular domain (ectodomain) of its receptor, FSHR, a large membrane glycoprotein that is coupled to G-proteins. This work provides new information about how FSH binds to its receptor and how this binding transmits a very specific signal into the cells responsible for reproduction. This knowledge will be utilized to guide the design of drugs that can modulate FSH receptor signaling to treat infertility.

FSH is already employed clinically to assist reproduction, but small-molecule drugs that can affect the FSH receptor directly may provide better treatments that can, for example, act longer or be administered orally. Previous research that determined protein structures of the interaction of FSH with its receptor were not able to resolve how FSH binding transmits a signal that activates the intracellular portion of the receptor. A central question in this process is the role of a flexible hinge region of the ectodomain of the receptor. This hinge region contains an amino acid at position 355, a sulfated tyrosine (sTyr), that has been determined to be critical to receptor activation and signal specificity. But without the structure of this region, it was impossible to determine which of a number of alternative models explained how this was accomplished.

Therefore, the researchers in this study, from Northwestern University Feinberg School of Medicine and the EMD Serono Research Institute set out to determine the structure of FSH in complex with the ectodomain of the receptor. Their structure, determined via x-ray diffraction at the LS-CAT beamline to a resolution of 2.5 Å, shows that the hinge region is not a separate domain that moves upon FSH binding to trans-



mit the signal, as had been hypothesized, but rather is an integral part of the ectodomain.

The structure looks like a right hand holding an American football. The ectodomain forms the palm of the hand with the hinge region protruding out like a thumb and the FSH nestled in like a football (Fig. 1). The sTyr of the hinge region of the receptor is held in the perfect orientation for interacting with the FSH.

But how is the signal transmitted if the

hinge region doesn't change its conformation when the FSH binds? The answer to this question is the central discovery of this work and relates to what FSH does when it recognizes its receptor. Once FSH binds to the ectodomain, it is induced to dramatically change its shape to accommodate the sTyr of the hinge region into a newly formed binding pocket. This is consistent with mutagenesis experiments that have highlighted both the importance of the sTyr of the receptor as well as amino acids that are located in the newly formed binding pocket of the FSH. The researchers hypothesize that the interaction between the sTyr and the induced pocket on FSH lifts the hinge region in a way that activates intracellular signaling. Experiments with mutated receptors in which the tyrosine was artificially lifted in the absence of FSH showed increased intracellular signaling activation, supporting their hypothesis.

Next up for this team is a focus on what happens after FSH binds to sTyr355 and on the development of drugs that may be able to help people with fertility problems related to FSH signaling. — *Sandy Field*

See: Xuliang Jiang¹, Heli Liu², Xiaoyan Chen², Po-Han Chen², David Fischer¹, Venkataraman Sriraman¹, Henry N. Yu¹, Steve Arkinstall¹, and Xiaolin He^{2*}, "Structure of follicle-stimulating hormone in complex with the entire ectodomain of its receptor," *Proc. Natl. Acad. Sci. USA* **109**(31), 12491 (July 31, 2012). DOI:10.1073/pnas.1206643109
Author affiliations: ¹EMD Serono Research Institute, ²Northwestern University Feinberg School of Medicine

Correspondence:

*x-he@northwestern.edu.

CAPTURING A VIRUS HIJACKER

Viruses use a process called transposition to help hijack cellular machinery and make new viruses. Some of the most important work in this process is performed by the bacteriophage Mu, a type of virus that infects bacteria. The enzyme inside Mu that facilitates this process is called the MuA transposase, which forms a complex between the cargo DNA of the Mu itself and the host bacterium's genome to become activated. Exactly how this binding regulates MuA activity has remained a mystery until recently. Studies performed by researchers from The University of Chicago utilizing x-ray crystallography at three APS beamlines generated structures of the MuA transposase in complex with its cargo DNA and the host DNA. These data create a better understanding of how viruses are able to deliver genes into organisms, potentially leading to a more effective route of therapy in the future.

Retroviruses such as the human immunodeficiency virus work by introducing a stretch of DNA into the infected host's genome, hijacking the machinery of the cell in order to make new viruses. Our understanding of the methods used by these retroviruses was facilitated by earlier studies using viruses that specifically target bacteriophages. These agents were also critical in helping to solidify an early understanding of the process known as transposition, where a gene would seem to "jump" from one group of bacteria to another. This process helps to ensure genetic diversity in bacteria since they do not reproduce sexually.

The bacteriophage Mu was a key player utilized in early studies to help understand transposition. Mu uses the enzyme called transposase to help move its genes into the bacterial genome. Transposase binds to the cargo gene of interest, binds randomly to the genome, and then leads an attack that temporarily destabilizes the host DNA and allows the Mu gene of interest to integrate. In the current study, with the help of the Bio-CARS 14-BM-C, SBC-CAT 19-ID-D, and LS-CAT 21-ID-F beamlines the research team answered the question of how transposase MuA is regulated.

The MuA transposase was previously known to be inactive until it was attached to the host genome while carrying a cargo gene from Mu. If either of these components is not in place, then the transposase will not be active.

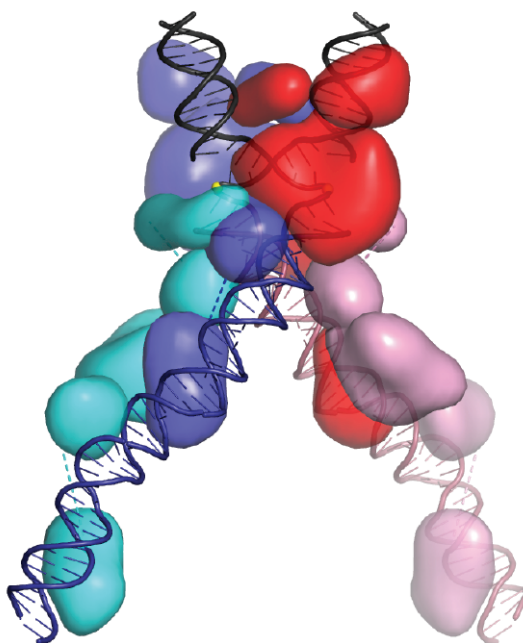


Fig. 1. The structure of MuA.

The crystal structures in this work demonstrated the types of interactions that needed to take place in order to promote bending of the host DNA and place it in a favorable position for attack by the active site of MuA. Without binding both the Mu cargo gene and the genome, the domains of MuA could not be situated correctly to promote the attack and transfer. This was the first structure of MuA interacting with DNA that helped confirm the previously-known biochemical data about this mechanism (Fig.1).

As an added bonus, this work helped to further characterize the class of enzymes known as DDE recombi-

nases, composed of D (aspartic acid) and E (glutamic acid) amino acids contained within the active site of many transposases. A comparison of the structure of previously-solved transposases provided evidence that MuA and its other DDE family members must have shared a common ancestor. While the DDE motif is present in many transposases, the enzymes have also acquired other domains that give them distinct traits. — *Emma Hitt*

See: Sherwin P. Montaño, Ying Z. Pigli, and Phoebe A. Rice*, "The Mu transpososome structure sheds light on DDE recombinase evolution," *Nature* **49**, 413 (5 November 2012). DOI:10.1038/nature11602

Author affiliation:

The University of Chicago

Correspondence:

*PRice@uchicago.edu

This work was funded in part by National Institutes of Health (NIH) grant GM086826 (to P.A.R.). Use of the BioCARS beamline was supported by the NIH, National Institute of General Medical Sciences grant P41GM103543 (formerly National Center for Research Resources P41RR007707). SBC-CAT is funded by the U.S. Department of Energy Office of Science (DOE-SC) Biological and Environmental Research Program under contract DE-AC02-06CH11357. Use of LS-CAT was supported by the Michigan Economic Development Corporation and the Michigan Technology Tri-Corridor (Grant 085P1000817).

14-BM-C • BioCARS • Life Sciences • Macromolecular crystallography, fiber diffraction, biohazards at the BSL2/3 level, subatomic (<0.85 Å) resolution, large unit cell crystallography • 8-14.9 keV • On-site • Accepting general users •

19-ID-D • SBC-CAT • Life sciences • Large unit cell crystallography, macromolecular crystallography, microbeam, multi-wavelength anomalous dispersion, single-wavelength anomalous dispersion, subatomic (<0.85 Å) resolution, ultra-low-temperature (15K) • 6.5-19.5 keV • On-site, remote, mail-in • Accepting general users •

21-ID-F • LS-CAT • Life sciences • Macromolecular crystallography, microfluorescence (hard x-ray), nano-fluorescence imaging, nanotomography • 6.5-20 keV • On-site, remote, mail-in • Accepting general users •

UBIQUITIN OR UBIQUITIN-LIKE: HOW IS A RECEPTOR TO KNOW?

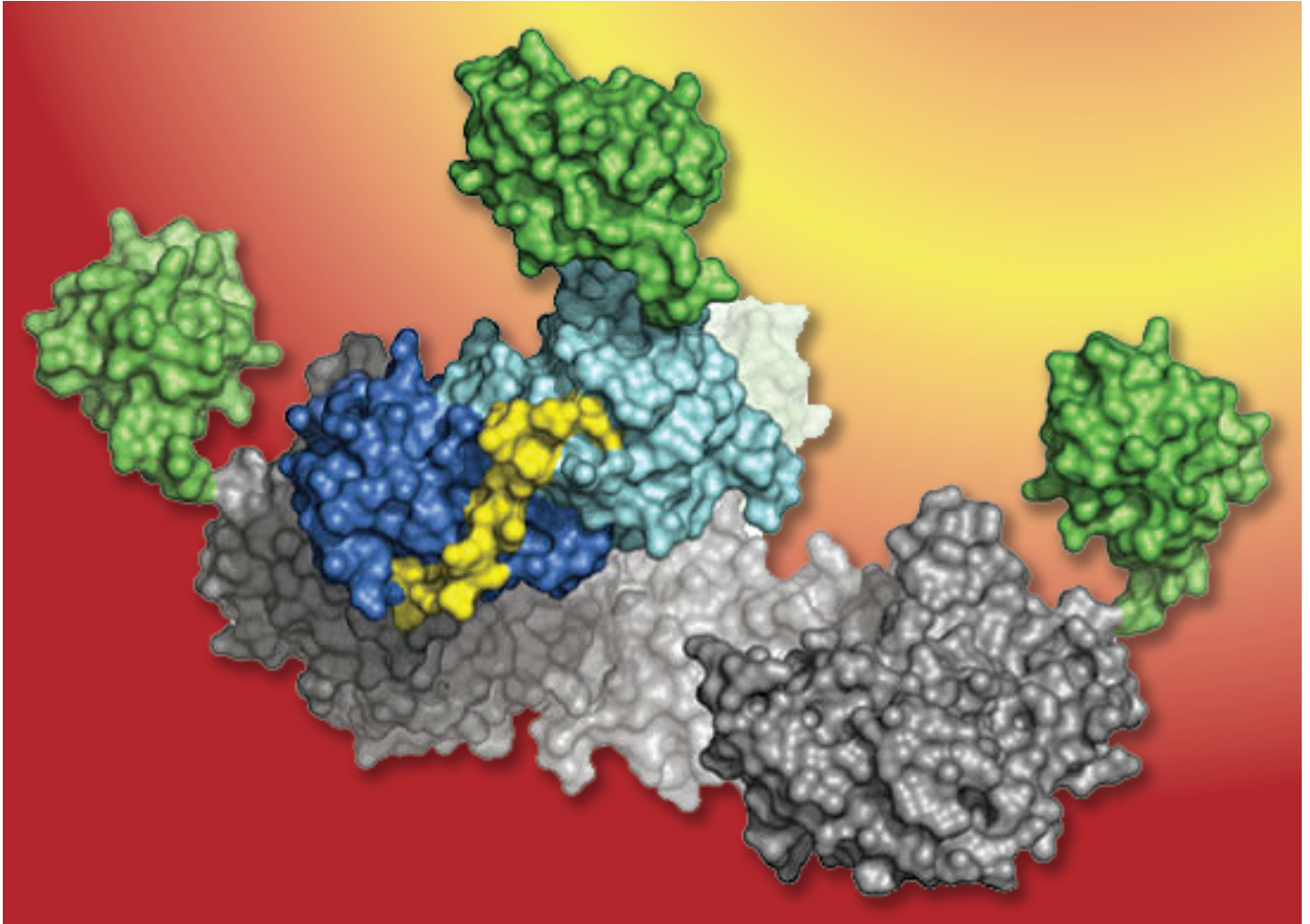


Fig. 1. The structure of SUMOK164-PCNA^{mono}.

Proteins within a cell can be modified by the addition of various molecules, changing their structure and activity. Recognition of protein modifications requires special interactions between the modified protein and the receptor that targets it. Until now, the mechanism for specific recognition of these post-translational modifications by receptors has remained largely unclear. X-ray crystallographic studies carried out at the NE-CAT 24-ID-C beamline at the APS showed for the first time that the receptor uses two different motifs to carry out modifications. This knowledge could lead to a better understanding of cell signaling related to certain protein modifications and important processes within the cell, such as DNA damage repair.

Proteins can undergo a variety of changes after being synthesized. One of the most important of these post-translational modifications involves the addition of ubiquitin (ubiquitylation) and the small ubiquitin-like modifier SUMO (SUMOylation). Ubiquitin is a small regulatory protein found in almost all cells with nuclei (eukaryotes). It directs proteins in recycling and other functions. SUMO are a family of small proteins that are covalently attached to and detached from other proteins in cells to modify their function. Ubiquitylation is a post-translational modification process in which the carboxylic acid of the terminal glycine from the diglycine motif in the activated ubiquitin forms an amide bond to the epsilon amine of the lysine in the modified protein. SUMOylation is a post-translational modification involved in various cellular processes, such as nuclear-cytosolic transport, transcriptional regulation, apoptosis, protein stability, response to stress, and progression through the cell cycle. Both of these modifications can regulate cellular processes such as differentiation, stress response, and proliferation among others; however, their functions are distinct. Ubiquitin, for example, typically targets proteins for destruction by the proteasome. By contrast, addition of SUMO often promotes the movement of proteins from one compartment, such as the nucleus, to another, such as the cytoplasm.

These are not the only roles for these modifications, but they act differently despite their structural similarities. The differences in function can be

mediated partially by different receptors that specifically recognize ubiquitin and SUMO-modified proteins; however, it has not been demonstrated how these receptors are able to differentiate between ubiquitin and SUMO. The proliferating cell nuclear antigen (PCNA) provides an interesting example of the consequences of this selectivity. When PCNA is ubiquitylated, it will promote DNA damage repair; however, if PCNA becomes SUMOylated, it recruits the helicase Srs2 to suppress repair. Therefore, two very similar modifications mediate polar opposite functions. Until recently, the means by which Srs2 is able to selectively recognize SUMOylated but not ubiquitylated PCNA has not been elucidated.

In this work, the researchers from the Sloan-Kettering Institute utilized x-ray crystallographic data collected at the NE-CAT beamline to show for the first time structural evidence for how this selective recognition is mediated.

A crystal structure of the PCNA with a SUMO modification was generated (Fig. 1). A structure was also solved with a peptide corresponding to the motif of the helicase Srs2 that binds to SUMO-modified PCNA. This peptide was shown to bind in two distinct locations on the PCNA, suggesting that Srs2 binds both the SUMO modification and PCNA itself. Biochemical data showed that binding to either SUMO alone or PCNA alone by this Srs2 peptide was significantly weaker than binding to SUMO-modified PCNA, suggesting that both the protein and the SUMO modification need to be in place for tight recognition.

This work presented the first structure of recognition of a SUMO-modified protein by a receptor. More than likely, other systems employ similar mechanisms to simultaneously recognize a protein and its post-translational modification. By understanding how this process works, other examples of SUMO-modified protein recognition in cells can be more easily characterized, which will provide a better understanding of important cellular processes such as differentiation, apoptosis, and DNA repair. — *Emma Hitt*

See: Anthony A. Armstrong, Firaz Mohideen, and Christopher D. Lima*, "Recognition of SUMO-modified PCNA requires tandem receptor motifs in Srs2," *Nature* **483**, 59 (1 March 2012). DOI:10.1038/nature10883

Author affiliation:

Sloan-Kettering Institute

Correspondence: *limac@mskcc.org

A.A.A., F.M., and C.D.L. are supported by National Institutes of Health (NIH) R01 GM065872 to C.D.L. and F32 GM086066 to A.A.A. NE-CAT is supported by grants from the National Center for Research Resources (5P41RR015301-10) and the National Institute of General Medical Sciences (8 P41 GM103403-10) from the NIH. Use of the Advanced Photon Source at Argonne National Laboratory was supported by the U.S. Department of Energy Office of Science under Contract No. DE-AC02-06CH11357.

24-ID-C • NE-CAT • Life Sciences • Macromolecular crystallography, microdiffraction, single-wavelength anomalous dispersion, single-crystal diffraction, microbeam • 6.5-23 keV • On-site • Accepting general users •

OUTSMARTING FLU VIRUSES

Smart viruses find ways around host defenses. In the case of the influenza viruses A and B, rapid genetic changes and resistance to available therapies make it hard to combat flu epidemics in humans. Mortality rates for influenza B viruses are higher than those reported for seasonal influenza A H1N1. Human monoclonal antibodies were previously shown to neutralize a wide variety of influenza A viruses, so extending that work to include influenza B viruses is critical because these flu strains cause a large proportion of the annual flu infections and are a major cause of seasonal epidemics every two to four years. Researchers working at a GM/CA-XSD beamline at the APS, as well as two other U.S. Department of Energy light sources, and building upon their earlier work with influenza A viruses, have now discovered a similar phenomenon for neutralizing influenza B viruses. Their results pave the way for development of a universal vaccine for all influenza A and B viruses.



Earlier work by the group, from The Scripps Research Institute, Crucell Vaccine Institute (The Netherlands), Gustav Wieds Vej (Denmark), and The University of Hong Kong on the influenza A viruses showed that monoclonal antibodies can neutralize the viruses by binding to a highly conserved region, called an epitope, in the stem region of a viral surface glycoprotein. To look for similar reactions in the influenza B virus, the research team focused on two co-circulating, antigenically distinct strains.

The researchers found three human monoclonal antibodies that protect against potentially lethal infection from these two influenza B strains. Two of the antibodies, CR8033 and CR8071, bind to conserved epitopes in the head region of the influenza B hemagglutinin (HA). The third antibody, CR9114, attaches to a conserved epitope in the HA stem, and, most important, provides protection against influenza A and B viruses.

The study showed that the three antibodies did not compete against

each other for HA binding sites and thereby concluded that they recognized different epitopes. The results pointed to the mechanism by which the antibodies CR8033 and CR8071 thwarted viral infection: although the virus gained entry to the cell and performed genome replication, propagation of the virus was prevented.

Antibodies CR8033 and CR8071 appear to prevent release of viral progeny from infected cells and disrupt the infection process. CR9114 uses a different mechanism and blocks infection by preventing the low pH conformational changes that trigger the fusion of the viral and endosomal membranes during the entry process (Fig. 1).

Several structures were solved using the GM/CA-XSD 23-ID-B beamline in order to study the interaction of CR9114 with group 2 influenza A viruses. A key aspect of these results is the finding that the CR9114 epitope appears to be highly conserved in all influenza A subtypes and in influenza B. These structures allowed the group to confirm the broad neutralizing activity of CR9114.

This finding is important primarily because it provides an inroad to the previously intractable problem of finding a universal influenza vaccine. A highly conserved epitope is likely to remain the same even if the virus undergoes repeated mutations and resistance cycles. When searching for a vaccine, a neutralizing epitope region

that remains constant and vulnerable to existing treatments is a beautiful thing. Antibodies such as CR9114 may be possible to elicit by vaccination and may already be present in the immune systems of some individuals.

Future directions for the researchers are to apply this knowledge toward the development of improved therapies and vaccines such as development of monoclonal antibody therapies and the design of small molecules that target the weak point in the virus defense.

Since previous work had shown that the influenza A viruses exhibited broadly neutralizing epitopes in the HA stem, those now found in the influenza B HA head point to both the head and stem regions of these viruses as targets for neutralizing antibodies.

Universal therapies against the many strains of influenza that may be circulating at any given time require somewhat of a "one vaccine fits all" approach. The work presented in this study — especially that concerning the CR9114 antibody — brings that dream into the realm of the possible.

— *Mona Mort*

See: Cyrille Dreyfus¹, Nick S. Laursen^{1,2}, Ted Kwaks³, David Zuijdgeest³, Reza Khayat¹, Damian C. Ekiert^{1†}, Jeong Hyun Lee¹, Zoltan Metlagel^{1‡}, Miriam V. Bujny³, Mandy Jongeneelen³, Remko van der Vlugt³, Mohammed Lamrani³, Hans J.W.M. Korse³, Eric Geelen³, Özcan Sahin³, Martijn Sieuwerts³, Just P.J. Brakenhoff³, Ronald Vogels³, Olive T.W. Li⁴, Leo L.M. Poon⁴, Malik Peiris⁴, Wouter Koudstaal³, Andrew B. Ward¹, Ian A. Wilson^{1*}, Jaap Goudsmit^{3**}, and Robert H.E. Friesen³, "Highly Conserved Protective Epitopes on Influenza B Viruses," *Science* **337**, 1343 (14 September 2012).

DOI:10.1126/science.1222908

Author affiliations: ¹The Scripps Research Institute, ²Gustav Wiedes Vej, ³Cruell Vaccine Institute, ⁴The University of Hong Kong. Present addresses: [†]University of California, San Francisco. [‡]Lawrence Berkeley National Laboratory

Correspondence: *wilson@scripps.edu; **jaap.goudsmit@cruell.com

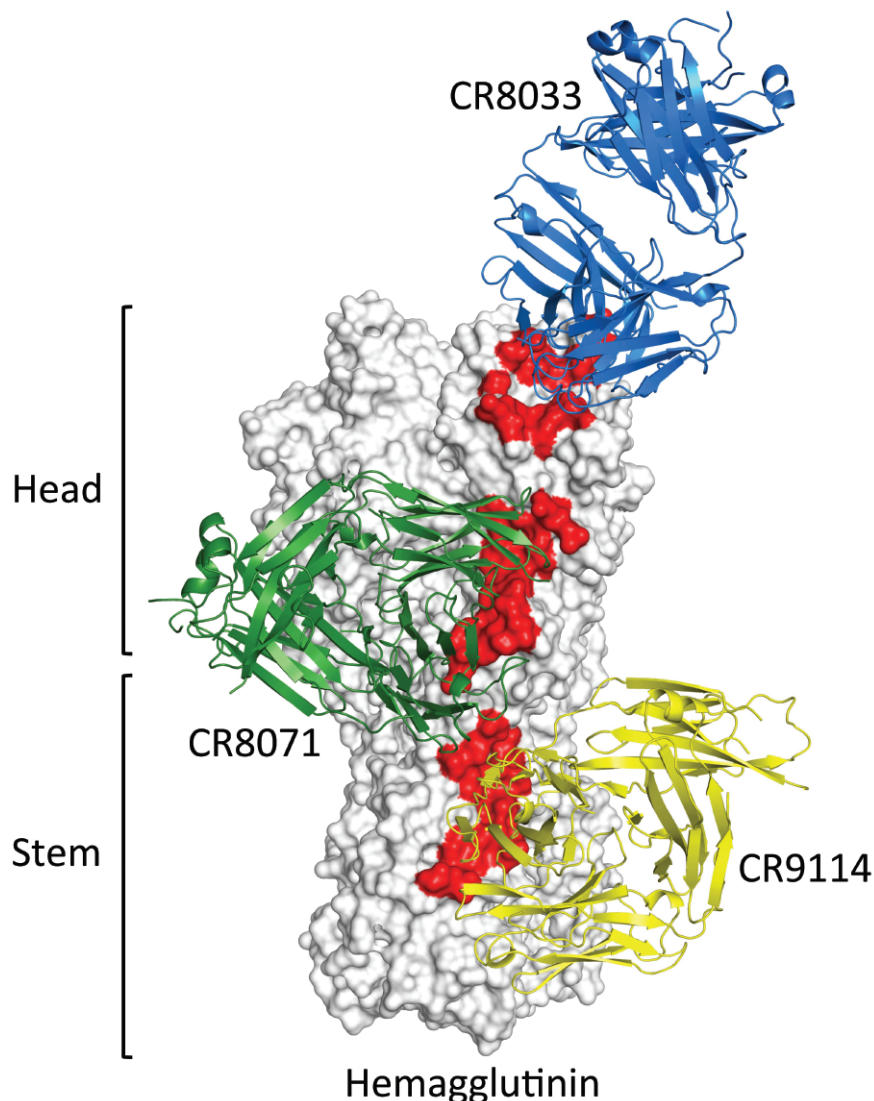


Fig.1. Surface representation of influenza hemagglutinin (white) with the newly identified sites of vulnerability colored red. Each site is unique and targeted by a different antibody. CR8033 (blue) binds to the head of HA, CR8071 (green) just below the head, while CR9114 (yellow) binds the stem. The stem binding CR9114, with its cross-neutralizing ability for influenza A and B viruses, provides proof of principle that a universal flu vaccine may be achievable.

This project has been funded in part by the Area of Excellence Scheme of the University Grants Committee, Hong Kong (grant AoE/M-12/06); a predoctoral fellowship from the Achievement Rewards for College Scientists Foundation (D.C.E.); grant GM080209 from the National Institutes of Health (NIH) Molecular Evolution Training Program (D.C.E.); a Saper Aude Postdoc grant from the Danish Council for Independent Research, Natural Sciences (N.S.L.), and the Skaggs Institute (I.A.W.). Portions of this research were carried out at the Stanford Synchrotron Radiation Lightsource at Stanford University and the Advanced Light Source at Lawrence Berkeley National Laboratory.

GM/CA-XSD is funded in whole or in part with federal funds from National Cancer Institute (Y1-CO-1020) and NIGMS (Y1-GM-1104). Use of the Advanced Photon Source at Argonne National Laboratory was supported by the U.S. DOE Office of Science under Contract No. DE-AC02-06CH11357.

23-ID-B • GM/CA-XSD • Life sciences • Large unit cell crystallography, macromolecular crystallography, microbeam, multi-wavelength anomalous dispersion, single-wavelength anomalous dispersion, subatomic (<0.85 Å) resolution • 3.5-20 keV • On-site, remote • Accepting general users •

TARGETING A NEW ENZYME TO COMBAT ANTIBACTERIAL RESISTANCE

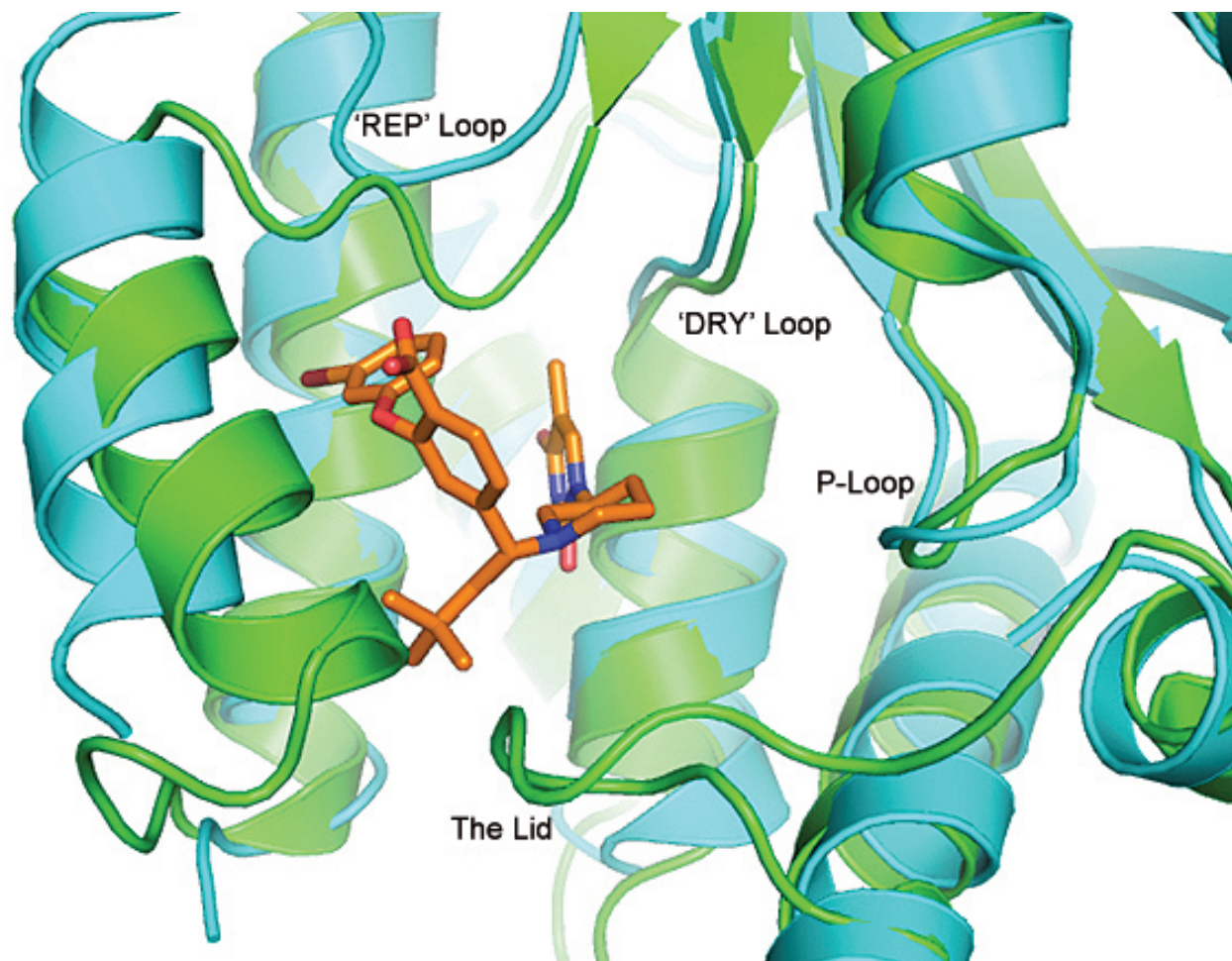


Fig. 1. Antibacterials need to block their bacterial targets, while safely avoiding any human counterpart. Antibacterial inhibitor TK-666 (orange) is shown bound to the *Staphylococcus aureus* TMK enzyme (green). Overlaid in cyan is the human TMK enzyme clearly showing, in several labeled regions, how there is much less space to accommodate TK-666. This smaller pocket is responsible for the remarkable selectivity of TK-666 for the bacterial enzyme over the human form.

Although antibiotics are one of the greatest discoveries of medical science, their widespread use has led to development of antibiotic resistance as bacteria constantly undergo genetic changes to evade their action. Infections caused by resistant strains of bacteria have risen at an alarming rate globally in recent years. The researchers in this study utilized the LRL-CAT insertion device beamline at the APS to obtain a high-resolution structure of an enzyme that affects the pathway that produces bacterial DNA. Their work is aimed at designing synthetic compounds that target and disrupt the action of that enzyme resulting in deadly consequences for bacterial cells that will no longer be able to replicate their DNA.

Antibiotics have been one of the most important medical discoveries of the 20th century. They play a key role in reducing illness and death due to infectious diseases. Overuse and misuse of antibiotics, however, have contributed to the emergence and spread of antibiotic resistance. This phenomenon represents a natural biological response of bacteria that allows them to adapt to adverse conditions. So, when faced with new antibiotics, they are able to mutate or change in such a way as to develop mechanisms to protect the biochemical targets with which the newly developed antibacterial agents interact. As a consequence, the effectiveness of the drug is reduced, or even eliminated. Antibacterial resistance is a costly and dangerous problem that can complicate patient treatment, result in longer and more serious illnesses, increase the duration of hospital stays, and even cause unnecessary death in some cases.

Bacteria are characterized as either Gram-positive or Gram-negative, according to how they react to the Gram staining technique that differentiates them based on their different cell wall constituents. In the United States, Gram-positive bacteria are common causes of bloodstream and other infections, and the incidence of hospital-acquired bloodstream infections caused by antibiotic-resistant Gram-positive bacteria is increasing. Infections by methicillin-resistant *Staphylococcus aureus* (commonly known as MRSA) and *vancomycin-resistant enterococci* (VRE) are especially concerning and have been rising dramatically throughout the world in recent years. Consequently, there is a critical need for new antibacterial

agents that can avoid current resistance mechanisms by attacking novel biochemical targets.

Thymidylate kinase (TMK) is an enzyme required by bacteria to synthesize DNA, the nucleic acid that stores the genetic information within cells. It acts by adding a phosphate group to deoxythymidine monophosphate (dTMP) to form deoxythymidine diphosphate (dTDP). Since this reaction comprises part of the biochemical pathway that is essential to produce DNA, interfering with TMK has a lethal effect on the cell due to blockage of DNA synthesis. TMK therefore has potential as a new antibacterial drug target.

An analysis of the structure of TMK has suggested that its dTMP binding pocket may be the most appropriate target for drug design. In this study, dTMP analogues were used as starting points for the design of synthetic compounds to target TMK in the bacterium *S. aureus*.

Utilizing data sets collected at the LRL-CAT 31-ID-D beamline, the researchers iteratively synthesized novel compounds and evaluated the crystal structures of these analogues when bound to TMK. This approach ultimately yielded TK-666, an inhibitor that showed potent broad-spectrum activity against Gram-positive bacteria, including activity against MRSA and VRE. It also demonstrated effective bactericidal activity, excellent selectivity for its biochemical target, and low resistance rates. Compared with human or Gram-negative bacterial TMK, differences in the binding pocket — the region of the enzyme where the inhibitor binds — were found to be responsible for the Gram-positive specificity of TK-666 (Fig. 1).

This study is the first to demonstrate TMK as a convincing antibacterial target for therapeutic drug discovery. The results of this research will be important in guiding future work in the development of novel compounds for the treatment of clinically relevant Gram-positive infections through TMK.

— Nicola Parry

See: Thomas A. Keating*, Joseph V. Newman, Nelson B. Olivier, Linda G. Otterson, Beth Andrews, P. Ann Boriack-Sjodin, John N. Breen, Peter Doig, Jacques Dumas, Eric Gangl, Oluyinka M. Green, Satenig Y. Guler, Martin F. Hentemann, Diane Joseph-McCarthy, Sameer Kawatkar, Amy Kutschke, James T. Loch, Andrew R. McKenzie, Selvi Pradeepan, Swati Prasad, and Gabriel Martínez-Botella†, "In Vivo Validation of Thymidylate Kinase (TMK) with a Rationally Designed, Selective Antibacterial Compound," *ACS Chem. Biol.* 7, 1866 (2012). DOI:10.1021/cb300316n

Author affiliation: AstraZeneca.

†Present address: Sage Therapeutics

Correspondence:

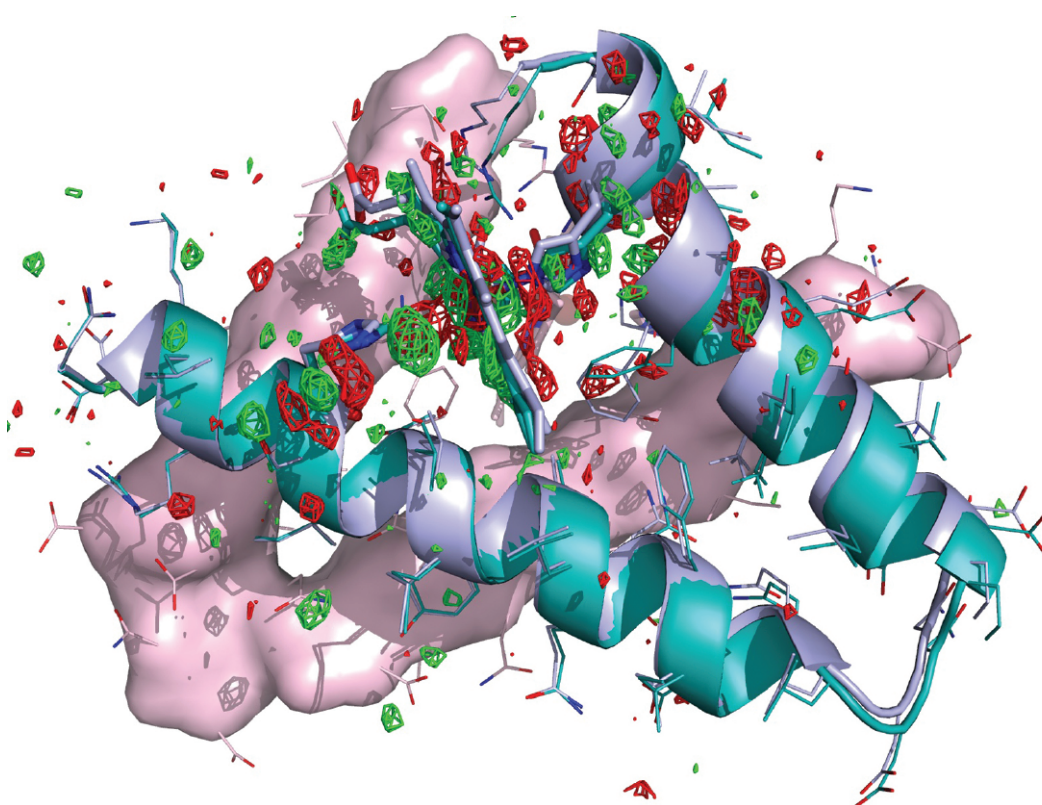
*thomas.keating@astrazeneca.com

Use of the Lilly Research Laboratories Collaborative Access Team beamline at Sector 31 of the Advanced Photon Source was provided by Eli Lilly Company, which operates the facility. Use of the Advanced Photon Source at Argonne National Laboratory was supported by the U.S. Department of Energy Office of Science under Contract No. DE-AC02-06CH11357.

31-ID-D • LRL-CAT • Life sciences • Macromolecular crystallography, single-wavelength anomalous dispersion, single-crystal diffraction • 4.7-28 keV • Mail-in • Accepting general users •

MOLECULAR SCISSORS AND PLIERS: HEMOGLOBIN ASSEMBLY

Protein molecules often have quite intricate and complex structures equaling that of the great cathedrals. Envisioning the mechanisms that achieve this structural complexity can be daunting. How do simple molecules assemble themselves into multi-subunit structures? The study of small subsets of molecules or a few steps in a complicated biochemical procedure can yield real insight about assembly mechanisms. But to get the big picture, and to get an entire picture, requires looking at multiple studies of many parts of the system. This is where meta-analysis — analyzing large numbers of results from a large number of studies — really shines and takes the daunting into the realm of the possible. A research team utilized meta-analysis and the BioCARS beamline 14-ID-B at the APS to reveal an assembly mechanism for the all-important hemoglobin molecule. They applied the results to an actual hemoglobin molecule to visualize the progression of construction events, greatly advancing our understanding of how hemoglobin assembly works and what to do when that mechanism malfunctions to create disease.



Four movies of the virus can be viewed at <http://www.pnas.org/content/109/1/107/suppl/DCSupplemental> or via this QR code.



Hemoglobin molecules transport oxygen in vertebrates and many invertebrates and generally consist of two or more subunits in each hemoglobin molecule, all of which orient to hold heme groups. The subunits must be able to communicate with each other in some way and coordinate to form the correct shape. The main question that these researchers set out to answer is how this communication between subunits occurs. The team answered this question by first performing a meta-analysis on invertebrate hemoglobin molecules in the Protein Data Bank. By analyzing such a large amount of data they were able to propose structural changes that would be expected to occur when subunits bind to each other. The researchers then applied this knowledge to actual hemoglobin assembly in the clam *Scapharca inaequivalvis* and by doing so have unveiled a detailed model for this previously mysterious process.

The research team, with members from The University of Chicago, the Mercer University School of Medicine, and the University of Massachusetts Medical School found that in this hemoglobin, which consists of two chemically identical subunits, binding in the first subunit triggers and facilitates binding in the second subunit. Evidence for this mechanism came from ultrafast time-resolved crystallographic data (Fig. 1).

An extremely interesting model arose from these analyses. The subunits function like a mechanical device with two identical parts, such as pliers or scissors (Fig. 2). Ligand-induced motion in one subunit is conveyed to the other subunit by way of pivot points. And, just like in pliers or scissors, the two partner subunits are

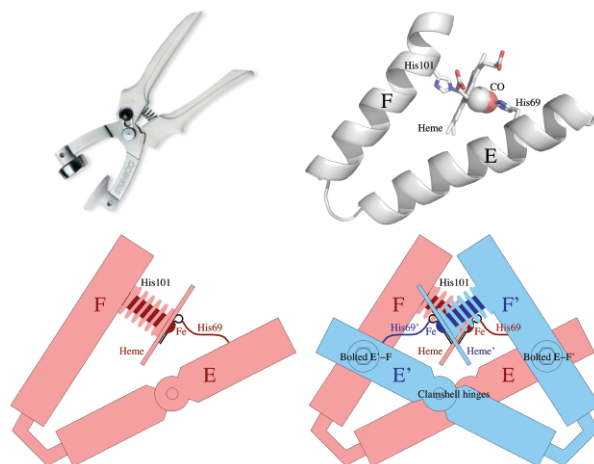


Fig. 2. The pair of helices with a heme group in between resembles specialty pliers. Oxygen binding or releasing acts like a spring that alters the space between the helices. When two subunits in pink and blue are bolted together at the crossings of helices by a unique sequence of amino acids, slight motion in one subunit is mechanically coupled to the other subunit. The inter-subunit communication achieves cooperative oxygen binding.

“bolted” together. This molecular bolting provides a stable interface between the subunits where relative pivot motion is possible but sliding is prevented.

The researchers identified relative rotations that account for previously observed changes in the three-dimensional structure of the hemoglobin molecules. The model is essentially a cooperative one in that movement of the subunits is interdependent. The location of the molecular hinge, in the middle of a helix rather than in the corner where two helices join, was also found to be of prime importance as was the tight interaction between the subunits. The latter finding explains why there is just enough motion to allow movement but not too much motion to cause sliding, which would prevent motion. This is just as would be expected when a pair of scissors or pliers is loose at the bolting point, making it difficult to cut or clamp properly. By using time-resolved experiments, the researchers were able to look at intermediate steps and able to see this molecular mechanical device stopped

< Fig. 1. The two subunits of the clam hemoglobin are assembled together at the interface between two identical pairs of helices. The pink surface in the background represents one pair of helices from a subunit, and the ribbon models in blue colors represent another pair from the partner subunit. The stick model between two helices is a heme group that carries oxygen. The differences between the oxygen bound and unbound forms are captured by Laue diffraction using the intense x-ray beam on 14-ID-B of APS. Here the gain and loss of electron densities are shown as green and red mesh, respectively. The changes in the blue subunit are driving the same changes in the pink one.

in motion, further supporting that it acts like scissors or pliers.

The research team identified a cooperative model, a cascade of structural events between the hemoglobin subunits. Such a tight linkage of events had been previously suspected, but the team used the results of meta-analysis applied to actual hemoglobin molecules to show that it actually happens.

In addition to providing major insight to hemoglobin assembly, the research has general applications for how motions and signals are transmitted across subunits and biochemical domains. Beginning their approach to this problem by using meta-analysis, the team obtained a big picture, which then allowed understanding of a specific hemoglobin system. Such an approach holds great promise for tackling hemoglobin-related disease and for understanding other protein assemblies.

— Mona Mort

See: Zhong Ren^{1*}, Vukica Šrajer¹, James E. Knapp², and William E. Royer, Jr.³, “Cooperative macromolecular device revealed by meta-analysis of static and time-resolved structures,” *Proc. Natl. Acad. Sci. USA* **109**, 107 (January 3, 2012).

DOI:10.1073/pnas.1109213108

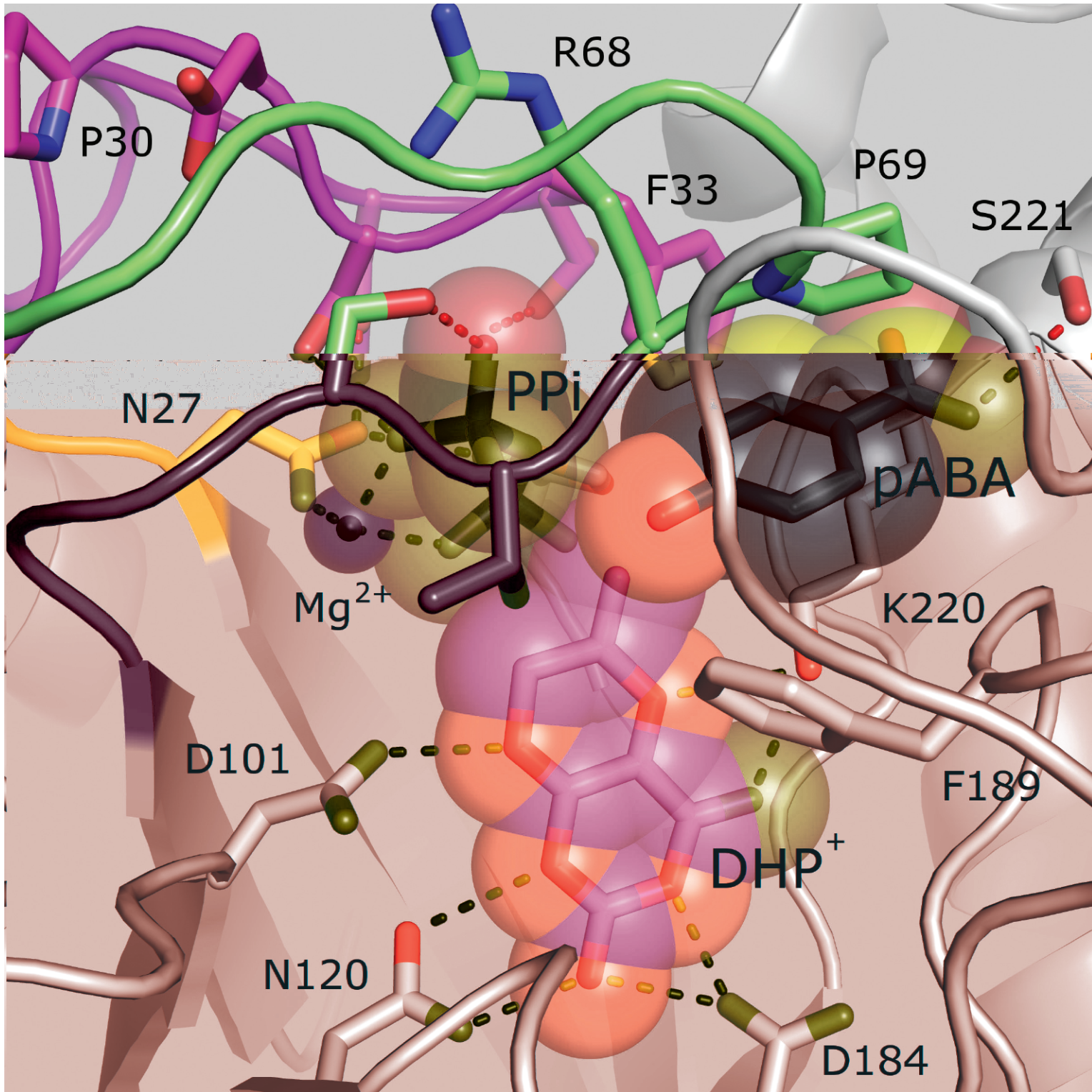
Author affiliations: ¹The University of Chicago, ²Mercer University School of Medicine, ³University of Massachusetts Medical School

Correspondence: *renz@uchicago.edu

Use of the BioCARS Sector 14 was supported by the National Institutes of Health (NIH), National Center for Research Resources, under Grant RR007707. Use of the Advanced Photon Source at Argonne National Laboratory was supported by the U.S. Department of Energy Office of Science under Contract No. DE-AC02-06CH11357.

14-ID-B • BioCARS • Life sciences • Time-resolved crystallography, time-resolved x-ray scattering, Laue crystallography, wide-angle x-ray scattering, biohazards at the BSL2/3 level, macromolecular crystallography • 7-20 keV • On-site • Accepting general users •

A NEW TWIST ON AN OLD DRUG TARGET



Students often believe that there are no more important discoveries to be made in science and that their textbook contains the final word on what we know about the natural world. Of course, nothing could be further from the truth. In work completed at the SER-CAT 22-BM-D and 22-ID-D beamlines at the APS, colleagues from St. Jude's Children's Research Hospital and the University of Tennessee Health Science Center have learned something new about an old topic: sulfonamide antibiotics. Their work explains the mechanism by which bacteria develop resistance to these drugs and provides detailed information about the catalytic action of the bacterial enzyme they inhibit. This information can guide the development of new antibiotics that will target the same pathway but not be as susceptible to resistance as previous antibiotics.

Introduced in the 1930s, sulfonamide (sulfa) drugs were the first antibiotics to act on a wide range of bacterial infections. They inhibit the bacterial enzyme dihydropteroate synthase (DHPS) by competing with the enzyme's natural substrate, *p*-aminobenzoic acid (PABA). DHPS is an enzyme in the folate pathway that is essential to bacterial growth. The sulfa drugs work because humans get folate from their diet and are not affected by the inhibitor, so bacteria are specifically targeted for killing. The sulfa drugs are still used but, due to mutations in DHPS that allow some bacterial strains to develop resistance to them, they are often only second- or third-line options.

However, some sulfa drugs have proven effective against infections that are resistant to other antibiotics and in immune-compromised patients, creating renewed interest in developing antibiotics that target DHPS but do not allow resistance to emerge. The St. Jude/Tennessee team is interested in developing antibiotics that target the binding of the other DHPS substrate, 6-hydroxymethyl 7,8-dihydropterin pyrophosphate (DHPP).

In previous structural and molecular studies of DHPS, it was determined that mutations allowing for resistance were clustered within two flexible, conserved loops near the enzyme's active site. However, these regions were not

well-visualized in crystal structures, leaving open many questions about how the mutations confer resistance and what role the loops play in enzyme catalysis. To gain more information about the catalytic mechanism of DHPS, the group approached the problem by trying to visualize the structure of DHPS in complex with both its substrates.

After soaking their DHPS crystals in PABA and DHPP, the researchers were surprised to find that the enzyme had catalyzed the reaction, leaving an intermediate molecule still bound in the active site (Fig. 1; DHP⁺). This intermediate structure provided two new findings. First, the structure showed that atoms involved in the catalysis were likely to undergo a unimolecular (SN¹) rather than a bimolecular (SN²) nucleophilic substitution reaction mechanism as was previously hypothesized. This provides important information about the catalytic mechanism of DHPS necessary for inhibiting its activity. Second, the structures of the flexible loops were stabilized in the presence of the intermediate; this allowed the team to see what was going on at that crucial point in catalysis.

Visualization of the loop 1 and loop 2 structures showed that during catalysis the loops form the pocket that binds to the substrate, PABA. This explains why amino acids in those loops are conserved in the enzyme and why mutations in those amino acids can confer antibiotic resistance. If they serve to inhibit sulfa drug binding but retain PABA binding, the bacteria can still make folate. Indeed, crystals soaked with the DHPP substrate and a sulfa drug instead of PABA showed that

the sulfa drugs insert directly into the pABA binding site.

Next, the team plans to use the insights gained from this study to develop drugs that can bypass these mutations and inhibit DHPS via the DHPP site. — *Sandy Field*

See: Mi-Kyung Yun^{1,2}, Yinan Wu¹, Zhenmei Li¹, Ying Zhao¹, M. Brett Waddell¹, Antonio M. Ferreira¹, Richard E. Lee¹, Donald Bashford^{1,2}, Stephen W. White^{1,2*}, "Catalysis and Sulfa Drug Resistance in Dihydropteroate Synthase," *Science* **335**, 1110 (2 March 2012). DOI:10.1126/science.1214641
Author affiliations: ¹St. Jude Children's Research Hospital, ²University of Tennessee Health Science Center
Correspondence:

*stephen.white@stjude.org

This work was supported by National Institutes of Health (NIH) grant AI070721 (S.W.W. and R.E.L.), NIH Cancer Center (CORE) support grant CA21765, and the American Lebanese Syrian Associated Charities. SER-CAT is an organization consisting of 22 member institutions, formed in 1997 to provide third-generation x-ray capabilities to macromolecular crystallographers and structural biologists in the southeastern region of the U.S. Use of the Advanced Photon Source at Argonne National Laboratory was supported by the U.S. Department of Energy Office of Science under Contract No. DE-AC02-06CH11357.

22-BM-D • SER-CAT • Life sciences • Macromolecular crystallography • 8-20 keV • On-site, remote • Accepting general users •

22-ID-D • SER-CAT • Life sciences • Macromolecular crystallography • Multi-wavelength anomalous dispersion • micro-beam • 6-20 keV • On-site, remote • Accepting general users •

< Fig. 1. Model of the DHPS active site with space-filling representation of the bound transition state intermediate (DHP⁺), the pyrophosphate leaving group (PPi), and pABA after the crystal was soaked in DHPP, pABA, and Mg²⁺. Loop 1 is shown in magenta and loop 2 in green.

ARCHITECTURE AND VIRAL DISEASE

Over decades of studying how viruses create disease, biologists have discovered that viral structure is a key factor. Thus, obtaining the structure of a disease-causing virus is usually the first step in finding ways to combat the disease. To that end, research at two APS x-ray beamlines determined the crystal structure of human enterovirus 71 (or EV71). This virus can, in infants and young children, cause polio-like paralysis and fatal encephalitis. Because large outbreaks of EV71 have occurred in the Pacific areas of Asia, the virus is now considered an emerging threat to public health. By unveiling the crystal structure of EV71, the research team has taken the essential first step in finding ways to prevent the virus from creating fatal disease, providing strong impetus for therapeutics and drug design to prevent and cure EV71 infection.

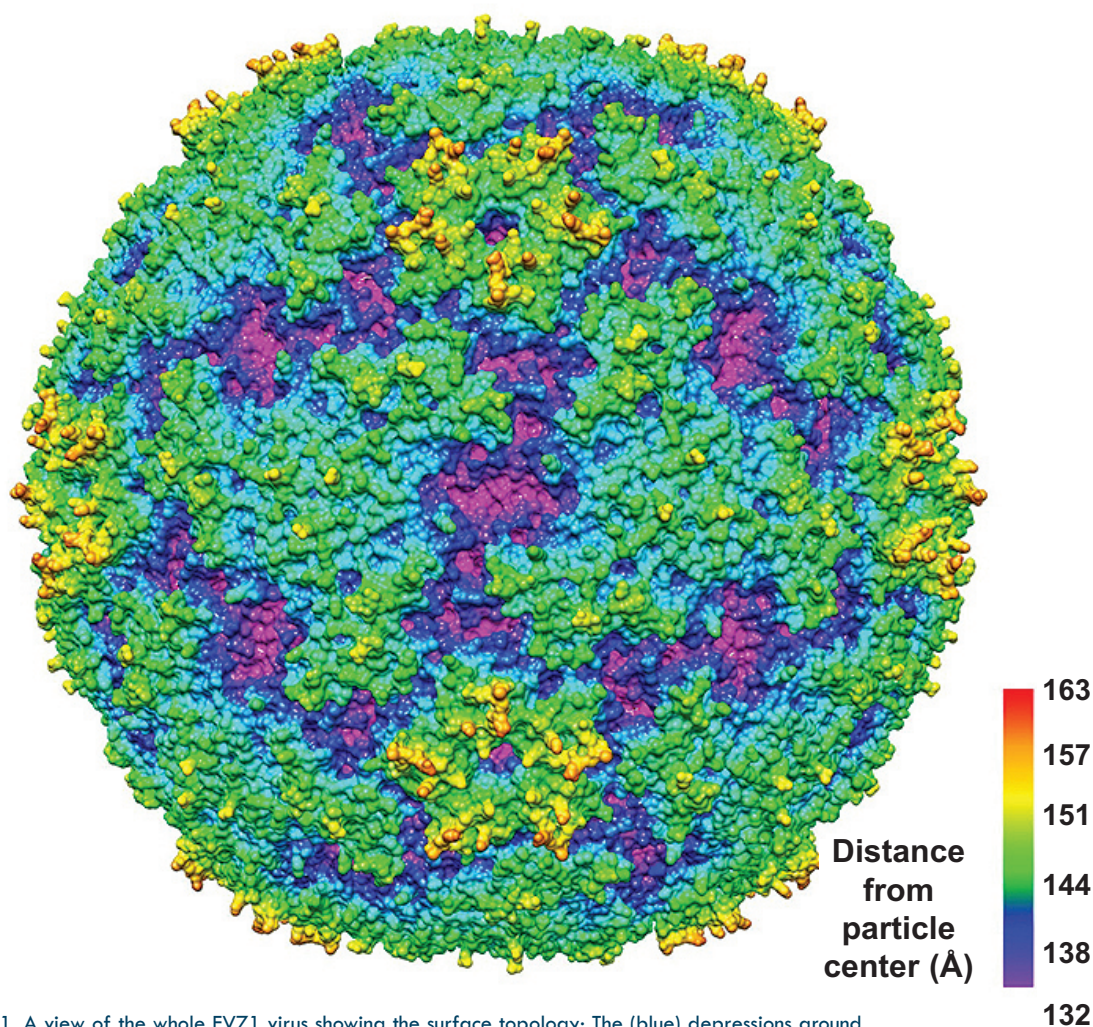


Fig. 1. A view of the whole EV71 virus showing the surface topology: The (blue) depressions around the 5-fold symmetry axes (near the top and bottom of the figure) are the "canyons", which are much deeper in other related viruses such as rhino (common cold) and polio viruses, where they function to bind to receptor molecules on the surface of potentially infected cells.

Viruses are just bits of DNA or RNA and proteins, but they have proved to be capable of immense destruction to human health. How have they achieved the ability to create such devastating diseases in organisms as complex as humans?

One key to understanding how viruses do so much damage appears to lie in their often complicated, and often breathtakingly beautiful architecture. Even though the virus itself is created from an amazingly small number of biochemical components and molecules, there seems to be a nearly infinite number of ways in which these building blocks are used.

The EV71 virus, which in a mild infection causes hand, foot, and mouth disease, belongs to a group called picornaviruses. Like other picornaviruses, EV71 has 60 copies of each of three viral proteins (VP1, VP2, VP3) that have a “jelly-roll” fold as well as 60 copies of a small protein (VP4) attached to the inner surface of the viral capsid. EV71 also has a feature, in common with other enteroviruses, called “canyons,” which are depressions around each fivefold axis (Fig. 1). This canyon is important because it is a place for immunoglobulin-like receptors to bind and will be key in anti-viral drug design.

Because genome release, and thus creation of viral progeny, seems to depend upon a destabilization process in the canyon, finding an antiviral compound that could bind there with high affinity would be an excellent way to inhibit viral infection. By carefully analyzing the EV71 crystal structure obtained at BioCARS beamline 14-ID-B and GM/CA-XSD beamline 23-ID-D the researchers from Purdue University and Sentinext Therapeutics were able to obtain important details about the size and shape of a pocket that may serve as a potential site for inhibitor binding (Fig. 2).

For picornaviruses such as EV71, the most variable regions are the loops

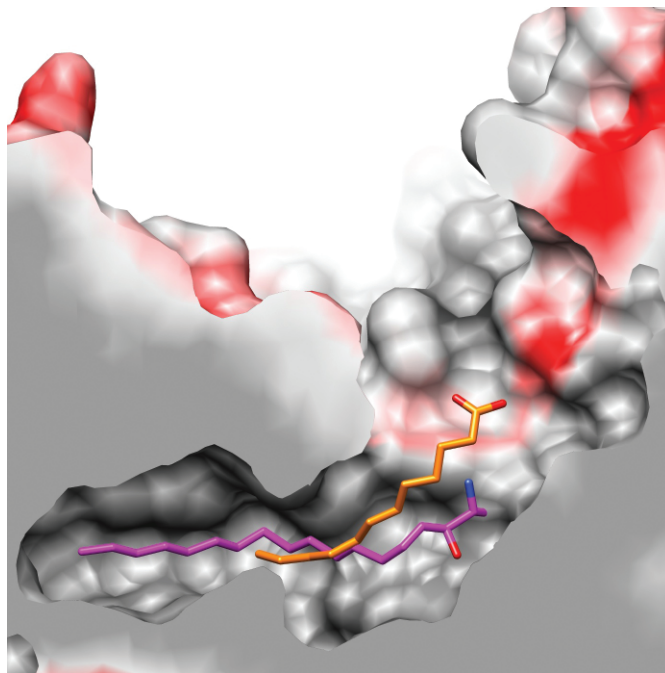


Fig. 2. Detail of the pocket within VP1 of the virus: this pocket might be usable as a target for antiviral compounds.

on the viral surface. In the case of EV71, the surface loops of VP1 create a northern “rim” of the canyon. In EV71 these loops are smaller and therefore the canyon is shallower than in other picornaviruses. Such a detail points to the importance of having a structure for every virus within a group, because such apparently small differences between viruses may thwart a general therapeutic treatment.

When it comes to viral structure, seemingly minute differences may determine the success, or failure, of a viral treatment.

The research group also determined that the VP2 loop is responsible for the “puff” forming the southern rim of the canyon, and that the VP3 loop creates a large surface structure known as the “knob.” In light of what has been found in other picornaviruses, these structures will be important in determining the site where neutralizing antibodies might bind.

Additional details of EV71 suggested that certain types of anti-EV71 compounds should bind into a hydrophobic pocket in VP1 and that these may require a hydrophilic head group that anchors these compounds onto the floor of the canyon. This is in contrast to rhinoviruses, another group of picornaviruses, in which similar com-

pounds have been shown to be highly effective anti-viral agents (albeit with undesirable side effects), but do not interact with residues on the canyon floor. Such details are veritable gold mines for drug designers.

By determining a crystal structure for EV71 in such detail, these researchers have contributed a large amount of critical information in the race to combat the polioliike diseases caused by this enterovirus. Their work opens the road for rapid progress in drug design and therapeutics for diseases caused by EV71.

— Mona Mort

See: Pavel Plevka¹, Rushika Perera¹, Jane Cardosa², Richard J. Kuhn¹, Michael G. Rossmann^{1*}, “Crystal Structure of Human Enterovirus 71,” *Science* **336**, 1274 (8 June 2012). DOI:

10.1126/science.1218713

Author affiliations: ¹Purdue University, ²Sentinext Therapeutics

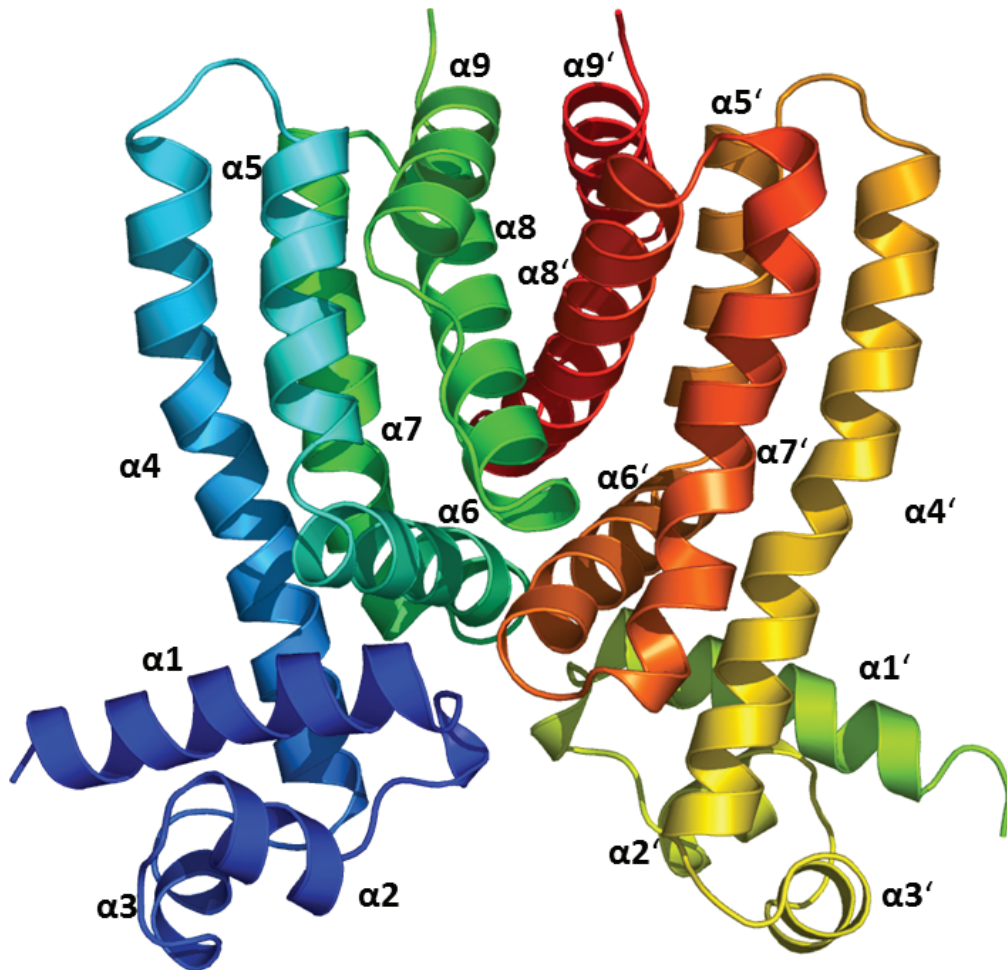
Correspondence: *mr@purdue.edu

This work was supported by National Institutes of Health grant AI11219 to M.G.R. Use of the BioCARS Sector 14 was supported by grants from the National Center for Research Resources (5P41RR007707) and the National Institute of General Medical Sciences (8P41GM103543) from the National Institutes of Health. GM/CA-XSD has been funded in whole or in part with federal funds from the National Cancer Institute (Y1-CO-1020) and the National Institute of General Medical Sciences (Y1-GM-1104). Use of the Advanced Photon Source at Argonne National Laboratory was supported by the U.S. Department of Energy Office of Science under Contract No. DE-AC02-06CH11357.

14-ID-B • BioCARS • Life sciences • Time-resolved crystallography, time-resolved x-ray scattering, Laue crystallography, wide-angle x-ray scattering, biohazards at the BSL2/3 level, macromolecular crystallography • 7-20 keV • On-site • Accepting general users •

23-ID-D • GM/CA-XSD • Life sciences • Macromolecular crystallography, microbeam, large unit cell crystallography, subatomic (<0.85 Å) resolution, multi-wavelength anomalous dispersion, single-wavelength anomalous dispersion • 5-20 keV • On-site, remote • Accepting general users •

PRIMING THE PUMP IN THE FIGHT AGAINST DRUG-RESISTANT TUBERCULOSIS



In recent years, drug resistance has become an increasing problem in the treatment of tuberculosis (TB), posing a significant challenge for efforts to prevent and control this disease, which has been a leading cause of death worldwide for more than 5000 years. Utilizing the NE-CAT facility at the APS, researchers unlocked the secrets of a protein that helps TB develop multidrug resistance. Understanding the results of this study will be important in guiding future research into new ways to control this disease.

Tuberculosis is a bacterial disease caused by *Mycobacterium tuberculosis*. It is easily transmitted through droplets in the air and predominantly affects the lungs. Although this is an ancient disease, it continues to pose significant problems to the public health. It is the leading cause of death from a curable infectious disease and is second only to human immunodeficiency virus/acquired immunodeficiency syndrome as the largest killer worldwide due to a single infectious agent.

TB is preventable and curable, but it is becoming more resistant to treatment. According to the World Health Organization, about 5% of cases are multidrug-resistant (MDR) – that is, they are resistant to isoniazid and rifampicin, two drugs that are first-line treatments for this condition.

The problem has further spiraled out of control as additional antibiotics have been used to attempt to control the situation, resulting in extensively drug-resistant TB, which is harder to control, and most recently, totally drug-resistant TB, which appears to be untreatable.

A better understanding of the molecular mechanisms of drug resistance in *M. tuberculosis* is therefore important for the continued development of new strategies to control this disease.

Recent studies have suggested that MDR strains of *M. tuberculosis* are associated with bacterial transporter pumps that, when switched on, can work to actively flush out a range of compounds from within the bacterial

cells. This includes the very medications that are being used to target the organism. One of these pumps is the Mmr multidrug efflux pump, which is involved in the development of multidrug resistance. Because very little has been known about what regulates the Mmr pump, this study aimed to investigate this mysterious biological device.

Utilizing the NE-CAT x-ray beamline 24-ID-E at the APS, researchers from Iowa State University and Cornell University determined the crystal conformation of the regulator protein Rv3066 (Fig. 1).

An important finding of their study provides insight into the structure and function of this regulator protein.

This protein, which regulates the Mmr bacterial pump, is an asymmetric, two-part regulator molecule with a flexible, spiral structure that allows it to recognize and respond to drugs.

The researchers found that in the presence of ethidium bromide, a toxic compound and substrate transported by the pump, the regulator changes its conformation. It undergoes a structural rotation, thereby switching on the pump that effectively gets rid of antimicrobial drugs from the bacterial organism.

Although further details behind the mechanism of multidrug resistance in TB remain to be determined, studying the structure of this regulator and how it acts to control the bacterial pump will lead to a better understanding of how the bacterium contributes to multidrug resistance and how it can change according to its environment.

These results will be important in guiding future research in the continued development of new ways to control TB, and could make a big difference in the fight against drug-resistant forms of the condition. — *Nicola Parry*

See: Jani Reddy Bolla¹, Sylvia V. Do¹, Feng Long¹, Lei Dai¹, Chih-Chia Su¹, Hsiang-Ting Lei¹, Xiao Chen¹, Jillian E. Gerkey¹, Daniel C. Murphy¹, Kanagalaghatta R. Rajashankar², Qijing Zhang¹, and Edward W. Yu^{1*}, “Structural and functional analysis of the transcriptional regulator Rv3066 of *Mycobacterium tuberculosis*,” *Nucl. Acids Res.* **40**(18), 9340 (2012). DOI:10.1093/nar/gks677

Author affiliations: ¹Iowa State University, ²Cornell University

Correspondence: *ewyu@iastate.edu

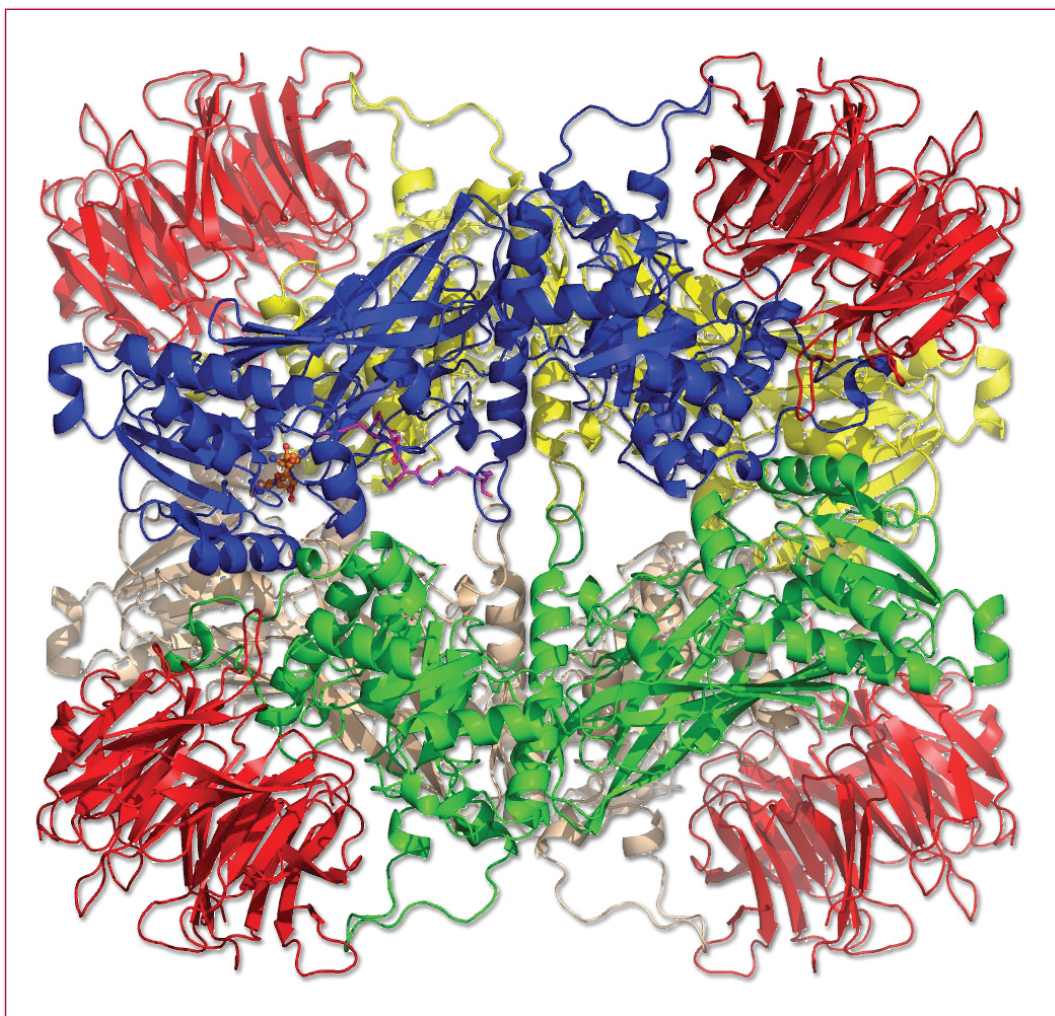
This work is supported by National Institutes of Health (NIH) DK063008 to Q.Z. and GM086431 to E.W.Y., a Community College Institute of Science Internship, and a Science Undergraduate Laboratory Internship from the U.S. Department of Energy (DOE) to J.E.G. and D.C.M. The Northeastern Collaborative Access Team is funded by Columbia University, Cornell University, Harvard University, the Memorial Sloan-Kettering Cancer Center, the Massachusetts Institute of Technology, Rockefeller University, Yale University, and the National Institute of General Medical Science. Use of the Advanced Photon Source at Argonne National Laboratory was supported by the U.S. DOE Office of Science under Contract No. DE-AC02-06CH11357.

24-ID-E • NE-CAT • Life sciences • Macromolecular crystallography, microbeam, microdiffraction, single-wavelength anomalous dispersion, single-crystal diffraction • 12.68 keV • On-site • Accepting general users •

< Fig. 1. This ribbon diagram shows the crystal structure of the asymmetric, two-part regulator molecule Rv3066. Each subunit of Rv3066 is composed of nine α helices. Helices $\alpha 1$ - $\alpha 9$ (left subunit) and $\alpha 1$ - $\alpha 9$ (right subunit) are labeled. Helices $\alpha 4$ through $\alpha 9$ contribute to the region involved in binding of ethidium bromide and drugs.

MODIFYING PROTEINS TO COMBAT DISEASE

Transmitting the genetic message encoded in DNA from one generation to the next is a well-understood concept in biology. There is now increasing awareness that chemical modifications of DNA and associated proteins are also transmitted across generations, and these changes are critical in determining the way the genetic message is read. Detailed understanding of the structures of the proteins that effect these changes is therefore highly coveted information. Thanks to the efforts of a research team from Eli Lilly and Company, with the help of the LRL-CAT beamline 31-ID-D at the APS, the structure of an important methylation enzyme is now known. The results of this research can be used to provide new direction and focus in the race to create drugs to combat disease, especially cancer.



A prime example of chemical modifications is the addition of a methyl group (methylation) to the side-chain of arginine residues of proteins, dramatically altering their activity and interactions. Aberrant methylation has been linked to a wide variety of diseases, most notably cancer.

The Lilly research team investigated a protein from a group of enzymes known as protein arginine methyltransferases (PRMTs), which play important roles in cell signalling, gene regulation, and the transport of proteins and nucleic acids.

The team focused on PRMT5, which had been previously shown to be part of a complex of partner proteins that help regulate its function and specificity. Because enhanced levels of PRMT5 have been observed in various types of cancer, it is a focus of anti-cancer drug research.

In particular, the researchers were interested in how PRMT5 interacts with methylome protein 50 (MEP50), known to be a critical mediator of binding with other members of the protein complex and with substrates. Phosphorylation of either MEP50 or of PRMT5 itself can control methyltransferase activity of PRMT5. Activation of the methyltransferase activity of PRMT5 was known to prolong survival of tumor cells while mutants that disrupt its association with MEP50 inhibited that methyltransferase activity.

Since MEP50 activity has been

< Fig. 1. Structure of the human PRMT5:MEP50 hetero-octameric complex bound to a substrate peptide and a cofactor analog. Cartoon representations of the PRMT5 monomers are colored blue, green, wheat, and yellow, while the MEP50 molecules are in red. Highlighted in stick representation are the substrate peptide derived from histone H3 in magenta, and the cofactor analog in orange.

linked especially to ovarian and prostate cancer, details of its structure and modes of interaction with PRMT5 and other members of the binding complex are prime targets of current research.

The research team determined a definitive structure for PRMT5 in interaction with MEP50, bound to a peptide derived from histone H4. The team combined data from chromatography, sedimentation analysis, enzymology, and x-ray crystallography using data collected at 31-ID-D to elucidate the structure and activity of the PRMT5:MEP50 complex.

The resulting structure yielded a surprise: a hetero-octameric complex that shows close interaction between a seven-bladed propeller-like MEP50 and the N-terminal domain of PRMT5 (Fig. 1). The structure offers a clear view of how substrate recognition occurs and points the way toward promising targets for drug design.

The researchers were able to compare their data from human PRMT5 with newly published data on PRMT5 from the nematode worm, which shows 31% sequence identity with human PRMT5. The dimeric PRMT5 complex in the nematode was strikingly different than the large octameric human PRMT5, in which four molecules of PRMT5 and four of MEP50 form the functional core of the PRMT5 complexes.

This important octameric structural core in human PRMT5 is proposed as the main driver of interactions with partner proteins to create a multimeric complex of subunits with different specificities and functions. In addition, when compared with what was previously known about PRMTs, important differences in the three-dimensional structure of PRMT5 and how it interacts with MEP50 were discovered.

Such critical details will be all-important in anti-cancer drug design. The structural data also allow the role of MEP50 to be expanded by suggesting its importance in recruiting substrates and partners to PRMT5.

By providing a detailed structure of PRMT5 in interaction with MEP50, the research team has revealed critical insights about post-translational methylation and identified promising target sites for drugs to combat cancer and other diseases related to methylation processes. — *Mona Mort*

See: Stephen Antonyamy*, Zahid Bonday, Robert M. Campbell, Brandon Doyle, Zhanna Druzina, Tarun Gheyi, Bomie Han, Louis N. Jungheim, Yuewei Qian, Charles Rauch, Marijane Russell, J. Michael Sauder, Stephen R. Wasserman, Kenneth Weichert, Francis S. Willard, Aiping Zhang, and Spencer Emtage**, "Crystal structure of the human PRMT5:MEP50 complex," Proc. Natl. Acad. Sci. USA **109**(44), 17960 (October 30, 2012). DOI:10.1073/pnas.1209814109

Author affiliation: Eli Lilly and Company
Correspondence:

*antonyamy_stephen@lilly.com,

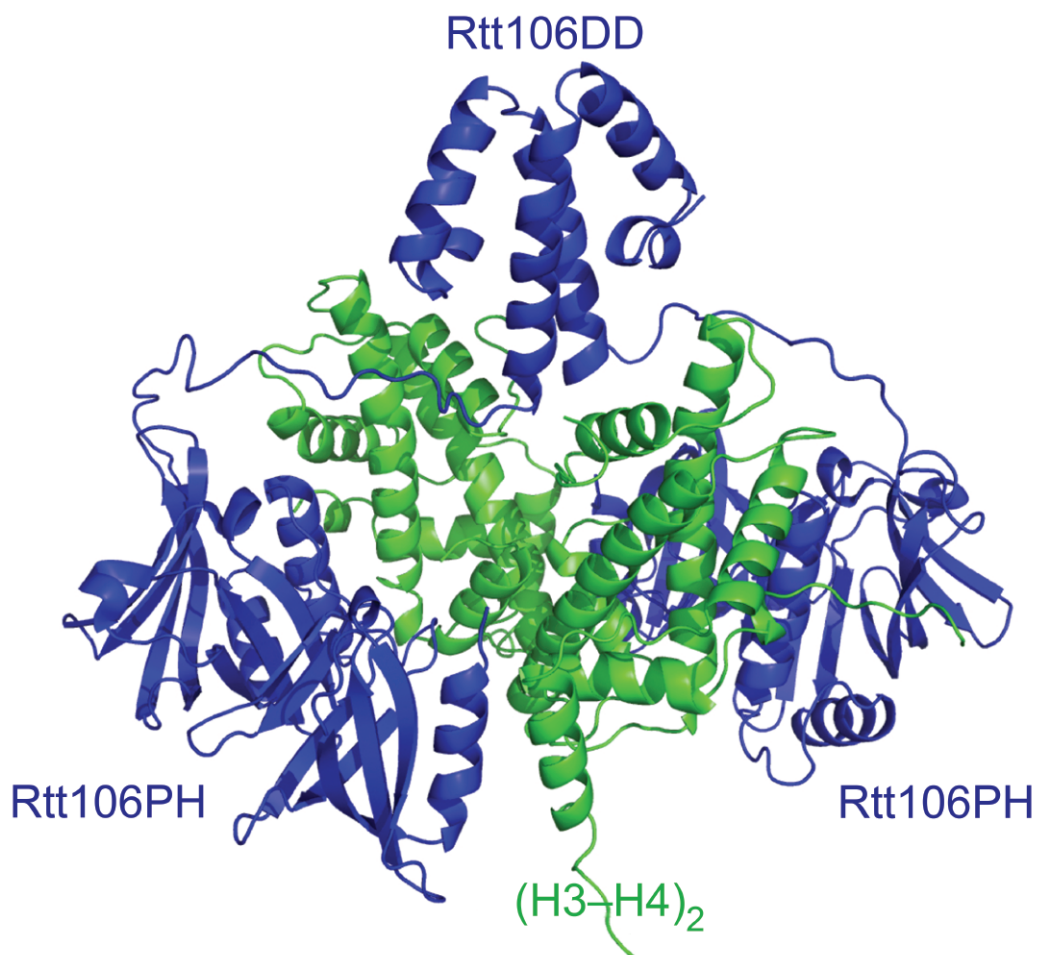
**semtage@gmail.com

Use of the Lilly Research Laboratories Collaborative Access Team beamline at Sector 31 of the Advanced Photon Source was provided by Eli Lilly Company, which operates the facility. Use of the Advanced Photon Source at Argonne National Laboratory was supported by the U.S. Department of Energy Office of Science under Contract No. DE-AC02-06CH11357.

31-ID-D • LRL-CAT • Life sciences • Macromolecular crystallography, single-wavelength anomalous dispersion, single-crystal diffraction • 4.7-28 keV • Mail-in • Accepting general users •

HOW A HISTONE CHAPERONE CONTROLS GENETIC DAMAGE IN YEASTS

In eukaryotic organisms, which are made up of cells that possess a membrane-bound nucleus (that holds genetic material) as well as membrane-bound organelles, changes in chromatin structure influence DNA-related processes and are regulated by post-translational modification, a process that modifies protein structure following synthesis. Researchers from the Mayo Clinic utilized the SBC-CAT beamlines 19-BM-D and 19-ID-D at the APS to investigate processes that are important for gene silencing and the DNA damage response, and will help guide future research into the mechanism of DNA replication, gene silencing, and maintenance of genomic stability in eukaryotic organisms.



In eukaryotic cells, genomic DNA is organized into chromatin, the molecular substance of chromosomes. Chromatin represents a combination of DNA and protein in the cell's nucleus. The proteins that bind to DNA comprise histones and nonhistone chromosomal proteins, and both classes complex with nuclear DNA to form chromatin. Histones are responsible for the most basic level of chromosome organization, the nucleosome, which contains two copies each of four core histones (H2A, H2B, H3, H4).

Changes in chromatin structure affect most DNA-related processes in eukaryotes, and are controlled partly by a late-stage chemical modification of histones during their synthesis, known as post-translational modification. One type of modification involves acetylation of histone lysine 56 (K56) in the amino-terminal α -helix (α N) region of histone H3. K56 is a core region localized at the entry and exit points of a nucleosome. Its acetylation is important in the control of nucleosome assembly during replication and repair of DNA, as well as the disassembly of nucleosomes during gene transcription, when genetic information is copied from DNA to RNA.

The acetylation of the histone H3 protein lysine 56 (H3K56ac) is a reaction considered especially important in the regulation of DNA replication and repair. Chaperones are proteins that have numerous important functions, including preventing newly made proteins from forming nonfunctional structures. In this way, they are involved in the assembly of nucleosomes from his-

tones and DNA. Histones are important for the most basic level of chromosome organization, the nucleosome. H3 and H4 are two histones that complex as a dimer (H3–H4) that makes the most important interactions with DNA. Two H3–H4 dimers in turn complex to form a tetramer (H3–H4)₂.

This deposition of H3–H4 molecules onto DNA requires histone chaperones. Chaperones are proteins that assist with the assembly and disassembly of other structures. One of their major functions is to stop polypeptide chains from forming nonfunctional structures, and as such, they are involved in the assembly of nucleosomes from histones and DNA.

In the yeast *Saccharomyces cerevisiae*, the histone chaperone Rtt106 contributes to the deposition of newly produced H3K56ac-carrying H3–H4 complex on replicating DNA. However, it remains unclear how Rtt106 binds H3–H4 and specifically recognizes H3K56ac.

The researchers from the Mayo Clinic utilized the SBC-CAT beamlines to collect data for the investigation of the three-dimensional (3-D) structure of Rtt106 and its association with histones in order to investigate its mechanism of action. They demonstrated that two regions of Rtt106 are involved in recognition of H3–H4: one, at the N-terminus of Rtt106, interacts with H3–H4 independently of acetylation, while another, a double pleckstrin-homology (PH) domain, binds the K56-containing region of H3. K56 acetylation markedly increases the affinity of H3–H4 for Rtt106, likely due to conformational and dynamic changes in the structure of H3.

These results suggest an interaction where the N-terminus of Rtt106 inserts between the two H3–H4 components of the (H3–H4)₂ tetramer, while two double PH domains in the Rtt106 dimer interact with both H3K56ac sites in (H3–H4)₂. The data additionally support a mechanism of interaction where the N-terminal region of Rtt106 inserts between the two H3–H4 components of

the (H3–H4)₂ tetramer (Fig. 1). Two double PH domains in Rtt106 also interact with the tetramer's two H3K56ac sites.

These structural and functional studies show that the interaction between Rtt106 and the (H3–H4)₂ tetramer is important for gene silencing, a regulatory process during which genes can be switched off, as well as the DNA damage response. The results of this study will therefore help guide further research into the mechanism of DNA replication, gene silencing, and maintenance of genomic stability in eukaryotic organisms. — *Nicola Parry*

See: Dan Su, QiHu, Qing Li, James R. Thompson, Gaofeng Cui, Ahmed Fazly, Brian A. Davies, Maria Victoria Botuyan, Zhiguo Zhang*, and Georges Mer**, "Structural basis for recognition of H3K56-acetylated histone H3–H4 by the chaperone Rtt106," *Nature* **483**, 104 (1 March 2012).

DOI:10.1038/nature10861

Author affiliation: Mayo Clinic

Correspondence:

**mer.georges@mayo.edu,

*zhang.zhiguo@mayo.edu

This work was funded in part by National Institutes of Health grants to Z.Z. and G.M. SBC-CAT is funded by the U.S. Department of Energy (DOE) Office of Science Biological and Environmental Research Program under contract DE-AC02-06CH11357. Use of the Advanced Photon Source at Argonne National Laboratory was supported by the U.S. DOE Office of Science under Contract No. DE-AC02-06CH11357.

19-BM-D • SBC-CAT • Life sciences • Ultra-low-temperature (15K), multi-wavelength anomalous dispersion, single-wavelength anomalous dispersion • 6-13.5 keV • On-site, mail-in • Accepting general users •

19-ID-D • SBC-CAT • Life sciences • Large unit cell crystallography, macromolecular crystallography, microbeam, multi-wavelength anomalous dispersion, single-wavelength anomalous dispersion, subatomic (<0.85 Å) resolution, ultra-low-temperature (15K) • 6.5-19.5 keV • On-site, remote, mail-in • Accepting general users •

< Fig. 1. Structural model of Rtt106 (blue) in complex with the (H3–H4)₂ tetramer (green). The structure of Rtt106 double PH domain (Rtt106PH) was determined using x-ray crystallography. The structure of Rtt106 amino-terminal dimeric domain (Rtt106DD) was determined using NMR spectroscopy. Atomic coordinates of the (H3–H4)₂ tetramer are from the structure of yeast *Saccharomyces cerevisiae* nucleosome core particle.

A NEW GATEWAY IN CELLULAR SIGNALING

When environmental conditions become adverse, people are free to move to another location and build a fire or make some hot cocoa. This is not possible for plants that must respond to changing conditions by changing their physiology. In response to stressful environmental conditions such as drought or cold, plants use the hormone abscisic acid (ABA) to modify processes such as water uptake and germination timing in order to conserve or reallocate resources. ABA acts by binding to receptors in plant cells that transmit signals to activate cellular processes such as gene expression. In work carried out at the LS-CAT beamlines at the APS, an exciting new aspect of ABA signaling has been discovered. These findings provide an important new paradigm for hormone signaling that will impact work in many areas of biology and increases our basic understanding of how ABA works. This is significant because ABA is currently being developed as a target for improving the tolerance of agricultural crops and as a treatment for humans because it displays anti-inflammatory and anti-diabetic properties.

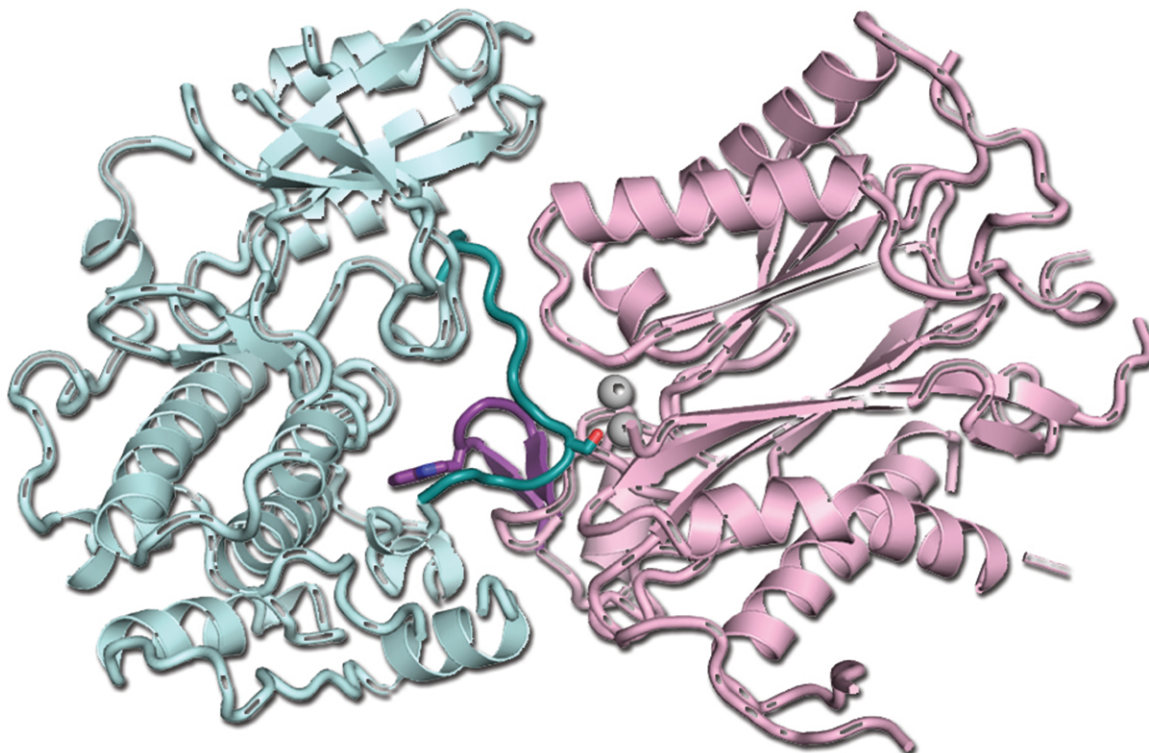


Fig. 1. Ribbon diagram of the crystal structure of the kinase/phosphatase complex showing how each one blocks the other's active site. The kinase is shown in light cyan with its activation loop in dark cyan. The phosphatase is shown in pink with its ABA receptor-locking loop and the ABA-sensing tryptophan in purple. The catalytic Mg^{2+} ions are presented as gray spheres.

When ABA binds to its receptor inside of plant cells, it activates a signaling network within the cell that involves the enzymes kinases and phosphatases. These enzymes regulate each other and downstream enzymes by addition and removal of phosphate groups to pass the signal along. For the ABA receptor, these enzymes interact with the receptor in a kind of gate, latch, and lock mechanism that responds to the presence of ABA. When no ABA is present, the gate is open, and the kinase and phosphatase are bound to each other, rendering the kinase inactive and keeping the signal quiet. When ABA binds the receptor, the gate closes and the receptor docks into the active site of the phosphatase, inactivating it. Then, a conserved tryptophan in the phosphatase that acts as an ABA sensor locks the gate by inserting between the gate and the latch in the receptor, leaving the kinase available to pass the signal downstream.

The researchers in this study, from the Van Andel Research Institute; the National University of Singapore; The Scripps Research Institute; Northwestern University; Purdue University; the Chinese Academy of Sciences, and the University of California, Riverside were interested in learning more about the next step. That is, what happens to the kinase while the receptor and the phosphatase are locking the gate?

In order to get insight into this process, they employed high-brightness x-rays from the APS at the LS-CAT 21-ID-D and 21-ID-F beamlines to solve the structure of the phosphatase in complex with the kinase. After some trial and error to find appropriate crystallization conditions, they were able to get crystals that diffracted to 2.6 Å. What the structure of the complex revealed was remarkable.

The kinase and the phosphatase

blocked each other's active site. Not only that, the mutual packing of kinase and phosphatase active sites directly mimicked the interaction of the ABA receptor with the phosphatase, forming the same gate, latch, and lock configuration. In the kinase-phosphatase complex, loops from each protein form the gate and latch in the same fashion as the receptor when ABA is present and the catalytic cleft of the kinase is occupied by the same conserved ABA-sensing tryptophan in the phosphatase to "lock" the complex (Fig. 1). When the structures are overlaid on each other, the interface between the kinase and phosphatase is nearly identical to the gate, latch, and lock of the phosphatase in complex with the receptor.

These findings suggest that the kinase and phosphatase evolved together to specifically regulate ABA signaling.

The researchers also believe they have uncovered a new paradigm for the way phosphatases regulate kinases. This has broad implications for biology because many cellular signals are regulated by kinase/phosphatase pairs and this will provide new information for how signals such as those from growth factors or neurotransmitters are regulated in cells.

Finally, the amazing discovery of the molecular mimicry displayed by these molecules to form two gate, latch, and lock mechanisms reveals important details about the ABA receptor signaling pathway that will be essential to understanding how ABA acts on plant and human cells.

— *Sandy Field*

See: Fen-Fen Soon^{1,2}, Ley-Moy Ng^{1,2}, X. Edward Zhou¹, Graham M. West³, Amanda Kovach¹, M.H. Eileen Tan^{1,2}, Kelly M. Suino-Powell¹, Yuanzheng He¹, Yong Xu¹, Michael J. Chalmers³, Joseph S. Brunzelle⁴, Huiming Zhang⁵, Huaiyu Yang⁶, Hualiang Jiang⁶, Jun

Li^{1,2}, Eu-Leong Yong², Sean Cutler⁷, Jian-Kang Zhu⁵, Patrick R. Griffin³, Karsten Melcher^{1*}, and H. Eric Xu^{1,6**}, "Molecular Mimicry Regulates ABA Signaling by SnRK2 Kinases and PP2C Phosphatases," *Science* **335**, 85 (6 January 2012).

DOI:10.1126/science.1215106

Author affiliations: ¹Van Andel Research Institute; ²National University of Singapore; ³The Scripps Research Institute; ⁴Northwestern University; ⁵Purdue University; ⁶Chinese Academy of Sciences; ⁷University of California, Riverside

Correspondence: v **eric.xu@vai.org, *Karsten.Melcher@vai.org

This work was supported by the Jay and Betty Van Andel Foundation and Amway (China) Limited (H.E.X.), the National Institutes of Health (H.E.X., P.R.G., and J.-K.Z.), the National Science Foundation (NSF) (S.C. and J.-K.Z.), and the Singapore Biomedical Research Council (E.-L.Y.). L.-M.N., F.-F.S., and M.H.E.T. were supported by an overseas Ph.D. scholarship from the National University of Singapore Graduate School for Integrative Sciences and Engineering. S.C. received funding from the NSF (grant IOS-0820508), and P.R.G. received funding from National Institute for General Medical Studies (grant GM084041) Use of the LS-CAT Sector 21 was supported by the Michigan Economic Development Corporation and the Michigan Technology Tri-Corridor for the support of this research program (Grant 085P1000817). Use of the Advanced Photon Source at Argonne National Laboratory was supported by the U.S. DOE Office of Science under Contract No. DE-AC02-06CH11357.

21-ID-D • LS-CAT • Life sciences • Macromolecular crystallography, microfluorescence (hard x-ray), nano-fluorescence imaging, nanotomography • 6.5-20 keV • On-site, remote, mail-in • Accepting general users •

21-ID-F • LS-CAT • Life sciences • Macromolecular crystallography • 12.7 keV • On-site, remote, mail-in • Accepting general users •

A NEW MECHANISM FOR REGULATION OF DNA DAMAGE REPAIR

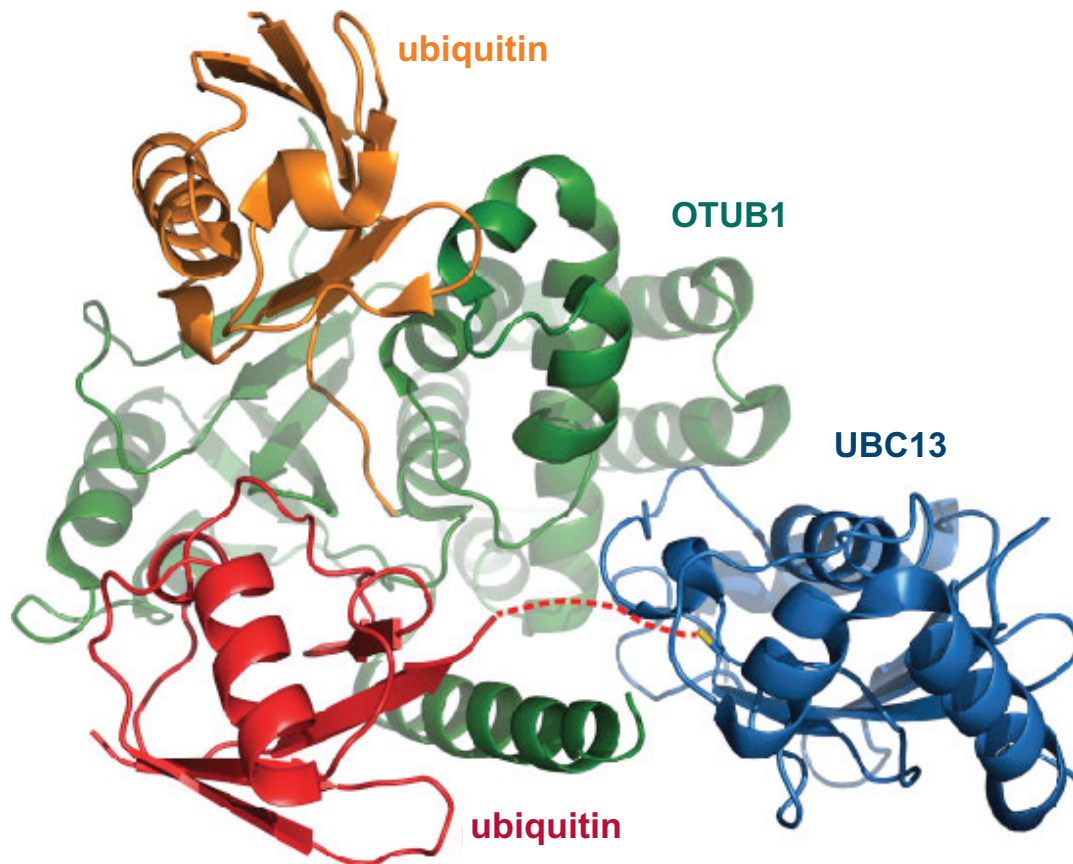


Fig. 1. Structure of OTUB1 (green) bound to a UBC13 (blue)~Ub (red) conjugate and mono-ubiquitin (gold).

The repair of DNA damage is an essential cellular function necessary for preventing complications including cancer or genetic conditions. One such pathway of repair involves the addition of the regulatory protein ubiquitin to histones (highly alkaline proteins found in eukaryotic cell nuclei that package and order the DNA into structural units called nucleosomes) in chromatin, the genetic material composed of DNA and proteins that condense to form chromosomes. Following DNA modification, ubiquitin removal is important to prevent overcorrection, which leads to the same complications as not repairing the damage at all. In work performed at the GM/CA-XSD x-ray facility at the APS, x-ray crystallography was utilized to find new information about how the ubiquitin-removing enzyme OTUB1 acts to prevent further damage.

Crystallography enabled the researchers to view the contacts OTUB1 makes with the ubiquitin-conjugating enzyme UBC13 on the atomic level (Fig. 1). This knowledge could eventually lead to drug development efforts to improve DNA damage repair and prevent disease in high-risk patients.

Genetic integrity is essential to maintain the balance of physiological processes within the cell. Many environmental factors such as ultraviolet radiation and free radicals can result in different forms of DNA damage. One of the most severe forms of DNA damage is a double-strand break, in which the DNA helix is severed, resulting in loss of structure or even dramatic alterations in gene sequences. Therefore, the cells of our body have evolved sophisticated machinery in order to reverse this type of damage. This DNA damage response is critical to normal function, and people with mutations that suppress the ability to repair DNA are at greater risk for developing diseases such as cancer.

The repair of double-strand breaks begins with the addition of ubiquitin to histone proteins near the site of damage. This attracts repair enzymes that facilitate the rejoining of strands. Ubiquitin addition is promoted by so-called ubiquitin-conjugating enzymes, such as UBC13. The cell keeps the response in check by removing excess ubiquitin, which is mediated by ubiquitin de-conjugating enzymes.

One deubiquitinating enzyme,

OTUB1, does not use catalytic activity, which is in contrast to the mechanism of action of most deubiquitinating enzymes. Instead, it binds and inhibits the addition of further ubiquitin proteins to DNA damage. In the present work, x-ray crystal structures of OTUB1 bound to UBC13 were prepared and diffraction data obtained from them at the GM/CA-XSD 23-ID-B and 23-ID-D beamlines. It was also shown for the first time that the levels of free ubiquitin in the system could regulate the binding of OTUB1 to UBC13.

The researchers describe several important events in the mechanism of UBC13 inhibition by OTUB1. The UBC13 binds to ubiquitin molecules and forms covalent attachments. Normally, this UBC13-ubiquitin intermediate would then engage a partner conjugating enzyme, but when the levels of free ubiquitin are higher, OTUB1 is bound by ubiquitin and undergoes a conformational change that promotes its binding to the UBC13-ubiquitin intermediate. This performs two inhibitory functions: UBC13 cannot form interactions with its attached ubiquitin to promote transfer to a different protein, and UBC13 will be blocked from interacting with its critical binding partner UEV1A. These two events strongly inhibit the conjugation of ubiquitin to histones in response to DNA damage.

The results suggest a novel regulatory approach whereby free ubiquitin levels inhibit ubiquitin conjugation of OTUB1 to histones. These findings

open the door for drug targeting strategies, since inhibition of OTUB1 could strengthen the DNA damage response in patients with mutations in this pathway that predispose them to diseases such as cancer. — *Emma Hitt*

See: Reuven Wiener, Xiangbin Zhang, Tao Wang[‡], and Cynthia Wolberger*, “The mechanism of OTUB1-mediated inhibition of ubiquitination,” *Nature* **483**, 618 (29 March 2012).

DOI:10.1038/nature10911

Author affiliation: Johns Hopkins University School of Medicine. [‡]Present address: National Institute of Allergy and Infectious Diseases

Correspondence: *cwolberg@jhmi.edu

GM/CA-XSD has been funded in whole or in part with funds from the National Cancer Institute (Y1-CO-1020) and the National Institute of General Medical Science (Y1-GM-1104). Use of the Advanced Photon Source at Argonne National Laboratory was supported by the U.S. DOE Office of Science under Contract No. DE-AC02-06CH11357.

23-ID-B • GM/CA-XSD • Life sciences • Large unit cell crystallography, macromolecular crystallography, microbeam, multi-wavelength anomalous dispersion, single-wavelength anomalous dispersion, subatomic (<0.85 Å) resolution • 3.5-20 keV • On-site, remote • Accepting general users •

23-ID-D • GM/CA-XSD • Life sciences • Macromolecular crystallography, microbeam, large unit cell crystallography, subatomic (<0.85 Å) resolution, multi-wavelength anomalous dispersion, single-wavelength anomalous dispersion • 5-20 keV • On-site, remote • Accepting general users •

CATCHING DNA POLYMERASE IN THE ACT

Enzymes are known for their lightning speed, working in our cells to catalyze normally slow biological reactions and speeding them up by millions of times. The enzymes that replicate our DNA for cell division, DNA polymerases, can add about 1000 nucleotides per second to a growing DNA strand. Structural studies have provided researchers with information about the position of molecules within the active sites of DNA polymerases but, until now, it hasn't been possible to see exactly what happens in that blindingly fast transfer of molecules that results in newly synthesized DNA. The researchers in this study developed a method for catalysis *in crystallo* that allows them to take molecular snapshots of DNA polymerase in action. Their work, using time-resolved x-ray crystallography, was completed at SER-CAT beamlines 22-BM-D and 22-ID-D at the APS. In addition to uncovering new details about transient elements involved in catalysis by DNA polymerase, this work extends current technology to allow real-time atomic resolution of an enzymatic reaction.

The researchers, from the National Institutes of Health, Kumamoto University (Japan), and the Institute of Nuclear-Agricultural Sciences (China) crystallized human DNA polymerase η (Pol η), which repairs breaks in DNA and works at a slower rate than other DNA polymerases. It catalyzes a reaction in which an activated phosphate from ATP is used to create a new bond between an -OH group from one base in DNA and a phosphate group in the next DNA base. The reaction also requires two magnesium ions. A key element of the method was to get the enzyme crystallized in an inactive "ground state" that could then be activated for observation.

The team first crystallized Pol η in complex with the reactants, DNA and ATP, in a low-pH and low-magnesium buffer that inhibited polymerase activity. The crystals were then placed in a buffer that brought them closer to physiological pH for crystal structure refinement to 1.50 Å.

Catalysis was initiated *in crystallo* by moving the crystals into a physiological pH buffer containing magnesium ions to start the reaction. To get snapshots of the enzyme in action, the reaction was terminated at 40-sec intervals by freezing the crystals in liquid nitrogen. The *in crystallo* reactions occurred ~20–100 times slower than the rate of the reaction in solution.

Structures for the crystals frozen at

various points in time showed the progression of the reaction much like an old-time movie. First, at 40 sec the magnesium ions from the new buffer started entering the active site and the binding of the second magnesium ion resulted in the alignment of the -OH group from the DNA with the ATP in their proper orientations. The new bond between this -OH and the ATP was starting to form by 80 sec and was 60–70% complete by 200 sec.

Also at 80 sec, an unexpected transient player in the reaction appeared. A water molecule that was involved in activation of the reactant, but incompatible with the product state, appeared to temporarily hydrogen bond with the -OH group.

In the next step, the nucleotide transfer occurred, lengthening the DNA by one unit, and the new backbone phosphate moved between the attacking and leaving oxygen atoms of the reaction. Between 200 and 250 sec the peak of chemical bond formation occurred and the pyrophosphate product from the ATP was in a transition state, ready to be released.

Finally, the team was surprised to find that as the products began to form, a third magnesium ion came in to stabilize the reaction products (Fig. 1). This aspect of the reaction and the water molecule at 80 sec were previously unobserved transient elements of the reaction.

These results provide a remarkable glimpse into the real-time mechanism of enzyme catalysis and uncover surprising transient elements in an enzyme reaction that had been thoroughly studied by current methods. The development of *in crystallo* catalysis clearly offers a new way to view enzymatic reactions. What will they capture next with their molecular snapshot? — *Sandy Field*

See: Teruya Nakamura^{1,2}, Ye Zhao^{1,3}, Yuriko Yamagata², Yue-jin Hua³, and Wei Yang^{1*}, "Watching DNA polymerase η make a phosphodiester bond," *Nature* **487**, 196 (12 July 2012). DOI:10.1038/nature11181

Author affiliations: ¹National Institutes of Health, ²Kumamoto University, ³Zhejiang University

Correspondence: *wei.yang@nih.gov

The research was supported by the intramural research program of the National Institute of Diabetes and Digestive and Kidney Diseases, National Institutes of Health (W.Y., T.N. and Y.Z.); the Japan Society for the Promotion of Science Institutional Program for Young Researcher Overseas visits, Kumamoto University, and the Kumayaku Alumni Research Fund (T.N.); Chinese Ministry of Education scholarship (Y.Z.); the National Natural Science Foundation of China (Y.-J.H.); and a Grant-in-Aid for Scientific Research from the Ministry of Education, Culture, Sports, Science, and Technology of Japan (Y.Y.). SER-CAT consists of 22 member institutions to provide third-generation x-ray capabilities to macromolecular crystallographers and structural biologists in the southeastern region of the U.S. Use of the Advanced Photon Source at Argonne National Laboratory was supported by the U.S. Department of Energy Office of Science under Contract No. DE-AC02-06CH11357.

22-BM-D • SER-CAT • Life sciences • Macromolecular crystallography • 8-20 keV • On-site, remote • Accepting general users •

22-ID-D • SER-CAT • Life sciences • Macromolecular crystallography • Multi-wavelength anomalous dispersion • microbeam • 6-20 keV • On-site, remote • Accepting general users •

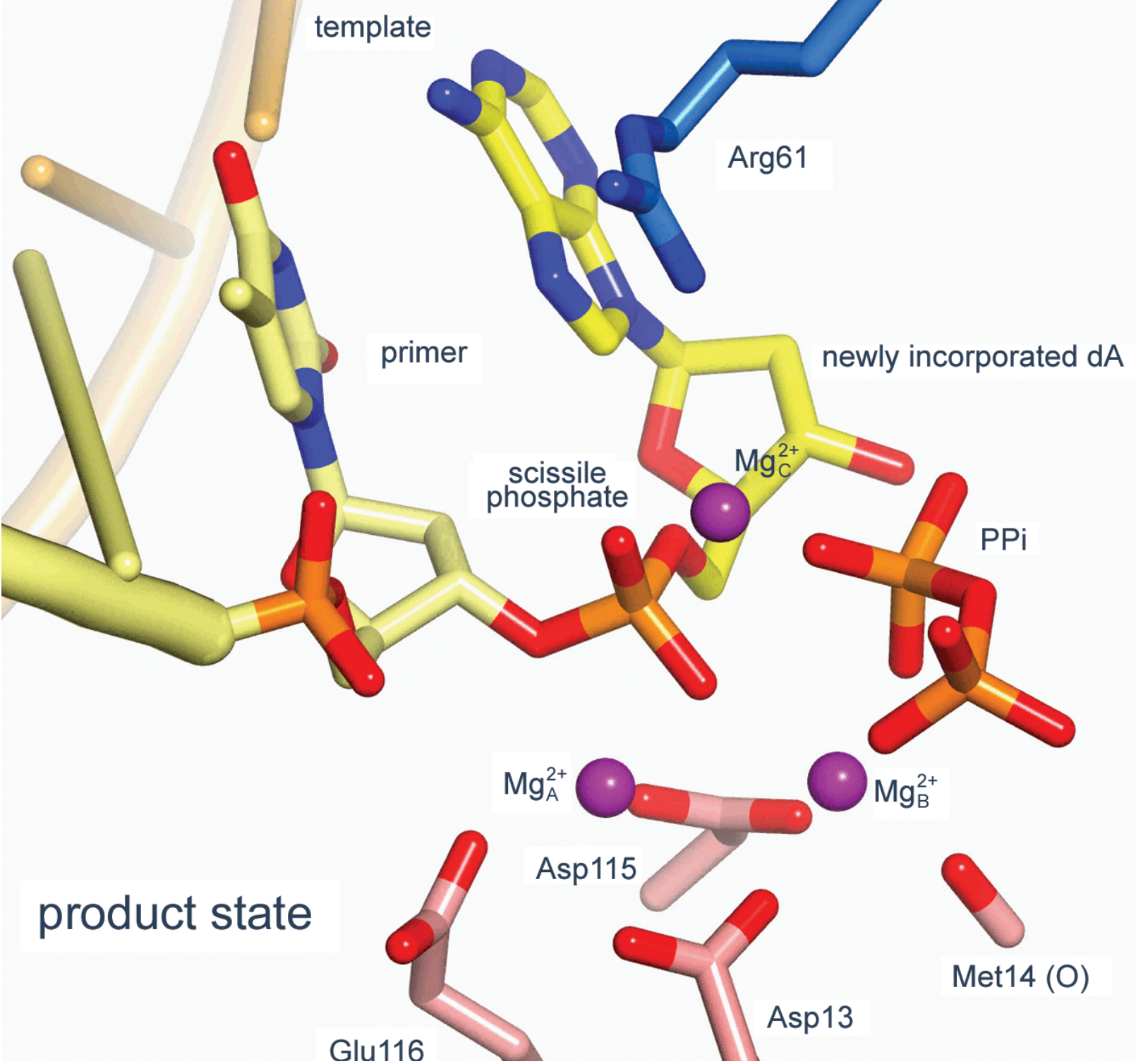


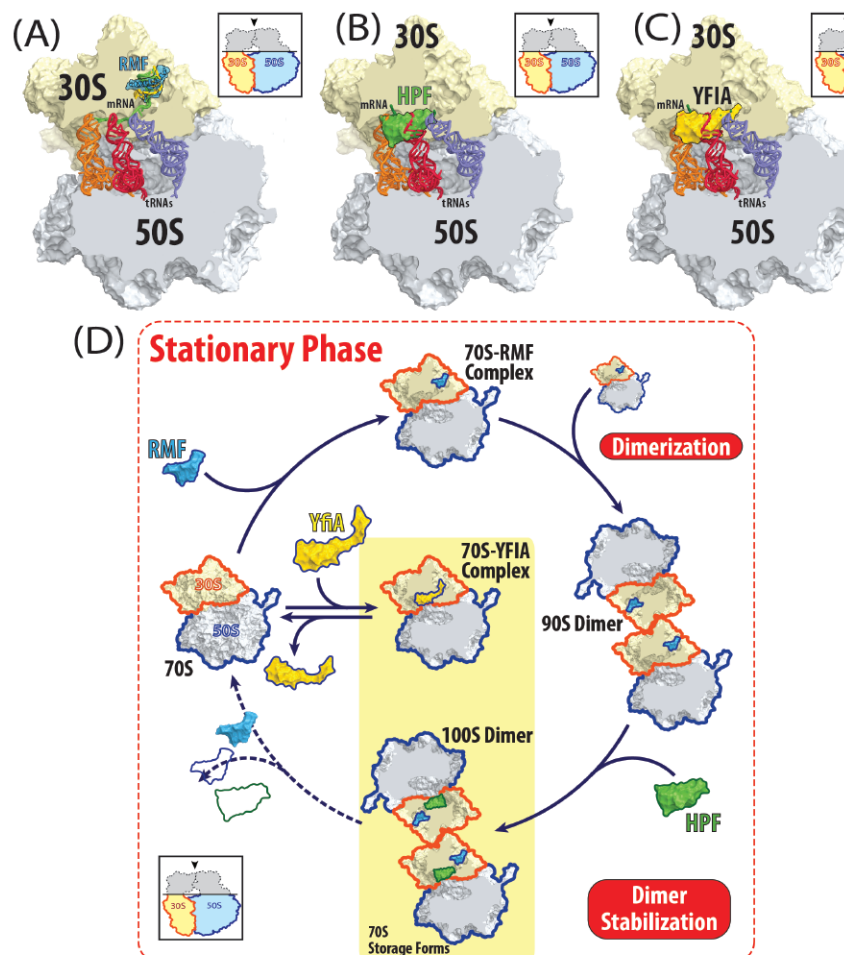
Fig. 1. A model of the Pol η active site after product formation. The newly formed phosphodiesterase bond (orange-red) created by Pol η is shown between DNA bases (yellow-red-blue) and surrounded by three coordinated magnesium ions (purple). The other reaction product, pyrophosphate (PPI, red-orange), and the Pol η active site amino acid residues (Arg, Glu, Asp, Met) are also shown in stick models.

A Quicktime animation of the figure is in the Supplementary Information at http://www.nature.com/nature/journal/v487/n7406/full/nature11181.html?WT.mc_id=EN0712MN13#/supplementary-information or via this QR code.



HOW BACTERIA STORE THEIR RIBOSOMES DURING STRESS

Pathogens (biological agents that cause disease or illness to the host) are becoming resistant to an increasing number of antimicrobial agents. Many of them escape antimicrobial action by acquiring spontaneous mutations. These can occur at a higher rate once the bacterial cell enters the stationary phase of the growth cycle in response to environmental stresses, such as exposure to antimicrobial agents or nutrient starvation. During this phase, many reactions essential for replication are dampened. One example is “ribosome hibernation,” protein synthesis due to reversible inactivation of the ribosome, the central player in this process. Ribosomes can hibernate in a cell either as pairs (100S dimers) or as individual 70S monomers. For pair formation, two protein factors are essential: ribosome modulation factor (RMF) and hibernation promoting factor (HPF). But for hibernation as individual monomers, only one factor is necessary: protein Y, or YfiA. Researchers from Yale University utilized data collected at an NE-CAT beamline at the APS and two National Synchrotron Light Source beamlines to study these ribosome structures found in bacterial cells during the stationary phase. Their findings provide important structural insight into how bacterial cells preserve ribosomes in an inactive, yet stable form, during the stationary phase of growth.



Two movies of the structure can be viewed at <http://www.sciencemag.org/content/336/6083/915/suppl/DC1> or via this QR code.



Bacteria encounter many stresses in their natural environments that lead to specific and regulated adaptive responses. One such response is entry into a stationary phase, occurring when nutrient supply is exhausted. This results in almost complete arrest of protein biosynthesis, and during this phase, bacterial cells are highly resistant to external stresses, including inhibition by antibiotics.

When bacteria actively grow and divide, they continually synthesize proteins according to the genetic information encoded in their DNA. With the help of adaptor molecules (transfer RNA or tRNAs), large macromolecular complexes called ribosomes translate the genetic information encoded in the messenger RNA (mRNA) into protein sequences. Rapidly growing cells require an adequate supply of amino acids to cope with the demands of protein synthesis. Consequently, in times of nutrient starvation when there are not enough amino acids, bacteria slow down protein synthesis and convert ribosomes into stable inactive forms. One such form, the 100S ribosome dimer, is important for cell survival during stationary phase. In this form indi-

< Fig. 1 (A-D). The structures of RMF (A), HPF (B) and YfiA (C) hibernation factors bound to the ribosome. Small ribosomal subunit (30S) is shown is light yellow, large ribosomal subunit (50S) is in light blue. Key players of the protein synthesis cycle, mRNA and three tRNA molecules, not actually present in the studied complexes, are shown in green, orange, red, and blue, respectively, to illustrate how hibernation factors inhibit protein biosynthesis. The views are indicated by the insets in each panel. (A) RMF (blue) prevents pivotal ribosome-mRNA interaction essential for initiation of protein synthesis by clashing with mRNA (green) and part of the ribosome (yellow). (B, C) HPF (green) and YfiA (yellow) bound to the ribosome prevent mRNA and tRNA molecules from interacting with the same ribosome. (D) Diagram showing the interplay between ribosomes and the three hibernation factors during stationary phase in bacteria.

vidual 70S ribosomes are arranged in pairs.

The process of 100S dimer formation in the bacterium *Escherichia coli* involves two small protein factors, Ribosome Modulation Factor (RMF) (Fig. 1A) and Hibernation Promoting Factor (HPF) (Fig. 1B). RMF binding results in dimerization, or pairing, of individual 70S ribosomes into 90S particles, which then become stabilized as 100S dimers following HPF binding. Although the *rmf* gene, which encodes for RMF protein, is dispensable during normal growth conditions, it becomes essential for cell viability during starvation, which highlights the importance of 100S dimer formation during stress. In contrast to *rmf*, a deletion of *hpf* gene does not affect either cell viability or dimer formation.

Alternatively, another protein factor, YfiA (also called protein Y) (Fig. 1C) can promote the formation of an inactive 70S ribosome monomer. Although YfiA and HPF have similar amino acid sequences, their effect on 100S dimer formation is different. HPF converts 90S dimers into 100S particles, while YfiA inhibits RMF-dependent ribosome dimerization. Previous studies suggested that HPF and YfiA could interfere with protein synthesis simply by competing with the binding of tRNAs to the ribosome.

The study conducted at the NE-CAT beamline 24-ID-C and National Synchrotron Light Source beamlines X29 and X25 (Brookhaven National Laboratory) by the Yale University researchers investigated the crystal structures of the bacterial 70S ribosome in complex with RMF, HPF, or YfiA to better understand how these proteins act. The team solved crystal structures of each of the three hibernation factors in complex with the bacterial ribosome to show how bacteria sequester the number of actively synthesizing ribosomes during stationary phase (Fig. 1D).

Their results revealed that RMF and HPF can bind simultaneously and

act together to interfere with initiation of protein synthesis. In their structure, the binding of RMF interferes with initiation of protein synthesis by preventing the crucial interactions between the ribosome and the mRNA — a carrier molecule of the genetic information. Because of the sequence similarity, the structural domains of HPF and YfiA in their binding sites are the same and overlap with those of the mRNA and tRNAs, as well as with initiation factors. However, only the binding of RMF and HPF, but not YfiA, enables the structural rearrangements of the ribosome required for the formation of 100S dimers.

The results of this study clarify how bacterial cells preserve ribosomes in an inactive, yet stable, form during starvation, and possibly during other stresses such as exposure to antimicrobial agents. Consequently, preventing this important process in bacterial cells might prove useful in the development of new strategies to combat the rise of antimicrobial drug resistance in pathogens. — [Nicola Parry](#)

[See:](#) Yury S. Polikanov, Gregor M. Blaha, and Thomas A. Steitz*, “How Hibernation Factors RMF, HPF, and YfiA Turn Off Protein Synthesis,” *Science* **336**, 915 (18 May 2012). DOI:10.1126/science.1218538

[Author affiliation:](#) Yale University

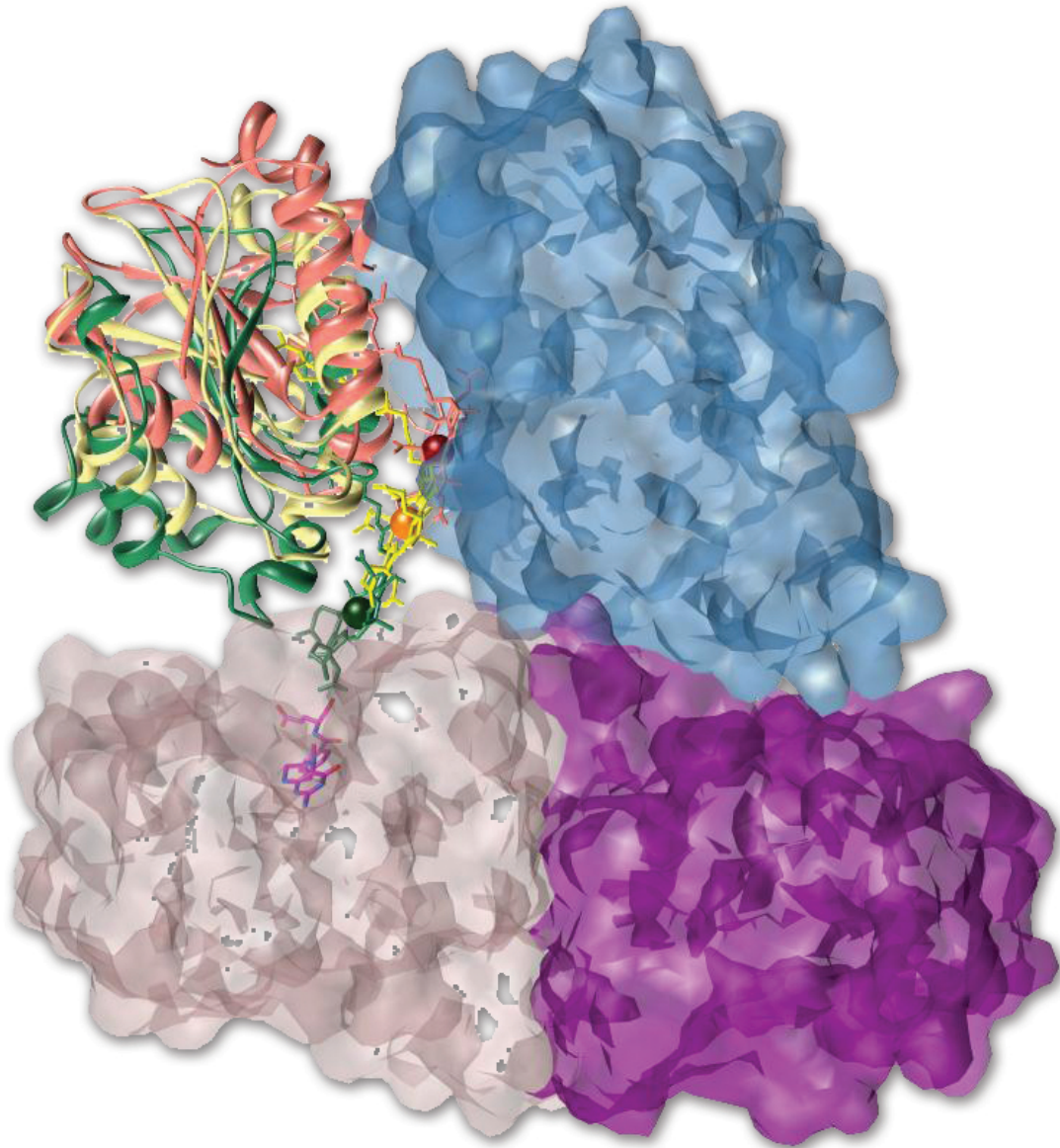
[Correspondence:](#)

*thomas.steitz@yale.edu

This work was supported by National Institutes of Health grant GM022778 awarded to T.A.S. Use of the Advanced Photon Source at Argonne National Laboratory was supported by the U.S. Department of Energy Office of Science under Contract No. DE-AC02-06CH11357.

24-ID-C • NE-CAT • Life sciences • Macromolecular crystallography, microdiffraction, single-wavelength anomalous dispersion, single-crystal diffraction, microbeam • 6.5-23 keV • On-site • Accepting general users •

A MOLECULAR JUGGLING ACT TO CONTROL BIOLOGICAL REACTIONS



B12-dependant methyl transfer is at the heart of numerous essential biochemical pathways. However, the exact nature of this process has remained elusive when it comes to understanding the structural changes that take place as the process advances. In work by researchers with the Howard Hughes Medical Institute and the Massachusetts Institute of Technology, the entire structure of a complete B12 methyl transfer complex has been determined for the first time. Utilizing x-ray crystallography at two U.S. Department of Energy Office of Science x-ray light sources, including the APS, the researchers observed key changes in the vitamin B12 binding region of a bacterial methyl transfer. These domain movements provide insight into the way these protein modules are regulated by bringing the vitamin B12 and catalytic domains together in a “swinging” and “clamping” motion, with implications for advances in greenhouse gas remediation and in the prevention and treatment of certain diseases and .

Many crucial biochemical pathways important for production of amino acid methionine and other molecules in humans rely on the process of B12 methyl transfer. Additionally, certain types of bacteria can also make use of this pathway in order to process carbon dioxide into a food source, which proved useful in the elucidation of the crystal structure. These methyl transfer reactions depend on an often buried vitamin B12 molecule to help them come about.

In anaerobic bacteria, vitamin B12 is bound by the corrinoid iron-sulfur protein (CFeSP) in order to bring it near methyltransferase (MeTr). Once the complex is assembled and a methyl folate (or folic acid) is recruited, B12 is activated to perform methyl transfer. Before this work, crystal structures of the individual pieces of the complex revealed the existence of two states, resting and active, individually but never bound together illustrating methyl transfer. This new work was able to solve the structure of the entire complex for the first time, and it extended the model of activation for the methyl transfer complex.

First, a high-resolution structure for the CFeSP/MeTr complex without folate, the donor of the methyl group, was solved (Fig. 1) via x-ray crystallography at the NE-CAT 24-ID-C beamline

< Fig. 1. Movement of B12 domain (shown as ribbons) away from protective domain (blue surface) towards the folate (magenta) in a methyltransferase domain (pink surface). Vitamin B12 is shown as sticks, with the central cobalt shown as spheres.

at the APS and the 5.0.2 and 8.2.2 beamlines at the Advanced Light Source (Lawrence Berkeley National Laboratory). The structure revealed that the vitamin B12 binding region undergoes a conformational change upon assembly of the complex. The complex no longer appeared to be in the resting state where vitamin B12 is completely shielded from reactions; however, it was also not found to be in the fully active state. The researchers termed this transition “en route,” and suggested that the enzyme is capable of being in more than just active and resting states as previously thought. In fact, with no bound folate, this intermediate state is preferred over the active or resting states. This led to the hypothesis that addition of folate would bias the complex toward the active state. Following the solving of the CFeSP/MeTR complex bound to folate, the vitamin B12 binding region was indeed favored to be positioned near MeTR, representing a more active conformation.

Overall, this work demonstrated for the first time that flexibility exists in the movement of the vitamin B12 binding region in methyl transfer. As opposed to a strict on/off state of activation, a continuum of intermediate states must therefore exist, supporting the “molecular juggling” mechanism of regulation whereby the vitamin B12 binding region has to move large distances to activate the complex. Learning more about the inner workings of methyl transfer can lead to a better understanding of human diseases related to methionine production. The use of carbon dioxide

through methyl transfer also has significant environmental importance, possibly leading to new ways to scavenge this greenhouse gas. — *Emma Hitt*

See: Yan Kung¹, Nozomi Ando¹, Tzanko I. Doukov^{1‡}, Leah C. Blasiak^{1‡‡}, Günes Bender², Javier Seravalli³, Stephen W. Ragsdale², and Catherine L. Drennan^{1*}, “Visualizing molecular juggling within a B12-dependent methyltransferase complex,” *Nature* **484**, 265 (12 April 2012). DOI:10.1038/nature10916

Author affiliations: ¹Massachusetts Institute of Technology, ²University of Michigan, ³University of Nebraska
Present addresses: [‡]Stanford Synchrotron Radiation Lightsource; ^{‡‡}University of Maryland Center for Environmental Science
Correspondence: *cdrennan@mit.edu

This work was supported by National Institutes of Health grants GM69857 (to C.L.D.) and GM39451 (to S.W.R.) and the Massachusetts Institute of Technology Energy Initiative (to C.L.D.). C.L.D. is a Howard Hughes Medical Institute Investigator. The NE-CAT beamlines are supported by award RR-15301 from the National Center for Research Resources at the National Institutes of Health. Use of the Advanced Photon Source at Argonne National Laboratory was supported by the U.S. Department of Energy Office of Science under Contract No. DE-AC02-06CH11357.

24-ID-C • NE-CAT • Life sciences • Macromolecular crystallography, microdiffraction, single-wavelength anomalous dispersion, single-crystal diffraction, microbeam • 6.5-23 keV • On-site • Accepting general users •

THE INNER WORKINGS OF THE SODIUM-CALCIUM EXCHANGE

Careful regulation of calcium levels in cells is essential for the proper function of many physiological processes. Ion concentrations can be actively regulated by ion exchange transporter proteins in the cell membrane. But the exact ion-exchange mechanism for sodium-calcium exchangers has not been determined, partly due to the lack of structural information. New data obtained by a research group utilizing SBC-CAT and GM/CA-XSD beamlines at the APS reveals for the first time the atomic-resolution structure of a sodium-calcium exchanger. The structure helps explain how the exchanger discriminates calcium from other ions and how the exchanger is able to move calcium ions rapidly out of the cell to maintain stability and limit damage. Determination of the atomic structure allows for insight into mechanisms of failure in disease states that become targets for drug development or studies into disease development.

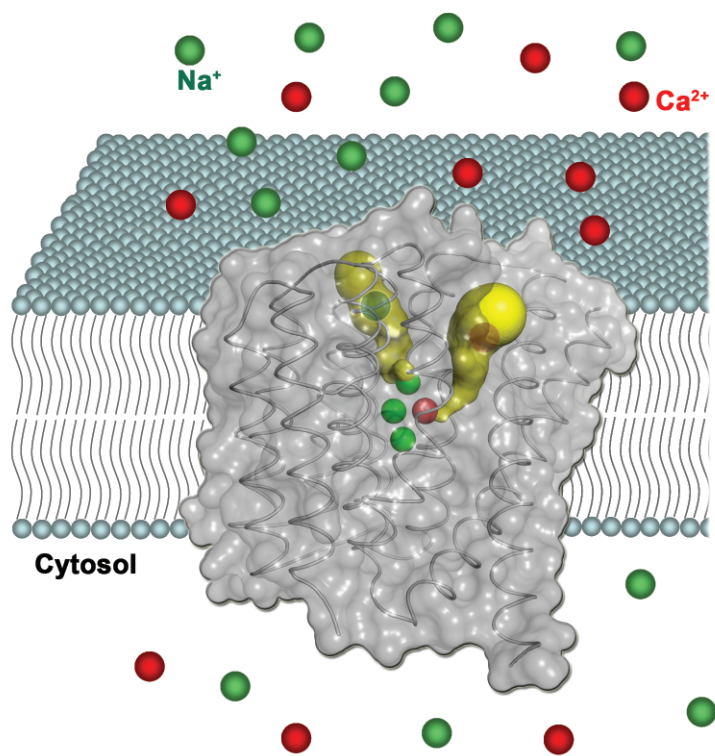


Fig. 1. The cartoon figure shows the NCX_Mj protein embedded in the membrane with outward-facing configuration for Na^+ binding and Ca^{2+} release. Na^+ (green spheres) and Ca^{2+} (red spheres) ions have higher concentrations extracellularly and lower concentrations in the cytosol.

Calcium stability, or homeostasis, is crucial for proper cell function. Therefore, tight regulation of calcium levels inside the cell has evolved across eukaryotes, organisms whose cells contain a distinct, membrane-bound nucleus. The sodium-calcium exchange transmembrane proteins maintain physiological levels of the ions necessary to prevent arrhythmia, brain damage, and other life threatening changes. Single calcium ions are pushed rapidly out of the cell in exchange for three sodium ions. This process represents one way in which intracellular levels of calcium can be kept from becoming too high. Modulation of calcium levels in the cell is essential in a number of body functions. For example, muscle contraction is facilitated by elevated calcium levels in the cell. In order to ensure relaxation of the muscle back to a resting state, exchangers can help rapidly move calcium back out.

Until this work, all data about how the sodium-calcium exchanger functions has been based on biochemical and physiological data. Previous work has been able to describe the potentially important features of the exchanger, but without the atomic resolution structure these features could not be known with certainty.

The exchanger from the archaea *Methanocaldococcus jannaschii* was used in this work to arrive at the first crystal structure for a sodium-calcium exchanger. Because biochemical experiments had proved that the archaeal sodium-calcium exchanger works very similarly to the eukaryotic transmembrane protein, the crystal structure would yield useful information about the exchanger in eukaryotes.

Thanks to the structures determined at the SBC-CAT 19-ID-D and GM/CA-XSD 23-ID-D beamlines, the researchers from the University of Texas Southwestern Medical Center were able to provide the first identification of the distinct subunits of the chan-

“Sodium” cont’d on page xx

HOW A POCKET FULL OF PROTEINS CAN INFLUENCE TUMOR DEVELOPMENT

Menin, a protein that controls cell growth in endocrine tissues, functions as a tumor suppressor protein, preventing tumor formation. The menin gene contains the information that codes for production of Menin, and mutations of this gene therefore predispose patients to multiple endocrine neoplasia 1 (MEN1), an inherited disorder that causes tumors in the endocrine glands and the duodenum. The researchers in this study, working at the LS-CAT beamlines 21-ID-D and 21-ID-F at the APS, collected data to investigate the crystal structures of menin. Understanding these results will be important in guiding future studies to further evaluate the mechanism of action of menin, a potential target for development of drugs to treat leukemia.

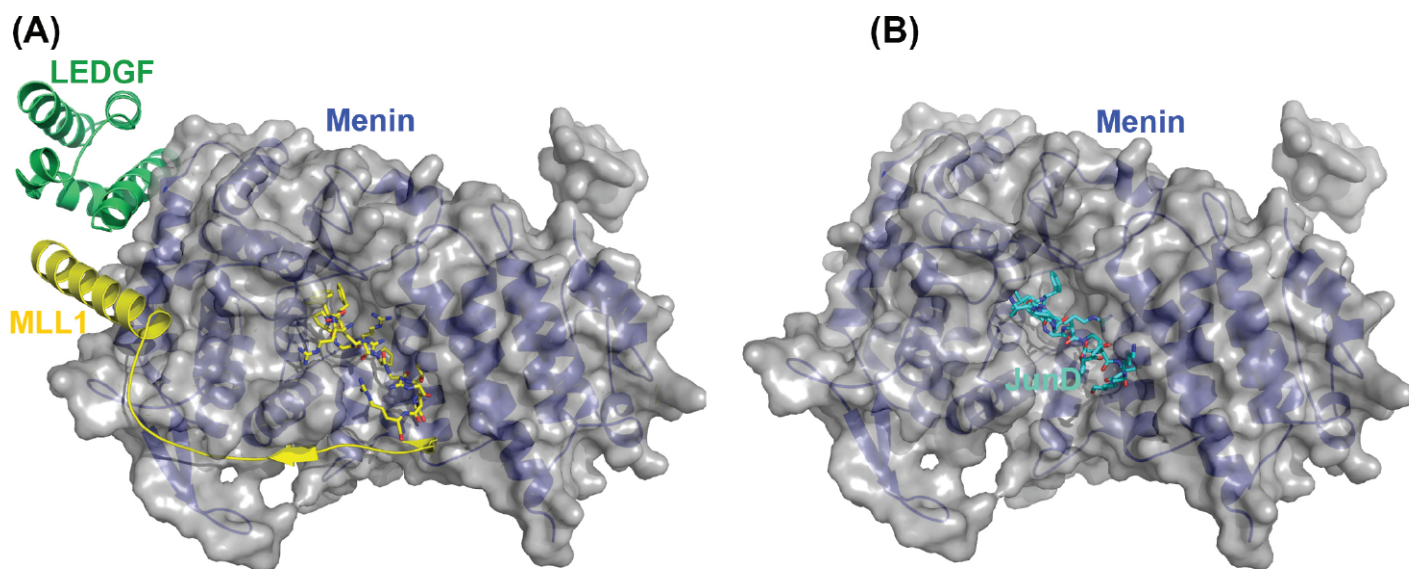


Fig. 1. The central pocket of menin binds both MLL1 and JUND in the same way. (A) the menin-MLL1 complex, further recruits a chromatin-associated protein-LEDGF; (B) the menin-JUND complex.

Menin interacts with other protein factors in its role as a tumor suppressor protein. It binds to JUND, a transcription factor, to block JUND-activated transcription. Conversely, it can also potentially cause cancer by interacting with mixed lineage leukemia (MLL) fusion proteins that are involved in the development of acute leukemias. A chromatin-associated protein, lens epithelium-derived growth factor (LEDGF), is also required for this process.

In its role as a tumor suppressor protein, menin has been shown to interact with numerous well-known transcription factors. These are proteins that bind to specific DNA sequences to control the flow of

genetic information from DNA to mRNA, and they do this by binding to enhancer or promoter regions of DNA near the genes that they regulate.

Menin's tumor suppressor activity involves direct binding to JUND, a member of the JUN family of transcription factors. In this way, it inhibits JUND-activated transcription. Since numerous MEN1 mutations interfere with the interaction between menin and JUND, there is considered to be a correlation between Menin's tumor-suppressor function and its suppression of JUND-activated transcription.

Importantly, it also acts as a cofactor of MLL fusion proteins that are involved in the development of acute leukemias. In this way it func-

tions as an oncogenic factor, a factor that has the potential to cause cancer, by enhancing gene transcription and promoting development of leukemia induced by the fusion protein MLL1.

LEDGF is a chromatin-associated protein that protects cells from stress-induced apoptosis, a form of cell death. It is known to be required for MLL1-dependent transcription and the development of leukemia.

A recent report on the attachment of MLL1 to LEDGF by menin indicates that it acts as a molecular adaptor that coordinates the functions of numerous proteins. However, despite the importance of menin, the mechanism by

"Pocket" cont'd on page xx

“Sodium” cont’d from page xx

nel involved in the recruitment and movement of sodium and calcium ions (Fig. 1). The structures contained trapped calcium and sodium, so key amino acids that interacted with the ions could be visualized. Large conformational changes could also be inferred from the crystal structure, revealing the mechanism that physically moves the ions into and out of the cell using the transmembrane protein.

In short, a calcium ion can enter into the channel on the intracellular side of the exchanger and induce a conformational change that causes it to close on the intracellular side and open on the extracellular side. High sodium concentrations outside the cell then drive three sodium ions into the channel and induce a conformational change that forces the calcium ion out of the exchanger. This then triggers the closure of the extracellular side and opening of the intracellular side of the protein, and the sodium flows out through diffusion. Then the cycle can be repeated.

Knowing the specific features of the sodium-calcium exchanger protein can lead to a better understanding of how it can become dysfunctional and lead to disease. This work represents a large step toward a conclusive understanding of the mechanism and properties of this enzyme. — *Emma Hitt*

See: Jun Liao, Hua Li, Weizhong Zeng, David B. Sauer, Ricardo Belmares[‡], and Youxing Jiang*, “Structural Insight into the Ion-Exchange Mechanism of the Sodium/Calcium Exchanger,” *Science* **335**, 686 (10 February 2012). DOI:10.1126/science.1215759

Author affiliation: University of Texas Southwestern Medical Center. [‡]Present address: North Crowley High School
Correspondence:

*youxing.jiang@utsouthwestern.edu

This work was supported in part by the Howard Hughes Medical Institute and by grants from the David and Lucile Packard Foundation and the Welch Foundation (grant I-1578 to Y.J.). Use of the Advanced Photon Source at Argonne National Laboratory was supported by the U.S. DOE Office of Science under Contract No. DE-AC02-06CH11357. GM/CA-XSD has been funded in whole or in part with federal funds from the National Cancer Institute

(Y1-CO-1020) and the National Institute of General Medical Sciences (Y1-GM-1104). SBC-CAT is funded by the U.S. DOE Office of Science Biological and Environmental Research Program under contract DE-AC02-06CH11357.

23-ID-D • GM/CA-XSD • Life sciences • Macromolecular crystallography, microbeam, large unit cell crystallography, subatomic (<0.85 Å) resolution, multi-wavelength anomalous dispersion, single-wavelength anomalous dispersion • 5-20 keV • On-site, remote • Accepting general users •

19-ID-D • SBC-CAT • Life sciences • Large unit cell crystallography, macromolecular crystallography, microbeam, multi-wavelength anomalous dispersion, single-wavelength anomalous dispersion, subatomic (<0.85 Å) resolution, ultra-low-temperature (15K) • 6.5-19.5 keV • On-site, remote, mail-in • Accepting general users •

“Pocket” cont’d from page xx

which this protein interacts with many factors and regulates their functions is still not fully understood.

The researchers in this study, from the University of Michigan Medical School, the University of Pennsylvania Perelman School of Medicine, and the University of Michigan evaluated the structure of menin in its free form and in complex with MLL1 or JUND, as well as in a complex consisting of both MLL1 and LEDGF.

Using data sets collected at the LS-CAT beamlines, the researchers showed that menin contains a deep structural pocket that binds short peptides of MLL1 or JUND in the same way. They also found, however, that it can have opposite effects on transcription in its associations with these two factors. The menin–JUND interaction blocks a phosphorylation reaction, thereby inhibiting JUND-induced transcription. In contrast, menin promotes gene transcription by binding MLL1 through this structural pocket, while still interacting with the protein LEDGF at a distinct surface formed by both menin and MLL1.

These structural and functional studies provide some explanation of how menin can both positively and negatively influence gene transcription. The findings also demonstrate that menin acts as a scaffold protein to assemble a three-dimensional complex of menin–MLL1–LEDGF, to coordi-

minate gene transcription and promote development of leukemia induced by MLL1 fusion-protein.

The results of this study will help guide further research into the mechanism of action of menin. And since direct association of menin with MLL fusion proteins is necessary for promoting development of leukemia, this interaction therefore represents a potential therapeutic target for production of anti-leukemia agents.

— *Nicola Parry*

See: Jing Huang¹, Buddha Gurung², Bingbing Wan¹, Smita Matkar², Natalia A. Veniaminova³, Ke Wan¹, Juanita L. Merchant³, Xianxin Hua^{2*}, and Ming Lei^{1**}, “The same pocket in menin binds both MLL and JUND but has opposite effects on transcription,” *Nature* **482**, 542 (23 February 2012). DOI:10.1038/nature10806

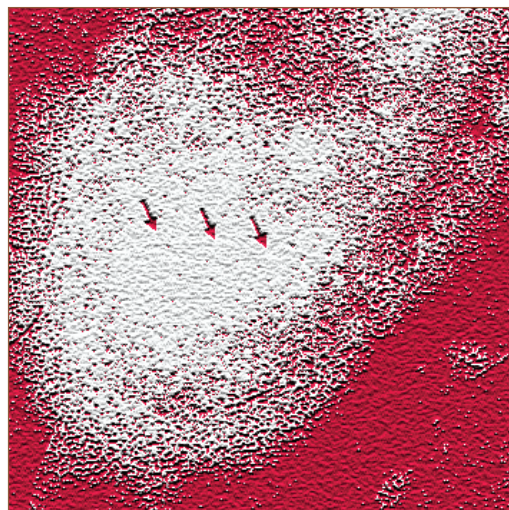
Author affiliations: ¹University of Michigan Medical School, ²University of Pennsylvania Perelman School of Medicine, ³University of Michigan

Correspondence: **leim@umich.edu, *huax@mail.med.upenn.edu

M.L. is a Howard Hughes Medical Institute Early Career Scientist. Work was supported by National Institutes of Health grants (GM 083015-01 to M.L., R01-DK085121 to X.H. and R37-DK45729 to J.L.M.), an American Cancer Society Research Scholar grant (to M.L.), and an American Association for Cancer Research Caring for Carcinoid Foundation Grant (to X.H.). The use of LS-CAT was supported by the Michigan Economic Development Corporation and the Michigan Technology Tri-Corridor for the support of this research program (Grant 085P1000817). Use of the Advanced Photon Source at Argonne National Laboratory was supported by the U.S. DOE Office of Science under Contract No. DE-AC02-06CH11357.

21-ID-D • LS-CAT • Life sciences • Macromolecular crystallography, microfluorescence (hard x-ray), nano-fluorescence imaging, nanotomography • 6.5-20 keV • On-site, remote, mail-in • Accepting general users •

21-ID-F • LS-CAT • Life sciences • Macromolecular crystallography • 12.7 keV • On-site, remote, mail-in • Accepting general users •



ENVIRONMENTAL,
GEOLOGICAL, &
PLANETARY SCIENCE

HOW MERCURY RISES INTO ZEBRAFISH LARVAE

Mercury is a common toxin in the modern environment, although the toxicity levels and their effects differ between the chemical forms of mercury. Organic mercury accumulates in tissue more readily and is more toxic than inorganic mercury, with methylated compounds posing the greatest threat to developing vertebrates. In this study, researchers utilized the XSD 20-ID-B,C beamline at the APS to investigate the tissue-specific accumulation patterns of four different mercury species in zebrafish larvae. Their work reveals substantial differences in the way different mercury species accumulate in tissue.

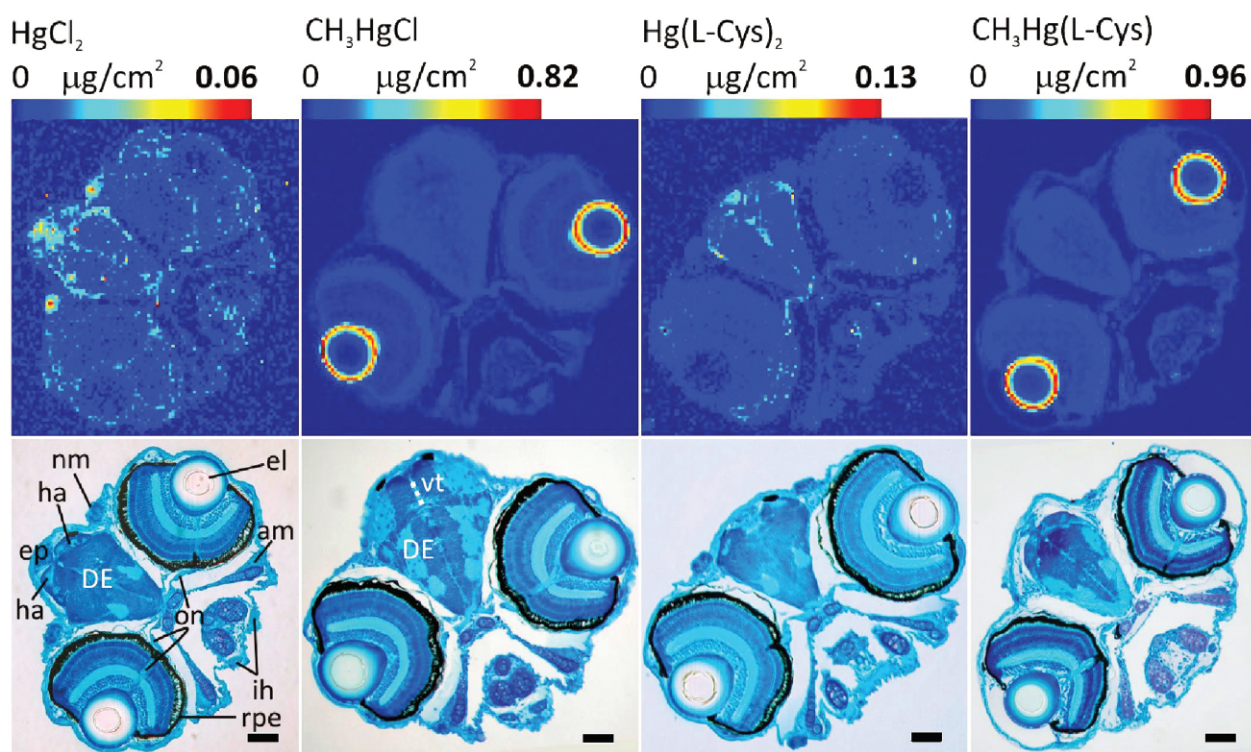
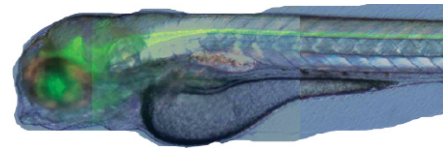


Fig. 1. Top row: Mercury distributions in zebrafish larvae following a 36-h exposure to four different mercury species. Bottom row: Histological images of a zebrafish brain and eye compared with the mercury distributions of the adjacent sections.

Their work reveals substantial differences in the way different mercury species accumulate in tissue



Mercury compounds, in both inorganic and organometallic forms, are common toxins in the environment. Examples of inorganic mercury include “silver” dental amalgams, some thermometers, and fluorescent light bulbs. An example of organometallic mercury is thiolate-bound methylmercury, which is present in marine fish and is particularly concentrated in predatory species. Mercury compounds that cross the blood-brain barrier and blood-placental barrier are especially harmful to developing organisms. Organic methylated mercury can cross these barriers and cause irreversible nervous system damage. The potential damage is especially great during pre- and post-natal development, resulting in recommended limits on fish consumption for pregnant women and young children. With so much mercury in the environment, it is important to understand the mechanisms that govern the transport and toxicity of different mercury species.

Zebrafish are an excellent vertebrate model organism because they develop an endothelial-based blood-brain barrier similar to mammals at only three days post-fertilization. In this investigation, the University of Saskatchewan researchers exposed zebrafish larvae (top of this page - not to scale) to two inorganic (mercuric chloride and mercuric bis-L-cysteinate) and two organic mercury (methylmercury chloride and methylmercury L-cysteinate) species mixed in water. Utilizing the high-flux, 5- μm -size synchrotron x-ray beam from XSD beamline 20-ID-B,C at the APS to carry out synchrotron x-ray fluorescence imaging, mapping the mercury accumulation patterns in different tissues.

The diversity of accumulation patterns between organic and inorganic mercury in zebrafish larvae proved to be striking. Although methylmercury

contributed far more to the overall mercury burden, each mercury species targets different cell types in the developing larvae. By far the highest concentrations in any tissues were of both forms of methylmercury in eye lens epithelial cells.

Prior to this study the explanation was that methylmercury had enhanced lipid solubility and higher permeability across the cell membrane. However, the data obtained by the group suggests that thiols substitute for hydroxide or chloride ligands in the larval body, resulting in higher permeability, although even this mechanism cannot account for the extremely high levels of methyl mercury in the cells. An additional active transport mechanism, most likely system L, a Na^+ -independent large neutral amino acid transporter, may transport methyl mercury across the blood-brain barrier.

Organic mercury was also much higher than inorganic mercury in the heart and brain, although inorganic mercury preferentially accumulated in the ventricular region of the brain. The likely explanation is that high levels of inorganic mercury target the ependymal cells that line the cerebrospinal fluid-filled ventricles and spinal cord. Selenoprotein P in the ependymal cells may sequester the mercury, for example, as HgSe nanoparticles in the blood plasma. There is evidence to support this idea: symptoms of mercury toxicity are relieved in mammals given intravenous sodium selenite and HgCl.

Although sensory hair cells in the fish are in direct contact with the mercury-contaminated water, different hair cell types also had different mercury concentrations. Neuromasts, mechanosensory organs responsible for detecting pressure changes in water, had twice as much organic as inorganic mercury. However, inorganic mercury was more concentrated in the

olfactory epithelium, which detects chemicals. While the high concentrations of inorganic mercury in the olfactory epithelium can be explained by passive transport, in the neuromasts, an active carrier across the cell membrane is likely. — *Dana Desonie*

See: Malgorzata Korbas, Tracy C. MacDonald, Ingrid J. Pickering, Graham N. George*, and Patrick H. Krone**, “Chemical Form Matters: Differential Accumulation of Mercury Following Inorganic and Organic Mercury Exposures in Zebrafish Larvae,” *Chem. Biol.* 7, 411 (2012). DOI:10.1021/cb200287c

Author affiliation:

University of Saskatchewan

Correspondence: *g.george@usask.ca, **pat.krone@usask.ca

This work was supported by the Canadian Institutes of Health Research (G.N.G., I.J.P.), the Saskatchewan Health Research Foundation (G.N.G., I.J.P.), the University of Saskatchewan, and a Natural Sciences and Engineering Research Council (NSERC) of Canada Discovery Grant (P.H.K.). G.N.G. and I.J.P. are Canada Research Chairs. The beamlines at APS Sector 20 are supported by the U.S. Department of Energy Office of Science (DOE-SC), a Major Resources Support grant from the Natural Sciences and Engineering Research Council of Canada, the University of Washington, the Canadian Light Source, and the Advanced Photon Source. Use of the Advanced Photon Source at Argonne National Laboratory was supported by the U.S. DOE-SC under Contract No. DE-AC02-06CH11357.

20-ID-B,C • XSD • Materials science, environmental science, chemistry • X-ray absorption fine structure, surface diffraction, x-ray Raman scattering, small-angle x-ray absorption fine structure, microfluorescence (hard x-ray), time-resolved x-ray absorption fine structure, x-ray emission spectroscopy • 4.3-27 keV, 7-52 keV • On-site • Accepting general users •

BACTERIAL DEFENSES AGAINST QUANTUM DOTS AND RELEASED TOXIC METALS

The use of manufactured nanomaterials (MNMs) is exploding. Semiconductor nano-crystals, called quantum dots (QDs), are used in bio-imaging, solar cells, drug delivery, and many other areas, increasing the possibility of their release into the environment. QDs are coated with stabilizing polymers, which enhance their biocompatibility and protects them from breaking down chemically. However, weathering may expose the core and shell components to chemical breakdown, releasing toxic heavy metals. Cadmium and selenium promote stress responses in a variety of organisms and threaten ecosystems. Bacteria provide essential ecosystem services, so understanding the effects of toxic chemicals released from MNMS on microbes is crucial. Also, research on microbial responses to QDs can help us estimate their potential effect on animals and humans. In this study, researchers working at the MR-CAT 10-ID-B beamline at the APS set out to understand the adaptations and defense mechanisms that microbes have against QD toxicity.

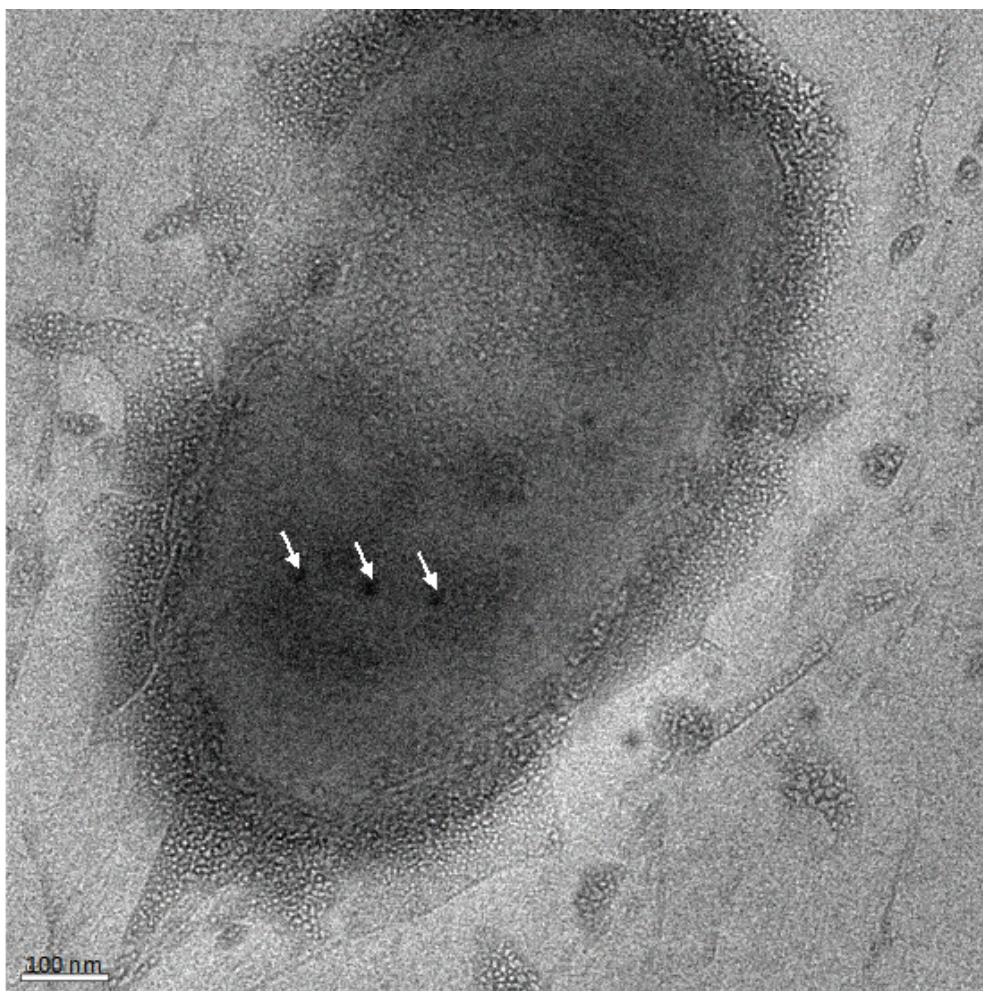


Fig. 1. Transmission electron microscopy image of a PAO1 and biogenic NPs, pointed by white arrows, synthesized during exposure to Cd- and Se-salts.

The common bacterium *Pseudomonas aeruginosa* PAO1 was chosen as a model for this study, because it has a greater capacity to resist heavy metals than other bacterial strains. The researchers exposed PAO1 to intact QDs, weathered QDs, and dissolved cadmium (Cd) and selenium (Se) salts at sub-lethal levels to mimic the low concentrations at which these compounds would enter the environment.

PAO1 is thought to defend against sub-lethal exposures to QDs in several ways. Increased expression of heavy metal efflux pumps and up-regulation of antioxidant enzymes within the cell, in addition to extracellular biosynthesis of metallic NPs, is believed to decrease metal bioavailability.

Figure 1 shows one bacterium growing with Cd and Se salts, and the formation of extra-cellular nanoparticles (arrow). With electron microscopy and energy-dispersive spectrometry, these particles were confirmed to contain Cd and Se. All three treatments up-regulated *czcABC* metal efflux transporters, although intact QDs had little to no release of metals and thus the least effect on *czcABC* expression. Surprisingly, weathered QDs had a greater transcriptional response than dissolved Cd and Se salts at similar concentrations.

Weathered QDs induced the superoxide dismutase gene *sodM*, which could be generated to repair oxidative damage. Again, there was a greater response in cells exposed to weathered QDs than to heavy metal salts. The up-regulation of DNA binding stress proteins suggests that PAO1 required DNA repair, possibly as a result of oxidative stress.

QDs also induced antibiotic resistant (ABR) genes, which increased antibiotic minimum

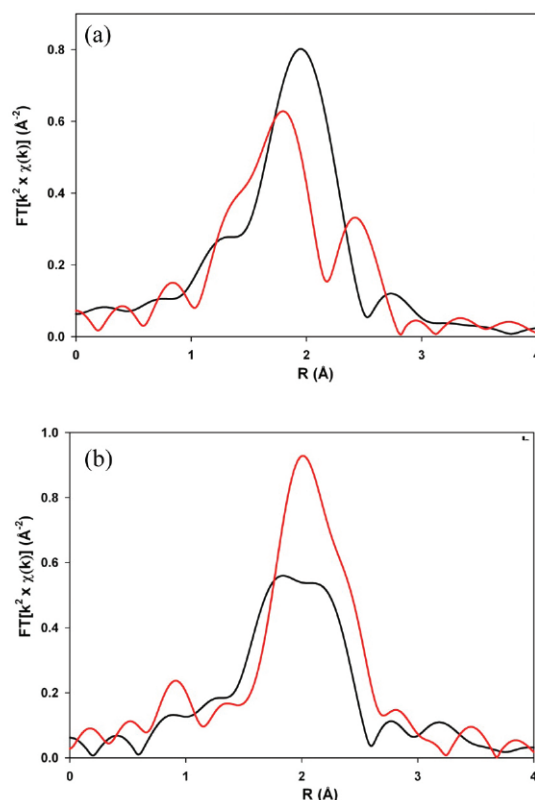


Fig. 2. The magnitude of k^2 -weighted Fourier transforms (FT) of EXAFS spectra. Panel (a) shows PAO1 exposed to Cd plus Se (red) and Cd alone (black) at Cd K edge, and panel (b) shows PAO1 exposed to Cd plus Se (red) and Se alone (black) at Se K edge. From Y. Yang et al., ACS Nano 6 (2012). ©2012 American Chemical Society.

inhibitory concentrations by between 50 and 100%. This increased tolerance to different antibiotics is similar to that observed in response to osmotic stress and pH extremes, suggesting the induction of a global defense mechanism.

Another adaptive mechanism is cell-mediated precipitation of released metals, which is likely a method of detoxification by reducing the bioavailability and toxicity of the metals. X-ray absorption fine structure (EXAFS) measurements at beamline 10-ID-B were collected by researchers from Rice University, the Illinois Institute of Technology, and Argonne to aid in understanding the structure and Cd and Se content in the biogenic NPs

(Fig. 2). EXAFS showed extracellular synthesis of biogenic cadmium- and selenium-NPs after exposure to Cd-nitrate and SeO₂.

Uncovering the exact metabolic pathways and enzymes involved in NP biosynthesis requires further research. Given the tremendous variety of bacteria, the number of possible responses to NPs is great. Further research will be needed to determine whether the responses uncovered in this study are common among other microbes. — Dana Desonie

See: Yu Yang¹, Jacques M. Mathieu¹, Soma Chattopadhyay², Jeffrey T. Miller³, Tianpin Wu³, Tomohiro Shibata², Wenhua Guo¹, and Pedro J.J. Alvarez^{1*}, "Defense Mechanisms of *Pseudomonas aeruginosa* PAO1 against Quantum Dots and Their Released Heavy Metals," ACS Nano 6(7), 6091 (2012). DOI:10.1021/nl3011619

Author affiliations: ¹Rice University, ²Illinois Institute of Technology, ³Argonne National Laboratory

Correspondence:

*alvarez@rice.edu

This research was supported by a Joint US-UK Research Program (Grant No. RD-834557501-0 by the U.S. Environmental Protection Agency and U.K. Natural Environment Research Council and Economic & Social Research Council). MR-CAT operations are supported by the U.S. Department of Energy (DOE) and the MR-CAT member institutions. Use of the Advanced Photon Source at Argonne National Laboratory was supported by the U.S. DOE Office of Science under Contract No. DE-AC02-06CH11357.

10-ID-B • MR-CAT • Materials science, environmental science, chemistry • X-ray absorption fine structure, time-resolved x-ray absorption fine structure, micro x-ray absorption fine structure, microfluorescence (hard x-ray) • 4.3-27 keV, 4.3-32 keV, 15-90 keV • On-site • Accepting general users •

A TINY TRACE OF THE SOLAR NEBULA

Fireballs streaking across the sky – they’re rare and they’re sensational when they strike. Possibly more sensational is what is found years later in a laboratory.

Scientists have gained tremendous clues about the origin of our solar system in fragments of the Allende meteorite, which burst across the Mexican sky in the early hours of February 8, 1969, sending thousands of fragments scattered across a 200-sq-mi (300-km) area in the Mexican state of Chihuahua near Pueblito de Allende, 340 mi (547 km) south of El Paso, Texas. It was the most important stony meteorite shower on record according to the Smithsonian National Museum of Natural History [1]. Panguite, a new mineral found in the carbonaceous chondrite Allende meteorite, likely condensed from the solar nebula before Earth and the other planets formed. X-ray diffraction studies of a panguite sample, carried out at the APS, are helping researchers understand panguite and other refractory minerals discovered in Allende. These results are a first step in gaining new understanding about the conditions under which the minerals formed and evolved in the early solar system.

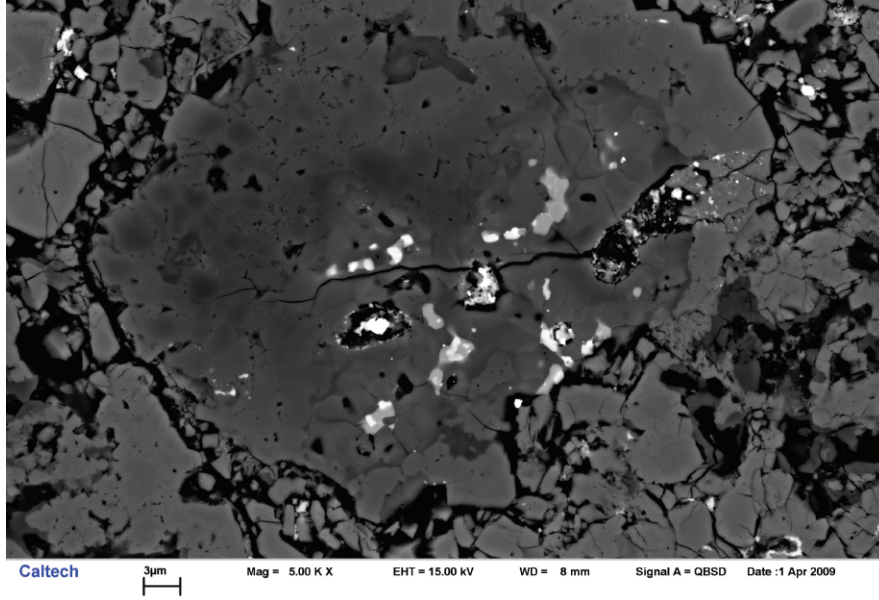


Allende is the largest carbonaceous chondrite and probably the most studied meteorite in the world. Carbonaceous chondrites are primitive meteorites that contain evidence of the processes, timing, and chemistry of the earliest stages in the evolution of our solar system. Researchers from the California Institute of Technology have been investigating the nanomineralogy of Allende since 2007, finding 10 new minerals including, most recently, panguite, a new titanium oxide. Besides being a newly discovered mineral, panguite is a new material. The International Mineralogical Association's Commission on New Minerals, Nomenclature, and Classification has approved both the mineral and its name. Synthetic panguite ($\text{Ti}^{4+}, \text{Sc}, \text{Al}, \text{Mg}, \text{Zr}, \text{Ca}$)_{1,8}O₃ is unknown and so the conditions in which panguite forms are difficult to characterize.

Panguite is one of the oldest minerals in the solar system, dating from long before Earth and the other planets solidified from the nebular cloud. The mineral is found in an ultra-refractory inclusion in Allende and other carbonaceous chondrites. "Refractory" refers to inclusions that contain minerals that are formed at high temperatures and in extreme environments. The minerals found in these refractory inclusions are thought to have condensed from primitive, high-temperature gases generated by the solar nebula. Panguite is among the solar system's first solid objects. Just as panguite condensed from the disorder of the nebular cloud, the mineral's name comes from Pan Gu, a giant from ancient Chinese mythology who separated heaven from Earth in the original chaos.

The panguite sample was first observed via scanning electron microscopy and characterized by electron backscatter diffraction (Fig. 1),

< A specimen of the Allende meteorite. Photo by Chip Clark, Smithsonian Institution. Inset: School children gather around a 7.5-kg Allende individual found by Manuel Gómez on February 13, 1969, approximately 3 km south of Rancho Santa Ana (NMNH 3493). Image from Smithsonian Institution Archives, photo by Roy S. Clarke, Jr.; image courtesy of National Museum of Natural History. Both ©copyright 2013 Smithsonian Institution.



micro-Raman spectroscopy, and electron probe microanalysis. The structure of the mineral phase was analyzed with synchrotron micro-Laue diffraction on one panguite grain at the XSD 34-ID-E undulator beamline of the APS by researchers from the California Institute of Technology; the University of Nevada, Las Vegas; and Argonne.

In the Allende inclusions, panguite occurs as irregular to subhedral orthorhombic grains only 500 nm to 1.8 µm in size. Refractory inclusions in the Allende carbonaceous chondrite are valuable because they have not undergone the alteration experienced by many phases in the meteorite.

The elements found in panguite yield clues to processes in the early solar system. Panguite has large concentrations of titanium (Ti), zirconium (Zr), scandium (Sc), and yttrium (Y), which gives it great potential as an environmental sensor. Both titanium and zirconium oxide are highly refractory in both oxidizing and reducing gases. Since nearly all Ti in panguite is 4+, it is likely that the mineral formed in an oxidizing environment. However, panguite is always found in contact with Ti-rich davisite, which has about twice as much Ti³⁺ as Ti⁴⁺, suggesting that it formed under reducing conditions.

Direct clues from Zr-Y-Sc-enriched phases are needed to understand the dichotomy in redox conditions. It is possible that davisite nucleated on panguite that had grown under previously oxidizing conditions, indicating that these two minerals are not genetically related. Additional research on panguite and other minerals in the

Fig. 1. Backscatter electron image of the ultra-refractory inclusion containing panguite in the Allende meteorite magnified at 5kx. The bright material is panguite with darker davisite in contact.

Allende meteorite will undoubtedly reveal much more about the origin and evolution of the early solar system.

— Dana Desonie

REFERENCE

[1] http://www.mnh.si.edu/onehundredyears/featured_objects/AllendeMeteorite.html

See: Chi Ma^{1*}, Oliver Tschauer^{1,2}, John R. Beckett¹, George R. Rossman¹, and Wenjun Liu³, "Panguite, (Ti⁴⁺, Sc, Al, Mg, Zr, Ca)_{1,8}O₃, a new ultra-refractory titania mineral from the Allende meteorite: Synchrotron micro-diffraction and EBSD," *Am. Mineral.* **97**, 1219 (2012).

DOI:10.2138/am.2012.4027

Author affiliations: ¹California Institute of Technology; ²University of Nevada, Las Vegas; ³Argonne National Laboratory

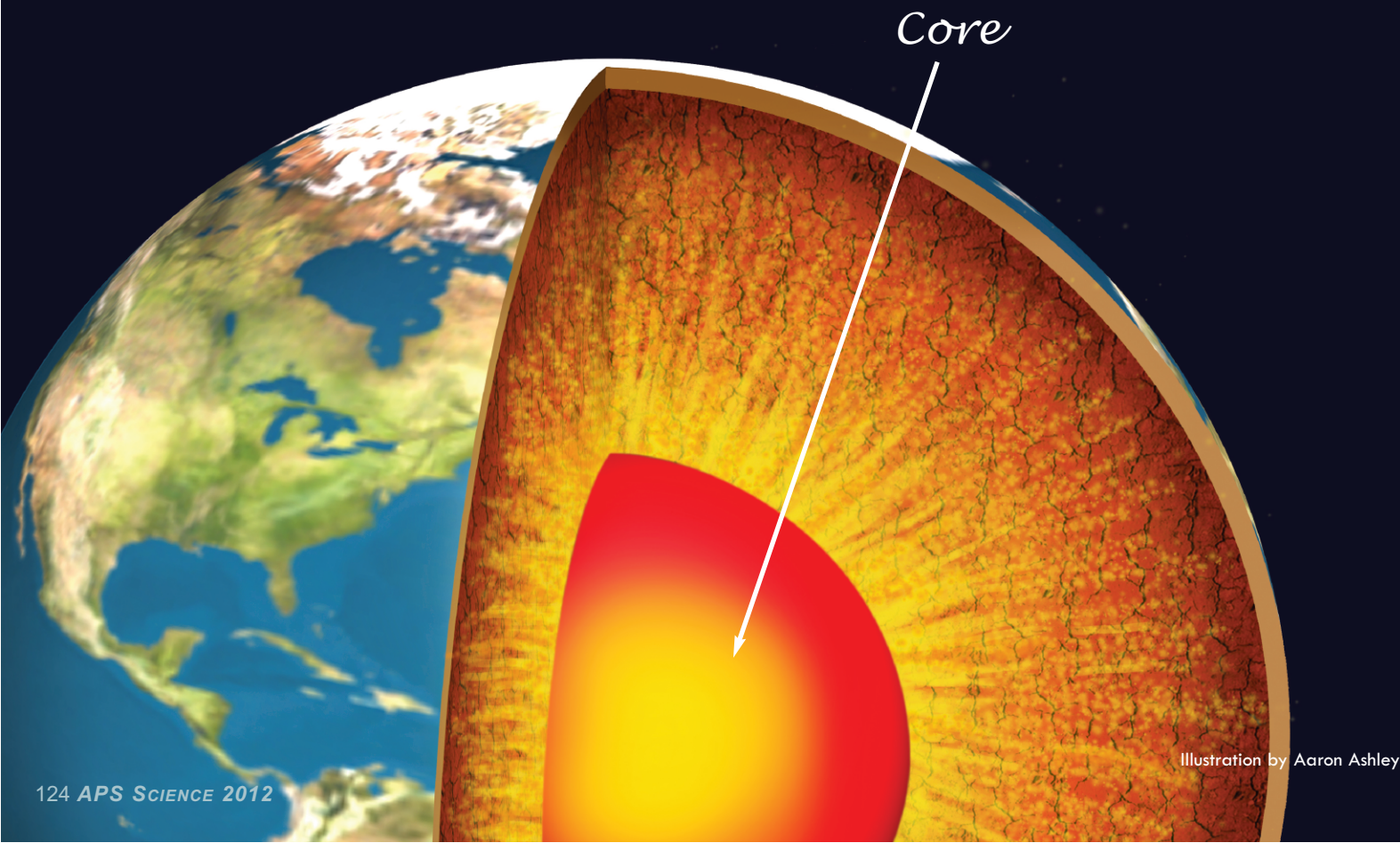
Correspondence: *chi@gps.caltech.edu

This research was supported by U.S. Department of Energy (DOE) National Nuclear Security Administration Cooperative Agreement DE-FC88-01NV14049, NASA OSS Grant NNX09AG40G, and National Science Foundation Grant EAR-0947956. Use of the Advanced Photon Source at Argonne National Laboratory was supported by the U.S. DOE Office of Science under Contract No. DE-AC02-06CH11357.

34-ID-E • XSD • Materials science, physics • Microdiffraction, Laue crystallography, microbeam • 7-30 keV • On site • Accepting general users •

DOUBLING ESTIMATES OF LIGHT ELEMENTS IN THE EARTH'S CORE

The inner core of the Earth is the remotest area on the globe, mostly impossible to study directly. It is an area of the planet that experiences both extremely high pressure ranging from 3,300,000 to 3,600,000 times atmospheric pressure, and extremely high temperatures somewhere from 5000 to 6000 K. One way to study this area is by recording how sound waves travel across the interior, matching these profiles to known information about how sound waves travel through candidate iron alloys, and attempting to discern which materials must be present. This method requires an understanding of how sound waves travel through the potential materials present in the core. A team of researchers utilized APS x-rays to develop a new model of how sound waves travel through iron and iron-silicon alloys, showing for the first time that increased temperatures will affect the sound wave profile, and that sound velocity and density correlate in a non-linear way. Their results suggest that the amount of light elements in the inner core could be two times more than estimated in previous studies without considering these effects.



The researchers from the University of Texas at Austin, Argonne, and the Carnegie Institute of Washington studied samples of what is known as hexagonal closest-packed iron (hcp Fe), which is believed to be the high-pressure phase of iron present in the Earth's core, as well as a hcp iron-silicon alloy because silicon is one of the most likely candidate light elements in the core.

The researchers measured the compressional wave velocity (in which the wave has the same direction of vibration as its direction of travel) of the samples using high-energy inelastic x-ray scattering (HERIX) and x-ray diffraction (XRD) in a resistively-heated diamond anvil cell at XSD beamline 3-ID-B,C,D of the APS (Fig. 1). They made their measurements under simultaneous high-pressure and high-temperature conditions to better simulate conditions in the Earth's core.

Previous studies had suggested that the compressional sound velocity of hcp Fe was generally linear with increased density. In contrast, by subjecting their samples to unprecedented extreme conditions, the team found that the effect of high temperature at a given density on the sound velocity of iron cannot be ignored (Fig. 1). As the temperature increased for a given density at high pressures, the sound waves slowed down. In addition, the relationship between the sound wave velocity and increased density was not linear, but instead could be better described by an empirical power-law function with concave behavior at higher densities.

The researchers incorporated this new information into models of the Earth's core to provide new estimates of the chemical composition there. The sound wave velocities that have been observed in the core correlate to a profile of hcp-Fe with approximately 8% of

silicon by weight at temperatures of 6000 K. This number represents nearly twice the amount estimated in previous studies.

The team hopes to explore additional alloys to further round out estimates of the core's composition and to explain a number of enigmatic behaviors of seismic waves in this most extreme region of the planet. Also, since this study observed temperatures and pressures that are still much lower than those of the inner core, these scientists hope future studies will push the experimental conditions even further. With direct measurements of compressional wave velocities at relevant pressure and temperature conditions on the horizon, such studies may eventually answer the long-standing question of the composition of the Earth's core. — *Karen Fox*

See: Zhu Mao^{1*}, Jung-Fu Lin¹, Jin Liu¹, Ahmet Alatas², Lili Gao², Jiyong Zhao², and Ho-Kwang Mao³, "Sound velocities of Fe and Fe-Si alloy in the Earth's core," Proc. Natl. Acad. Sci. USA **109**(26), 10239 (June 26, 2012). DOI:10.1073/pnas.1207086109

Author affiliations: ¹University of Texas at Austin, ²Argonne National Laboratory, ³Carnegie Institution of Washington

Correspondence:

*zhumao@mail.utexas.edu

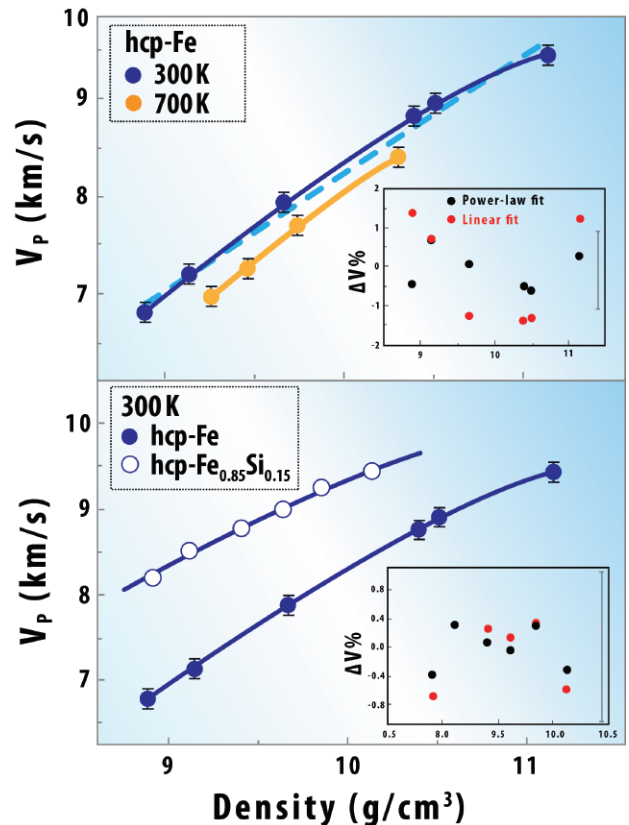
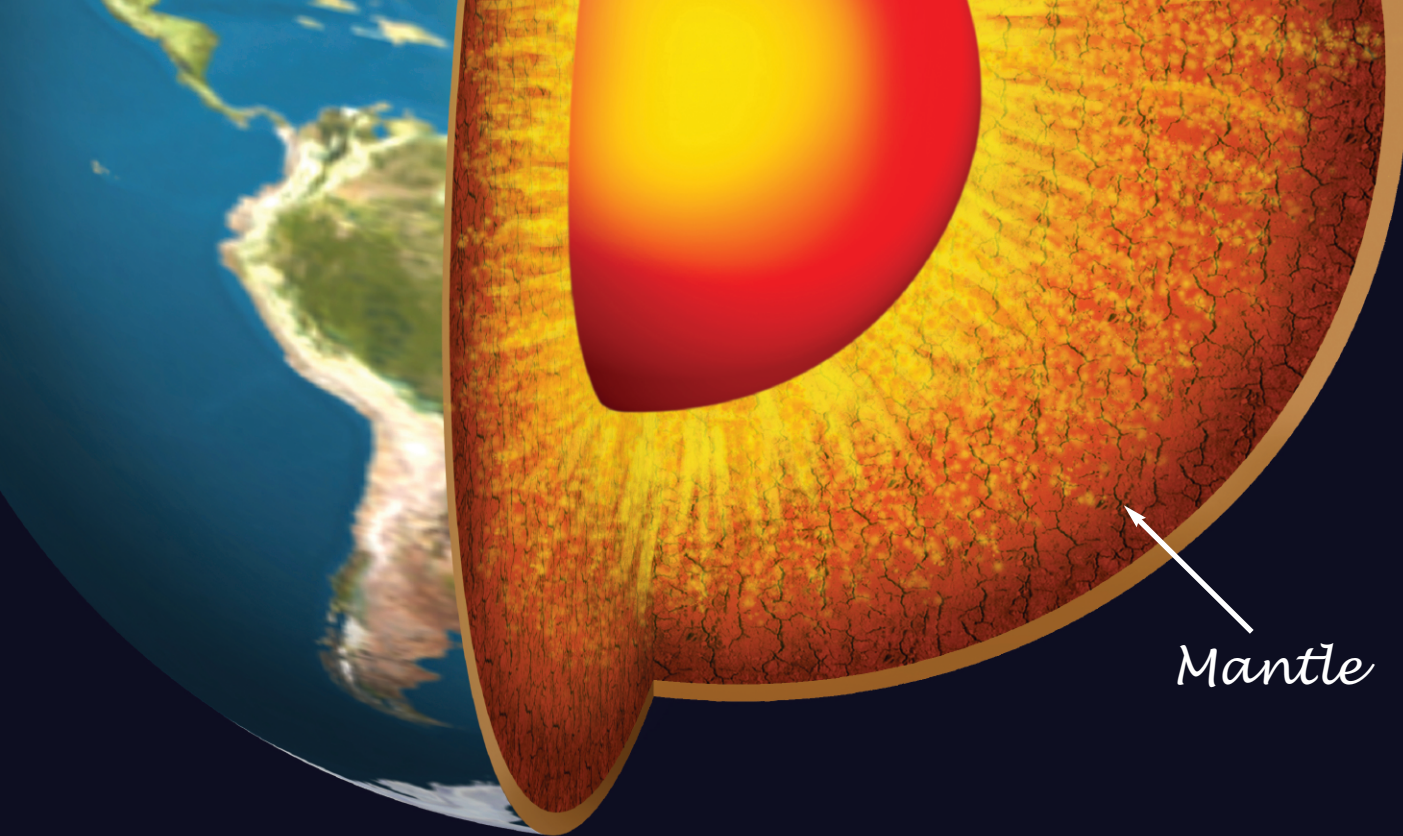


Fig. 1. Velocity-density plots of the samples at high pressures and temperatures. The top panel shows the velocity-density plot for hcp-Fe at both 300 K and 700 K. The dashed lines show the linear fit, while the solid line shows the power law fit, which matches the data more closely. The bottom panel shows the velocity-density relation of both hcp-Fe and the iron-silicon alloy at 300 K.

Work at the University of Texas, Austin, was supported by the National Science Foundation (NSF) (EAR-1056670 and EAR-1053446), and the Carnegie/ Department of Energy (DOE) Alliance Center. H.-K.M. would like to acknowledge support from NSF EAR-1119504 and EAR-0911492. Use of the Advanced Photon Source at Argonne National Laboratory was supported by the U.S. DOE Office of Science under Contract No. DE-AC02-06CH11357.

3-ID-B,C,D • XSD • Physics • Nuclear resonant scattering, inelastic x-ray scattering, high-pressure diamond anvil cell • 7-27 keV, 14.41-14.42 keV • On-site • Accepting general users •



Mantle

IRON-BEARING PEROVSKITE IN THE MANTLE

Illustration by Aaron Ashley

Although we are confined to Earth's crust, we live every day with the impacts that the large-scale motions of subterranean tectonic plates can have on our planet, such as changes to terrain or weather. Under the crust, Earth's mantle convects, transporting heat from the core outward, uplifting continental plates at their boundaries, recycling oceanic plates, and creating new crust and upper mantle rocks. Understanding the convection of the mantle gives us insight into processes that affect us locally. But Earth's mantle is a 2900-km-thick layer that makes up the majority of Earth by volume. Its temperature ranges from 773 K to 4273 K and its pressure soars as high as 140 GPa. What tools do we have to measure its characteristics? One proven method is replicating in a laboratory those temperatures and pressures, applying them to samples of relevant materials, and studying them with high-brightness x-rays from synchrotron light sources such as the APS. One team of researchers employed a GSECARS beamline at the APS to study an iron-bearing perovskite thought to exist in the lower Earth mantle. Their results indicate that the mantle could indeed contain an iron-bearing perovskite, adding another potential piece to the puzzle of the Earth's composition.

Seismic probing of the mantle maps out hot and cold masses where compressional and shear waves traveling through the rock slow down and speed up, respectively.

Seismic waves reflect and refract off mineral, thermal, and composition boundaries, indicating where changes occur. From volcanic eruptions; subducting slabs that meet, driving one of them down into the mantle; and inferences based on the compositions of meteorites, geologists postulate the lower mantle comprises $(\text{Mg,Fe})\text{SiO}_3$, or perovskite, and MgO , periclase. But without accurate information about how these rocks deform when stressed and then return to their original shape, geodynamicists cannot accurately model the mantle.

Research published in 2003 and 2004 showed unexpected iron partitioning in $(\text{Mg,Fe})\text{SiO}_3$ under lower mantle conditions, raising questions about the effect of additional iron in the structure of perovskite silicates. These silicates are crystal structures with alternating layers of SiO_3 and some combination of aluminum, iron, and magnesium. These three elements all fit into the same location in the crystal lattice, potentially changing the characteristics of the mineral. An iron-bearing perovskite such as $\text{Mg}_{0.95}\text{Fe}^{2+}_{0.04}\text{Fe}^{3+}_{0.01}\text{SiO}_3$ may form within subducting oceanic crust as it sinks through the mantle and would behave differently than MgSiO_3 in the same environment.

A team of researchers from University Bayreuth (Germany), the European Synchrotron Radiation Facility (France), and The University of Chicago characterized $\text{Mg}_{0.95}\text{Fe}^{2+}_{0.04}\text{Fe}^{3+}_{0.01}\text{SiO}_3$ and MgSiO_3 under pressures as high as 25 GPa and temperatures of 1200 K. They measured the compressional and shear wave velocities and densities using the 13-ID-C,D

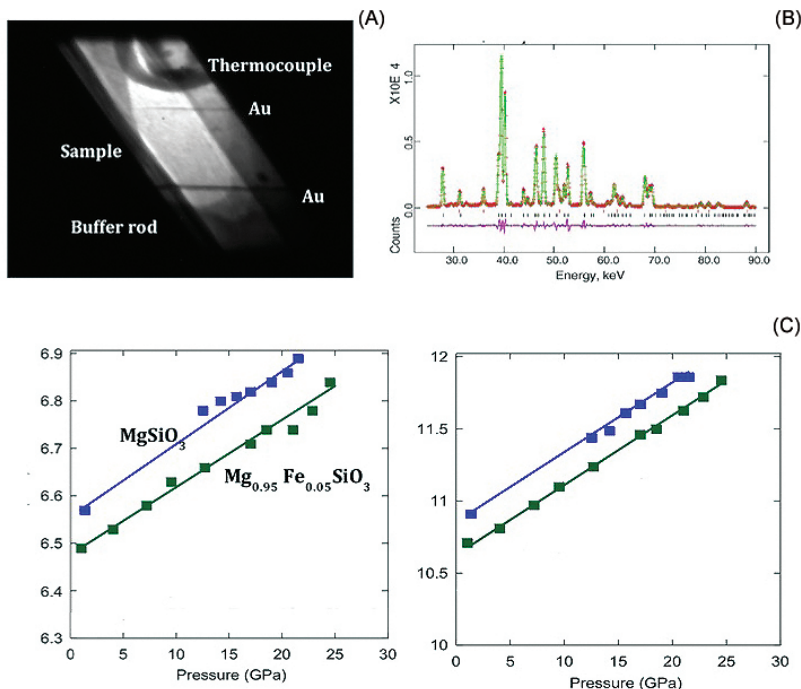


Fig. 1. Experimental setup for ultrasonic interferometry measurements and x-ray diffraction. (A) X-ray radiography. (B) Energy dispersive x-ray diffraction. (C) Sound wave velocities.

beamline of GSECARS at the APS. Measurements were taken at a range of pressures and temperatures representative of the mantle to the upper limit of the lower mantle.

They measured the travel times of both shear and compressional waves through the silicate samples with ultrasound. Using simultaneous *in situ* x-ray radiographic imagery, they measured the length of each sample. From these data they calculated the bulk and shear moduli—the measure of how the minerals return to their original shape after experiencing compression and shear, respectively—for each sample at each temperature and pressure.

The team found that the bulk modulus of $\text{Mg}_{0.95}\text{Fe}^{2+}_{0.04}\text{Fe}^{3+}_{0.01}\text{SiO}_3$ was approximately 2% lower than that of MgSiO_3 , implying that the iron-bearing mineral does not compact as much as MgSiO_3 due to compressional waves. To check this conclusion, the team calculated the bulk modulus using a procedure that does not require x-ray density data. While the value for MgSiO_3 remained consistent with the scientific literature, the $\text{Mg}_{0.95}\text{Fe}^{2+}_{0.04}\text{Fe}^{3+}_{0.01}\text{SiO}_3$ value was still lower. The shear modulus values for both minerals agreed with previously published work, indicating that additional iron does not affect

shear-wave properties.

But can this iron-bearing form of perovskite postulated to appear in the mantle produce the measured seismological profile? The team input their derived moduli data into a standard bulk silicate Earth model and calculated the resulting shear and compressional wave velocities. Even with the presence of $\text{Mg}_{0.95}\text{Fe}^{2+}_{0.04}\text{Fe}^{3+}_{0.01}\text{SiO}_3$, the velocity estimates were consistent with models based on seismological data. The team concluded that the mantle could indeed contain an iron-bearing perovskite, based on their measured characteristics for $\text{Mg}_{0.95}\text{Fe}^{2+}_{0.04}\text{Fe}^{3+}_{0.01}\text{SiO}_3$.

— Mary Alexandra Agner

See: Julien Chantel^{1,2*}, Daniel J. Frost¹, Catherine A.

McCammon¹, Zhicheng Jing³, and Yanbin Wang³, “Acoustic velocities of pure and iron-bearing magnesium silicate perovskite measured to 25 GPa and 1200 K,” *Geophys. Res. Lett.* **39**, L19307 (2012).

DOI:10.1029/2012GL053075, 2012

Author affiliations: ¹University Bayreuth, ²European Synchrotron Radiation Facility, ³The University of Chicago

Correspondence:

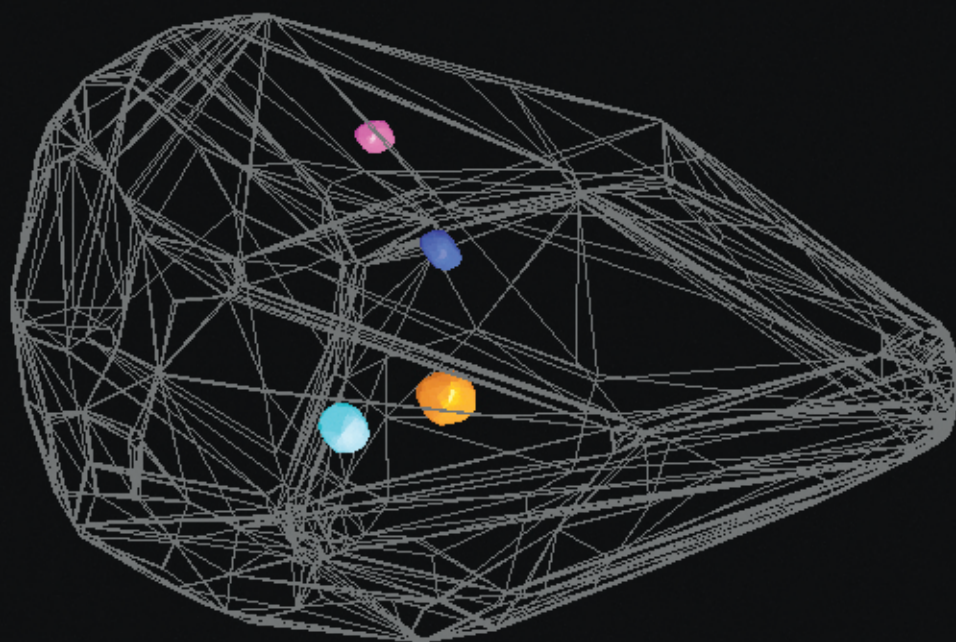
*julien.chantel@esrf.fr

This work was funded through the support of a European Research Council (ERC) advanced grant 227893 “DEEP.” GSECARS is supported by the National Science Foundation - Earth Sciences (EAR-1128799) and U.S. Department of Energy (DOE) - Geosciences (DE-FG02-94ER14466). Use of the Advanced Photon Source at Argonne National Laboratory was supported by the U.S. DOE Office of Science under Contract No. DE-AC02-06CH11357.

13-ID-C,D • GSECARS • Geoscience, environmental science • Inelastic x-ray scattering, small x-ray absorption fine structure, microdiffraction, x-ray absorption fine structure, microfluorescence (hard x-ray), high-pressure diamond anvil cell, high-pressure multi-anvil press • 4-45 keV • On-site • Accepting general users •

SUPERVOLCANOES ARE LESS STABLE THAN BELIEVED

On California's eastern edge, bordering Nevada, lies what is known as the Long Valley Caldera – a 20-mile-long stretch of collapsed land formed by a gigantic volcanic eruption 760,000 years ago. The super eruption cast a thin layer of volcanic deposits almost as far as the midwestern United States. Closer to the eruption, hotter clouds traveling close to the surface deposited material up to tens of miles away, creating the Bishop Tuff. Studying the history of this magma body can help shed light on modern gigantic pools of magma, such as that at Toba on the island of Sumatra in Indonesia. Radiometric dating of various ingredients such as zircon from the Bishop Tuff rocks has suggested that the magma pool was long-lived, evolving slowly over more than 100,000 years before erupting. Now, research carried out at the GSECARS beamlines at the APS has produced new evidence that the magma probably erupted less than 10,000 years after being fully formed and more likely between 500-3000 years.



Previous studies focused on zircon found in the material from the eruption. That zircon, which is naturally long-lived, has been dated to 100,000-150,000 years prior to the eruption. Zircon is easily dated, which is one reason why it is an attractive material to study, but it makes up just a small fraction of the total composition from the eruption. So the team turned instead to quartz, which makes up 60-70% of the crystals in the magma remains.

To examine the quartz, the team of researchers from Vanderbilt University, OFM Research-West, and The University of Chicago utilized six pumice clasts from the Chalfant Quarry in the southeastern portion of the Bishop Tuff and five pumice clasts from the Aeolian Buttes in the northern portion of the deposit. These samples encompass much of the spectrum of pumice characteristics observed throughout the Bishop Tuff.

The samples were studied utilizing a variety of observational methods, including documentation of sizes and shapes of the whole quartz crystals; cathodoluminescence imaging of individual quartz crystals; trace element analysis at low spatial resolution using laser ablation mass spectrometry; trace element analysis at high resolution using synchrotron x-ray microfluorescence at the GSECARS 13-ID-C,D beamline, and x-ray tomography performed at the GSECARS 13-BM-D beamline, both at the APS. The team

< Fig. 1. This processed version of a tomographic image shows a crystal from the Bishop Tuff with a group of four inclusions shown as colorful solids. The inclusions are shown in their real positions inside of the host crystal (gray wireframe), and each is a different size and faceted to a different extent. The processing routines quantify size, shape (i.e., how round or faceted they are), and their position within the crystal. These three parameters can be used to limit residence times of the inclusions within a crystal, which, in turn, provides information on the lifetime of the magma body itself.

employed their results to constrain the lifetime of the quartz by analyzing the data in a handful of different ways.

The first method examined how long the quartz had resided in hot magma by looking at diffusional relaxation of titanium across the sample. The sharpness of contacts between chemically distinct zones in crystals can constrain the residence times of these internal contacts, and the durations and rates of crystal growth. Once originally established, the concentrations relax over time by diffusion, leading to less sharp divisions throughout the crystal. The typical values showed crystals that were 500-1000 years old at the time of eruption, with the longest time being 2700 years old. The uncertainties are close to 200%, leading to an upper bound close to 13,000 years at a maximum, and more typically under 5000 years.

The team also looked at melt inclusion faceting times, which involves comparing how many different shapes of glass inclusions in crystals are found, since round inclusions naturally become more faceted over time. The best estimate of how long it takes for inclusions to become more faceted implied that the residence time for the quartz had been some 600-1500 years at the time of eruption. Assuming much slower rates of faceting would lead to time estimates of more like 2200-5300 years.

The third method was cataloguing the number of different sizes of crystals. Since crystals grow larger over time, one can estimate the age of the quartz based on how many smaller or larger crystals are in residence. The calculations based on crystal size distributions suggest residence times for the quartz crystals on the order of 1000 years.

Since zircon is long-lived and rugged, the team believes measurements of zircon are in fact showing the history of the entire life span of growth of the magma pool, which seems to take place over hundreds of thousands

of years. The new quartz information, however, supports a model that says that once the pool is formed, it is more unstable than believed and can erupt within 1000 years.

The creation of the pools may evolve very slowly, but on a geological time scale they are not long-lasting after being fully formed. While similar magma bodies on Earth today are still not expected to erupt in any of our lifetimes, they are likely to be more dynamic and variable than previously thought. — *Karen Fox*

See: Guilherme A.R. Gualda^{1*}, Ayla S. Pamuku¹, Mark S. Ghiorso², Alfred T. Anderson, Jr.³, Stephen R. Sutton³, and Mark L. Rivers³, "Timescales of Quartz Crystallization and the Longevity of the Bishop Giant Magma Body," *PLoS ONE* 7(5), e37492 (1 May 2012).

DOI:10.1371/journal.pone.0037492

Author affiliations: ¹Vanderbilt University, ²OFM Research-West, ³The University of Chicago

Correspondence:

*g.gualda@vanderbilt.edu

GSECARS is supported by the National Science Foundation (EAR-0622171) and the U.S. Department of Energy (DOE) – Geosciences (DE-FG02-94ER14466). Use of the Advanced Photon Source at Argonne National Laboratory was supported by the U.S. DOE Office of Science under Contract No. DE-AC02-06CH11357.

13-BM-D • GSECARS • Geoscience, environmental science • Tomography • High-pressure diamond anvil cell, high-pressure multi-anvil press, x-ray absorption fine structure • 4.5-70 keV • On-site • Accepting general users •

13-ID-C,D • GSECARS • Geoscience, environmental science • Inelastic x-ray scattering, small x-ray absorption fine structure, microdiffraction, x-ray absorption fine structure, microfluorescence (hard x-ray), high-pressure diamond anvil cell, high-pressure multi-anvil press • 4-45 keV • On-site • Accepting general users •

ADVANCED PHOTON SOURCE AND CANADIAN LIGHT SOURCE STRENGTHEN TIES



Top: Birdseye view of the CLS booster and storage rings.

Image courtesy of the Canadian Light Source, Inc.
Bottom: Sector 1 in the APS experiment hall.



techniques of the laboratories, we hope to more quickly discover answers to the challenges of our high-tech world."

This new agreement will provide Canadian scientists with more research time to use the x-ray light source facilities and more time on a larger number of APS beamlines. Using varied x-ray and imaging capabilities will

broaden the range of experiments Canadians may undertake at the APS to augment their research done at the Canadian Light Source. X-ray science offers potential solutions to a broad range of problems in surface, material, environmental and earth sciences, condensed matter physics, chemistry, and geosciences.

Since the Sector 20 beamlines at the APS became fully operational, scientists from Canada and other areas who have used these beamlines at the APS have produced an average of 51 scientific publications a year. This research includes the study of more effective mineral exploration strategies, ways to mitigate mine waste and mercury contamination, and novel ways to fabricate nanomaterials for use in fuel cells, batteries, and LEDs.

"Having secure access to brilliant beams of hard x-rays has allowed the CLS to concentrate our local efforts on those applications best suited to the performance characteristics of our lat-

Seeking to solve some of today's greatest global problems, scientists using x-ray light source facilities at national research laboratories in the United States and Canada are sharing more expertise.

The Canadian Light Source, Inc. (CLS) and the APS agreed in January 2012 to a Partner User Proposal that cements a stronger working relationship between the two facilities for the next three years. These two premier light sources use different but complementary x-ray techniques to probe materials in order to understand chemical and structural behavior.

"The ravages of disease, the shortage of sustainable energy sources, and the need for high-performance materials cross all borders," said Brian Stephenson, Argonne Associate Laboratory Director for Photon Sciences and APS Director. "By sharing technological expertise and offering scientists the complementary research

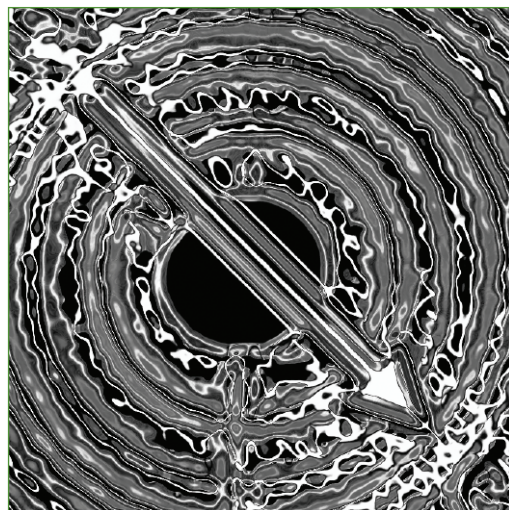
tice while continuing to support Canadian scientists in programs that are truly best served by doing the science at the CLS or the APS, whichever provides the best performance," said Josef Hormes, CLS Executive Director.

Before the Canadian Light Source began operation in 2004, a Canadian group led by Daryl Crozier of Simon Fraser University, working in partnership with colleagues at the University of Washington and the Pacific Northwest National Laboratory, helped found the Sector 20 beamlines at the APS as part of the Pacific Northwest Consortium Collaborative Access Team. Parts of this team were included in the X-ray Science Division of the APS when it was formed.

This long-standing partnership has led to scientifically significant upgrades to the beamline. The new agreement will provide the valuable manpower and expertise to allow the APS to continue to push the innovation envelope.

Scientists from the APS and the Canadian Light Source will work together on R&D projects to improve light-source technology. In particular, scientists will upgrade even further the two beamlines at Sector 20 in four key areas. This will provide a unique capability to prepare and measure *in situ* films and interfaces, a new technique to create quantitative three-dimensional chemical maps of samples, and improved forms of spectroscopy to expand the range of elements and types of environments that can be examined.

"Canadian researchers have been strongly involved with the APS since its inception," Stephenson said. "This expanded agreement builds on our long history of successful collaboration and promises a continued future of plentiful science results and technological innovations."



NANOSCIENCE

TURQUOISE + YELLOW = GREEN: AVIAN STRUCTURAL COLORS AND PHOTONICS INNOVATION

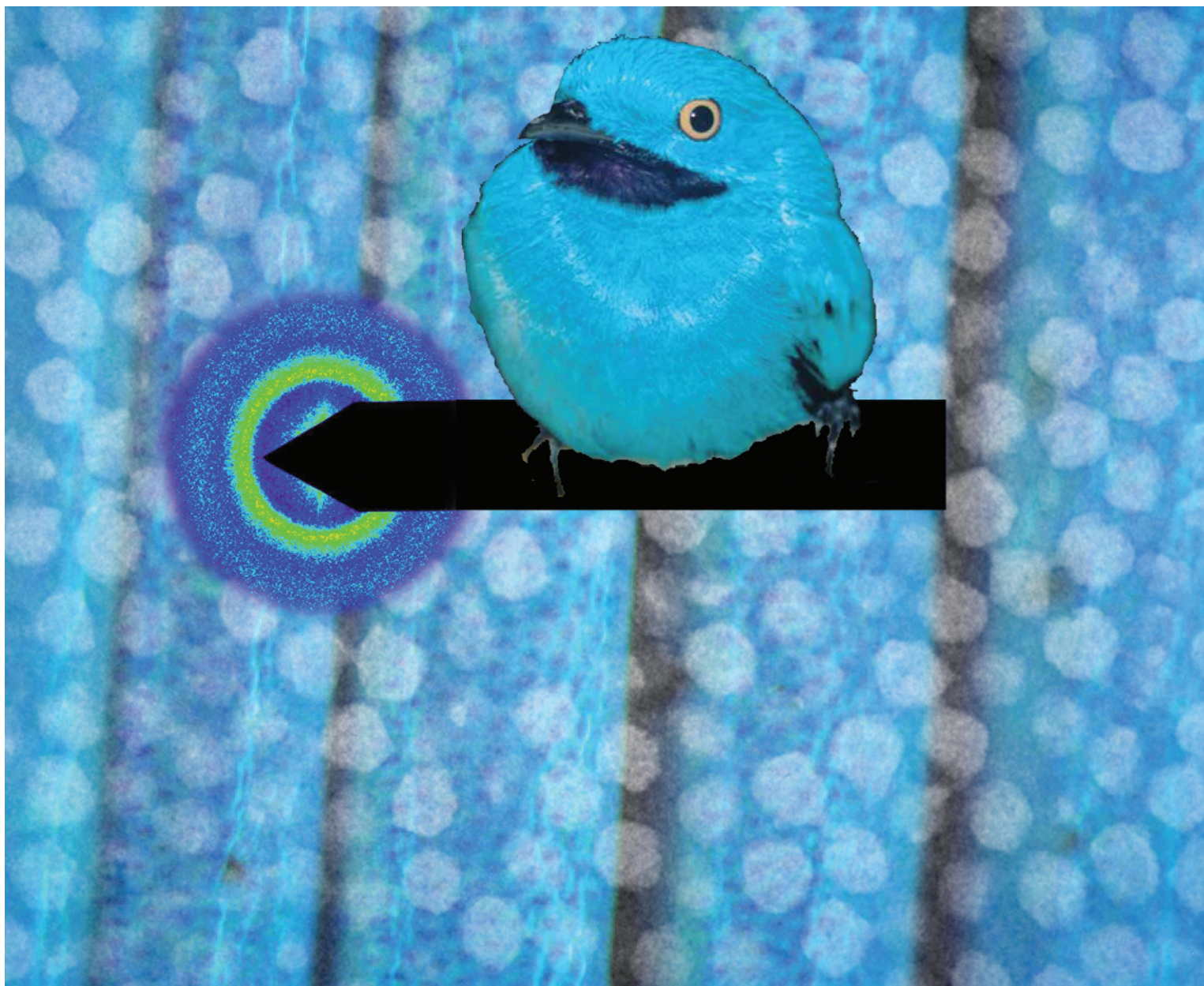


Fig. 1. A collage of the ring-shaped x-ray diffraction pattern documenting isotropic nanostructure and a superimposed light and electron micrograph showing the quasi-random arrangement of air bubbles in feather keratin within the amorphous biophotonic nanostructure in the spongy medullary feather barbs responsible for the vivid turquoise blue color of Plum-throated Cotinga (*Cotinga maynana*). Collage by Vinod Saranathan, photograph of Plum-throated Cotinga (*Cotinga maynana*) by Thomas Valqui.

The vivid blue and green non-iridescent hues of bird plumage are produced by the nanostructure of feathers, unlike much of the avian palette, which is a product of pigmentation. The unique, saturated colors produced by these nanostructures are part of the vital information communicated between birds by their plumage, including breeding status and camouflaging displays. Research utilizing the XSD 8-ID-I beamline of the APS to examine bird feathers at nanometer resolution investigated the ability of these structures to scatter the same color light in multiple directions and establishes a case for bio-mimicking them to manufacture components for devices that benefit from omnidirectional optical properties, such as optical disc drives and fiber-optic cables.

Bird feathers consist of a rachis, or primary shaft, from which numerous barbs branch. Barbs are colored by pigment, structure, or a combination of the two. Barb pigment molecules absorb and re-emit light, producing a color determined by the density and shape of the pigment molecule. Structural colors are produced by the scattering of light at the boundaries between two materials with differing refractive indices. The barb nanostructures are made of beta-keratin proteins pleated into sheets and include hollow areas shaped like spheres or channels; they also include pigment granules filled with melanin. Pigments and structural colors interact to produce colors in tandem when light passes through a layer of pigment molecules prior to scattering off a layer of nanostructures. Many shades of non-iridescent green result from the interaction of yellow pigment with a structural green layer.

Scientists from Yale University and Donostia International Physics Center (Spain) utilized synchrotron small-angle x-ray scattering (SAXS) at 8-ID-I to examine 297 distinctly colored feathers from 230 species belonging to 163 genera in 51 avian families. The scattering results showed three basic nanostructures: spheres, channels, and disordered networks. The nanostructures were quasi-ordered over short distances (hundreds of nanometers), resulting in scattering at the same wavelength in all directions. For a human engaged in bird-watching, this means the color of the feathers is the same no matter the angle or lighting conditions under which they spot the bird. For an engineer, recreating this omnidirectional quality in synthetic materials means reflecting light no mat-

ter the incident angle, improving transmission through the optical fibers used in telephone and internet communication.

The short-range quasi-order of the nanostructures causes them to double-scatter light. The researchers found that double scattering produces two reflectance peaks — one in the visible spectrum and one in the ultraviolet — that is perceived by birds. The role this ultraviolet plumage plays in avian communication is still being studied.

To understand the formation of the nanostructures, the team compared the scattering results from the feathers to those of synthetic materials self-assembled through two methods of phase separation: spinodal decomposition and nucleation-and-growth. Spinodal decomposition is the unmixing of an unstable molecular mixture that creates channels with fractal-like patterns. Nucleation-and-growth is the unmixing of a meta-stable molecular mixture that creates spherical droplets.

The scattering profiles from the spinodally decomposed materials agreed with those of the avian channel nanostructures. Similarly, the profiles of the nucleated-and-grown materials agreed with those of the avian sphere nanostructures. The similarities of the scattering profiles support the hypothesis that feather nanostructures self-assemble by arrested phase separation of the beta-keratin from the cells' cytoplasm.

However, the team cautions that the similarities between the avian nanostructures and the synthetics are insufficient evidence to conclude that their method of formation is the same. While the hypothesis that feather barb nanostructures form through phase

separation is undergoing further testing, these data suggest that phase separation of synthetics could be used to manufacture photonic devices with the desirable omnidirectional optical properties of the feather nanostructures. — *Mary Alexandra Agner*

See: Vinodkumar Saranathan^{1*†}, Jason D. Forster¹, Heeso Noh¹, Seng-Fatt Liew¹, Simon G.J. Mochrie¹, Hui Cao¹, Eric R. Dufresne¹, and Richard O. Prum^{1,2**}, "Structure and optical function of amorphous photonic nanostructures from avian feather barbs: a comparative small angle X-ray scattering (SAXS) analysis of 230 bird species," *J. R. Soc. Interface* **9**(75), 2563 (7 October 2012).

DOI:10.1098/rsif.2012.0191

Author affiliations: ¹Yale University, ²Donostia International Physics Center.

[†]Present address: University of Oxford

Correspondence:

*vinod.saranathan@zoo.ox.ac.uk,

**richard.prum@yale.edu

This work was supported with seed funding from the Yale NSF-MRSEC (DMR 1119826) and NSF grants to R.O.P. (DBI-DBI-0078376), H.C. (PHY-0957680) and E.R.D. (CAREER CBET-0547294) as well as Yale University funds to V.S. and R.O.P. R.O.P. would like to acknowledge support of the Ikerbasque Science Fellowship and the Donostia International Physics Center. Use of the Advanced Photon Source at Argonne National Laboratory was supported by the DOE's Office of Science under Contract No. DE-AC02-06CH11357.

8-ID-I • XSD • Materials science, physics, polymer science • Intensity fluctuation spectroscopy, small-angle x-ray scattering, x-ray photon correlation spectroscopy • 6-12.5 keV, 7.35-7.35 keV, 7.35 keV • On-site • Accepting general users •

ENGINEERING NANOCRYSTAL-BASED FUNCTIONAL MATERIALS

Engineered nanocrystals (NCs) are set to become the building blocks of a new generation of solar cells, light-emitting devices for displays and other applications, and catalysts that work when light shines on them. Extended x-ray absorption fine structure (EXAFS) measurements of manganese K-edge undertaken on the MR-CAT 10-ID-B and XSD 9-BM-B,C beamlines at the APS are helping scientists pin down the details and show the way to tuning the properties of engineered nanocrystals for specific applications.

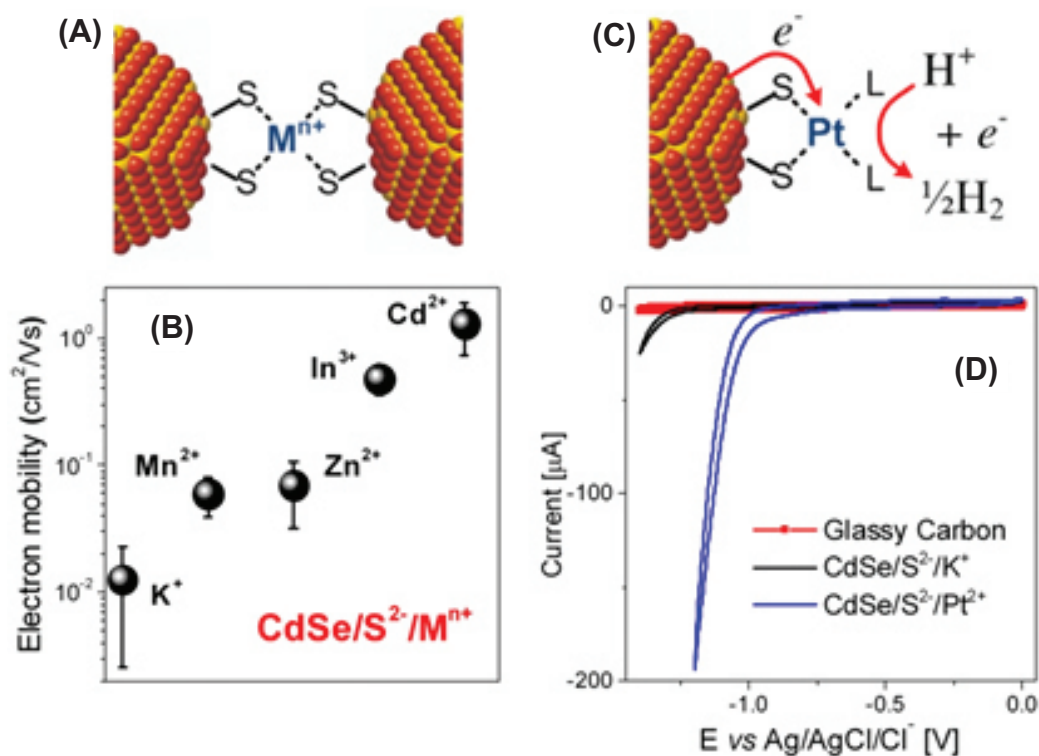


Fig. 1. (A) Semiconductor nanocrystals linked with metal ions. (B) The effect of different metal ions on the field-effect electron mobility in $\text{CdSe}/\text{S}^{2-}$ nanocrystal films. (C) Schematics of $\text{CdSe}/\text{S}^{2-}$ NC surface with coordinated Pt^{2+} ions showing that electrons supplied by NC can drive proton reduction. (D) Cyclic voltammograms measured for $\text{CdSe}/\text{S}^{2-}/\text{K}^+$ and $\text{CdSe}/\text{S}^{2-}/\text{Pt}^{2+}$ nanocrystals in aqueous solution at pH 6.5. The increase of current shows electrocatalytic reduction of water.

Nanocrystalline pieces of inorganic semiconductors, a few billionths of a meter across, can be stirred into a liquid to form a colloid suspension in which the particles never settle out. Such mixtures are ideal for evaporating the liquid to form thin films and layered structures. The layers left behind can be electrically active, respond to or generate light, or catalyze various chemical transformations.

A research team from The University of Chicago and Argonne utilized a range of techniques, including EXAFS at the MR-CAT 10-ID-B beamline, sulfur K-edge XANES spectra measured at the XSD 9-BM-B,C beamline, electron paramagnetic resonance spectroscopy to characterize the materials, and SQUID magnetometry to investigate the nanocrystals' magnetic properties.

The researchers demonstrated that by engineering these cations they can control almost every property of the nanocrystals including photoluminescence efficiency (how brightly they glow when a current is applied), electron mobility (how well they themselves conduct electricity), and their electrocatalytic performance. The same approach to engineering the cations on the surface of a nanocrystal can also be used to adjust the type and concentration of free-charge carriers in the nanocrystal layer and the materials' magnetic susceptibility. Such fine control of the nanocrystals will allow scientists to tune their properties for specific applications, whether boosting solar energy conversion or adjusting the color of the light they produce in a display panel.

Until now, most research into inorganic semiconductor nanocrystals has faced a problem in that the surface of

the nanocrystals must be "capped" with organic compounds. The team hoped to avoid this problem so that they could exercise greater control of their nanocrystals for the development of the particles into photovoltaic solar energy materials, thermoelectrics, light-emitting diodes, and photodetectors for light sensors.

The alternative is to find small and conductive inorganic molecules to cap the nanocrystals. So the use of sulfide, selenide, and telluride anions has been investigated as a way to provide an inorganic protective coating on nanocrystals. Of course, this brings its own problems in that the anions then give the surface an overall negative charge, making the nanocrystals repel each other, which is undesirable if the aim is to make them pack neatly together in a layer.

In previous work the researchers employed ammonium and hydrazinium cations to counteract this repulsive effect and to balance the surface charges. Those cations decomposed into gaseous fragments upon mild heating and could not be used to tailor the material properties. However, there has been one example of other researchers utilizing a more complex cation, didodecyldimethylammonium, to make the nanocrystals soluble in non-polar solvents. The researchers in this study have now simplified the concept and opened a whole new range of options by binding lead, calcium, potassium, manganese, or indium ions to their semiconductor nanocrystals. Platinum ions could also be utilized to create photocatalytic arrays of nanocrystals made from the semiconductor material cadmium selenide.

The team found that these cations not only allow them to make fully inor-

ganic systems but also give them a way to hook together individual nanocrystals in the lattice in a way that was not possible with previously utilized capping materials. The result is nanocrystals with increased luminescence efficiency, greater electron mobility, greater catalytic activity, and superparamagnetism.

— David Bradley

See: Angshuman Nag¹, Dae Sung Chung¹, Dmitriy S. Dolzhnikov¹, Nada M. Dimitrijevic², Soma Chattopadhyay², Tomohiro Shibata², and Dmitri V. Talapin^{1,2*}, "Effect of Metal Ions on Photoluminescence, Charge Transport, Magnetic and Catalytic Properties of All-Inorganic Colloidal Nanocrystals and Nanocrystal Solids," *J. Am. Chem. Soc.* **134**, 13604 (2012).

DOI:10.1021/ja301285x

Author affiliations: ¹The University of Chicago, ²Argonne National Laboratory

Correspondence:

*dvtalapin@uchicago.edu

MR-CAT operations are supported by the Department of Energy and the MR-CAT member institutions. Use of the Advanced Photon Source and the Center for Nanoscale Materials was supported by the U.S. Department of Energy Office of Science under Contract No. DE-AC02-06CH11357.

10-ID-B • MR-CAT • Materials science, environmental science, chemistry • X-ray absorption fine structure, time-resolved x-ray absorption fine structure, micro x-ray absorption fine structure, microfluorescence (hard x-ray) • 4.3-27 keV, 4.3-32 keV, 15-90 keV • On-site • Accepting general users •

9-BM-B,C • XSD • Materials science, chemistry • X-ray absorption fine structure • 2.1-23 keV • On-site Accepting general users •

ORDER AND STRENGTH FROM DISORDER IN A SOLID-STATE MATERIAL

Disorder often starts out as order, but sometimes disorganization can be persuaded into a new sort of order. Solid-state crystalline structures such as fullerenes (C₆₀ molecules) are highly ordered at both the short-range and long-range scales, while amorphous and quasi-crystalline materials display lesser degrees of organization. What happens when different categories of these materials are blended together? A team of American and Chinese researchers working at two APS beamlines has discovered the first example of a hybrid crystalline-amorphous material at the atomic level, results that could have important implications for practical applications.

Working at the GSECARS 13-ID-C and HP-CAT 16-ID-B and 16-ID-D beamlines at the APS, the team synthesized a new material by compressing solvated fullerenes, in which the structure of the C₆₀ lattice is altered by the incorporation of “guest” molecules. Among other characteristics, this affects the vibrational properties and hence the infrared and Raman spectroscopic qualities of the C₆₀ molecules.

The experimenters, from the Carnegie Institution of Washington, Jilin University (China), the University of Nebraska, Argonne, Stanford University, and the SLAC National Accelerator Laboratory used C₆₀*m-xylene as a starting point, studying it on a diamond anvil cell (DAC) at pressures up to 60 GPa, with a variety of techniques including x-ray diffraction (XRD) at HP-CAT and GSECARS, Raman spectroscopy, infrared absorption spectroscopy, and inelastic x-ray scattering (IXS) at HP-CAT. Quantum molecular dynamics (QMD) simulations were also conducted to shed light on the high-pressure phase transformation of the material.

While XRD revealed a hexagonal, close-packed (hcp) structural periodicity in the long range that remains preserved even up to 60 GPa, the C₆₀*m-xylene showed other intriguing behaviors under high pressure. Raman spectroscopy of the original sample and samples after decompression from different pressures suggested that the C₆₀ cages began to collapse at about 32 GPa to form into ordered amorphous carbon clusters (OACCs, Fig. 1).

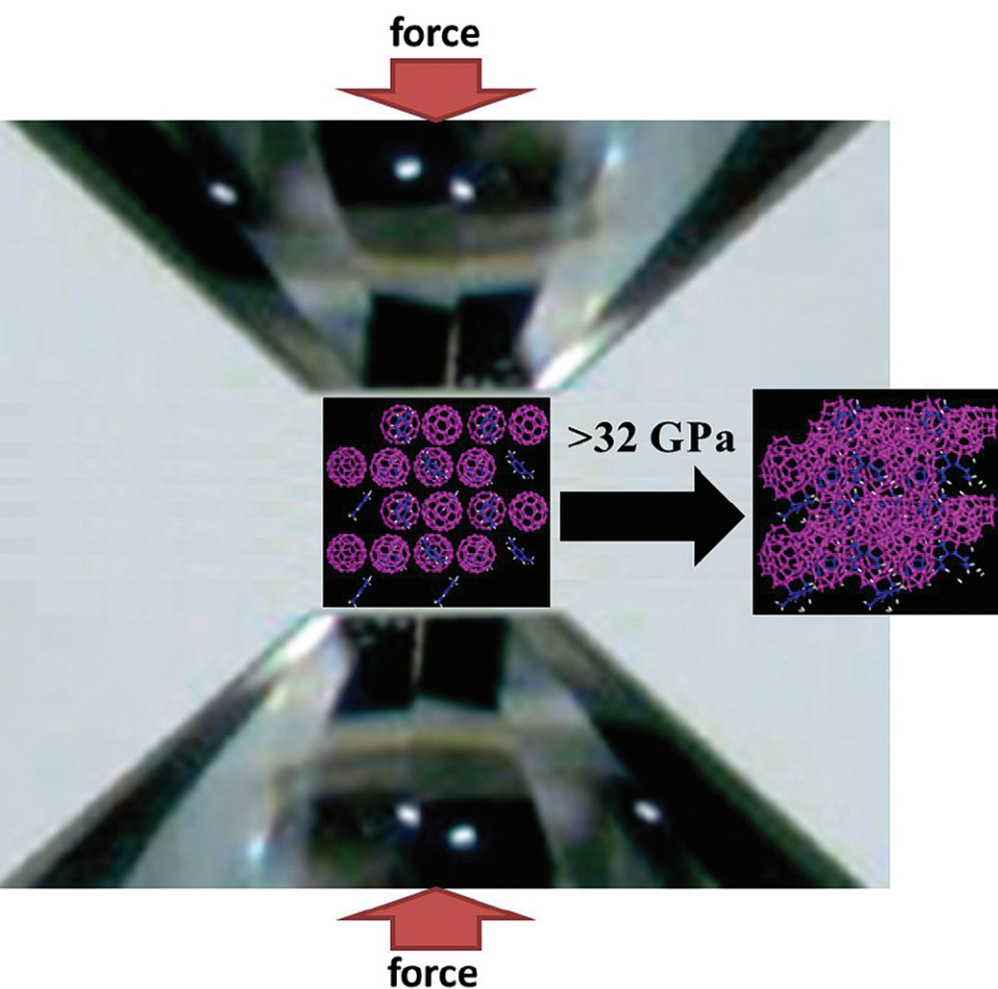


Fig. 1. Diagram of the synthesis of ordered amorphous carbon clusters at an extremely high pressure superimposed on a photo of a DAC.

Examination of vibrational modes indicated that even as the cages began to fragment, they still retained their pentagonal and hexagonal rings. The XRD and IXS studies revealed that most of the phase changes that occurred at high pressure remained even when the material was brought back to ambient pressure (Fig. 2).

The phase transition began to occur at about 32 GPa, as sp^2 hybrid C-C double bonds started to break and formed sp^3 hybrid C-C bonds. Some of the sp^3 bonds transformed back to sp^2 upon decompression, but most remained. Below 32 GPa, the process was elastic, and the deformed C60 cages returned to their normal shapes at ambient pressure. But above 32 GPa, the transformation into OACC was irreversible. Even with the collapse of the C60 cages, the C60 molecules were isolated from each other on the lattice sites by the solvent molecules, which maintained the long-range order.

The researchers confirmed the crucial role of the solvent molecules by evaporating them from the material with heat treatment, which caused the material to lose its long-range periodicity and become amorphous. Because the structure of solvated fullerenes is dependent upon the type of solvent, this finding suggests that it might be possible to synthesize different carbon materials with this same structure but different cluster sizes and packing symmetry.

The QMD simulations demonstrated that this behavior was not unique to this particular material. Examining a similar close-packed, face-centered-cubic system the simulations showed the phase transition above 30 GPa at which the bonds of the C60 cages began to break and the cages deform into ellipsoidal structures, followed by complete collapse and formation of OACCs at 32 GPa and above, all consistent with the experimental observations.

The OACC structure proved its ultra-incompressibility by actually creating ring crack indentations on the surface of the diamond anvils, a phenomenon previously only observed when one diamond anvil is pressed into another equally hard surface, such as another diamond anvil.

Such hardness, and the manner in which OACC maintains its other high-pressure structure and characteristics even after being returned to ambient pressures could have important implications for possible practical applications.

The team's discovery of the hybrid crystalline-amorphous OACC demonstrates that sometimes, blending different things together can create something more useful than either component on its own.

— Mark Wolverton

See: Lin Wang^{1,2*}, Bingbing Liu², Hui Li³, Wenge Yang¹, Yang Ding⁴, Stanislav V. Sinogeikin¹, Yue Meng¹, Zhenxian Liu¹, Xiao Cheng Zeng³, and Wendy L. Mao^{5,1}, "Long-Range Ordered Carbon Clusters: A Crystalline Material with Amorphous Building Blocks," *Science* **337**, 825 (17 August 2012).

DOI:10.1126/science.1220522

Author affiliations: ¹Carnegie Institution of Washington, ²Jilin University, ³University of Nebraska, ⁴Argonne National Laboratory, ⁵Stanford University, ⁶SLAC National Accelerator Laboratory

Correspondence: *lwang@ciw.edu

This work was supported as part of EFree, an Energy Frontier Research Center funded by the U.S. Department of Energy (DOE) Office of Science under DE-SC0001057. The use of HP-CAT is supported by the Carnegie Institute of Washington, the Carnegie DOE Alliance Center, the University of Nevada at Las Vegas, and Lawrence Livermore National Laboratory through funding from the DOE National Nuclear Security Administration, DOE Basic Energy Sciences, and the National Science Foundation. GSECARS is supported by the National Science Foundation - Earth Sciences (EAR-1128799) and Department of Energy - Geosciences (DE-FG02-

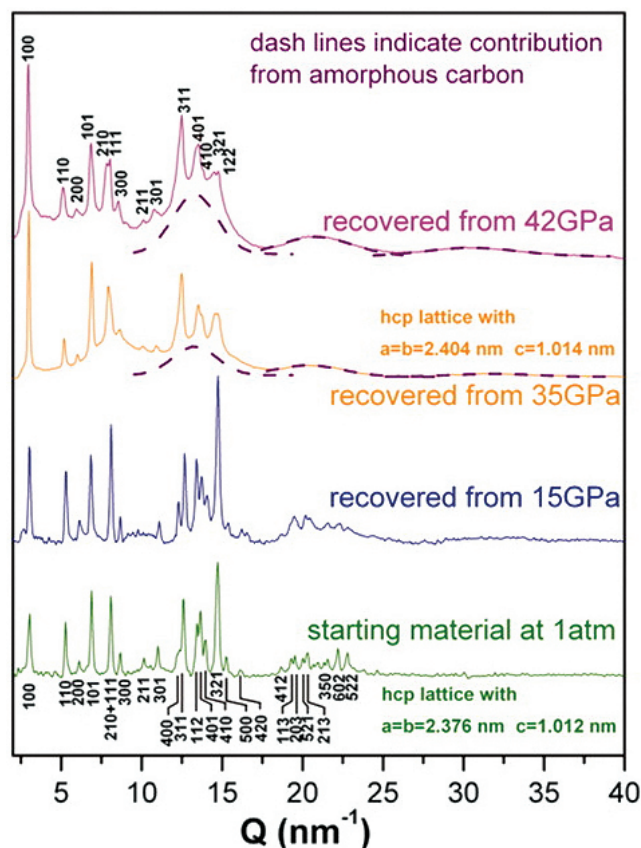


Fig. 2. XRD patterns of samples decompressed from different maximum pressures and the phase diagram at room temperature. The backgrounds were carefully subtracted during the measurement of the XRD patterns. There are several broad bands (indicated by the dashed lines) that represent the contributions from the amorphous carbon clusters and coexist with the sharp diffraction peaks from the hcp lattice. From L. Wang et al., *Science* **337** (2012). © 2012 American Association for the Advancement of Science.

94ER14466). Use of the Advanced Photon Source at Argonne National Laboratory was supported by the U.S. DOE Office of Science under Contract No. DE-AC02-06CH11357.

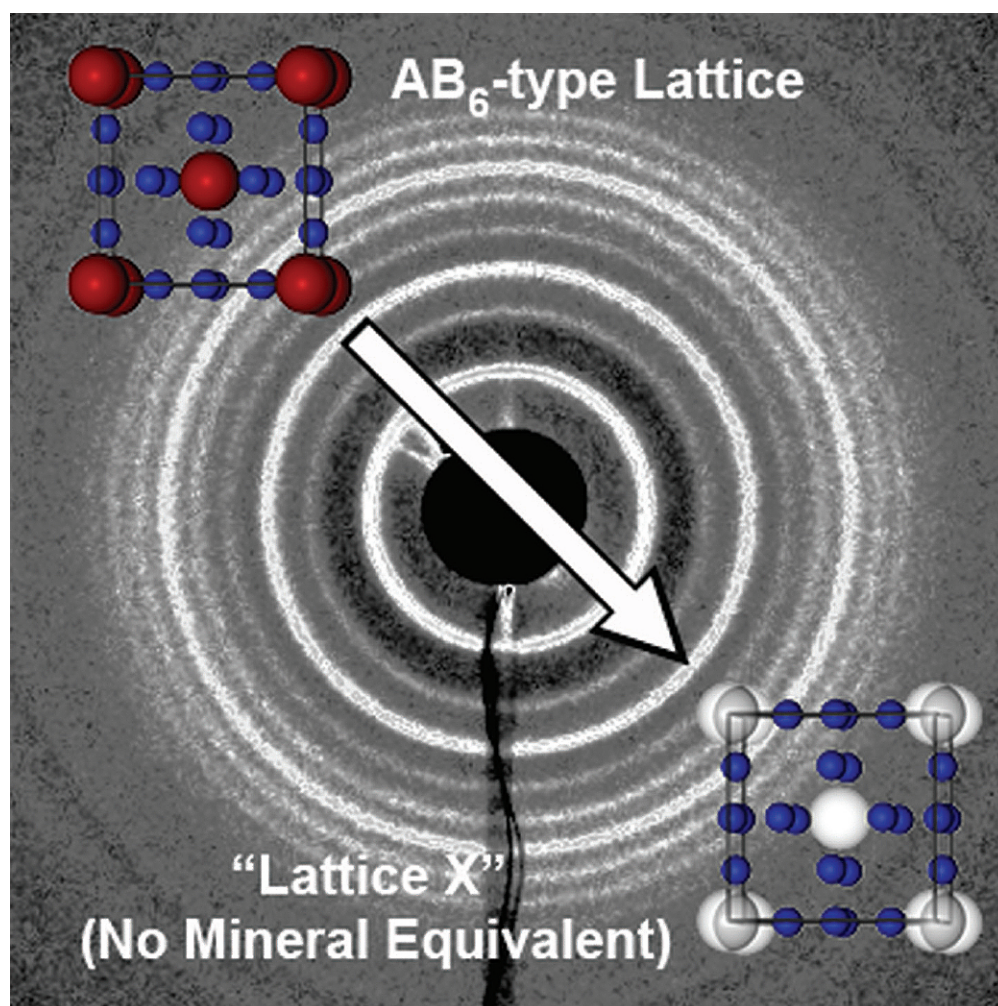
13-ID-C,D • GSECARS • Geoscience, environmental science • Inelastic x-ray scattering, small x-ray absorption fine structure, microdiffraction, x-ray absorption fine structure, microfluorescence (hard x-ray), high-pressure diamond anvil cell, high-pressure multi-anvil press • 4-45 keV • On-site • Accepting general users •

16-ID-B • HP-CAT • Materials science, geoscience, chemistry, physics • Microdiffraction • single-crystal diffraction, high-pressure diamond anvil cell • 24-35 keV • On-site • Accepting general users •

16-ID-D • HP-CAT • Materials science, geoscience, chemistry, physics • Nuclear resonant scattering, inelastic x-ray scattering (1-eV resolution), x-ray raman scattering, x-ray emission spectroscopy, high-pressure diamond anvil cell • 6-25 keV, 14.41-14.42 keV • On-site • Accepting general users •

CREATING NOVEL SUPERLATTICE SYMMETRIES USING HOLLOW DNA SPACERS

Scientists have synthesized a spherical nanoparticle superlattice resembling graphite and have also created a new superlattice nanostructure unlike any crystalline material ever assembled in nature or in the lab. These are among five lattice symmetries achieved using a novel approach incorporating hollow particles, or spacers, composed almost entirely of DNA to replace inorganic gold nanoparticles inside spherical nucleic acids (SNAs). These particles, despite consisting solely of crosslinked DNA, were found to behave much like crystalline nanoparticles with an inorganic gold core and have great promise for applications from gene regulation to approaches to cancer therapy, with clinical trials of therapeutic uses of SNAs under way. The structure of the nanoscale superlattices was characterized using small-angle x-ray scattering (SAXS) at the DND-CAT 5-ID-B,C,D beamline at the APS.



In the simplest structure synthesized in the study, a team of researchers from Northwestern University modified a precursor lattice with a body-centered cubic (bcc) arrangement consisting of SNAs bound to gold nanoparticles (SNA-AuNP). They achieved this by replacing the center particle of the unit cell with a hollow spacer to yield a simple cubic lattice. The SNA-AuNPs and spacer particles were mixed in a 1:1 ratio, and the amorphous aggregates were then annealed to just below their melting point, the temperature at which the aggregate dissociates into free particles. This process resulted in the formation of an ordered, lattice structure. The SAXS data showed that the hollow spacer occupied the center of a simple cubic lattice.

Unlike previous synthesis strategies involving electrostatic or hydrogen-bonding interactions, with the hollow-spacer approach it is possible to manipulate the length of the DNA linker and the size of the nanoparticles in structures while maintaining the original lattice shape.

Synthesized lattices with hollow SNAs were found to behave much like SNA-AuNPs in many respects, including their ability to self-assemble through cooperative binding.

The Northwestern University researchers also used the spacer approach to assemble more complex crystalline lattices, types AB₂ and AB₆, isostructural with AlB₂ and Cs₆C₆₀, respectively. SAXS data confirmed the synthesis of AB₂-type precursor lattices, which consisted of both A-type

< Fig. 1. Schematic of the precursor lattice of the AB₆ type with SNA-AuNPs (red spheres) superimposed on a SAXS image of lattice X with hollow SNA particles (white spheres) replacing the gold nanoparticles in the precursor lattice.

and B-type gold nanoparticles.

However, when the A-type particle was replaced with a hollow spacer, a simple hexagonal lattice was formed, as predicted. Similarly, the team showed that when hollow SNAs replaced the B-type particles, a structure similar to graphite was detected. This is the first time such a structure has been achieved by any nanoparticle assembly method.

With the AB₆ precursor, when the B-type particles were replaced with hollow spacers, an entirely new structure undocumented in synthetic or natural materials was formed, called lattice X by the researchers (Fig. 1).

In order to visualize the structure of the superlattices, the team used transmission electron microscopy (TEM) to produce “snapshots” of slices of crystals embedded in a polymer resin. The TEM images of the AB₆-type superlattices showed that the hollow spacers were not perturbed during this process, but instead remained surprisingly stable. Additionally, the team used electron tomography to generate a three-dimensional lattice reconstruction of a bcc superlattice.

The synthesis of novel, programmable superlattice structures using hollow DNA spacers represents a significant contribution to the emerging area of SNA research, a field which was pioneered by members of this research team. SNAs, with their unique biological, chemical, and physical properties are showing great promise for applications in gene regulation and nanotherapeutic uses that may yield new approaches to cancer therapy. Indeed, clinical trials of therapeutic uses of SNAs are already under way.

With this recent work in materials science, the research team has demonstrated that it is possible to exert great control over the different crystal structures that can be synthesized with

nanoparticles, and they have also created crystal structures with no mineral equivalent. — *Elise LeQuire*

See: Evelyn Auyeung*, Joshua I. Cutler, Robert J. Macfarlane, Matthew R. Jones, Jinsong Wu, George Liu, Ke Zhang, Kyle D. Osberg, and Chad A. Mirkin**, “Synthetically programmable nanoparticle superlattices using a hollow three-dimensional spacer approach,” *Nat. Nano.* **7**, 24 (January 2010).

DOI:10.1038/NNANO.2011.222

Author affiliation:

Northwestern University

Correspondence:

*evelyn.auyeung@u.northwestern.edu

**chadnano@northwestern.edu

C.A.M. acknowledges support for the Northwestern Nonequilibrium Energy Research Center from the U.S. Department of Energy (DOE) (DE-SC0000989) as well as support from the Air Force Office of Scientific Research and the Department of Defense (for a National Security Science and Engineering Faculty Fellowship). E.A. acknowledges a Graduate Research Fellowship from the National Defense Science and Engineering Graduate Fellowship. E.A., R.J.M., M.R.J., and K.D.O. acknowledge Ryan Fellowships from Northwestern University. M.R.J. and K.D.O. acknowledge Graduate Research Fellowships from the National Science Foundation. DND-CAT is supported by E.I. DuPont de Nemours & Co., The Dow Chemical Company, and Northwestern University. Use of the Advanced Photon Source at Argonne National Laboratory was supported by the DOE Office of Science under Contract No. DE-AC02-06CH11357.

5-ID-B,C,D • DND-CAT • Materials science, polymer science • Powder diffraction, x-ray standing waves, x-ray optics development/techniques, small-angle x-ray scattering, surface diffraction, x-ray reflectivity, wide-angle x-ray scattering • 5-20 keV • On-site • Accepting general users

SELF-ASSEMBLING NANOPORES FOR TRANSPORTING WATER AND IONS

Many living cells incorporate microscopic structures for expelling and replenishing water and other substances. For example, aquaporins are proteins that help regulate the movement of water across the membranes of animal, plant, and bacterial cells by forming transmembrane pores. Scientists have pursued various strategies to create artificial structures that mimic the basic transport properties of biological pores. One such strategy relies on creating self-assembling molecules that form nanoscale tubes, typically featuring pores with inner diameters less than 2 nm. Up until now, attempts to produce self-assembling nanotubes to efficiently conduct water and other substances have met with very limited success. However, researchers carrying out studies at the APS reported utilizing molecular rings to form tubes possessing sub-nanometer diameters that efficiently conduct ions and water across lipid (i.e., fat) membranes. Potential applications for these new nanotubes include water purification, and molecular sensing and separation.

The researchers, from Beijing Normal University (China); Shanghai Jiao Tong University (China); The University at Buffalo, The State University of New York; the Chinese Academy of Sciences; the University of Nebraska-Lincoln; and Argonne employed computer modeling to construct synthetic nanopores exhibiting optimal performance. X-ray diffraction (XRD) and other imaging techniques characterized the size, shape, and performance of the self-assembled nanotubes. The diffraction measurements were carried out at the XSD 2-ID-D beamline at the APS.

The type of molecular ring chosen to form the core of the nanotubes consisted of a rigid macrocycle. The term “cycle” refers to compounds consisting of atoms joined in a closed ring or loop; “macro” indicates larger cycles, typically those possessing 15 or more atoms. The top half of Fig. 1 shows the basic structure of the macrocyclic molecule used for this research. It consists of a large hydrocarbon molecule based upon the simpler benzene ring. The benzene molecule (C_6H_6) is a flat, rigid ring of six carbon atoms bonded to six peripheral hydrogen atoms. The macrocyclic molecule depicted in Fig. 1 acquires its rigidity from the benzene units connected via two triply-bonded carbon atoms. When these donut-like rings lie flat against one another, a type

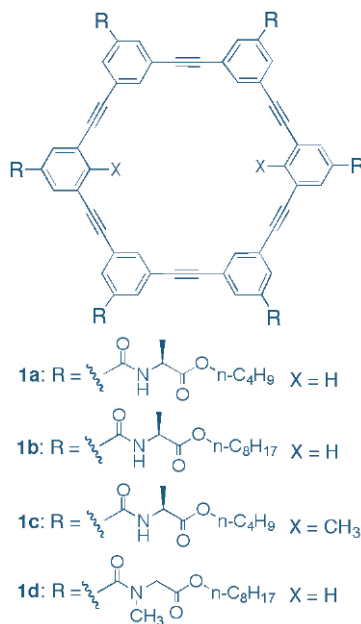


Fig. 1. Top portion depicts the chemical structure of the macrocycle used in this research; the six smaller hexagonal cycles are benzene rings. Side chains, denoted “R,” are attached to the macrocycle’s periphery. The inner “X” indicates either a hydrogen atom or a methyl radical. Lower portion: 1a through 1d indicate the specific chemical formula of each side chain, R, attached to the macrocycle’s periphery, as well as an attached interior hydrogen atom or methyl radical denoted X. By altering the functional groups attached to the inside or outside of the macrocycle (i.e., by changing R and/or X) the researchers could change the resulting nanotube properties.

of molecular bond arises called a π - π interaction, also known as π stacking.

Attached side chains (denoted R) encircle the macrocycle, producing highly directional hydrogen-bonding interactions that “tie up” the macrocycle’s benzene rings. The side chains are also classified as functional groups, because substituting different side chains changes the core macrocycle’s chemical functioning. Four distinct molecules, each consisting of a macrocycle and six attached molecular side chains, were synthesized and investigated. The four side chains are denoted 1a through 1d in Fig. 1.

Computer simulations were performed to theoretically confirm that particular macrocycle/side chain combinations would indeed self-assemble into stable nanotubes. The simulations indicated that hydrogen bonding of the side chains, and π stacking of the macrocycles, are both crucial to nanotube formation and stability. Figure 2 illustrates the core macrocycle and attached side chains, and reveals that the resulting nanotube forms a helical shape.

X-ray diffraction measurements at beamline 2-ID-D were made utilizing a solid sample featuring 1b nanotubes. From the XRD measurements, a nanocolumnar diameter of 34.2 Å (3.42 nm) was calculated. This width is only about 8% less than the actual 1b nan-

otube width. The slight difference between the expected and XRD-measured widths is most likely due to positioning of the side chains—for instance, the 1b side chains may not have fully extended from the macrocycle.

XRD measurements further revealed a strong diffraction peak indicative of π stacking associated with planar-stacked macrocycles. Analysis of the π stacking data indicated a long-range macrocycle ordering of approximately 23 to 26 nm, corresponding to a nanotube consisting of 65 to 73 stacked macrocycles.

Aggregations of both 1a and 1b nanotubes on a solid surface were investigated using scanning electron microscopy, transmission electron microscopy, and atomic force microscopy (AFM). Images derived from AFM revealed that the nanotubes assembled into long, closely-packed nanofilaments.

Fluorescence spectroscopy and other techniques determined the capacity of different nanotube types for transmembrane water and ion transport. In a solution containing hydrochloric acid (HCl), for instance, 1a nanotubes transported protons (H^+ , the nucleus of a hydrogen atom) through a membrane over 3000 times more efficiently than chloride ions. Transmembrane ion conductance was also observed for aqueous potassium chloride, but was absent for sodium chloride, thereby demonstrating that the nanotubes exhibit a considerable selectivity in ion transport. Additionally, it was found that 1a nanotubes — in spite of possessing hydrophobic interiors — performed transmembrane water transport at 22% the efficiency of the biologically-important protein aquaporin 1.

This investigation demonstrated that properly constructed macrocycles utilizing π stacking and side-chain hydrogen bonding can self-assemble into stable nanotubes capable of efficient transmembrane water transport and ion selection. Moreover, the macrocycles' interior and exterior functional groups can be synthetically changed to alter nanotube properties. Potential applications for these new nanotubes

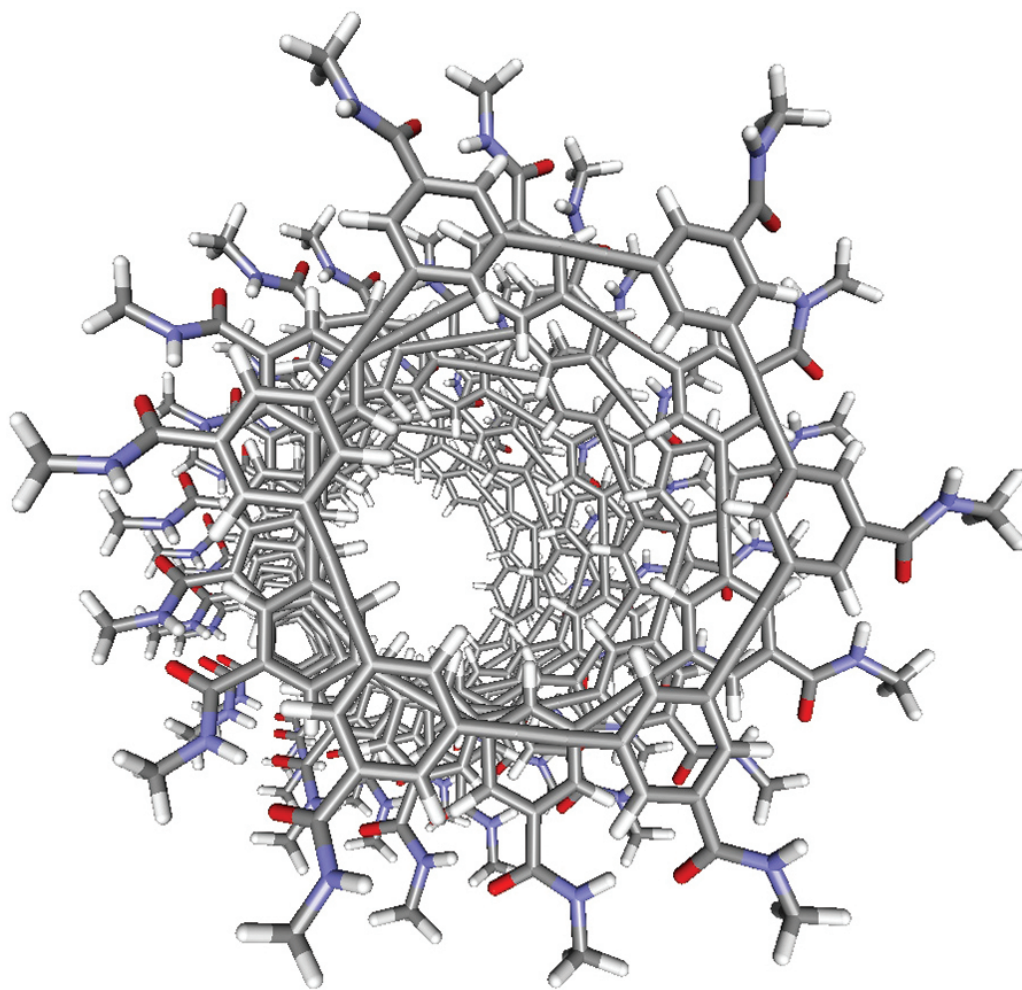


Fig. 2. A self-assembling nanopore consisting of rigid macrocyclic building blocks possessing a fixed, sub-nanometer diameter. The hydrophobic sub-nanometer pore has demonstrated the ability to selectively conduct metals ions and allow rapid passage of water molecules.

include water purification, and molecular sensing and separation.

— Philip Koth

See: Xibin Zhou¹, Guande Liu², Kazuhiro Yamato³, Yi Shen⁴, Ruixian Cheng¹, Xiaoxi Wei³, Wanli Bai¹, Yi Gao^{4,5}, Hui Li⁵, Yi Liu¹, Futao Liu¹, Daniel M. Czajkowsky⁴, Jingfang Wang², Michael J. Dabney³, Zhonghou Cai⁶, Jun Hu⁴, Frank V. Bright³, Lan He¹, Xiao Cheng Zeng⁵, Zhifeng Shao², and Bing Gong^{1,3*}, “Self-Assembling Subnanometer Pores with Unusual Mass-Transport Properties,” *Nat. Comm.* **3**, 949 (17 July 2012). DOI: 10.1038/ncomms1949

Author affiliations: ¹Beijing Normal University; ²Shanghai Jiao Tong University; ³University at Buffalo, The State University of New York; ⁴Chinese Academy of Sciences; ⁵University of Nebraska-Lincoln; ⁶Argonne National Laboratory

Correspondence: *bgong@buffalo.edu

This work was supported by the National Natural Science Foundation of China (91027020, 21072021), MOST (2007CB936000, 2010CB529205), RFDP (20070027038), KNDCDP (2009ZX09502008), STCSM (1052nm07700, 10PJ1405100), K.C. Wong Foundation (H.K.), the Changjiang Scholar Program, Beijing Municipal Commission of Education and FRFCU (2009SC-1), and the U.S. National Science Foundation (CBET-1036171 and CBET-1066947). Use of the Advanced Photon Source at Argonne National Laboratory was supported by the DOE Office of Science under Contract No. DE-AC02-06CH11357.

2-ID-D • XSD • Life sciences, materials science, environmental science • Microfluorescence (hard x-ray), microdiffraction, small x-ray absorption fine structure • 5-30 keV • On-site • Accepting general users

MEASURING HOW GOLD NANOPARTICLES STACK UP

Ordered arrangements of nanoparticles can be designed to have electronic, optical, or magnetic characteristics for many potential applications. If the nanoparticles themselves have shapes more complex than simple spheres, their characteristics can take on still greater variety. A team of scientists utilized XSD beamline 12-ID-C,D at the APS to show that triangular gold nanoparticles suspended as colloids in an ionic solution spontaneously assembled into stacks of a dozen or so, with spacing that could be controlled by chemical means. The “tunability” of the method has potential for making nanoarrays that can be assembled into materials capable of being configured to a range of desired properties.

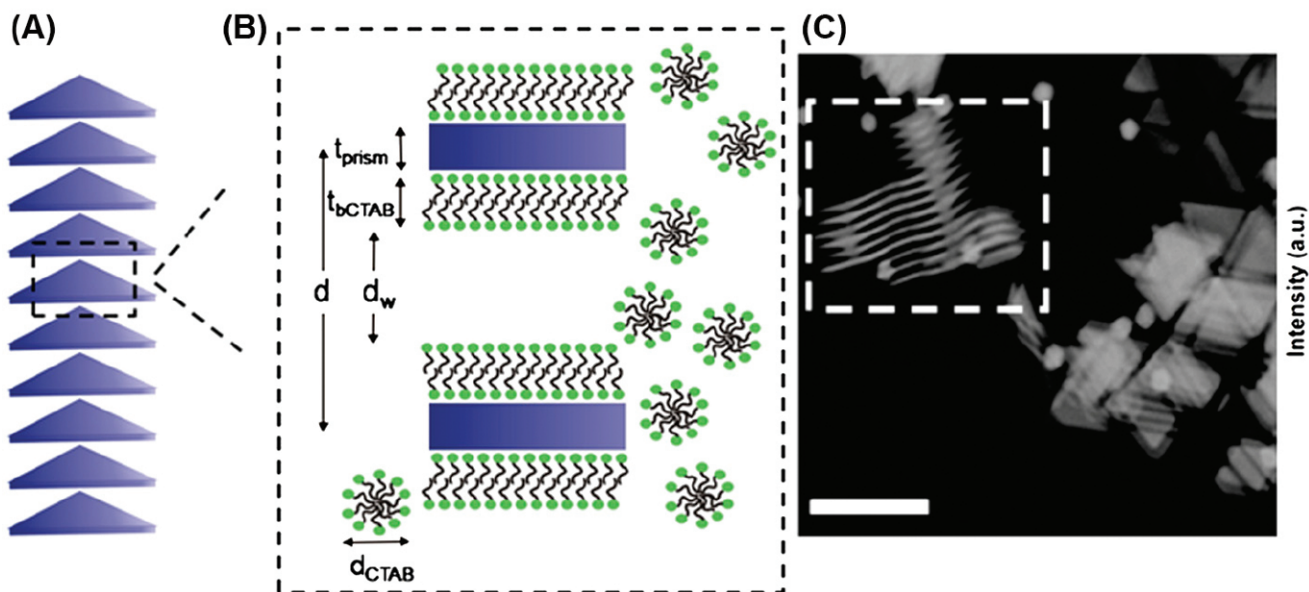
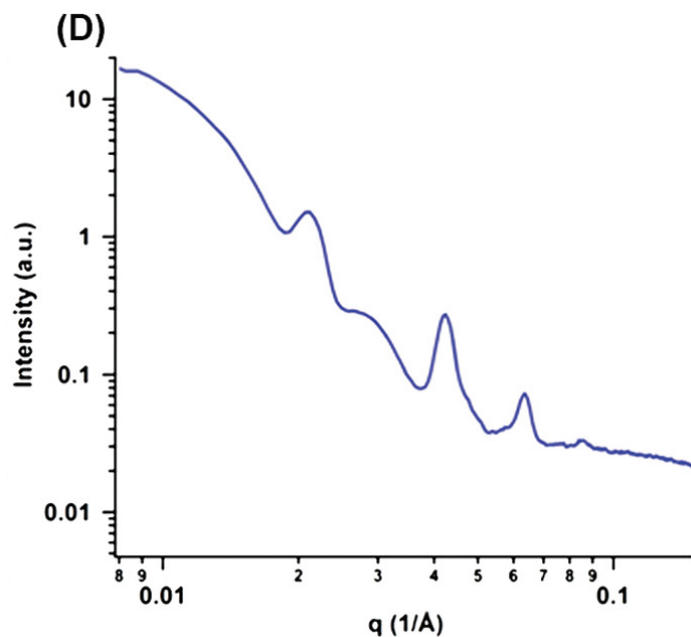


Fig. 1. Columnar superlattices of anisotropic gold nanoprisms. (A) Nanoprisms form 1-D lamellar crystals in solution with an average of 10–15 prisms per crystal. (B) A zoomed-in edge-on view of two nanoprisms within a lamellar superlattice where d is the d spacing, d_w is the water region, t_{prism} is the thickness of the nanoprism, t_{bCTAB} is the thickness of the CTAB bilayer, and d_{CTAB} is the diameter of the CTAB micelles. (C) Cryoscanning transmission electron microscopy image of the lamellar crystals. The outlined region highlights an edge-on view of the nanoprism crystals. (Scale bar: 200 nm.) (D, facing page) One-dimensional SAXS profile of the as-synthesized Au nanoprisms (145-nm edge length) in solution. The sharp diffraction peaks at $q = 0.021, 0.042, 0.063,$ and 0.084 1/\AA indicate a periodic lamellar structure. From K.L. Young et al., *Proc. Natl. Acad. Sci. USA* **109** (2012). ©2012 National Academy of Sciences

The researchers from Northwestern University, the Universidad Autonoma de Mexico, and Argonne grew gold nanoparticles in the shape of flat triangular tiles, or prisms, 7.5-nm thick and 145 nm on each side. The prisms were created in an aqueous solution of the surfactant molecule cetyltrimethylammonium bromide (CTAB), a negative ion. CTAB is a long molecule with one end hydrophilic with strongly polar groups that readily interact with water, and the other hydrophobic with little or no affinity for water. At sufficiently high concentrations, CTAB agglomerates into spherical micelles approximately 6

nm in diameter, with the hydrophobic tails forming a core and the hydrophilic group facing out toward the surrounding solvent. In addition, CTAB forms a bilayer on the surfaces of the gold prisms. The inner layer consists of CTAB molecules with their hydrophilic ends at the gold surface and the hydrophobic ends pointing outward; another CTAB layer with the opposite orientation covers this first layer.

Small-angle x ray scattering (SAXS) studies at beamline 12-ID-C,D revealed the presence of one-dimensional (1-D) arrays consisting of 10 to 15 gold prisms, their flat faces parallel



to each other and spaced about 30 nm apart. The prisms were far enough apart that micelles could have entered into the gaps between them. Further x-ray scattering studies at energies close to the absorption edges of gold and bromine showed that the micelles mostly stayed out of the prism arrays and could be detected only around them.

To explain the interactions between prisms and micelles, the group drew on arguments involving chemistry, electrostatics, and thermodynamics. Because the micelles are made of negative ions, they repel each

other and try to collectively stay as far apart as they can. But the gold prisms take up space that could otherwise be occupied by micelles, and they exclude more space when dispersed than when stacked well. The implication is that the micelles tend to squeeze the prisms as close together as possible — like stacks of poker chips — to create the maximum room for them.

But the prisms, by virtue of their CTAB coatings, also have a charge and repel each other. Moreover, the charges on both the micelles and the prisms mean that their effective sizes are larger than their physical dimensions. Putting all these elements together into a theoretical analysis that determines the optimum balance of the electrostatic repulsion between the prisms and the compressive force from the micelles, the scientists calculated that the equilibrium separation of the stacked prisms should be 28.8 nm, very close to the observed value.

Further verification of these arguments came from experiments in which the concentration of CTAB in solution was made higher, increasing the compressive force on the prisms and squeezing them closer together. In another test, adding sodium chloride changed the ionic balance of the solution, screening the charges on the prisms and reducing the electrostatic repulsion between them. As expected, the prisms moved closer together. Diluting the CTAB or NaCl concentration reversed these effects, so that the team could make the gold prisms assemble into arrays with chosen

parameters.

The ability to fine-tune the way the prisms self-assemble makes it possible to create arrays with reconfigurable characteristics. Using nanoparticles of different shapes would offer still greater scope for design variations.

— David Lindley

See: Kaylie L. Young¹, Matthew R. Jones¹, Jian Zhang¹, Robert J. Macfarlane¹, Raul Esquivel-Sirvent^{1,2}, Rikkert J. Nap¹, Jinsong Wu¹, George C. Schatz¹, Byeongdu Lee^{3*}, and Chad A. Mirkin^{1**}, "Assembly of reconfigurable one-dimensional colloidal superlattices due to a synergy of fundamental nanoscale forces" *Proc. Natl. Acad. Sci. USA* **109**, 2240 (2012).

Author affiliations: ¹Northwestern University, ²Universidad Nacional Autonoma de Mexico, ³Argonne National Laboratory

Correspondence:

**chadnano@northwestern.edu,
*blee@aps.anl.gov

C.A.M and G.C.S. acknowledge the Department of Energy (DOE Award DE-SC0000989) for support through the Northwestern University Nonequilibrium Energy Research Center. C.A.M. is also grateful for a National Security Science and Engineering Faculty Fellowship from the Department of Defense. K.L.Y. acknowledges the National Science Foundation and the National Defense Science and Engineering Graduate Research Fellowships. M.R.J. and R.J.M. acknowledge Northwestern University for Ryan Fellowships. R.E.-S. acknowledges Dirección General Asuntos del Personal Académico-Universidad Nacional Autónoma de México, Consejo Nacional de Ciencia y Tecnología Project 82474. Use of the Advanced Photon Source at Argonne National Laboratory was supported by the U.S. DOE Office of Science under Contract No. DE-AC02-06CH11357.

12-ID-C,D • XSD • Chemistry, physics, materials science • Small-angle x-ray scattering, grazing incidence small-angle scattering, wide-angle x-ray scattering, surface diffraction • 4.5-36 keV • On-site • Accepting general users •

CREATING ROBUST NANOPOROUS MATERIALS VIA CONTROLLED POLYMERIZATION

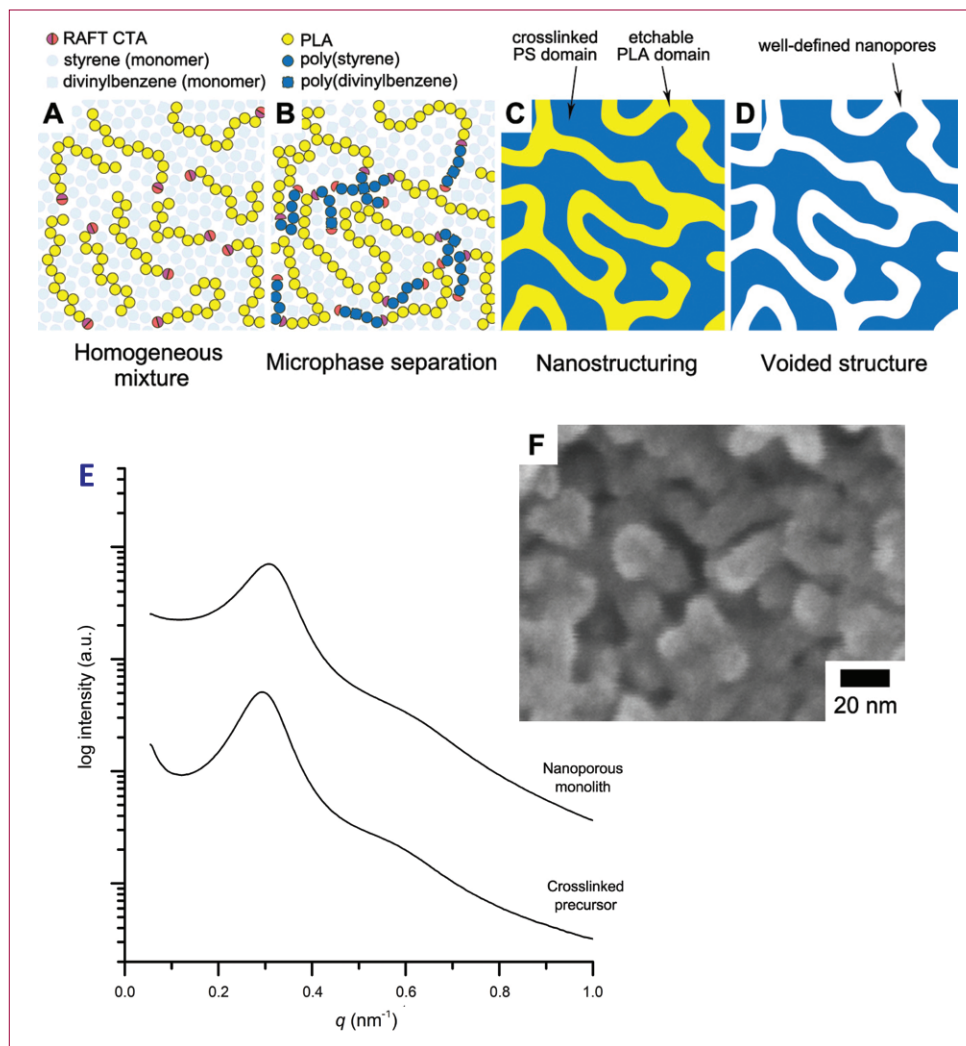


Fig. 1. (A–D) Schematic depiction of nanoporous monolith generation by a controlled polymerization-induced microphase separation process. (A) A macro-CTA consisting of an etchable polymer (yellow) dissolves in the mixture (light blue) of a monomer and a cross-linker. (B) The controlled growth of chains (dark blue) of a monomer and a cross-linker generates a block polymer structure. (C) Microphase separation occurs over a small time interval, creating a nanostructure with a cross-linked polystyrene domain (blue) and a chemically etchable polymer domain (yellow). (D) Removal of the etchable polymer produces well defined, percolating nanopores (white) in a cross-linked and mechanically robust matrix (blue). (E) Representative SAXS profiles of the crosslinked precursor (depicted in C) and the nanoporous monolith (depicted in D). (F) A representative scanning electron microscope image of the nanoporous monolith. The image was taken after ca. 1 nm of Pt coating.

Polystyrene foam, one of many forms of polymers, is well suited for one-time use as a cup to keep a drink hot or cold. It is, however, quite brittle, and it cannot be exposed to high temperatures for long before it begins to melt. In the realm of nanoporous polymer materials, similar limitations — thermal instability and lack of mechanical strength — have presented challenges in broadening the useful applications of these materials. Based in part on small-angle x-ray scattering (SAXS) analysis of the nanoscale structure of specimens performed at the DND-CAT beamline 5-ID-B,C,D at the APS, researchers from the University of Minnesota have devised a new strategy for creating more-robust nanoporous polymers derived from a cross-linked and microphase-separated block polymer precursor. Growth of a block polymer and cross-linking-induced microphase separation and arrested the emerging structure, resulting in a bicontinuous structure that can readily be converted into a nanoporous form with potential for applications in wide-ranging areas including drug delivery systems, catalysis, and environmental remediation.

Mesoporous materials with pore sizes in the 2-50-nm range are already proving useful in many advanced applications. Nanoporous materials with a bicontinuous structure comprising a rigid framework and a porous space can be fabricated from metals, ceramics, or polymers. Nanoporous polymers are attracting increased attention because their pore size and structure, and their mechanical and chemical properties, can be finely tailored. Especially, utilization of microphase separation of block polymers possessing etchable blocks provides fascinating opportunities to generate well-defined nanoporous polymers. But progress in fabricating useful, tunable, and mechanically robust nanoporous polymers has been slowed by the difficulty of achieving this structure in a simple process, the demand for ever-smaller pore diameters, and the typically poor mechanical properties of the final nanoporous polymer.

The researchers tackled this problem by cross-linking the block polymer precursor during synthesis. They conducted controlled copolymerization of styrene and divinylbenzene (DVB) in the presence of a chemically etchable polylactide (PLA) attached to a chain transfer agent (PLA-CTA). As polymerization proceeded over time, polystyrene grew from the end of the PLA to generate a PLA-polystyrene block polymer *in situ*. At one point during the polymerization, they became incompatible, resulting in microphase separation into two distinct domains: a polystyrene domain — the framework of the mate-

rial — and a chemically etchable PLA domain. At the same time, copolymerization with DVB promoted cross-linking of the polystyrene domain and arrested the emerging bicontinuous morphology. Then PLA was removed by immersion in a caustic solution of sodium hydroxide in methanol and water, leaving nanoscale voids throughout the samples. Dramatic increases in SAXS intensity after removal of the PLA, compared with the precursor specimen, confirmed the nanoporous structure of the material.

Scanning electron microscopy (SEM) images showed that pore diameters within the structure can be controlled by manipulating the molar mass of the PLA-CTA. Molar masses of the PLA-CTA samples were 11, 22, and 41 kg mol⁻¹ (PLA-CTA-11, PLA-CTA-22, and PLA-CTA 41). Nitrogen sorption experiments indicated pore diameters as small as 4 nm were achieved using monoliths prepared with PLA-CTA-11, and 8 nm when prepared using PLA-CTA-41. According to a model for PLA-polystyrene, it may be possible to further reduce pore diameters to 2 nm.

SEM images of the PLA-CTA-22 sample showed even distribution of the continuous percolating nanopores, indicating a structure similar to inorganic materials with a bicontinuous structure produced by spinodal decomposition. One example is Vycor, a porous glass with high thermal stability.

SAXS data of these nanoporous polymers also shared characteristics with other materials formed by spinodal decomposition processes. This struc-

ture is expected to provide efficient transport through the porous space without dead ends. With higher thermal stability and greater mechanical robustness than those prepared with non-cross-linked polystyrene materials, these nanoporous polymers have promising applications in areas as diverse as drug delivery systems, catalysis, and environmental remediation. — *Elise LeQuire*

See: Myungeun Seo and Marc A. Hillmyer*, "Reticulated Nanoporous Polymers by Controlled Polymerization-Induced Microphase Separation," *Science* **336** 1422 (15 June 2012). DOI:10.1126/science.1221383

Author affiliation:

University of Minnesota

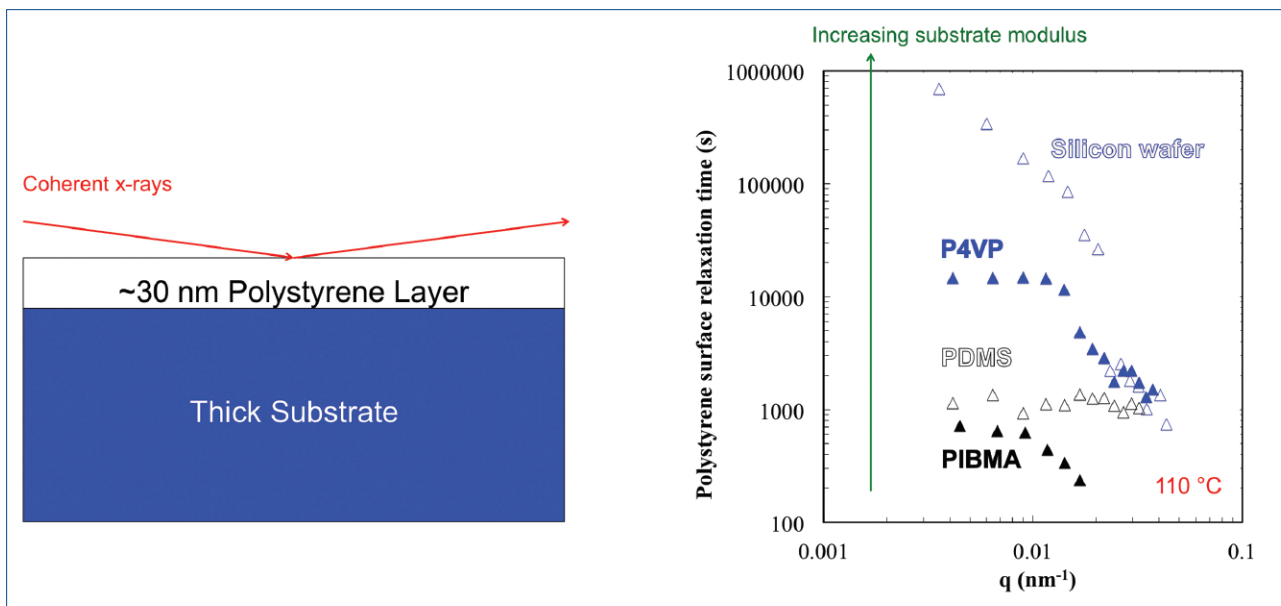
Correspondence: *hillmyer@umn.edu

The authors thank The Dow Chemical Company for financial support. Partial support for this work was also provided by the National Science Foundation (DMR-1006370). DND-CAT is supported by E. I. DuPont de Nemours & Co., The Dow Chemical Company, and Northwestern University. Use of the Advanced Photon Source at Argonne National Laboratory was supported by the U.S. Department of Energy Office of Science under Contract No. DE-AC02-06CH11357.

5-ID-B,C,D • DND-CAT • Materials science, polymer science • Powder diffraction, x-ray standing waves, x-ray optics development/techniques, small-angle x-ray scattering, surface diffraction, x-ray reflectivity, wide-angle x-ray scattering • 5-20 keV • On-site • Accepting general users

STIFFNESS AND THICKNESS IN NANOSCALE POLYMER FILMS AND SUBSTRATES

Nanoscale-thickness polymer films are suited to many applications such as fast-response microdevices, sensors, and microactuators. But maximizing their utilization means taking uncertainties out of the manufacturing process. Polymers, when positioned on top of various substrates, have exhibited major changes in their properties — depending on substrate stiffness and thin-film thickness — when compared with non-nanoscale (bulk) sizes. Past research utilizing a number of different techniques has produced conflicting results as to the interplay of polymer dynamics involving film and substrate. Much of the data produced by such investigations was based on bulk properties rather than those at the nanoscale level. Researchers working at XSD beamline 8-ID-I at the APS employed new experimental methods to better understand the importance of film thickness and substrate properties relating to film surface dynamics. Based on this research, companies that manufacture devices using nanoscale polymer films will know which films and substrates to use together for specialized applications, both those in use today and those being developed for the future.



The researchers in this study, from Northwestern University and Argonne utilized x-ray photon correlation spectroscopy (XPCS) at beamline 8-ID-I to study polystyrene (PS) because XPCS is an excellent method for examining surface and interface dynamics where the coherent x-rays probe only the approximately top 10 nm of a thin film. These coherent 7.35-keV x-rays were reflected off the surfaces of polystyrene films to measure thermally induced capillary waves that travel along the surface of such films and are affected by its surface tension and viscosity.

The researchers examined thin polystyrene layers — from 27 nm to 127 nm in thickness — held by silicon wafers and polymer substrates with varying elastic modulus (Fig. 1). Intensities and fluctuations of the capillary waves on the surface of the PS film were measured after being heated to a temperature above the polymer's glass transition temperature (T_g).

From their studies, the researchers found just how important thickness and stiffness of the polystyrene films are to the dynamics of relaxation times when polystyrene is confined to the nanoscale and when different substrates are used. In fact, they found that thickness and stiffness controlled the amount of capillary wave relaxation

< Fig. 1. Surface dynamics of thin, supported polystyrene films are investigated using x-ray photon correlation spectroscopy. Relaxation times for surface capillary waves are measured as a function of in-plane wavevector q , which is inversely proportional to the length scale being probed on the surface. When measured 10° C above the glass transition temperature (T_g) of PS, surface relaxation times vary by orders of magnitude depending on the modulus of the supporting substrate. These effects disappear if measurements are taken 40° C above T_g .

that occurs near the polystyrene T_g specifically, showing that lower substrate stiffness values led to faster polystyrene layer relaxations, and decreasing polystyrene layer thickness values resulted in increasing surface capillary wave relaxation times.

The researchers conclude that measurements at 10° C above the T_g of polystyrene show widely varying surface capillary wave relaxation times when thin polystyrene films are placed on substrates with elastic modulus values that range from about 1 MPa to over 100 GPa.

Further, the surface dynamics on the softer substrates are faster moving (they are less stiff, with shorter surface relaxation times) when compared to those on the harder ones, even for the films with thicknesses exceeding 100 nm. At such thickness levels, polystyrene did not display any T_g confinement effects but did show stiffness effects from substrate modulus.

The stiffness effect was much more noticeable when probing longer length scales on the surface and within 10° C of the polystyrene's T_g . However, the effect became much less obvious at shorter length scales and at 40° C above bulk T_g .

In addition, thinner, stiffer polystyrene films with longer surface wave relaxations times were found to be slower moving when compared to thicker films for a given substrate. The effects of substrate modulus and film thickness disappear when measurements are taken 40° C above the polystyrene T_g . This analysis of length scales and temperatures on polystyrene bilayers is important because both are impacted in very different manners when the film is confined to the nanoscale.

These studies reinforce the importance of substrate dynamics on sup-

ported thin films and emphasizes that the dynamics associated with substrate modulus and polystyrene layer thickness exerts a large influence on the surface wave relaxations of a thin top layer, even over thicknesses exceeding 100 nm. Consequently, the factors of modulus and thickness can be effectively applied when fine-tuning the dynamics of thin polymer layers, an ability that is very important when preparing to manufacture bilayer polymer films near the glass transition temperature. — *William A. Atkins*

See: Christopher M. Evans¹, Suresh Narayanan², Zhang Jiang², and John M. Torkelson^{1*}, "Modulus, Confinement, and Temperature Effects on Surface Capillary Wave Dynamics in Bilayer Polymer Films Near the Glass Transition," *Phys. Rev. Lett.* **109**, 038302 (2012).

Author affiliations: ¹Northwestern University, ²Argonne National Laboratory

Correspondence:

*j-torkelson@northwestern.edu

This work was supported by the National Science Foundation Materials Research Science and Engineering Centers Program (DMR-0520513), Northwestern University (C.M.E.), and 3M (C.M.E.). Use of the Advanced Photon Source at Argonne National Laboratory was supported by the U.S. Department of Energy Office of Science under Contract No. DE-AC02-06CH11357.

8-ID-I • XSD • Materials science, physics, polymer science • Intensity fluctuation spectroscopy, small-angle x-ray scattering, x-ray photon correlation spectroscopy • 6-12.5 keV, 7.35-7.35 keV, 7.35 keV • On-site • Accepting general users •

IMAGING STRESS, STRAIN, AND TENSION IN THE NANOWORLD

Nanowires are microscopic structures with lengths typically on the order of micrometers and thicknesses measured in nanometers. One class of nanowires consists of transition metals such as nickel (Ni). These tiny structures are increasingly drawing attention for potential use in a multitude of technological applications, including sensors, magnetic devices, and catalysts, but first we need an understanding of their detailed physical properties. To that end, scientists utilized x-ray beams from the APS to characterize and image Ni nanowires. The diffraction images revealed important nanoscale characteristics of the wires in three dimensions, including their internal strains and stresses. Their results provide an important first step toward utilizing Ni nanowires in new scientific and commercial applications.

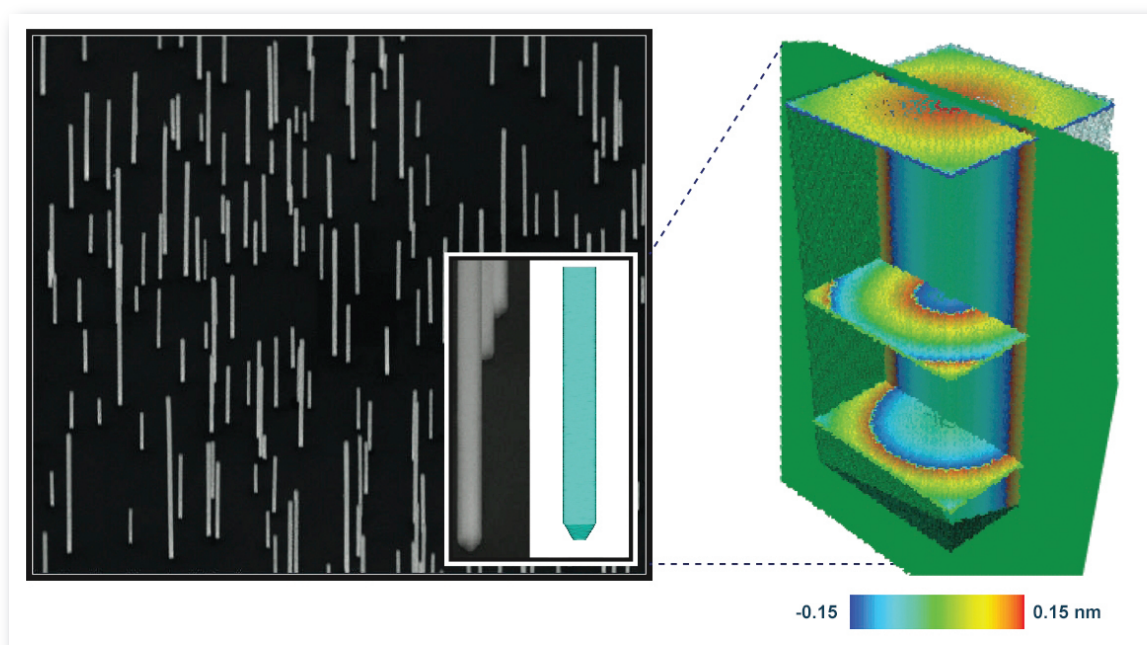


Fig. 1. The left side shows scanning electron micrographs of the sample revealing that the nanowires are well-oriented with smooth facets. The inset highlights the basal part of the nanowire exhibiting pronounced tapering features and orthogonal faceting. Right side of figure: Coherent x-ray diffraction datasets were used to reconstruct the shape and 3-D atomic displacement field (strain) within a single nickel nanowire.

One method of synthesizing nanowires involves chemical vapor deposition (CVD). The researchers in this study from the University of California, San Diego, and Argonne employed a high-temperature version of CVD (reaching 650° C) to grow nickel nanowires upon a thin layer of silicon oxide (SiO₂) that coated a silicon wafer. The size and distribution of the deposited nanowires were characterized using surface electron microscopy (SEM). Micrographs produced with SEM revealed vertical clusters of nickel nanowires populating the SiO₂ substrate, as shown in the left side of Fig. 1.

The nanowires stretched up to 5 μm in height, with widths varying from approximately 50 to 300 nm. SEM also indicated that the nickel nanowires possessed smooth facets along their lengths, were free of crystalline defects (such as lattice dislocations), and that each exhibited basal constriction, i.e., each nanowire was tapered near its base.

To obtain additional key information, the researchers carried out coherent x-ray diffraction (CXD) experiments at XSD beamline 34-ID-C of the APS. When properly reconstructed, the data derived using CXD yields highly detailed structural information (images) of nanostructures without destroying the sample. By sufficiently focusing and narrowing the synchrotron x-ray beam the research team was able to probe single nanowires.

To obtain three-dimensional (3-D) data for a particular nanowire, the sample was rotated tomographically in tiny increments of 0.005° through the Bragg condition. The diffracted x-rays were recorded at each increment by a detector. The individual diffraction measurements were later combined to form a 3-D x-ray diffraction dataset of nanowire structure. This dataset was then reconstructed using a computer algorithm to produce the color-coded representation of nanowire shape and strain shown in the right side of the figure.

Because there was no obstructing lens, and because x-rays are not affected by external magnetic and electric fields, this technique offers a promising way to see through the working devices encompassing tiny samples with atomic resolution.

Previous research had demonstrated that nanowires synthesized under conditions similar to those in this study contain small amounts of impurities concentrated near and on their surface. These surface impurities produce a distortion in the nanowire's crystalline lattice, which causes x-rays diffracting near the nanowire's surface to suffer a phase distortion. In contrast, x-rays diffracted from nearer the nanowire's center — where there are few impurities — do not suffer a phase distortion.

To account for this location-dependent diffraction difference, the researchers constructed a model in which the nanowire consists of two distinct regions: core and near-surface (or shell). The nanowire core was modeled as having a constant, homogeneous density, while the shell was considered to possess a varying, heterogeneous density. This core/shell idealization was crucial to successfully processing the CXD data to obtain 3-D information about nanowire structure.

The 3-D diffraction data showed that the nanowire core exhibited a compressive strain (i.e., an internal, inward force), which was greatest at its base. In contrast, the outer nanowire shell was characterized by a tensile stress, or dislocation, which manifested itself as a stretching apart of the crystalline lattice along the nanowire's length.

By probing nanowires of various sizes it was determined that for greater widths the tensile strain in the shell also increased until it reached a constant value (i.e., the tensile strain in the nanowire became directly proportional to its width). By contrast it was found that compressive strain in the nanowire core rapidly decreased with increasing nanowire width.

Concerning the basal taper present in the nanowires, the researchers posit that the taper forms as a consequence of the surface tensile strain opposing the internal compression at the nanowire's base.

The imaging techniques employed in this research demonstrate the capability of coherent x-ray diffraction utilizing synchrotron x-rays to non-destructively probe key properties of individual nanowires. The researchers were able to use their findings to calculate values for Young's Modulus, which is a standard measure indicating the stiffness of elastic materials. Determining nanowire properties such as internal stress, strain, and elasticity constitutes a crucial step in developing methods to tune such properties, with the ultimate goal of utilizing Ni nanowires in new scientific and commercial applications.

— Philip Koth

See: E. Fohtung^{1*}, J.W. Kim¹, Keith T. Chan¹, Ross Harder², Eric E. Fullerton¹, and O. G. Shpyrko¹, "Probing the Three-Dimensional Strain Inhomogeneity and Equilibrium Elastic Properties of Single Crystal Ni Nanowires," *Appl. Phys. Lett.* **101**(3), 033107 (2012).

DOI:10.1063/1.4737440.

Author affiliations: ¹University of California, San Diego; ²Argonne National Laboratory

Correspondence:

*efohtung@physics.ucsd.edu

E.F., J.W.K., and O.G.S. were supported by the U.S. Department of Energy (DOE) Office of Science, Basic Energy Sciences under Contract DE-SC0001805. K.T.C. and E.E.F. were supported by National Science Foundation Award DMR-0906957. Use of the Advanced Photon Source at Argonne National Laboratory was supported by the U.S. DOE Office of Science under Contract No. DE-AC02-06CH11357.

34-ID-C • XSD • Materials science, physics • Coherent x-ray scattering • 5-15 keV, 7-25 keV • On-site • Accepting general users •

AN EXPANDED SYNCHROTRON SCIENCE PROGRAM FOR EXEMPLARY STUDENTS



Above: Neuqua Valley High School students at GSECARS beamline 13-ID-E at the APS and (below) preparing samples under the guidance of GSECARS staff scientist Matt Newville (The Univ. of Chicago; second from left).



During the 2011-2012 school year the Exemplary Student Research Program spearheaded by the Argonne National Laboratory Education Division (CEPA-ED) brought three teams of high school students and teachers to Argonne where, working under the watchful eyes of APS resident users and Argonne Electron Microscopy Center staff scientists, the students gained hands-on experience in seeing a research project through from idea to reality.

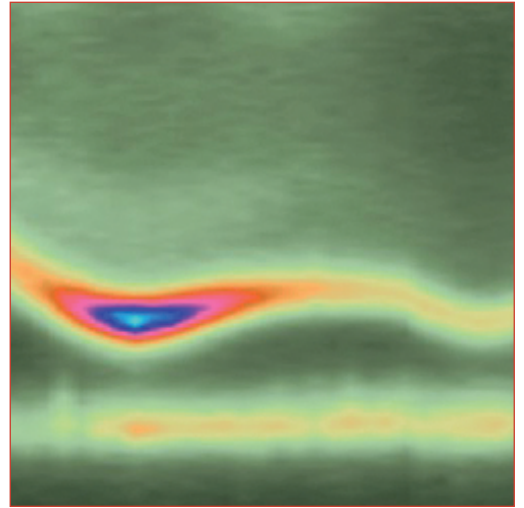
The program requires teams to “construct a doable project based on the techniques and limitations within a specific research group; prepare and submit a research proposal; setup the experiment; gather and analyze their results; make conclusions; and prepare a final poster.” The teams, from Naperville North High School and Neuqua Valley High School in Illinois, presented their posters at the May 2012 APS/CNM/EMC Users Meeting.

Building on that initial success, the program is being greatly expanded for 2013, providing a greater number of student teams with access to more APS user facilities.

Lou Harnisch of CEPA-ED, working with Susan Strasser and Connie Vanni of the APS User Office, has expanded the APS portion of the program from one sector (GSECARS at APS Sector 13) to five: GSECARS again, LS-CAT at Sector 21, NE-CAT at Sector 24, and XSD sectors 7 and 20. Students will have the opportunity to gain experience with a range of synchrotron x-ray research techniques including tomography, x-ray absorption fine structure, x-ray emission spectroscopy, microprobe mapping, protein crystallography, and elemental and structural studies.

The expanded program began with an intensive workshop in July 2012 for high school teachers who will serve as project mentors for STEM-, Honors-, or Advanced Placement-level student teams during the academic year, as well as for 1 or 2 students per teacher.

“We are delighted to be able to offer students and their teachers an opportunity to learn at our facility and we’re looking forward to seeing the next set of results,” said Brian Stephenson, Argonne Associate Laboratory Director for Photon Sciences and Director of the APS. “I especially want to thank the APS resident users and staff who are encouraging the next generation of synchrotron scientists by participating in the program.”



ATOMIC, MOLECULAR
&
OPTICAL PHYSICS

NEW PHYSICS IN IRIDIUM COMPOUNDS

Unraveling the complexities of spin-orbital coupling could someday lead to new high-temperature superconductors and workable quantum computers via an elusive phase of matter called a “quantum spin liquid.” Two groups of researchers utilizing two x-ray beamlines at the APS are delving into the new physics required to develop just such a material.

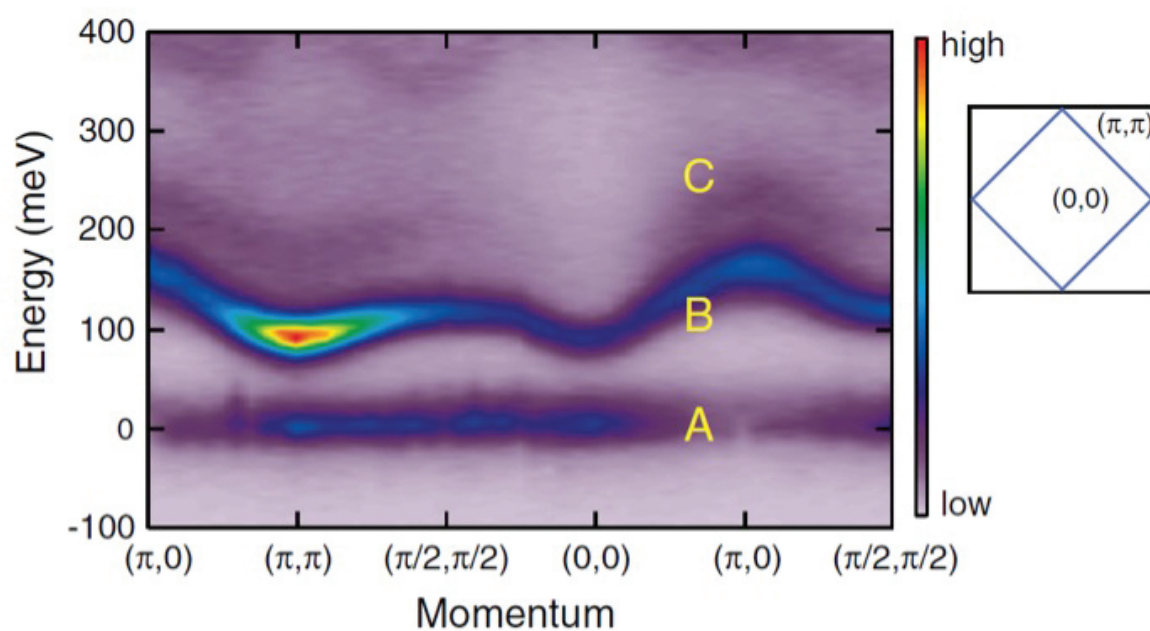


Fig. 1. An unprecedented “magnon gap” of $\text{Sr}_3\text{Ir}_2\text{O}_7$ was revealed by resonant inelastic x-ray scattering at the APS. This implies that dipolar interactions, analogous to classical bar magnets, are extremely strong in a composite spin-orbit coupled state and that these interactions control the behavior of magnetic moments at the quantum level. Three main features in the spectra (shown by yellow letters) are (A) elastic or quasielastic peaks near the zero energy, (B) an intense and dispersive band in the range 90–160 meV, and (C) a rather weak and broad feature above the dispersive band suggestive of two-magnon states.

The electrons that surround an atom’s nucleus usually possess independent degrees of freedom including orbital momentum and spin. But in certain circumstances, these two entangle, resulting in a composite state. Spin-orbital coupling is not a new phenomenon, but the way it alters the behavior of novel materials is not yet well-understood.

Because these materials have great fundamental and technological promise, deciphering the effects of spin-orbital coupling is a research priority. Iridates are being explored now because they are one of very few systems that have been predicted to behave as quantum spin liquids, and because tools were developed that can reliably study the spin-orbital coupling. One such tool is resonant inelastic x-ray scattering (RIXS), which is

available to users of the APS.

X-ray measurements of spin-orbit coupling in iridium oxide materials show exciting new results, which are the basis of two papers published back-to-back in *Physical Review Letters*. In one paper, a group composed of scientists from Brookhaven National Laboratory, Argonne, IFW Dresden (Germany), and the University of Kentucky used RIXS on XSD beamline 9-ID-B,C to study electronic excitations and deduce the wave function of the iridium electrons (Fig. 1). They reported that the model commonly used to describe electronic structure in iridium oxides is flawed.

The other paper, authored by a group including researchers from Argonne, IFW Dresden, and the Max Planck Institute for Solid State Research in Stuttgart reported finding novel magnetic behavior in a different iridium oxide compound.

The shape of the electron cloud surrounding an atom affects how that atom interacts with nearby atoms. This shape changes when the orbitals are entangled with spin. The researchers looked at the electronic structure of $\text{Sr}_3\text{CuIrO}_6$, a compound in which the iridium atoms are surrounded by oxygen atoms in a slightly distorted octahedron.

Such a system is typically modeled by assuming that the octahedron is perfectly regular and thus the orbital degree of freedom is being quenched in certain ways. If the shape is not perfect, then the layout of the electron cloud is deformed, but previous research groups have assumed that minor irregularities made little difference and could be ignored. In this case, the structure of $\text{Sr}_3\text{CuIrO}_6$ is close to the ideal.

When the Brookhaven-led group gathered data on the actual structure, they found that the irregularity makes a noticeable and important change to the wave function, which thus deforms the orbitals of the active electrons, as shown in the graphic. When the spin couples to the orbitals, the effect cannot be ignored. Although the fundamental physics for spin-orbit coupling is clear, this work suggests that the ideal case is not true in real materials.

The study allows researchers to

describe such systems more realistically by including distortion as a parameter in models. And, because the orbital shape determines how each electron interacts with its neighbors, this has important consequences on the magnetism in these solids.

The spin-orbital coupling in another iridate compound, $\text{Sr}_3\text{Ir}_2\text{O}_7$, results in a magnetic behavior not seen before. The research carried out by the Argonne-led team showed that the coupled states in this material behave — on an atomic scale — just like classically sized bar magnets, with two magnetic poles, although the mechanism from which it arises is different. Typical assumptions that charge interactions dominate over spin interactions are not correct in this case, in which the spin-orbit coupling is strong. This could be the basis for creating new materials.

This coupling between pairs of spins is extremely weak so there was no hope of seeing it with conventional materials. The group probed the material utilizing XSD beamline 30-ID-B,C at the APS.

Both groups investigated the spin-orbital coupling in their iridate compounds utilizing RIXS. In both cases, the novel behavior due to spin-orbital coupling could be observed clearly in the iridium compounds because iridium is a large atom and the effects of the coupling are larger than for smaller atoms, and also because RIXS can measure the subtle effects of spin-orbital coupling.

RIXS is similar to neutron scattering because both probe the dynamics in a system, but RIXS has the advantage that it couples to both the electron orbitals and spin. Neutron scattering doesn't "see" the charge part of the electrons.

While neutron scatterings is good for low energies, RIXS is appropriate for looking at the high energies of the electrons. The technique can also operate on very small amounts of material. — *Yvonne Carts-Powell*

See: X. Liu^{1*}, Vamshi M. Katukuri², L. Hozoi², Wei-Guo Yin¹, M.P.M. Dean¹, M.H. Upton³, Jung-ho Kim³, D. Casa³, A. Said³, T. Gog³, T.F. Qi⁴, G. Cao⁴, A.M. Tsvelik¹, Jeroen van den Brink², and J. P. Hill¹, "Testing the Validity of

the Strong Spin-Orbit-Coupling Limit for Octahedrally Coordinated Iridate Compounds in a Model System $\text{Sr}_3\text{CuIrO}_6$ " *Phys. Rev. Lett* **109**, 157401 (2012).

Author affiliations: ¹Brookhaven National Laboratory, ²IFW Dresden, ³Argonne National Laboratory, ⁴University of Kentucky
Correspondence: *xliu@bnl.gov

The work at Brookhaven was supported by the U. S. Department of Energy (DOE) Division of Materials Science, under Contract No. DE-AC02-98CH10886. The work at IFW Dresden was supported by the Computational Materials and Chemical Sciences Network program of the Division of Materials Science and Engineering, U. S. DOE through Grant No. DE-SC0007091. Use of the Advanced Photon Source was supported by the U. S. DOE Office of Science under Contract No. DE-AC02-06CH11357. T.F.Q and G.C. were supported by the National Science Foundation through Grant No. DMR-0856234.

See: Jung-ho Kim¹, A.H. Said¹, D. Casa¹, M.H. Upton¹, T. Gog¹, M. Daghofer², G. Jackeli³, J. van den Brink², G. Khaliullin³, and B.J. Kim^{2*}, "Large Spin-Wave Energy Gap for the Bilayer Iridate $\text{Sr}_3\text{Ir}_2\text{O}_7$: Evidence for Enhanced Dipole-like Interactions near the Mott Metal-Insulator Transition," *Phys. Rev. Lett* **109**, 157402 (2012).

Author affiliations: ¹Argonne National Laboratory, ²IFW Dresden, ³Max Planck Institute for Solid State Research
Correspondence: *bjkim@anl.gov

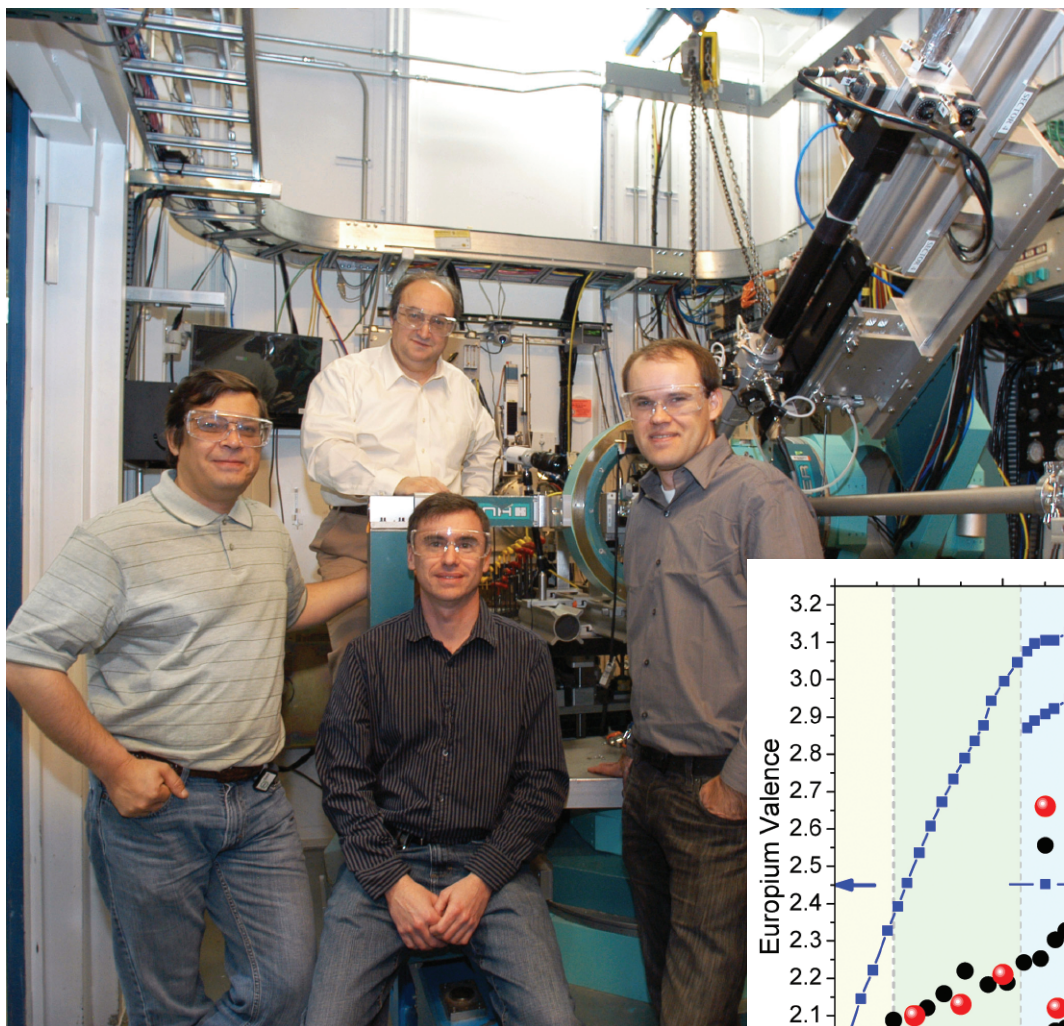
Work in the Materials Science Division and the use of the Advanced Photon Source at Argonne National Laboratory was supported by the U.S. DOE under Contract No. DE-AC02-06CH11357. G. . acknowledges support from GNSF/ST09-447. M.D. acknowledges support from the DFG (Emmy-Noether program).

9-ID-B,C • XSD • Physics, materials science
• Resonant inelastic x-ray scattering, inelastic x-ray scattering, liquid scattering • 4.5-24 keV
• On-site • Accepting general users

30-ID-B,C • XSD • Physics, materials science
• Inelastic x-ray scattering, resonant inelastic x-ray scattering • 5-14 keV, 5-30 keV, 23.7-23.9 keV • On-site • Accepting general users •

VALENCE-BOND-MODEL INADEQUACIES

Nature makes science fun by never failing to surprise. Just when scientists think they have a thing figured out, nature sends them scurrying to the whiteboard because of some unexpected result. The latest involves the so-called “bond-valence model,” which for years has been utilized to relate the number of nearest neighbors of the central atom of molecule or crystal (coordination number) and the interatomic distances between the atoms to the valence state. (Valence represents the number of bonds that an atom can form with one or more other atoms. The bond-valence sum rules provided an easy way to calculate valence from the coordination number and interatomic distances.) Research at several APS beamlines has shown that gaining valence information requires a lot more work when it comes to mixed-valence systems.



Researchers and co-authors Stas Sinogeikin, Daniel Haskel, Narcizo Souza-Neto (front), and (back) Ercan Alp in the experiment station at XSD beamline 4-ID-D, where the high-pressure x-ray absorption spectroscopy measurements were carried out. (Not pictured: co-authors Jiyong Zhao, Guoyin Shen, and G. Lapertot.)

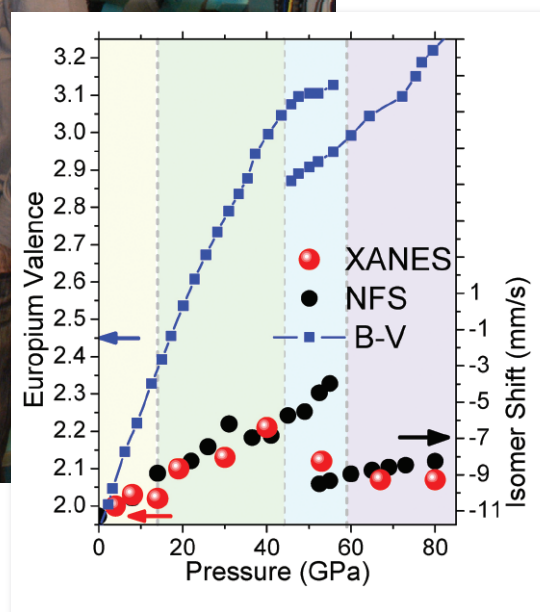


Fig. 1. Europium valence determined by XANES, NFS, and bond-valence (B-V) parameterization. XANES and NFS results are in good agreement but are at odds with the bond-valence parameterization method. Shading differentiates the four different valence regimes as described in the text.

The culprit that caused all this trouble was europium monoxide (EuO), which is known to be a bit unruly even under ideal circumstances. Under ambient conditions, EuO has the same crystal structure as common table salt, sodium chloride (NaCl), and, as with salt, the two atoms inside each molecule exist as positively and negatively charged ions.

The Eu ion usually has a +2 valence (Eu^{2+}) under ambient conditions, but the Eu^{+3} valence state is energetically close by, meaning that it wouldn't take much to induce a shift to the Eu^{+3} valence state. That's because Europium's valence state is not primarily due to the electrons occupying a single orbital level inside the atom, as is true of less obstreperous materials, but to the combined effect of electrons from different orbits. This is what makes EuO a mixed-valence system.

The scientists in this study loaded polycrystalline samples of EuO into a diamond anvil cell and performed x-ray diffraction (XRD) on HP-CAT beamline 16-BM-D, and x-ray absorption near-edge spectroscopy (XANES) and nuclear forward scattering (NFS) experiments under high pressure on XSD beamlines 4-ID-D and 3-ID-B,C,D, respectively. The XRD experiments allowed the scientists to determine how the EuO volume changed upon being squeezed by pressures as high as 92 GPa, which is more than 13 million pounds per square inch. The XANES measurements directly probed the electronic structure of EuO as a function of lattice contraction, thus providing valence information. The pressure dependence of Eu valence was verified using the NFS technique.

The XRD data indicated that the EuO volume decreased steadily with increasing pressure until a pressure of about 45 GPa was reached, where a sudden 7% volume collapse was seen. From there on, the volume decreased continuously once again.

Pressurizing a material usually causes a gradual decrease in volume, which tails off at high pressures because core electrons in atoms repel each other. Sudden volume changes, however, are rare and require a different explanation. The volume collapse was found to be due to a shift in crystal

structure from the NaCl structure to the cesium chloride (CsCl) structure, which has a higher coordination number and a longer bond length. This much was well known, leading people to speculate that the Eu^{2+} ions changed into Eu^{3+} ions at the same time.

The ionic size of Eu^{3+} is approximately 20% smaller than Eu^{2+} . Because the Eu^{3+} state is close to the Eu^{2+} state in energy, it has been assumed that the volume collapse is accompanied, and possibly driven, by a valence transition to the Eu^{3+} state. The research team found that this is not the case.

The researchers, from Argonne, the Brazilian Synchrotron Light Laboratory, the Carnegie Institution of Washington, and Commissariat à l'énergie atomique-CEA (France) discovered that europium ions remained in the Eu^{2+} state until a pressure of 14 GPa was reached. Between 14 and 44 GPa, the europium ions displayed a mixed-valence state composed of discrete and fluctuating Eu^{2+} and Eu^{3+} ions that were distributed homogeneously throughout. NaCl and CsCl structures coexisted from 44 GPa to 59 GPa, with the Europium ions in the CsCl structures displaying a nearly Eu^{2+} state. Above 59 GPa, the CsCl structure was seen throughout, with the europium ions being in the Eu^{2+} state.

The Eu ions initially moved toward a 3+ state as the pressure went up, but the volume collapse was accompanied by a decrease in valence and an increase in ion size, which the CsCl structure allowed, as it gives the Eu ions more room to expand, permitting them to revert to the 2+ valence.

The numerous facilities for high-pressure research at the APS allowed the team to obtain a picture of the electronic transition. As it turns out, the bond-valence model cannot deal with the fluctuating valence state observed up to 45 GPa, because the dynamics of this fluctuation are too fast for the lattice to respond, causing the relationship between valence and bond distance to break down.

Europium monoxide may not be found in the typical household today, but that could soon change. Because of its properties as a spin-polarized ferromagnetic semiconductor, much

research is being directed toward manufacturing EuO spintronic devices. Spintronics is the emerging technological field that has already given us high-capacity computer hard drives based on the giant magnetoresistance effect.

— Vic Comello

See: Narcizo M. Souza-Neto^{1,2,*}, Jiyong Zhao¹, Ercan E. Alp¹, Guoyin Shen³, Stas V. Sinogeikin³, G. Lapertot⁴, and Daniel Haskel^{1,**}, "Reentrant valence transition in EuO at high pressures: beyond the bond-valence model," *Phys. Rev. Lett.* **109**, 026403 (2012).

DOI:10.1103/PhysRevLett.109.026403
Author affiliations: ¹Argonne National Laboratory, ²Brazilian Synchrotron Light Laboratory, ³Carnegie Institution of Washington, ⁴CEA-France

Correspondence:

*narcizo.souza@lnls.br,

**haskel@aps.anl.gov

See also: *Science* magazine Editors' Choice, Physics, "Bond Valence Under Pressure," by Jelena Stajic.

Work at Argonne was supported by the U.S. Department of Energy (DOE) Office of Science under Contract No. DE-AC-02-06CH11357. HP-CAT is supported by the Carnegie Institution of Washington, the Carnegie DOE Alliance Center, the University of Nevada, Las Vegas, and Lawrence Livermore National Laboratory through funding from DOE-National Nuclear Security Administration, DOE-Basic Energy Sciences, and the National Science Foundation. Use of the Advanced Photon Source at Argonne National Laboratory was supported by the DOE Office of Science under Contract No. DE-AC02-06CH11357.

3-ID-B,C,D • XSD • Physics • Nuclear resonant scattering, inelastic x-ray scattering, high-pressure diamond anvil cell • 7-27 keV, 14.41-14.42 keV • On-site • Accepting general users •

4-ID-D • XSD • Physics, materials science • Anomalous and resonant scattering (hard x-ray), magnetic x-ray scattering, magnetic circular dichroism (x-ray magnetic circular dichroism, hard x-ray) • 2.7-40 keV • On-site • Accepting general users •

16-BM-D • HP-CAT • Materials science, geoscience, chemistry, physics • Powder angular dispersive x-ray diffraction, x-ray absorption near-edge structure, single-crystal diffraction, high-pressure diamond anvil cell • 6-70 keV • On-site • Accepting general users •

K-SHELL PHOTOIONIZATION OF XeF₂ YIELDS EVIDENCE OF INTERATOMIC COULOMBIC DECAY

The x-ray photoionization of a deep inner-shell electron in a heavy atom sets off a cascade of radiative and nonradiative transitions as the atom relaxes. If the cascade occurs in an atom that is part of a molecule, it can also lead to the removal of valence electrons on more than one atomic site, leaving the molecule with multiple positive charges whose mutual repulsion may break the molecule apart, an event called a Coulomb explosion. This type of molecular damage may prove useful in several application areas including the emerging technique of photon activation therapy, which generally uses a pharmaceutically inert agent that accumulates in the target cells and is activated using x-rays by irradiation of the target cells and surrounding tissue. In one version of this method, an iodinated compound is inserted into the DNA of a malignant tumor during cell replication and then irradiated with monochromatic x-rays, leading to selective local destruction of the cancerous tissue. Among the issues to be addressed before photon activation therapy can become a viable treatment option is the very basic question of the effect of a heavy atom's local environment on the final amount of ionization that photoionization of the atom produces. Researchers carrying out investigations at an APS beamline recently found evidence that challenges the commonly held belief that deep inner-shell photoionization produces the same final total charge whether a heavy atom is isolated, or part of a molecule or cluster.

The researchers from Argonne, the DESY Center for Free-Electron Laser Science (Germany), and the University of Hamburg (Germany) carried out both experimental and theoretical investigations of the relaxation mechanisms of atomic xenon (Xe) and xenon difluoride (XeF₂) following Xe *K*-shell photoionization, with XeF₂ serving to model the ionization and fragmentation of iodinated compounds. The researchers found that the fluorine atoms also participate in the decay cascade, increasing total charge production. They also discovered that fragmentation of the XeF₂ molecule begins during, not after, the decay process. The observed enhancement in total charge production was attributed to interatomic Coulombic decay-like (ICD-like) processes that involve decay channels that open only in the presence of neighboring atoms, producing higher charge states in a molecular environment than would be expected from an isolated atom. All of

the measurements were made at the XSD 7-ID-B,C,D beamline of the APS.

The choice of Xe and XeF₂ was motivated by the proximity of Xe to iodine in the periodic table and the fact that both heavy atom systems may be studied in the gas phase, making it possible to resolve the fragmentation channels and energies of the fragments in a way that would not be possible in a condensed-phase experiment. Effusive beams of Xe or XeF₂ were subjected to x-ray pulses, creating Xe *K*-shell vacancies that predominantly decayed via x-ray fluorescence, with the appearance of the *K* α fluorescent line serving as the start signal for coincidence measurements of ion creation using a multiple-hit ion time-of-flight (ITOF) spectrometer. The ions were accelerated electrostatically and detected in the ITOF spectrometer using a Z-stack microchannel-plate (MCP) detector (Fig. 1). Achieving a well-defined initial state meant using the APS bunch-timing signals to correct

for the slow rise time of the low-energy photon spectrometer that detected the *K* α fluorescent line, making it possible to identify in real time the particular 80-ps bunch that was associated with each event.

The multiple-hit ITOF spectrometer allowed the researchers to look at second and third hits, enabling the possibility of recording all three ion fragments of XeF₂. The XeF₂ data were taken with the beamline monochromator set near a pre-edge resonance associated with the excitation of a Xe 1s electron to the lowest unoccupied molecular orbital. Use of resonance excitation was important because resonant photoabsorption preferentially excites molecules whose internuclear axes are aligned with the x-ray polarization direction. The resultant on-resonance fluorine ion peaks showed distinct splittings into faster and slower components corresponding to ions ejected toward and away from the detector, respectively. This separation

between the backward- and forward-going ions provided a means to extract information about the breakup modes.

The ion spectra showed that charge on the Xe atom was redistributed to the F ligands and that there was a significant increase in the total charge produced following photoionization of XeF_2 compared to atomic Xe, indicating that some breakup modes produced more charge than the atomic Xe case (Fig. 2). The breakup kinetic energies of the F ions were determined from time-of-flight measurements of the faster and slower ions and compared with the Coulomb repulsion energies the ions would have, if they were formed instantaneously at the ground state Xe–F internuclear separation of 1.97 Å. The measured energies were found to be lower than the Coulomb energies, suggesting that the ions began moving away from their ground state positions before their charges were fully developed.

This circumstance was examined in more detail by simulating the decay cascade for atomic Xe after K-shell ionization using the XATOM code. The number of inner-valence and core holes in Xe was found to reach its final value after about 2 fs, causing the Xe atom to have an average charge of +4 to +5 at this time. Holes produced in the outer valence shell appeared later; two such holes were produced on average during the first 10 fs.

Although XeF_2 can be regarded as a model for iodinated compounds, such compounds would typically provide the iodine atoms with a larger number of neighbors, which could lead to even more pronounced breakup effects than reported in this study.

— Vic Comello

See: R.W. Dunford^{1*}, S.H. Southworth¹, D. Ray¹, E.P. Kanter¹, B. Krässig¹, L. Young¹, D.A. Arms¹, E.M. Dufresne¹, D.A. Walko¹, O. Vendrell², S.-K. Son², and R. Santra^{2,3}, “Evidence for interatomic Coulombic decay in Xe K-shell-vacancy decay of XeF_2 ,” *Phys. Rev. A* **86** (2012) 033401. DOI: 10.1103/PhysRevA.86.033401

Author affiliations: ¹Argonne National Laboratory, ²DESY Center for Free-Electron Laser Science, ³University of Hamburg

Correspondence: *dunford@anl.gov

This work was supported by the Chemical Sciences, Geosciences, and Biosciences Divisions of the U.S. Department of Energy (DOE). Use of the Advanced Photon Source at Argonne National Laboratory was supported by the DOE Office of Science under Contract No. DE-AC02-06CH11357.

7-ID-B,C,D • XSD • Materials science, atomic physics, chemistry • Time-resolved x-ray scattering, time-resolved x-ray absorption fine structure, phase contrast imaging • 6-21 keV • On-site • Accepting general users •

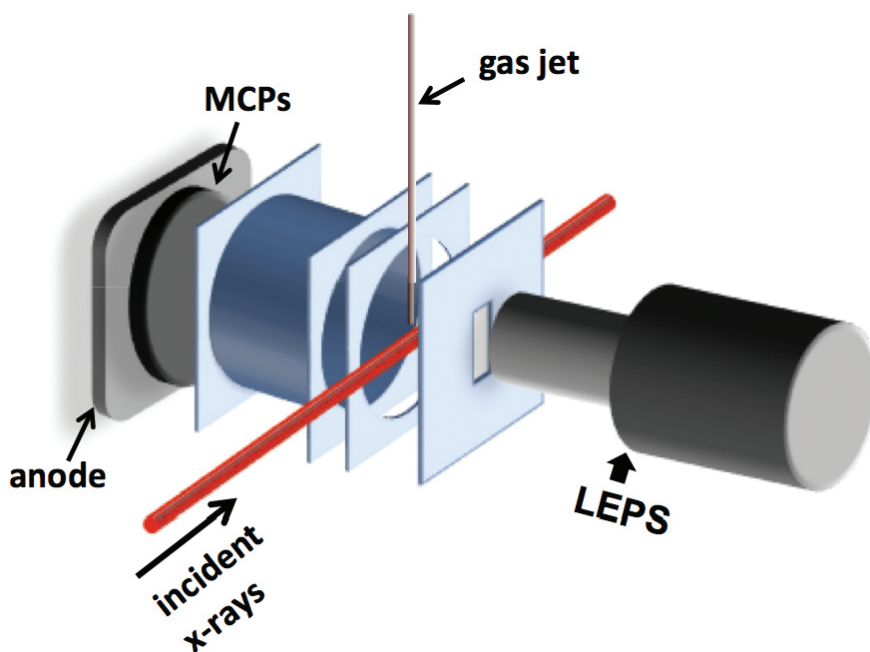


Fig. 1. The x-ray beam from the APS was crossed with effusive beams of Xe or XeF_2 . A germanium x-ray fluorescence spectrometer (LEPS) on one side of the interaction region measured x-rays from the target, while an ion time-of-flight (ITOF) spectrometer on the opposite side measured the charge-to-mass ratios of the ion fragments produced.

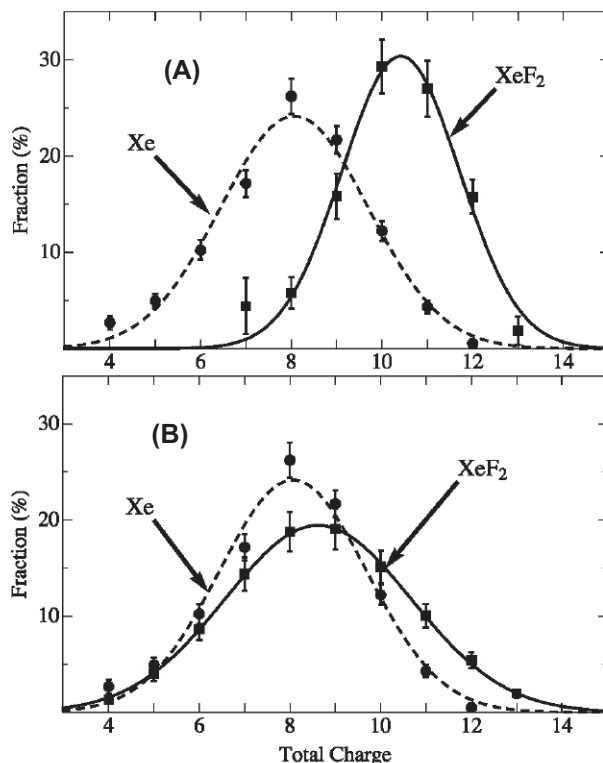


Fig. 2. Charge state distributions for XeF_2 (squares with solid curve) compared with Xe (circles with dashed curve) in coincidence with $K\alpha$ photons. (A) XeF_2 breakup pattern for the subset of events involving two fluorine ions in the final state with charge states F^{3+} and F^{2+} . Plotted is the fraction of events (in %) vs. the total charge (i.e., the Xe charge state plus 5). (B) The distribution of total charge averaged over all XeF_2 breakup modes.

THE INADEQUACIES OF SEVERAL THEORIES

Plутonium dioxide (PuO_2) has received intense interest in recent years owing to its use in mixed-oxide nuclear fuels and because of the theoretical challenges posed by its $5f$ electron states, which come from the presence of plutonium, arguably the most complex element known. Because of the difficulties in preparing and handling PuO_2 , much theoretical work has proceeded without rigorous experimental testing. In particular, the lattice vibrations of PuO_2 , which are critical for understanding phase stability and thermal transport, are known only through predictions made using theoretical approaches such as density functional theory (DFT), DFT plus the Hubbard U (DFT + U), and dynamical mean-field theory (DMFT), all of which are known to model the phonon behavior of PuO_2 in approximate fashion. Research at XSD beamline 30-ID-B,C at the APS measured the phonon density of states (DOS) of PuO_2 (+2% Ga), utilizing the high-resolution inelastic x-ray scattering (HERIX) instrument. The results provide critical guidance for improving theoretical models, and that adding new physics to the calculation (e.g., DFT to DFT+ U or DMFT) improves on the predictive capability of electronic structure theory when applied to the lattice vibrations.

The HERIX instrument is a high-energy-resolution (1.5-meV), four-circle diffractometer designed for making phonon measurements in solids and liquids, and has proven effective for measuring phonons in actinides. To obtain an accurate representation of the phonon DOS with a powder sample, the researchers from Lawrence Livermore National Laboratory, and Columbia University positioned nine equally spaced analyzers at overlapping angles to cover the complete range of momentum transfers.

At low energies, all three predictions match the measured transverse acoustic (TA) peak in the DOS fairly well. However, the longitudinal acoustic (LA) peak, measured at 22.8 meV, is significantly higher in energy than the 19.5-meV prediction obtained using DFT [1]. Including the Hubbard U (DFT + U) [2] in the calculation appears to correct for this shortcoming. The DMFT calculation [3] also correctly predicts the measured LA modes to about the same degree. In contrast, the DFT + U calculation places the small feature between the TA and LA peaks closer to the TA peak than actual measurement, which shows this feature to be about halfway between these peaks, as does the DFT calculation. Since the DMFT and DFT + U calculated dispersions

overlap in the acoustic region, it appears that DMFT also probably misplaces the feature between the main TA and LA peaks.

At midrange energies, the DFT calculation continues to underestimate the energies of the features by about 6 meV, while the DFT + U result accurately captures the two most significant optic mode features. The DMFT dispersion data clearly differ from the DFT + U result, but are too limited to pinpoint optic mode features of the phonon DOS in this range.

At the highest energies (>50 meV), little correspondence can be found between any of the measured and predicted features. A comparison of all of the results indicates that measurement reveals some expected splitting whose amount is overestimated by all of the calculations.

In the analysis of thermal conductivity, all three calculations agree with experiment regarding the TA mode. The LA mode, however, is not handled consistently by the calculations. Finally, although DFT and DFT + U obtain reasonably accurate predictions of the experimental heat capacity curve using quite different phonon DOS curves, their success does not translate to phase stability predictions where even small shifts in the phonon DOS pro-

duce vibrational entropy changes that can dramatically reshape phase diagram predictions. Therefore, there is a practical need to improve lattice vibration calculations to enhance their predictive capabilities with regard to phase stability and thermal transport in extreme environments not easily accessible by experiment.

Comparing the measured results with the three sets of theoretical predictions shows how adding new physics to the calculation (e.g., DFT to DFT + U or DMFT) improves on the predictive capability of electronic structure theory when applied to lattice vibrations, but also that further work is needed. Future calculations incorporating these advances will likely provide more reliable predictions of thermodynamic and transport properties of this important nuclear fuel material. — *Vic Comello*

See: M.E. Manley^{1†*}, J.R. Jeffries¹, A.H. Said², C.A. Marianetti³, H. Cynn¹, B.M. Leu², and M.A. Wall¹, "Measurement of the phonon density of states of PuO_2 (+2% Ga): A critical test of theory," *Phys. Rev. B* **85** (2012) 132301.

DOI:10.1103/PhysRevB.85.132301

Author affiliations: ¹Lawrence Livermore National Laboratory, ²Argonne National Laboratory, ³Columbia University.

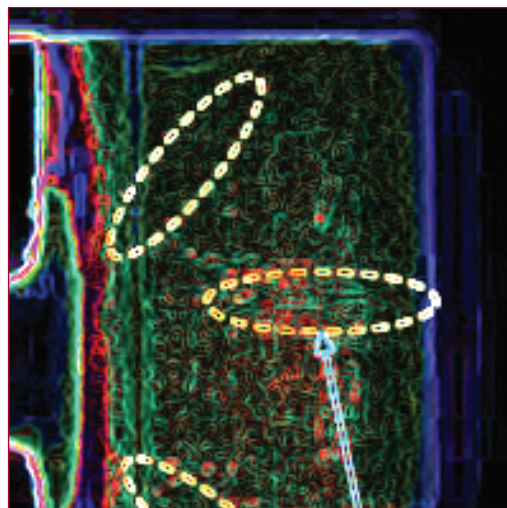
[†]Present address: Oak Ridge National Laboratory

Correspondence: *manley@ornl.gov

This work was performed under the auspices of the U.S. Department of Energy (DOE) by Lawrence Livermore National Laboratory under Contract No. DE-AC52-07NA27344. Use of the Advanced Photon Source at Argonne National Laboratory was supported by the DOE Office of Science under Contract No. DE-AC02-06CH11357. The construction of HERIX was partially supported by the National Science Foundation under Grant No. DMR-0115852. C.A.M. acknowledges funding from the Columbia RISE program.

REFERENCES

- [1] S. Minamoto, M. Kato, K. Konashi, and Y. Kawazoe, *J. Nucl. Mater.* **385** (2009) 18.
- [2] P. Zhang, B.-T. Wang, and X.-G. Zhao, *Phys. Rev. B* **82** (2010) 144110.



NOVEL X-RAY TECHNIQUES & INSTRUMENTATION

THREE-DIMENSIONAL NANOSCALE IMAGING FROM COHERENT X-RAY SURFACE SCATTERING

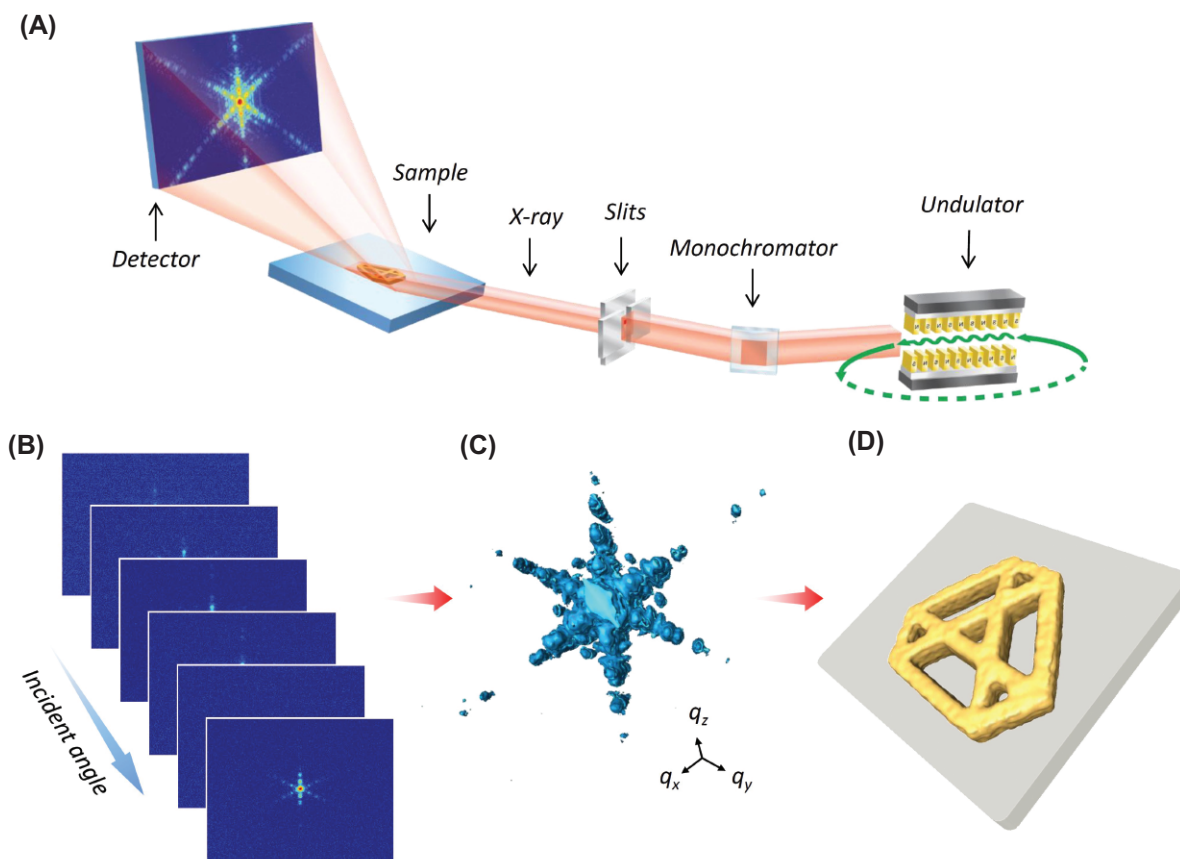


Fig. 1. (A) Schematic of experiment geometry of coherent surface scattering imaging; (B) A series of scattering patterns collected at different incident angles; (C) Iso-surface rendering of 3-d scattering intensity data; (D) three-dimensional reconstruction of the logo pattern.

Beginning slightly more than ten years ago, the development of methods to construct images of objects from the way they diffract a beam of coherent x-rays has offered a high-resolution means of investigating the structure of physical and biological materials. But the technique has mostly been used in transmission mode, limiting the kinds of objects that can be studied. Working at XSD beamline 8-ID-E, scientists have now demonstrated a form of coherent diffraction imaging based on reflection scattering of x-rays at grazing angles, enabling them to map out nanoscale surfaces in three dimensions, a technique that could lead to nanoscale imaging and even time-resolved growth studies in materials science and biology.

All surfaces have a critical angle of incidence, typically less than a degree in the hard x-ray regime, below which x-rays do not penetrate the material but instead undergo total external reflection. At incident angles just above the critical angle, scattering is still strong and also sensitive to the detailed near-surface structure of the material. A collaboration among Argonne scientists sought to make use of these phenomena in order to extend previous efforts to perform coherent diffraction imaging by reflection rather than transmission.

As a first demonstration, the team, working at the Argonne Center for Nanoscale Materials, created a simple test surface consisting of two gold stripes 1- μm wide, approximately 2- μm long, and 1- μm apart, on a silicon substrate.

Utilizing beamline 8-ID-E the team then recorded the diffraction pattern produced by a beam of 7.35-keV APS x-rays striking the surface parallel to the stripes at a grazing angle of 0.6°, near the critical angle for gold but above that of silicon. Theoretical calculation of the expected diffraction intensity profile — due mostly to scattering off gold, with a weaker contribution from silicon — showed excellent agreement with the results. More important, the team was able to use standard image reconstruction algorithms to reason backward from the diffraction pattern and thereby deduce directly the size and placement of the two gold stripes.

The team then moved on to a more complex pattern, a representation in gold-on-silicon of the Argonne National Laboratory logo. The pattern was chosen to be elongated, 400 μm in the direction parallel to the x-ray beam, but 5 μm in the transverse direction because the grazing angle geometry gives very different resolution in the two directions. To extract as much information as possible from the experiment, nine different detector positions were used for a given incident angle, and the results from all positions were combined to create a single pattern that included a large number of diffraction speckles.

Making only the assumption that the scattered intensity at any point was the result of interference from one wave scattered by gold and another by silicon surfaces, the scientists succeeded in deducing a three-dimensional (3-D) reconstruction from diffraction patterns (speckles) collected at a number of different angles of incidence, from 0.56° to 0.9°. Variation of the scattering intensity with incident angle provided additional data on the structure of the target object in the dimension perpendicular to the surface, allowing the team to produce a full 3-D map of the Argonne logo, with height correctly determined to be 37 nm (Fig. 1).

The image resolution obtained by this technique as applied to this study differed markedly with orientation: 22-nm parallel to the beam but only 2.6- μm transverse to it, with 2.7-nm height

resolution. Fortunately, higher coherent flux and more efficient detectors can readily improve these resolutions. Taking further data from different azimuthal angles in the plane of the target could reduce the discrepancy between the two lateral resolutions. Ultimately, the technique could prove useful for nanoscale imaging and even time-resolved growth studies in materials science and biology.

— David Lindley

See: Tao Sun*, Zhiang Jiang, Joseph Strzalka, Leonidas Ocola, and Jin Wang**, "Three-dimensional coherent X-ray surface scattering imaging near total external reflection," *Nat. Photonics* **6**, 586 (2012).

DOI:10.1038/NPHOTON.2012.178

Author affiliation:

Argonne National Laboratory

Correspondence:

*taosun@aps.anl.gov,

**wangj@aps.anl.gov

Use of the Advanced Photon Source and the Center for Nanoscale Materials at Argonne National Laboratory were supported by the U.S. Department of Energy Office of Science under Contract No. DE-AC02-06CH11357.

8-ID-E • XSD • Materials science, polymer science, physics • Grazing incidence small-angle scattering, x-ray photon correlation spectroscopy, intensity fluctuation spectroscopy, grazing incidence diffraction • 7.35-7.35 keV, 12-12 keV • On-site • Accepting general users •

UNDERSTANDING STRAIN IN NANOSCALE SEMICONDUCTORS

Exploring the world at the nanoscale requires tools that compensate for our inability to actually see such small materials, and the difficulty of characterizing their behavior in real time and under meaningful working conditions. Researchers utilizing the APS and the Argonne Center for Nanoscale Materials (CNM) have now added a new technique for understanding the internal strain behavior of a prototype semiconductor consisting of a 65-nm silicon-germanium (SiGe) film overlying a 15-nm silicon-on-insulator (SOI) layer. The device was embedded in a silicon dioxide insulator on a silicon substrate. This type of SiGe-SOI technology is currently in use and is constantly being refined as part of the ongoing search for faster, cheaper, and smaller nanoelectronic and nanocrystalline devices.

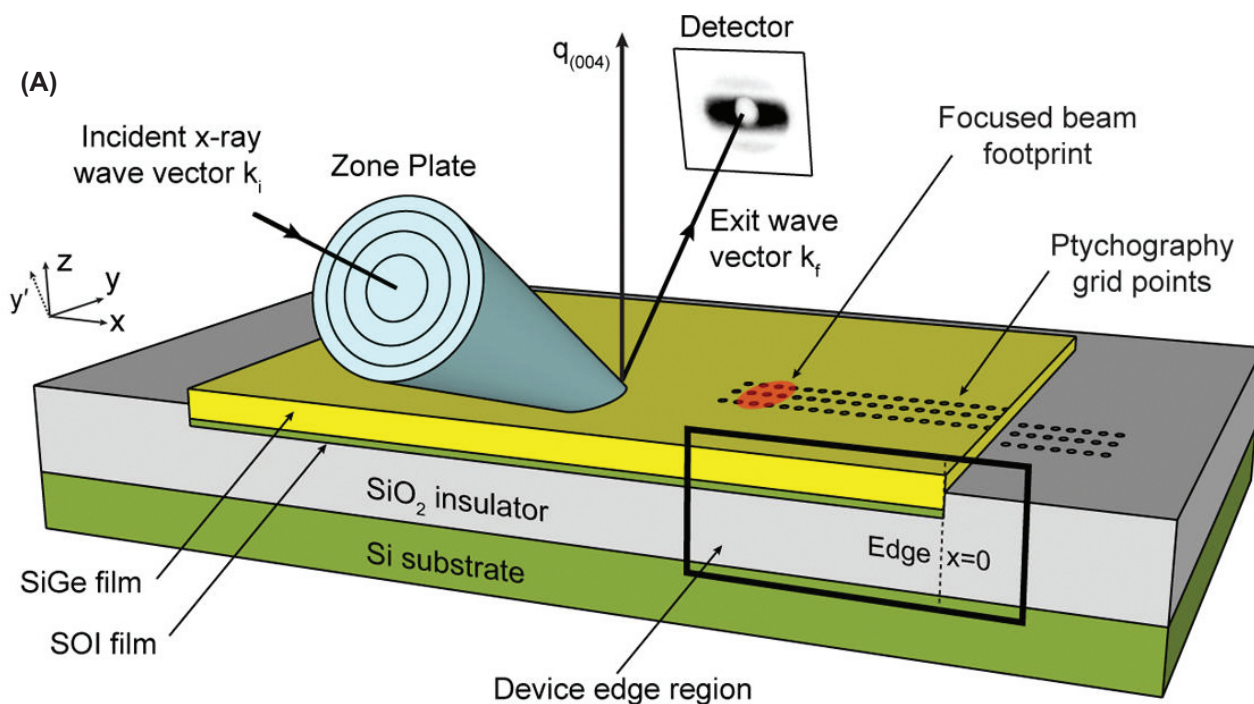
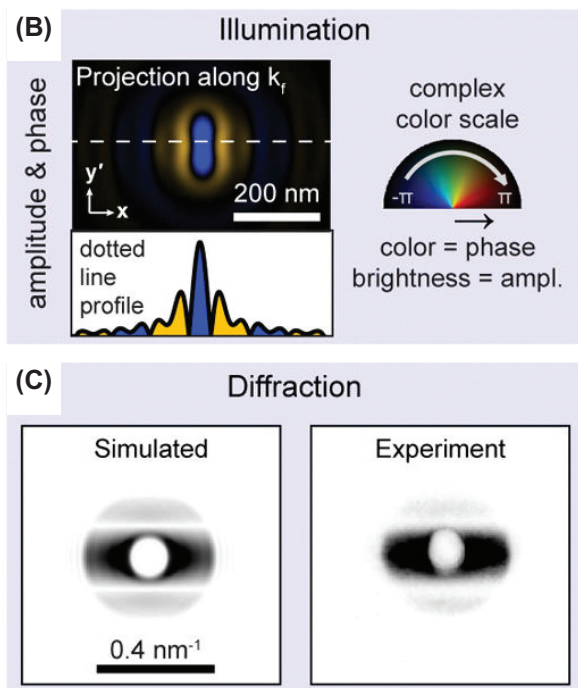


Fig. 1. X-ray Bragg projection ptychography from thin film heterostructures. (A) A schematic of the thin-film heterostructure studied in this work is shown, composed of layered SiGe (65 nm), SOI (15 nm), and SiO₂ films on a Si substrate. The incident coherent x-ray beam was focused down to an 85-nm-diameter spot size using a Fresnel zone plate, and diffraction patterns from the SiGe layer were measured with an area detector in the far field at the (004) Bragg condition. Also depicted in (A) are a focused beam footprint and overlapping grid points (to scale) at which diffraction patterns were collected for Bragg projection ptychography imaging of the device edge. The calculated focused beam amplitude in the SiGe layer projected along k_f is shown in (B, next page), and its two-dimensional Fourier transform amplitude is shown in (C, next page). This simulated diffraction pattern replicates the envelope and pattern of the experimental diffraction measured far from the edge, where the film is fully constrained in a biaxial stress state. This Fourier relationship between the beam projection and the far field area diffraction plane enables Bragg projection ptychography. From S.O. Hruszkewycz et al., *Nano Lett.* **12**, 5148 (2012). ©2012 American Chemical Society.

Many approaches have been employed to understand the lattice strain in such devices, but all of these so far have limitations. A major challenge has been to examine such devices in a non-destructive manner so that they continue to operate as



intended, unperturbed by the measurement technique. Another obstacle to accurate imaging is that the lenses utilized in some conventional probes can introduce aberrations that are hard to disentangle from the characteristics of the material itself.

Motivated by this challenge, a team of researchers from Argonne; IBM; and the University of California, San Diego, have developed a new non-destructive imaging tool, called nanofocused x-ray Bragg projection ptychography.

X-ray beams from the Hard X-ray Nanoprobe operated jointly at APS

Sector 26 by the CNM and XSD were focused on a prototype nanoscale device manufactured at IBM research and development facilities, in order to characterize the epitaxial stressor behavior of the SiGe-on-SOI device.

The beam was focused on an 86-nm-diameter spot on the thin-film heterostructure utilizing a hard-x-ray zone-plate optic.

To determine the lattice strain at the edge of the SiGe/SOI, the team collected focused beam coherent nanodiffraction patterns at incremental 25-nm steps, profiling the sample edge. Using the iterative two-dimensional coherent diffraction imaging approach known as ptychography, the researchers were able to produce for the first time a high-resolution image of the SiGe near the edge of the device, revealing detailed structural information about film density and lattice distortions without relaxing any boundary

conditions (Fig. 1).

Understanding strain is critical to tailoring the elastic and electronic properties needed to improve the performance of nanoelectronic devices. In this case, two sources of lattice strain were identified: the intrinsic epitaxial strain that occurs due to the lattice mismatch between the SiGe and the SOI films, and the strain introduced during the thermal processing of the device. Bragg projection ptychography clearly confirmed these two different sources of lattice distortions in the SiGe layer and simultaneously imaged the nanofocused beam, allowing for a much

higher potential imaging resolution.

Using a combination of nanodiffraction and coherent imaging, the researchers have developed a technique to explore, in a non-destructive way, lattice strain and film structure at a scale well below that of the 85-nm diffraction x-ray beam. This new ptychographic approach allowed the research team to resolve the lattice features of the prototype nanodevice to 16-nm resolution, providing the strictest test to date of continuum elastic modeling of nanoscale lattice behavior.

— Elise LeQuire

See: S.O. Hruszkewycz^{1*}, M.V. Holt¹, C.E. Murray², J. Bruley², J. Holt², A. Tripathi³, O.G. Shpyrko³, I. McNulty¹, M.J. Highland¹, and P.H. Fuoss¹, “Quantitative Nanoscale Imaging of Lattice Distortions in Epitaxial Semiconductor Heterostructures Using Nanofocused X-ray Bragg Projection Ptychography,” *Nano Lett.* **12**, 5148 (2012).

DOI:10.1021/nl303201w

Author affiliations: ¹Argonne National Laboratory; ²IBM; ³University of California, San Diego

Correspondence: *shrus@anl.gov.

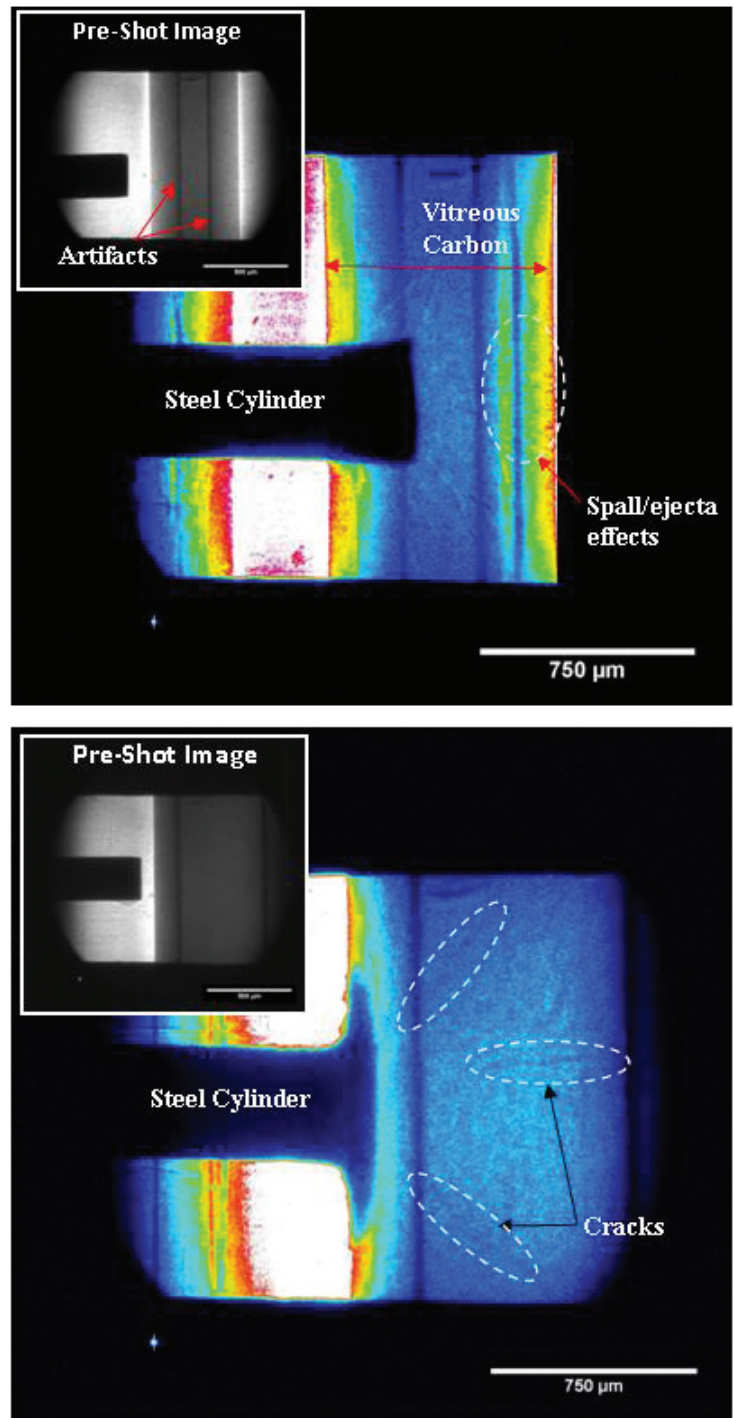
This work, including the use of the Argonne Center for Nanoscale Materials and Advanced Photon Source, was supported by the U.S. Department of Energy (DOE) Office of Science under Contract No. DE-AC02-06CH11357. S.O.H., M.J.H., and P.H.F. were supported by the U.S. DOE, Basic Energy Sciences, Materials Sciences and Engineering Division.

26-ID-C • CNM/XSD • Physics, materials science • Nanofluorescence imaging, microdiffraction, nanotomography • 8-12 keV • On-site • Accepting general users •

HIGH-RESOLUTION AND ULTRAFAST IMAGING OF HIGH-SPEED IMPACTS

The high-speed impact of two objects produces a shock wave that can crack, spall, or otherwise deform the colliding objects. In laboratory experiments, shock waves typically travel entirely through centimeter-scale objects within microseconds. While high-speed photography has long been used to image materials undergoing rapid structural change, it can only directly reveal the surface effects caused by shock events. Previous research that matched powerful synchrotron x-ray radiation with the “phase contrast imaging” (PCI) technique demonstrated the ability of PCI to capture dynamic changes throughout an object’s volume over microsecond timescales. Recently, researchers with Los Alamos National Laboratory and Argonne carrying out experimentation at the APS further refined synchrotron-based PCI to capture high-resolution, high-speed impact features occurring within ultra-short, nanosecond time frame, with spatial resolutions of $3\ \mu\text{m}$ (Fig. 1). This new capability promises to yield new information about the impact of shock waves on materials, advance studies of the physics of materials subjected to high strain rates, and lead to critical studies of materials strength, failure, and compaction.

Fig. 1. PCI data obtained during impact of a $300\text{-}\mu\text{m}$ -diameter stainless steel cylinder into vitreous carbon (experiment 1, top) and boron carbide plates (experiment 2, bottom). The pre-shot images (insets) show the cylinders at rest about $100\ \mu\text{m}$ from impact surface. The vitreous carbon plate was $\sim 0.5\text{-mm}$ thick and the boron carbide plate was $\sim 1\text{-mm}$ thick. Penetration of boron carbide (bottom) is markedly lower than that of vitreous carbon (top).



Phase contrast imaging is increasingly being exploited to reveal fine structural details that are absent from conventional x-ray images. While conventional x-ray imaging depends upon the attenuation (absorption) of x-rays passing through an object, PCI utilizes subtle phase shifts. These phase shifts occur because some regions in an object can slow the speed of photons slightly more than other regions, rendering the x-rays passing through the different regions slightly out-of-phase with one another. With a sufficiently intense x-ray source, these phase discontinuities can yield high-contrast images that reveal minute differences in a material's structure.

The experimental setup at XSD beamline 32-ID-B,C that was employed to create and image impacts is depicted schematically in Fig. 2. A specially-designed gun launched projectiles at high speed against a stationary target. A narrow slit and shutters controlled the flow of x-rays to the target area. X-rays that illuminated the target travelled to a scintillator that absorbed the x-ray radiation and re-emitted visible light, which was then focused onto an intensified charge-coupled device (ICCD) optical detector to form images.

In utilizing the PCI technique, the research team faced a challenge: the x-rays were so powerful that overexposing the target could induce structural changes *before* the impact event. Because it was important that any structural changes seen in the target material were caused by the impact and not by radiation damage, x-ray overexposure had to be prevented. Reducing x-ray exposure also protected the sensitive scintillator. Shielding the target and detector from excessive radiation was accomplished by electromechanical shutters that could rapidly block or pass the x-ray beam. The shutters blocked the x-rays for as long as possible, opening just before impact and closing quickly after.

Three separate impact experiments were conducted. Synchronizing the events within each experiment was performed electronically. A "master gun system" initiated launch of a projectile from the gun, while simultaneously opening the two shutters. This allowed x-rays to pass through the shutters and

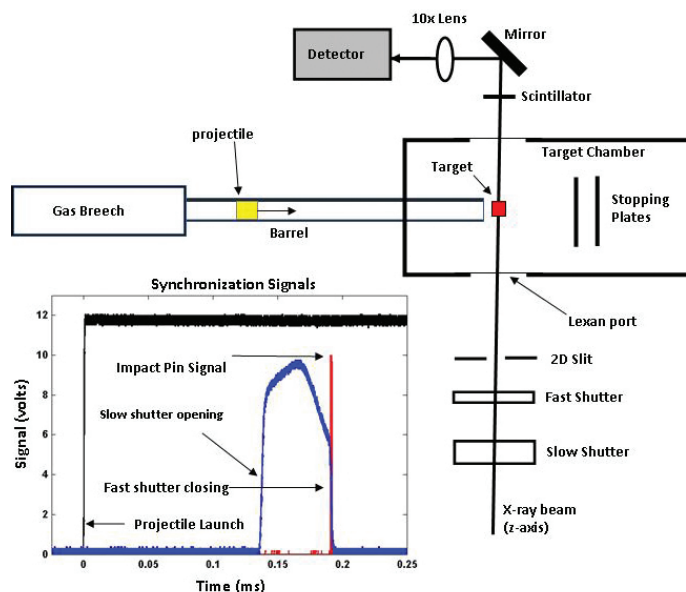


Fig. 2. Schematic of configuration for impact experiments using phase contrast imaging. Inset: timing signals used for synchronization include the 12-V signal sent by the gun control system (marked Projectile Launch), the photodiode signal (scaled for visibility) indicating the approximate duration of x-ray beam illumination of the target, and the impact pin signal.

illuminate the target before striking the scintillator. Just prior to colliding with the target, the projectile hit a piezoelectric impact. This pin sent an electrical current to a signal generator for timing, synchronizing, and triggering events. The signal generator quickly activated the ICCD, allowing imaging of the impact event with a single bunch of synchrotron x-rays spanning 80 nsec, followed immediately by closure of the second shutter. Proper operation of the shutters and the ICCD limited the target area's exposure to 60 msec, which proved sufficient to prevent x-ray damage to both the sample and detection system.

12.6-mm-diameter projectiles were fired from the gas gun utilizing compressed helium. The velocities of the three projectiles were measured at 619 m/s, 657 m/s, and 350 m/s. The two higher-speed projectiles consisted of aluminum cylinders featuring a protruding stainless steel pin designed to impact the target. The target in the first experiment consisted of vitreous, glass-like carbon; the second target was made of boron carbide.

The impact data gathered from these experiments demonstrates that synchrotron-based phase contrast imaging can provide high-resolution images of dynamic changes in materials on the nanosecond timescale. The team that conducted this proof-of-concept research continues to refine their experimental techniques and equipment. For example, the development of

a robust and remotely operated detection system has yielded even higher-resolution images and the first shock compression "movies" produced by synchrotron-based PCI techniques. Efforts are under way to obtain x-ray diffraction data to identify the atomic structure of new phases generated during impact, as well as examine the details of explosion events, such as so-called "hot-spot formation."

— Philip Koth

See: B.J. Jensen^{1*}, S.N. Luo¹, D.E. Hooks¹, K. Fezzaa², K.J. Ramos¹, J.D. Yeager¹, K. Kwiatkowski¹, T. Shimada¹, and D. M. Dattelbaum¹, "Ultrafast, High Resolution, Phase Contrast Imaging of Impact Response with Synchrotron Radiation," *AIP Advances* **2**(1), 012170 (2012). DOI:10.1063/1.3696041

Author affiliations: ¹Los Alamos National Laboratory, ²Argonne National Laboratory

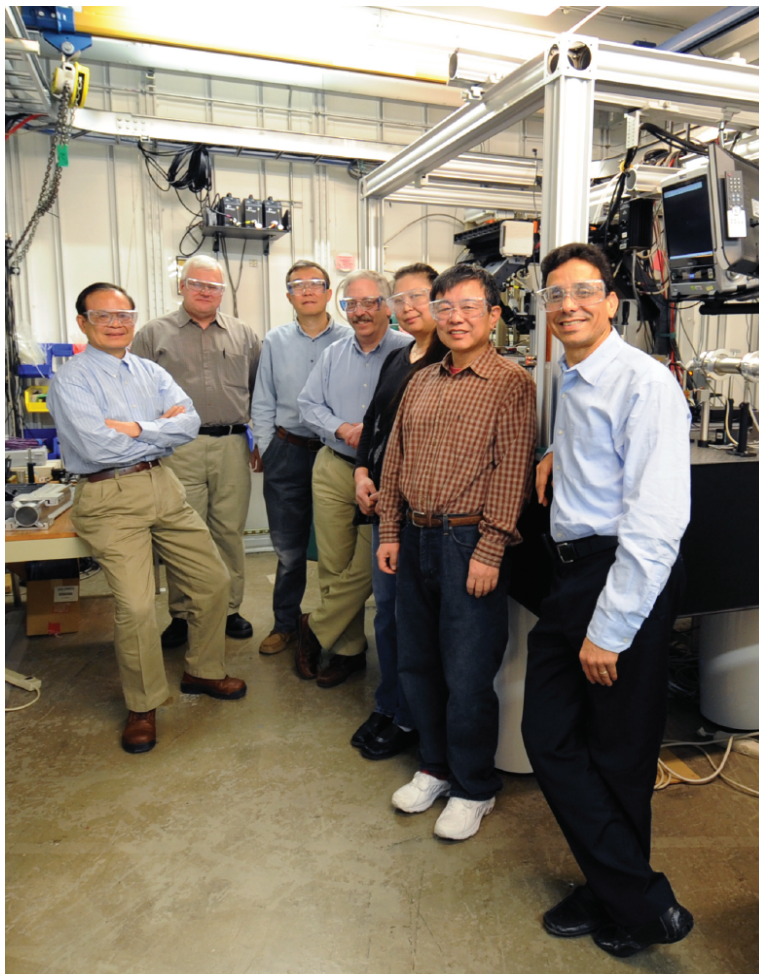
Correspondence: *bjjensen@lanl.gov

This work was supported by the Science Campaign and LDRD programs at Los Alamos National Laboratory. Use of the Advanced Photon Source at Argonne National Laboratory was supported by the U.S. Department of Energy Office of Science under Contract No. DE-AC02-06CH11357

32-ID-B,C • XSD • Materials science, life sciences, geoscience • Phase contrast imaging, radiography, transmission x-ray microscopy, tomography • 7-40 keV • On-site • Accepting general users

FOCUSING SYNCHROTRON BEAMS TO NANODIMENSIONS

Kirkpatrick-Baez (K-B) mirror systems are utilized to focus synchrotron x-ray beams down to spot sizes of microns in order to study materials, chemical, and biological samples. But traditional K-B mirror systems lack the precision necessary to focus intense synchrotron beams down to nanometer dimensions. Moreover, elliptical mirrors for aberration-free focus are very costly to produce. But a new nested (as opposed to the usual sequential arrangement), or Montel K-B mirror system solves these problems by incorporating two innovations into the fabrication process. This new mirror system will provide a more efficient and less expensive way to fabricate precise nested K-B mirrors. In addition, these newly designed mirrors can be used — for the first time — for ultra-precise micro- and nanofocusing of intense synchrotron x-ray beams.



Seven of the coauthors in the 34-ID-E enclosure. From left to right: Chian Liu, Michael Wieczorek, Wenjun Liu, Jon Tischler, Bing Shi, Jun Qian, and Lahsen Assoufid (all XSD). The nested K-B nanofocusing mirror assembly was tested in the experimental setup behind the group.

Researchers from the Argonne and Oak Ridge national laboratories developed these new mirrors in order to overcome the shortcomings of existing K-B systems. The ones employing benders to bend flat trapezoid silicon mirrors to elliptical reflecting surfaces have stability problems and are bulky, hard to adjust, and difficult to focus in the nanometer range. The mirrors made by computer-controlled surfacing are very expensive to manufacture, with each costing around \$100,000 and involving many fabrication steps.

The new design of nested Montel K-B mirrors (Fig. 1) is compact and easy to use, with no need for benders. Overall, this new system, which features highly precise, profile-coated elliptical reflecting surfaces that are able to efficiently focus hard x-rays to less than 100 nm, can be employed in many applications where x-ray nanobeams are required.

The main challenge overcome by these scientists involved eliminating the imperfections at the edges where the two perpendicular elliptical mirrors come together. The problem was solved by developing a profile coating technique that converts inexpensive, flat silicon substrates into precise elliptical mirrors. The technique uses a contoured aperture mask in a magnetron sputtering system that coats a predetermined profile onto mirror substrates. During the development, gold and platinum were found to be suitable coating substances. Taking only a few

hours per coating run, a primary coat and a follow-up corrective coat were determined to be all that was needed to produce precise elliptical K-B mirrors. Multiple mirrors can be coated during each run. A focal spot as small as 70 nm was achieved using the profile coating method when applied to a flat silicon substrate.

Another problem solved was the way the mirror systems were produced and aligned. Instead of cutting the mirrors at 45° to their surface and then assembling them through an alignment that requires 2 degrees of freedom on each end, the mirrors were polished at 90° to their surface. The polished surface was then pushed against the other mirror's surface so that only 1 degree of freedom was required. The mirror edges were made in two ways: the side of the mirror was polished and then the two mirrors together were coated to produce identical elliptical mirrors; and a wider mirror was coated first, then cut into two mirrors, and the side of one of them was polished.

The nested K-B mirrors were tested at the XSD 34-ID-E beamline of the APS (Fig. 2). The beamline test showed a point focus of around 100 nm, which was considered excellent. A larger incident divergence was able to be focused because of the new nested arrangement of mirrors. This improvement led to an increased demagnification factor and potentially smaller focusing when compared to a sequential K-B system.

This beamline test proved that nested Montel K-B mirrors can be fabricated successfully for synchrotron beamlines, and that the profile coating technique is capable of producing high-quality Montel K-B mirrors using flat silicon substrates.

Because of this successful first-ever test of a synchrotron hard x-ray nested K-B mirror system, the developers are confident that scientific research will benefit from the new Montel optics. — *William A. Atkins*

See: Chian Liu^{1*}, G.E. Ice², W. Liu¹, L. Assoufid¹, J. Qian¹, B. Shi¹, R. Khachatryan¹, M. Wieczorek¹, P. Zschack¹, and J.Z. Tischler¹, "Fabrication of nested elliptical KB mirrors using profile coating for synchro-

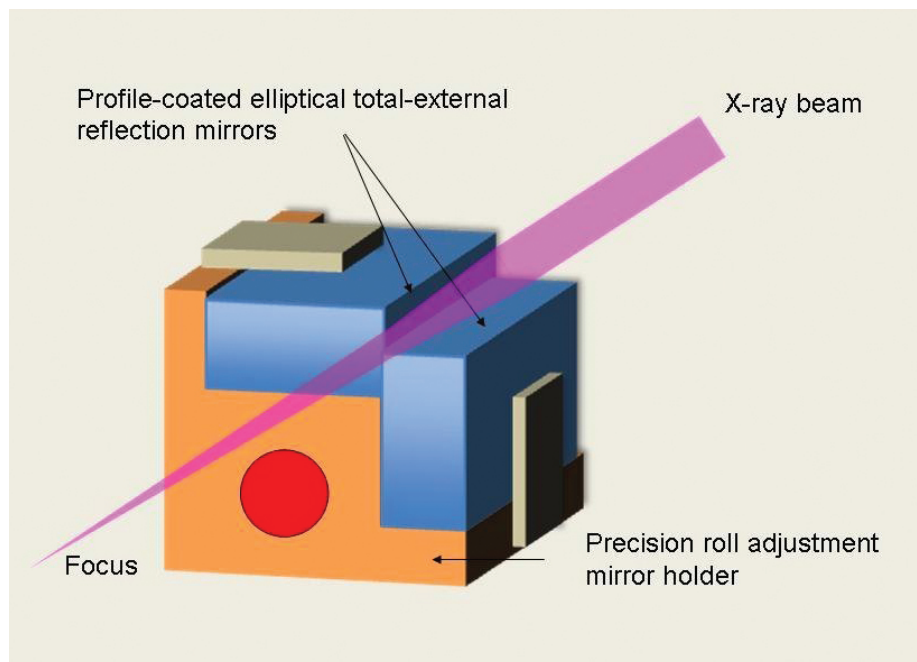


Fig. 1. A prototype Montel K-B mirror design. Two profile-coated elliptical total-external reflection mirrors are seen, along with the precision roll adjustment mirror holder. The x-ray beam is seen coming in from the top-right, with the focus at the bottom-left. From C. Liu et al., *Appl. Surf. Sci.* **258**, 2182 (2012).

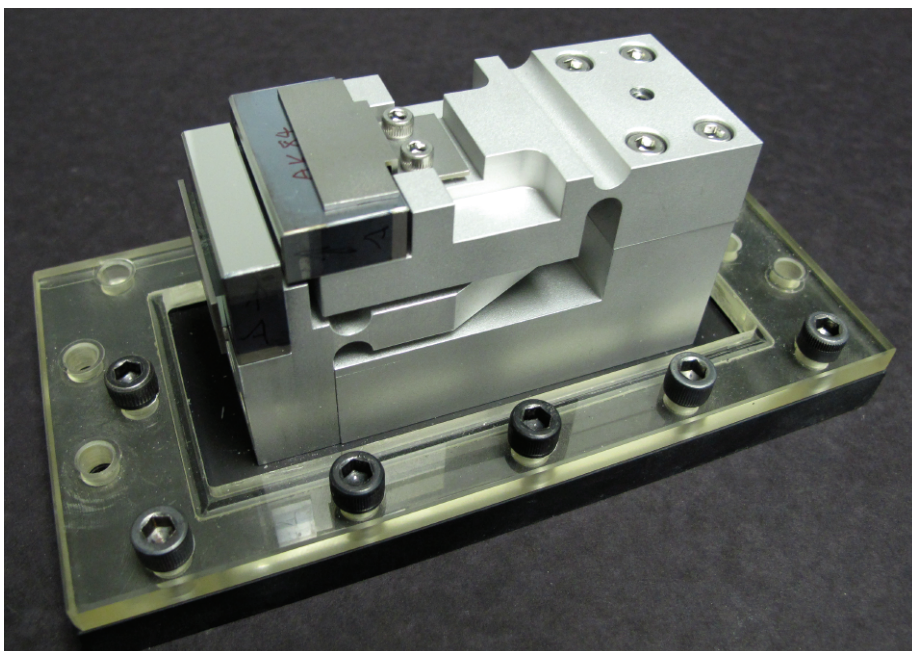


Fig. 2. Nested K-B mirror/mount assembly tested at APS 34-ID-E beamline. The mirrors are at the top left in the photo. The reflecting surface of the vertical mirror is visible, and the reflecting surface of the horizontal mirror faces towards the left.

tron radiation X-ray focusing," *Appl. Surf. Sci.* **258**, 2182 (2012).

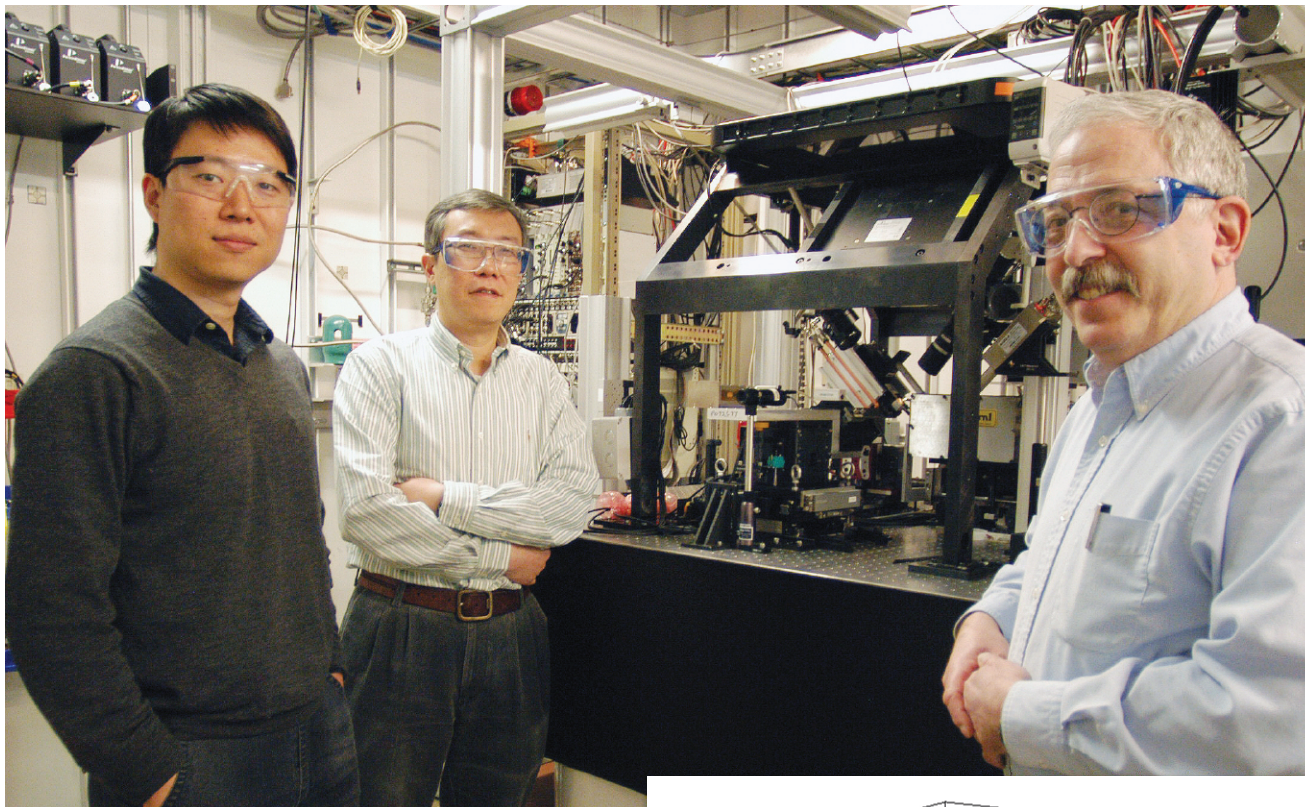
Author affiliations: ¹Argonne National Laboratory, ²Oak Ridge National Laboratory

Correspondence: *cliu@aps.anl.gov

This work is supported by UChicago

Argonne, LLC, Operator of Argonne National Laboratory, a U.S. Department of Energy (DOE) Office of Science laboratory operated under Contract no. DE-AC02-06CH11357. G.E.I and J.Z.T. are supported by the Center for Defect Physics, an Energy Frontier Research Center funded by the U.S. DOE Office of Science under Award Number ERKCS99.

HIGH-SPEED MICRODIFFRACTION AT 34-ID-E



Left to right: Ruqing Xu, Wenjun Liu, Jon Tischler (all XSD) in the 34-ID-E microdiffraction station.

The microdiffraction station on XSD beamline 34-ID-E at the APS has been a world leader in utilizing sub-micron-sized x-ray beams for a wide range of diffraction problems in materials science and condensed matter physics since it was first built in 2001 [1]. With its small white (or monochromatic) beam size of only a few hundred nanometers and the ability to depth-resolve the scattering along an x-ray beam, it provides the ability to measure strain or orientation of all the volume elements in a three-dimensional (3-D) solid [2]. This capability has been used as a source for probing the strain in deformed metals [3], the deformation around a nano-indent [4], structures in a diamond anvil cell [5], the strain at the base of a tin whisker [6], and identification of embedded phases [7], as well as the strain and orientation from many other small structures.

Many of these studies require a 3-D volumetric measurement, which means scanning three spatial dimensions; this is inherently time consuming. So the utility of this technique has always been limited by the rate at which measurements could be made. With the acquisition of fast area detectors, the time for acquiring a single image dropped from 8 s to 0.1 s. This has made it practical to measure the scattering from vol-

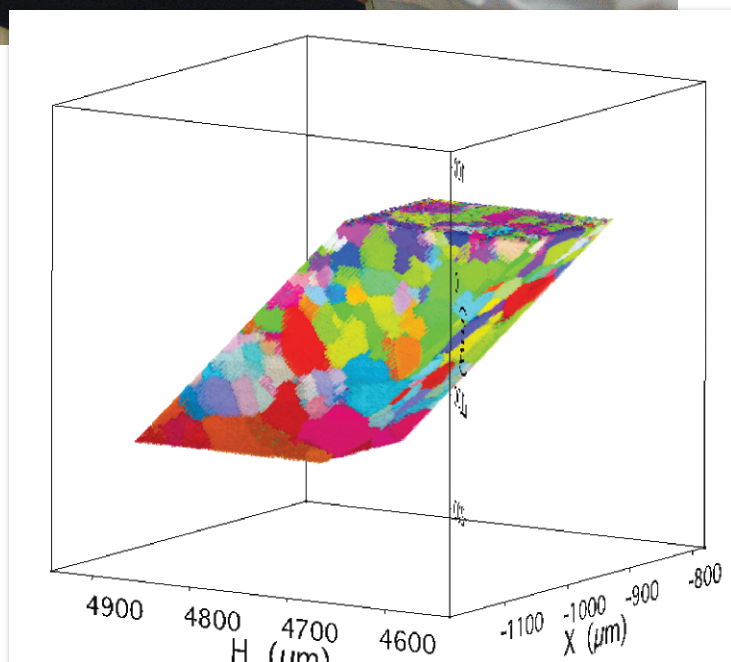


Fig. 1. Orientations in a 3-D volume of aluminum. Each color represents a different orientation; the grains show themselves as volumes of constant color. The top is the only external surface, the height of the visible volume is 212 μm , and the base of the volume is 135 \times 186 μm . The average rms orientation error for all of the measured points is than 0.01°. Image courtesy of John Budai, Oak Ridge National Laboratory.



Chen Zhang (Michigan State Univ.) at the 34-ID-E control station, monitoring his experiment utilizing microbeam Laue diffraction to characterize the microstructure beneath the sample surface of a deformed titanium specimen. The information gathered will be the basis for a 3-D computational model that will allow direct comparison between simulation and experimental data. The lower-left screen shows the diffraction pattern being obtained from the sample under study. The control panels in the lower center are to monitor the beam and systematically move the specimen. The top center screen shows real-time video of the measurement from four points of view. The upper right screen shows a birds-eye view of the material area being investigated.

umes containing the order of half-a-million points.

Once the detector speed increased, it then became necessary to speed up all of the other parts of the data collection and processing. The first step was to change from a step-scan mode to a fly-scan mode where images are continuously acquired while the depth-resolving wire is scanned repeatedly over the same $\sim 500\text{-}\mu\text{m}$ range. This removed all of the time lost stopping and starting the scanning motor for each image. The second step was to increase the data transfer rate and storage capacity. Operating at 10 images per second requires storing 80 MB/s continuously. For a one-day measurement this adds up to 6 TB of data. And the third step was to improve the analysis; if one is collecting terabytes of data per day, then one must be able to analyze terabytes of data per day. This required providing the data files with all of the information needed to process the data, the programs

capable of processing the data, and a cluster capable of running everything.

One recent measurement of grain growth in an aluminum alloy is pictured in Fig. 1 showing the result from a single annealing step. The data for this volume came from 7 TB of images collected in two days; this represents a 15-fold increase in data size and speed over non-fly scanning. Before this upgrade, measuring a volume of this size would have required one month of continuous measuring.

This advance was the result of a close collaboration between the APS and the Materials Science and Technology Division at Oak Ridge National Laboratory.

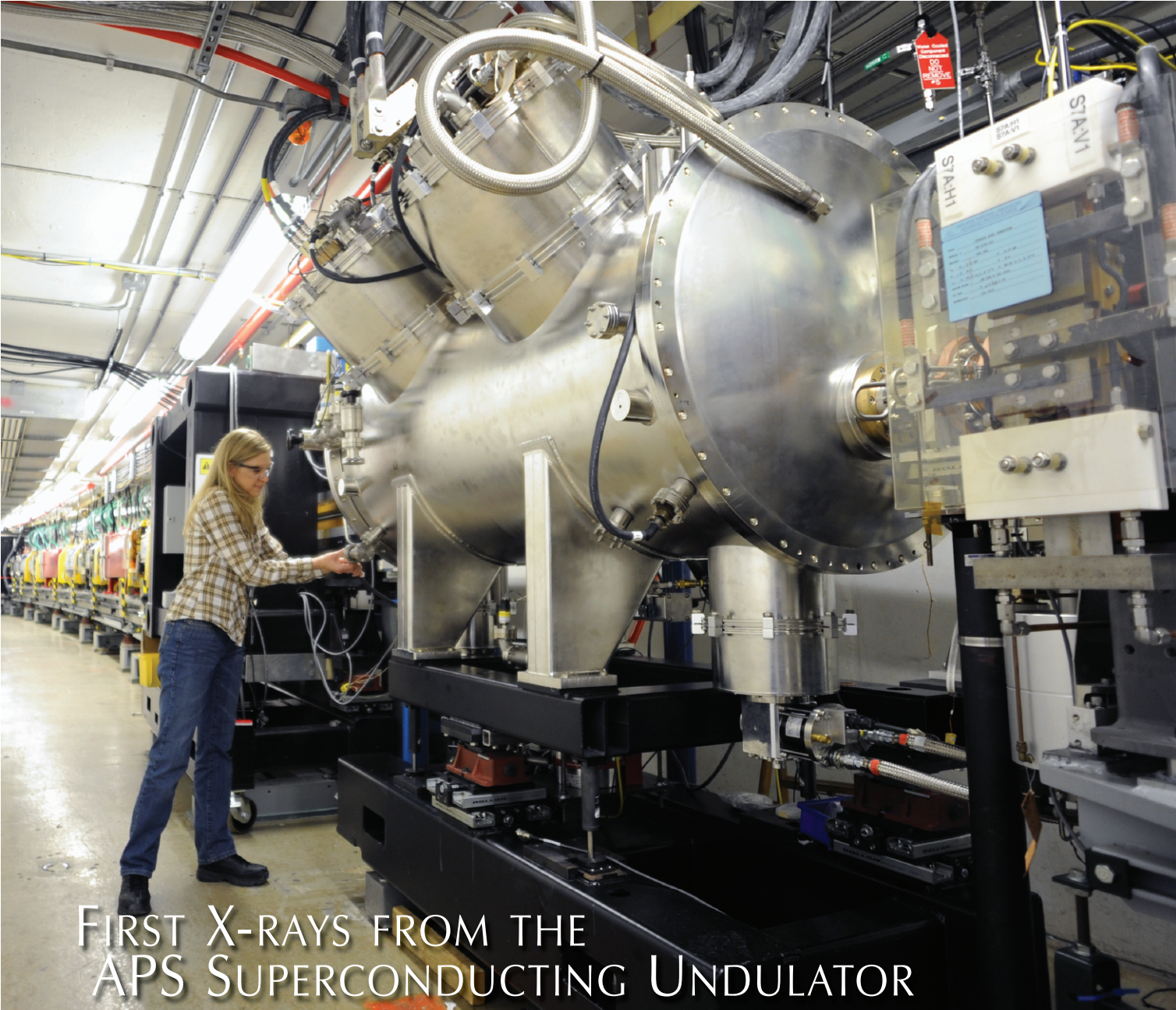
Contact: Jon Tischler,
tischler@aps.anl.gov;
Wenjun Liu, wjliu@aps.anl.gov;
Ruqing Xu, ruqingxu@aps.anl.gov

REFERENCES:

- [1] D.E. Ice and B.C. Larson, *Adv. Eng. Mater.* **2**(10), 643, (2000). DOI:10.1002/1527-2648(200010)2:

- 10<643::AID-ADEM643>3.0.CO;2-U
[2] B.C. Larson, Wenge Yang, G.E. Ice, J.D. Budai, and J.Z. Tischler, *Nature* **415**, 887 (2002). DOI:10.1038/415887a
[3] Lyle E. Levine, B.C. Larson, et al., *Nat. Mater.* **5**, 619 (2006). DOI:10.1038/nmat1698
and
Lyle E. Levine, Peter Geantil, B.C. Larson, et al., *Acta Mater.* **59**, 5803(2011). DOI:10.1016/j.actamat.2011.05.056
[4] W. Yang, B.C. Larson, G.M. Pharr, et al., *J. Mater. Res.* **19**, 66 (2004). DOI:10.1557/jmr.2004.19.1.66
[5] Wendy L. Mao, Lin Wang, Yang Ding, Wenge Yang, Wenjun Liu, et al., *Proc. Natl. Acad. Sci. USA* **107**, 9965 (2010). DOI:10.1073/pnas.1005279107
[6] M. Sobiech, M. Wohlschlägel, U. Welzel, et al., *Appl. Phys. Lett.* **94**, 221901 (2009). DOI:10.1063/1.3147864
and
Z.W. Pan, J.D. Budai, Z.R. Dai, W.J. Liu, et al., *Adv. Mater.* **21**, 890 (2009). DOI:10.1002/adma.200802138
[7] Chi Ma, Oliver Tschauner, John R. Beckett, et al., *Am. Mineral.* **97**, 1219 (2012). DOI:10.2138/am.2012.4027

34-ID-E • XSD • Materials science, physics • Microdiffraction, Laue crystallography, microbeam • 7-30 keV • On site • Accepting general users •



FIRST X-RAYS FROM THE APS SUPERCONDUCTING UNDULATOR

Fig. 1. Sue Bettenhausen (ASD) in the APS storage ring at the SCU prototype installed on Sector 6. An APS Undulator A can be seen just upstream of the SCU.

A decade-long R&D program for development of an APS superconducting undulator (SCU) culminated in January 2013 with the installation and testing at the APS of the first prototype, SCU0. On January 21, the SCU0 produced the first photon beam for the users at APS Sector 6.

During the 2012-13 winter shutdown of the APS accelerator, the SCU0 was installed in the downstream part of straight section 6 in the APS storage ring (Fig. 1). The undulator was cooled down, filled with liquid helium, and commissioned in a two-week period.

Every synchrotron radiation (SR)

facility is designed to cover as wide a spectral range of radiation as can be delivered to users. This leads to the utilization of a variety of magnetic devices, such as specialized bending magnets, or undulators and wigglers. In recent years, many SR facilities around the world have adopted an in-vacuum undulator (IVU) technology that permits extension of the high-energy spectrum of SR radiation. But IVU technology is approaching its physical limits. A significant leap in the development of a new generation of undulators belongs to superconducting technology.

For many years, scientists and

engineers at different SR facilities, such as the Budker Institute of Nuclear Physics (BINP) in Russia, the National Synchrotron Light Source, ANKA in Germany, and the Singapore Synchrotron Light Source attempted to employ SC undulators as a radiation source. None of these attempts, for various reasons, have resulted in long-term utilization of the devices. Superconducting wigglers, on the other hand, have found much wider acceptance at SR facilities including third-generation SR sources. The majority of these wigglers have been successfully built by the BINP.

The APS is the first third-genera-

tion x-ray facility to make significant investments in the development of novel undulators based on SC technology. The main goal is to achieve unsurpassed performance from short-period, high-magnetic-field undulators. With well established SC materials, superconducting undulator performance will exceed the brightness of the high-energy x-rays delivered by APS Undulator A. But in the future, novel SC materials, such as Nb_3Sn and high-temperature superconductors, will lead to an ultimate performance that will exceed the best possible IVU devices.

The cryostat of the first APS superconducting device was designed and built following the BINP concept for SC wigglers. The superconducting magnetic structure and the cooling system were developed at the APS during the R&D program. This part of the project included magnetic modeling as well as building and testing several magnet prototypes.

A special cryostat was built to test cooling of the undulator superconducting coils with liquid helium by utilizing a thermosyphon concept. The cooling design was improved by thermally insulating the undulator beam chamber from the superconducting coils and cooling it with two cryocoolers. Two more cryocoolers in the undulator cryomodule cool the liquid-helium circuit. The undulator is first filled with approximately 50 L of liquid helium and then operated as a closed system.

The SCU0 magnet, which is wound with NbTi superconducting wire, has a 42-pole structure with a period length of 16 mm, twice as small as APS Undulator A. The SCU0 undulator peak field is 0.4-0.64 T, which corresponds to the photon energy at the fundamental of 20-25 keV.

The detailed design of the SCU0 was done at the APS in collaboration with scientists and engineers from the BINP. Parts of the cryomodule were manufactured in industry, while the magnetic structure was built at the

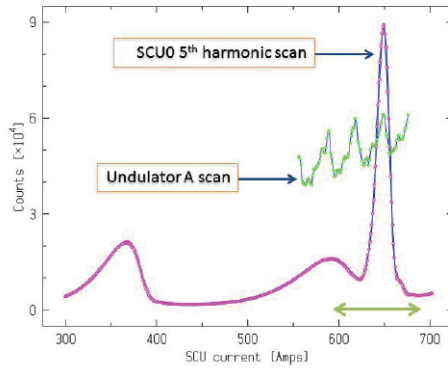


Fig. 2. SCU0 5th harmonic and APS Undulator A at 85 keV. SCU0 flux at 85 keV is 1.4x higher than Undulator A.

APS. The undulator was assembled by the SCU0 team in a new high-bay facility at Argonne. In parallel with manufacturing the SCU0, a dedicated measurement system was designed and built.

Assembly of the SCU0 in spring 2012 was followed by rigorous cold test and magnetic measurements in summer of that year. During the tests, the SCU0 performed well both cryogenically and magnetically, thus confirming the design principles.

Although the SCU0 magnet is only 330-mm long, it is nevertheless comparable in photon brightness at 50-100 keV with the 2.4-m-long Undulator A. The very first experience of operating the superconducting undulator in the storage ring indicates stable cryogenic behavior of the device and minimal effects on stored beam. More studies are on the way, but it is already clear that superconducting undulator technology can deliver on its promises to the synchrotron radiation community.

The next step will be the design and fabrication of an SCU with 72 periods (the same number as APS Undulator A) and replacement of the prototype with this longer SC magnet. The existing cryostat, with all auxiliary



Main photo: Members of ASD, AES, and the APS Upgrade Project team in the Bldg. 314 high bay at Argonne. Behind them is the large cryostat for the superconducting undulator. Left to right: Marion White (ASD); Joe Gagliano, Jr. (ASD); John TerHAAR (ASD); Joel Fuerst (ASD); Chuck Doose (ASD); Matthew Kasa (ASD); Denise Skiadopoulos (AES); Jack Burke (AES); Kurt Boerste (ASD); Susan Bettenhausen (ASD); Mike Merritt (ASD); Yury Ivanyushenkov (ASD); Emil Trakhtenberg (AES); Efim Gluskin (ASD); George Srajer (APS-U); and Quentin Hasse (ASD). Inset: Scott Wesling (left) and Bill Jansma (both AES), who aligned the SCU prototype.

systems, will accommodate this 1.2-m long, 72-period SCU. The new device will increase by almost an order of magnitude x-ray brightness at 60 keV (Fig. 2). In addition, both the prototype and future devices, as real undulator sources, will provide users with orders-of-magnitude “cleaner” (much better signal-to-noise ratio) high-energy radiation than that available from any existing SR source in the world.

Contact: Efim Gluskin,
gluskin@aps.anl.gov;
Yury Ivanyushenkov, yury@aps.anl.gov

SHORT-PULSE X-RAYS AT THE ADVANCED PHOTON SOURCE

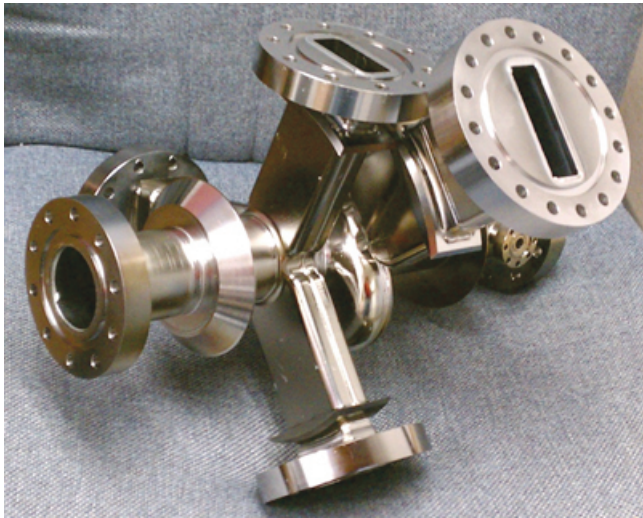


Fig. 1. SPX Mark-II deflecting cavity made of niobium.

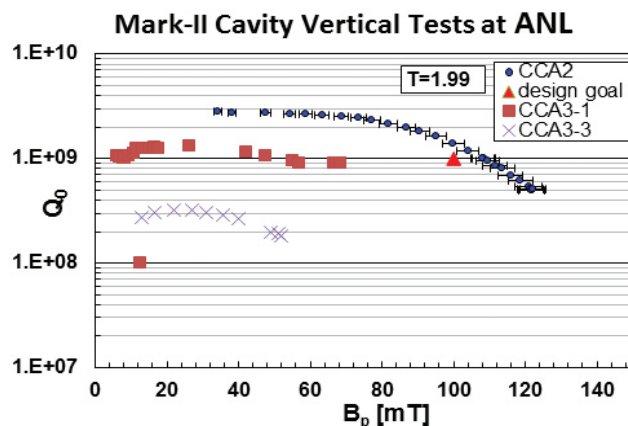


Fig. 2. SPX Mark-II deflecting cavity vertical test result. Quality factor, Q_0 vs. surface magnetic field.

The Short-Pulse X-ray (SPX) facility planned as part of the APS Upgrade is designed to be a unique-in-the-world facility. It will provide tunable polarized x-ray pulses of variable duration (1-100 ps), repetition rate (1 kHz–6.5 MHz), and bandwidth (10^{-4} or 10^{-2}) over a wide energy range (200 eV–40 keV) at high average flux ($\sim 10^{15}$ /s for the widest bandwidth, longest pulse duration). The SPX facility utilizes a scheme suggested by Zholents et al. [1] that incorporates a pair of radio-frequency (rf) deflection cavities in the APS storage ring. The first rf-deflection cavity chirps the 100-ps-duration electron pulse such that different parts of the pulse acquire different vertical

momenta, producing a fan of radiation as the pulse passes an undulator. The second cavity restores the beam to its original phase space. The variable repetition rate can be readily achieved, as the time between pulses in the APS standard 24-bunch mode—153 ns—is long enough for mechanical choppers. Detailed beam physics simulations and implementation are discussed in [2] and [3].

The envisioned facility will have three independently operating beamlines and co-located ultra-fast laser infrastructure. Two beamlines fed by insertion devices will operate in the hard x-ray regime. The hard x-ray spectroscopy and scattering beamline will feature

a slit to extract short pulses and operate as a traditional spectroscopy/diffraction beamline with interchangeable Si and multilayer monochromators, variable speed chopper, and microfocusing capability. The hard x-ray microscopy and imaging beamline will have the unique capability of accepting the entire 1-mrad fan of x-ray radiation, which then can be used for time-dispersed diffraction or coherent imaging. The soft x-ray beamline (200-2000 eV) will be based on bending magnet radiation. In the bending magnet, the electron beam produces a vertically elongated source, and imaging a section of the source will produce a short pulse, and in addition, a means to control and

chop polarization by selecting on- or off-axis components.

Significant R&D progress toward the SPX facility has been made in the past year. In collaboration with Jefferson National Laboratory, superconducting rf deflecting cavities (Mark-II) operating at 2815 MHz in continuous mode have been constructed and tested at the Argonne Physics Division superconducting test facility (Figs. 1 and 2). In addition, the past year has seen the completion of a 5-kW rf power amplifier unit and significant progress in the design, testing, and characterization of silicon carbide material utilized for the higher-order-mode waveguide dampers. In collaboration with Lawrence Berkeley National Laboratory (LBNL), a fully functional digital low-level rf control system has been designed and fabricated, which is being utilized in the SPX R&D phase. Ongoing collaboration with LBNL on the development of a precision timing/synchronization system for the SPX facility is progressing well to meet the demanding requirements on the control of both amplitude and phase of the field in the SPX superconducting cavities. The Beam Technology Group at LBNL has developed and demonstrated a system for distributing stable rf signals over optical fiber capable of achieving less than 20-fs rms drift and jitter that meets SPX rf and timing/synchronization specifications. Current plans call for a first test of the rf deflection cavities in the APS storage ring in 2015.

Contact: *Ali Nassiri*,
nassiri@aps.anl.gov

REFERENCES

- [1] A. Zholents, P. Heimann, M. Zolotarev, and J. Byrd, *Nucl. Instrum. & Methods A* **425**, 385 (1999). DOI:10.1016/S0168-9002(98)01372-2
- [2] M. Borland, *Phys. Rev. Special Topics - Accelerators and Beams* **8**, 074001 (2005). DOI: 10.1103/PhysRevSTAB.8.074001
- [3] A. Nassiri et. al, 2012 International Particle Accelerator Conference (IPAC12) Proceedings, p. 2292, (2012).

DEVELOPMENT OF NEXT-GENERATION X-RAY BEAM POSITION MONITORS

Development of a next-generation x-ray beam position monitor (XBPM) is a collaboration between the ASD Diagnostics Group, and the AES Mechanical Engineering and Design; Mechanical Operations and Maintenance, Controls; and Survey and Alignment groups. The effort reached a critical milestone in 2012 with the first high-power, first-article tests at the inelastic x-ray scattering beamline, 29-ID. The final design for this grazing-incidence insertion device (GRID) XBPM supporting APS Upgrade high-heat-load front ends was completed, and procurement of components was initiated, in December 2012.

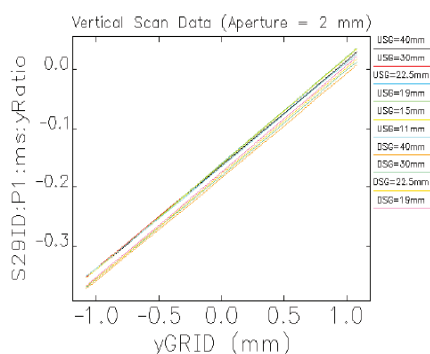


Fig. 1. Vertical beam position measurements with USG and DSG undulators.

The first production model is expected to be ready in 2013 to support the new resonant inelastic x-ray scattering beamline planned for 27-ID. A second unit will be deployed at the new Dynamic Compression Sector beamline 35-ID. This development will improve long-term x-ray beam stability at a level below 500-nrad rms, and is planned for all new insertion device front ends as part of the APS Upgrade.

With the high-quality feedback systems used in today's synchrotron radiation sources, the actual beam stability achieved is often determined by the accuracy of beam position measurements. Located approximately 20 m from the source, the APS XBPMs are uniquely suited for very-high-resolution beam-angle measurements. The existing APS XBPMs, based on photoemission, were designed more than 20

years ago; their signal is strongly dependent on the undulator gap due to severe contamination from bending magnet radiation background. Following a several-year development effort in ASD, hard x-ray BPMs have been demonstrated to be immune from this background.

In all third-generation sources, beamlines use only the core of the undulator beam, approximately 100 μ rad in radius. A set of grazing-incidence apertures was designed to intercept the useless wings of the radiation pattern outside of this central cone. When hard x-ray photons are absorbed by the copper apertures, they generate copious fluorescence photons and produce a footprint of the undulator beam. A novel hard x-ray BPM was proposed several years ago to image this partial footprint on the apertures and infer the position of the core beam.

The first article based on this design principle was tested in user-beam Run 2012-1 at beamline 29-ID (which had two in-line undulators installed at the time), delivering up to 10 kW of x-ray power. The test demonstrated that the bending magnet background signal was reduced by two orders of magnitude, which will significantly improve beam stability for users.

A simple aperture-based x-ray imaging system for the vertical position readout also performed excellently. Figure 1 shows the x-ray beam position readout during electron beam angle scans. The undulator gaps were varied from 10.5 mm to 40 mm, with x-ray power changing by more than 1000-fold. Remarkably, almost no gap dependence was found in the upstream undulator (USG). The change in the signal seen with the downstream undulator (DSG) and between the two undulators is due to minute differences in steering occurring in the end sections of the two undulators. Monochromatic x-ray beam measurements showed that the central cone position correlates well with the XBPM measurements, in contrast with electron BPMs, which cannot

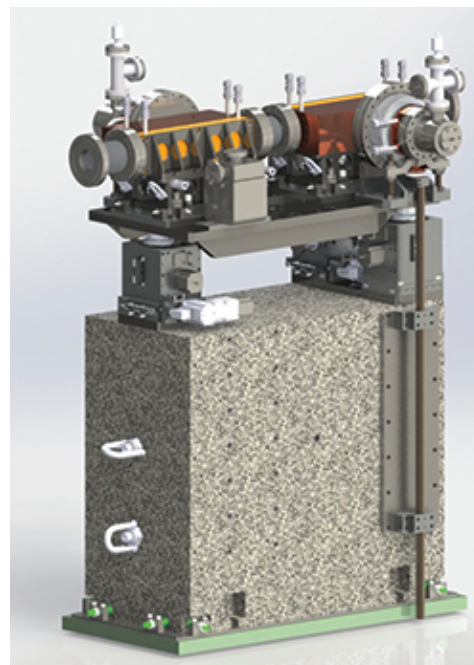


Fig. 2. Solid model for GRID-XBPM in a high-heat-load front end.

detect internal steering effects.

Deployment of next-generation XBPMs is planned for all new APS Upgrade front ends; mechanical designs are in a very advanced stage. Figure 2 shows a solid-model XBPM design for the high heat-load undulator front end. During the 29-ID test, it was discovered that x-ray heating of the BPM eventually caused the support structure to expand, resulting in a temperature-dependent drift of the vertical position readout. The new design decouples the absorber from the readout optics utilizing bellows, and the vertical detector positions will be monitored in real time. Corrections of the detector motion relative to a hydrostatic level system will be made during machine operations.

Contact: Glenn Decker,
decker@aps.anl.gov

See: B.X. Yang, G. Decker, S.-H. Lee, P. Den Hartog, and K.W. Schlax, "Progress in the Development of a Grazing-incidence Insertion Device X-ray Beam Position Monitor," PAC 2011, Brookhaven National Laboratory (2011), 441.

THE NEWLY RECONFIGURED BEAMLINE 1-BM



Repurposing and reconfiguring 1-BM are (l. to r.): Jonathan Almer¹, John Okasinski¹, Naresh Kujala², Albert Macrander², Lahsen Assoufid², Robert Bradford³, Lisa Gades³, Shashidhara Marathe², Matthew Moore³, and Russell Woods³ (all XSD). ¹Materials Physics and Engineering Group—high-energy and energy dispersive diffraction, ²Optics Group—optics testing, ³Detectors Group—detector testing

In recognition of the vital role played by optics and detectors at the APS, the 1-BM bending magnet beamline is being reconfigured to host optics and detectors testing programs. These new optics characterization capabilities will feature Talbot interferometry and both monochromatic and white-beam topography for characterizing crystal optics as large as 90 mm. A unique resource, 1-BM is currently the only domestic monochromatic topography program, and will soon be the only U.S. facility for white-beam topography once the National Synchrotron Light Source (NSLS) at Brookhaven National Laboratory is shut down for transition to NSLS II.

The 1-BM detectors program will serve as a test bed for new x-ray detectors and will provide in-house facilities for calibrating the numerous detectors in use at the APS. Beam time will eventually be shared with a high-energy diffraction program being developed by the XSD Materials Physics and Engineering Group.

The reconfiguration began in summer 2012. By August of that year, two mirrors were removed, a new flat crystal had been installed in the existing monochromator, and monochromatic beam was delivered to the C-hutch. Both optics and detectors efforts took first data with mono beam in the fall 2012 run, and white beam was delivered to the B hutches during the first run of 2013. To support the future high-energy diffraction program, a new Laue-Laue monochromator will be installed in the A-hutch. Users will be

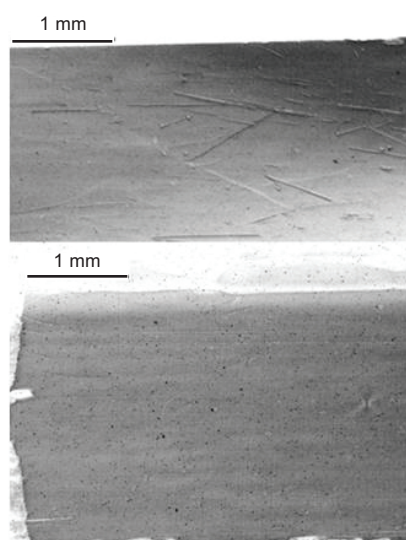


Fig. 1. Topographs of sapphire samples obtained at 1-BM at 8 keV for the (0006) reflection. No dislocations were observed for the sample for the lower part of the figure. As a caveat, note that RIXS analyzers ideally would be larger in size.

able to select from either of the two monochromators and the beamline will be configured for rapid change-overs. First users were hosted February 1-5, 2013.

In anticipation of producing sapphire analyzers for the resonant inelastic x-ray scattering (RIXS) beamline that is part of the APS Upgrade, the XSD Optics Group has tested topographic techniques for screening sapphire. To match a specific resonance, a backscattering analyzer must have specific lattice spacing, and this dictates specific materials [1]. Meeting this need dictates the use of sapphire with ultralow defect density, and x-ray

topography is well suited to screening material prior to analyzer fabrication. Figure 1 shows monochromatic beam topographies for two sapphire samples from the same supplier. The upper sample shows a large number of dislocations; the lower sample does not. These results demonstrate that lower dislocation density sapphire can be obtained, and also the utility of topography as a screening step.

The goal of the associated detectors testing program is to provide in-house facilities for detector calibration and studies of detector performance. The effort will develop standardized calibration techniques for beamline detectors. Early emphases of the program include flat-field calibration of area detectors and characterization of scintillation crystals. During the fall 2012 run, the program kicked off with a study of scintillation counters, looking at count-rate dependence and dead-time corrections. This study will include side-by-side comparisons of several different models, including new counters from Oxford Instruments.

1-BM will also be utilized to commission new detectors developed by the XSD Detectors Group; the next-generation of the FastCCD will be tested in early 2013. The testing effort continues to develop mechanical facilities and the analysis codes needed to extract calibrations.

With a successful first run for both the Optics and Detectors groups, the new effort at 1-BM is off to a fast start. The effort will continue to evolve in coming months as white beam is established in the B-hutch, and as Sector 1 brings the high-energy diffraction program online.

Contact: Al Macrander,
macrander@aps.anl.gov;
Robert Bradford, rbradford@aps.anl.gov

REFERENCE

- [1] T. Gog, D.M. Casa, A.H. Said, M.H. Upton, J. Kim, I. Kuzmenko, X. Huang, and R. Khachatryan, *J. Synchrotron Rad.* **20**, 74 (2013).
DOI:10.1107/S0909049512043154

This work supported by the U.S. Department of Energy Office of Science under Contract No. DE-AC-02-6CH11357.

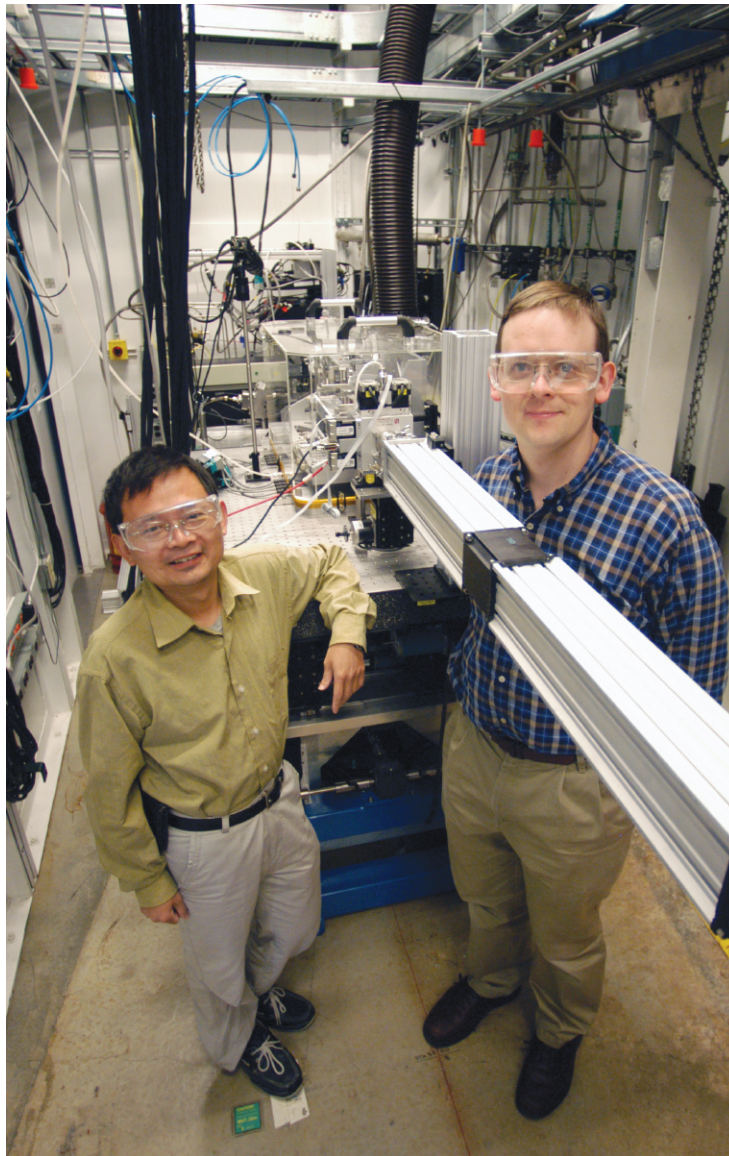
A DEDICATED FUEL-SPRAY RESEARCH BEAMLINE AT THE APS

The structure and dynamics of the high-pressure, high-speed fuel sprays from engine injectors are key to increasing fuel efficiency and reducing pollutants. But because liquid sprays are difficult to image with conventional optical techniques, particularly in the region close to the nozzle, quantitative information about the structure of these sprays has been elusive.

Research on this critical subject has been ongoing at the APS for several years, utilizing ultrafast x-radiography as the technique of choice and carried out mainly at XSD Sector 1 at the APS, and at the Cornell High Energy Synchrotron Source, with microsecond x-ray tomography also being employed. Results, which have seen wide circulation in several peer-reviewed journal articles, have yielded information on quantitative fuel mass distribution and high-speed spray and combustion models.

Now, a dedicated fuel-spray beamline is in operation on the XSD 7-BM bending magnet beamline at the APS. This new resource is made possible through a partnership between the DOE Office of Vehicle Technologies/Office of Energy Efficiency and Renewable Energy (VT/EERE) and the DOE Basic Energy Sciences Program.

The facility provides fast x-ray imaging techniques for experiments in a new, centralized resource for cutting-edge research on transportation engine technologies, high-throughput measurement of fuel sprays and combustion via the synchrotron x-ray techniques,



Jin Wang (left) and Alan Kastengren in the 7-BM research station

microsecond x-radiography, and microsecond x-tomography. It is anticipated that this facility will serve a large user community

The Vehicle Technologies office made a significant investment in repurposing the 7-BM beamline, where two research stations and a front end were already in place. The beamline makes available ultrafast (microsecond) x-radiography, ultrafast (microsecond) x-tomography, high beam intensity, wide-bandpass mono (10^{13} - 10^{14} ph/s, tunable from 6 to 12 keV), and flexible

beam size. Instrumentation includes a sagittal focusing double-multilayer monochromator, a harmonics rejection mirror for use with ultrafast area detectors, a secondary Kirkpatrick-Baez focusing mirror for use with point detectors, modular sample stations, pressurized chambers, unpressurized chambers, and rapid compression machines. Major emphasis is placed on safe operation under high-pressure, high-temperature conditions.

The APS, supported by the BES, supplied all construction manpower to complete the project. The EERE's investment, through the Transportation Technology R&D Center at Argonne, was built upon the previous development of the beamline infrastructure that had been supported by the BES. The beamline is administered by XSD, with science and engineering R&D coming from XSD, AES, and the Vehicle Technologies office through programmatic support to staff scientists and engineers.

Beamline 7-BM is expected to be one of the APS flagship beamlines for industrial applications on energy-related projects and a symbol of collaborations between BES and

EERE.

The beamline is in full operation and is now accepting general users through the APS General User Program.

*Contact: Jin Wang
(wangj@aps.anl.gov),
Alan Kastengren
(akastengren@anl.gov)*

7-BM-B • XSD • Physics • Radiography, tomography, microfluorescence (hard x-ray) • 5.5-12 keV • On-site • Accepting general users •

DECKER OF ASD ELECTED TO APS FELLOWSHIP

Argonne Senior Scientist **Glenn Decker** has been named a fellow of the American Physical Society, an honor limited to no more than one-half of one percent of the society's membership of more than 50,000. Decker's fellowship recognizes his "outstanding contributions to the design, commissioning, and enhancement



of synchrotron light sources, and for innovative developments in the field of particle beam diagnostics. In particular for the accelerator alignment technique necessary to reduce stray radiation background signals from photoemission-type photon beam position monitors and for the subsequent development of the largest deployment in the world of such monitors in a global closed-loop orbit feedback system." The alignment technique is known as the "Decker distortion." He was awarded The University of Chicago Medal for Distinguished Performance in 1996 for his work as storage ring manager on APS design and commissioning.

ALP OF XSD IS VICE-CHAIR OF FIP EXECUTIVE COMMITTEE

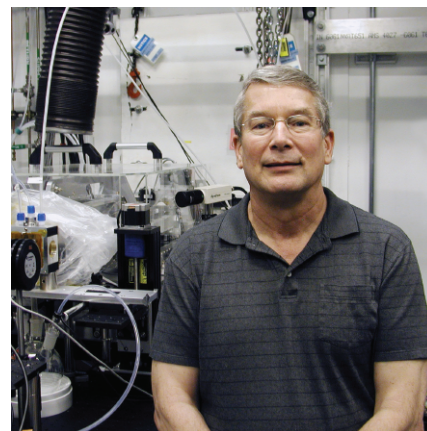
Argonne Senior Scientist **Esen Ercan Alp** has been elected to Vice-Chair and the 4-Year Chair Line term of the American Physical Society Forum on International Physics (FIP) beginning in January 1 of 2012. Alp has been a member of the Argonne scientific staff since



1984 and is also a Visiting Professor at Northern Illinois University and at the University of Illinois at Champaign-Urbana. He is widely known for his work in nuclear resonant x-ray spectroscopy. He was a member of the Canadian Light Source Science Advisory Committee from 1999 to 2009, and co-chair of the first Scientific Committee for the Synchrotron-light for Experimental Science and Applications in the Middle East project in Jordan. Alp also chairs the International Science Advisory Committee for the Turkish Accelerator Center. He has worked at different synchrotron radiation facilities in France, Germany, Japan, and the U.S. The FIP is a voluntary association of American Physical Society members who are interested in advancing the knowledge of physics and its diffusion by fostering cooperation and communication among physicists of all countries. Programs such as international book exchanges, equipment exchanges, travel grants, etc. have been established via initiatives of FIP members.

SOUTHWORTH OF XSD ELECTED TO APS FELLOWSHIP

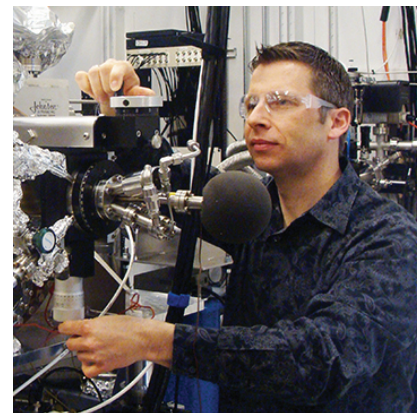
Argonne Senior Scientist **Stephen H. Southworth** has been named a Fellow of the American Physical Society.



He is recognized for "pioneering the development of atomic and molecular spectroscopies with third- and fourth-generation light sources, including such new effects as higher multipole asymmetries, double-shell photoionization, and femtosecond electronic response of atoms to ultra-intense x-rays." Southworth is leader of the Atomic, Molecular, and Optical Physics Group in XSD. His work has had a major impact on atomic and molecular physics. In synchrotron-based work, he did innovative experiments on the anisotropy of polarized x-ray emission from molecules, where distinctly different angular distributions were obtained for x-ray emission involving molecular orbitals of different symmetry. He also performed seminal experiments on double K-shell photoionization of atoms and non-dipole asymmetries in photoelectron angular distributions. He emphasizes the importance of teamwork and is grateful to have worked with excellent collaborators on every project.

DOE EARLY CAREER AWARD FOR ROSE OF XSD & CNM

Volker Rose, assistant physicist with the XSD Microscopy Group and the Argonne CNM was one of four Argonne researchers to receive 2012 Early Career Research Program awards, granted by the DOE to exceptional researchers beginning their careers. Rose's award will allow him to



develop a novel high-resolution microscopy technique for imaging nanoscale materials with chemical, electronic, and magnetic contrast combining sub-nanometer spatial resolution of scanning probe microscopy with the chemical, electronic, and magnetic sensitivity of synchrotron radiation. This technique will enable fundamentally new methods of characterization, which will be applied to the study of energy materials, nanoscale magnetic systems, and site-specific heterogeneous catalysis. Rose's earlier research achievements include an International Student Exchange Program Award sponsored by DOE and the American Nuclear Society in 2004, as well as sharing an R&D 100 Award in 2009 for the Hard X-ray Nanoprobe at APS Sector 26.

TOBY OF XSD CHAIRS U.S.N.C.C.

Argonne Senior Scientist **Brian H. Toby** was elected Chair of the U.S. National Committee for Crystallography of the National Academies for a 3-year term beginning January 1 of 2012. This committee represents the interests of U.S. crystallographers and facilities within the International Union for Crystallography (IUCr). Toby has been a member of the Argonne scientific staff since 2005 and is well known for his research in powder diffraction crystallography and for his development of x-ray and neutron powder diffraction instrumentation. He has also produced a number of very widely-used computer codes for that field. He has served on committees for the American Crystallographic Association, the International Centre for Diffraction Data, the IUCr, and the American Institute of Physics. Before coming to Argonne he was a staff scientist at the National Institute of Standards and Technology Center for Neutron Research and has held positions in industry and academia.



He has also produced a number of very widely-used computer codes for that field. He has served on committees for the American Crystallographic Association, the International Centre for Diffraction Data, the IUCr, and the American Institute of Physics. Before coming to Argonne he was a staff scientist at the National Institute of Standards and Technology Center for Neutron Research and has held positions in industry and academia.

GERIG OF ASD NAMED CHAIR OF USPAS BOARD

Rodney E. Gerig was selected chair of the Board of Governors of the U.S. Particle Accelerator School (USPAS). Gerig is Deputy Associate Laboratory Director, Accelerators, for Photon Sciences at the APS, and is also the director of the Argonne Accelerator Institute.



The USPAS is a partnership of nine U.S. DOE national laboratories, two National Science Foundation-supported universities, and one office of the Department of Homeland Security dedicated to providing rigorous academic courses in accelerator science and engineering.

Gerig has served on the USPAS board since 2003. He replaces Derek Lowenstein of Brookhaven National Laboratory, who decided to step down from the chairmanship after serving two three-year terms. Gerig brings to the board a strong perspective of accelerator operations and R&D at a national user facility. He was a motivating force behind the establishment in 2008 of the Lee Teng Internships, a three-way partnership of Argonne, Fermilab, and USPAS, which brings 10 talented undergraduates annually to Argonne and Fermilab for a summer of research in accelerator science or technology.

AWARD-WINNING ENERGY CONSERVATION

Innovative heat-recovery systems for APS buildings were recognized with the 2012 U.S. Department of Energy (DOE) Federal Energy and Water Management (FEWM) Award. These system designs, developed by the AES Division Site Operations Group and implemented in cooperation with the Argonne Facilities Management and Services (FMS) Division, have been utilized as part of a more comprehensive building retrofit to remodel lab/office module (LOM) 438 (see "Sustainability through Collaboration: An APS/Argonne Success Story," *APS Science* 2011, page 183). Executive Order 13514, "Federal Leadership in Environmental, Energy, and Economic Performance," requires that 15% of the buildings at Argonne meet the high performance and sustainable building (HPSB) guiding principles by the year 2015. These efforts resulted in Argonne being among the first DOE facilities to bring an existing building into compliance with the Executive Order.

The FEWM Awards, founded in 1981, recognize federal and partner organization employees for outstanding efforts related to federal energy, water, and fleet management, and the development and implementation of cost-effective projects and programs that embody the principles of sustainable design, institutionalization, and culture change. The APS has played a leading role in Argonne efforts to achieve compliance with federal requirements for energy sustainability. The APS-FMS project team gathered detailed energy and water usage information to develop conservation measures and calculate returns on investment. A number of audits, procedure reviews, and building modifications were made to LOM 438 to meet the HPSB standards. The facility renovations include:

- Upgrading the building lighting system from T-12 fluorescent light fixtures to LED lighting along with the installation of 77 occupancy sensors for a 60% reduction in lighting energy consumption, saving 77-MW h/y.
- Restroom fixtures and urinal control valves were replaced with motion-activated high-efficiency devices.
- Retrofitting the office and laboratory ventilation system heating source added recovered heat generated by the APS scientific tools and instruments. Low-grade (80° F) waste heat from the electron storage ring cooling system is utilized to preheat the LOM outdoor ventilation air, saving an estimated 125 M Btu (43 Mw/h equivalent) of energy per year.

A post-implementation energy audit determined that the lighting upgrade and the installation of occupancy sensors, combined with heat recovery from the APS beamlines, have reduced the LOM 438 total energy costs by 23.8%, meeting the minimum HPSB goal of 20% energy cost savings. Following the upgrades, a survey of the building's occupants confirmed their approval of the building's temperature, acoustics, air quality, lighting levels, and cleanliness.

Continuing in this effort, the design of the new addition to LOM 438 in the form of pentagon F will further exploit the use of waste heat by employing state-of-the-art, high-efficiency heat-transfer heat exchangers. These devices will permit the use of very-low-grade waste heat for laboratory and office ventilation reheat, expanding the ability of the APS to tap into and recycle this underutilized energy stream.

Contact: [Marvin Kirshenbaum, kirshen@aps.anl.gov](mailto:Marvin.Kirshenbaum@aps.anl.gov)



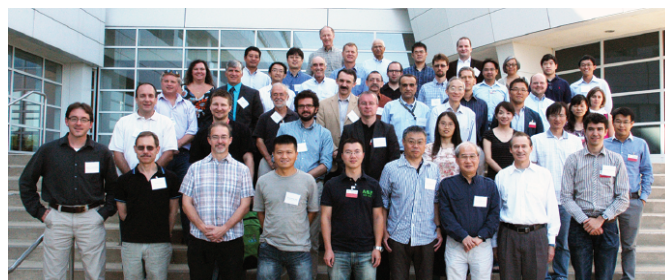
NATIONAL SCHOOL ON NEUTRON AND X-RAY SCATTERING • AUGUST 12-25 • The school, which educates graduate students on the utilization of major neutron and x-ray facilities, includes lectures on the principles of scattering theory and the characteristics of the sources, seminars on the application of scattering methods to a variety of scientific subjects and short experiments at the APS and the Oak Ridge National Laboratory (ORNL) Spallation Neutron Source and High Flux Isotope Reactor facilities. The target audience is graduate students attending U.S. universities and majoring in physics, chemistry, materials science, or related fields. The school is jointly conducted by Argonne and ORNL. *Contact: nxschool@dep.anl.gov*

X-RAY INTERFACE SCIENCE AT THE ADVANCED PHOTON SOURCE: NEW SECTOR DEVELOPMENT • JANUARY 10-11 • This workshop shaped the final design on a new sector for x-ray interface science at the APS. As a part of the strategic initiative of Argonne and the APS, this sector will have 9 experimental stations allowing 4 stations (1 tunable, 3 fixed-energy) running at the same time. It is expected that teams will start to form after this workshop to build specialized instrumentation for materials synthesis such as oxide-MBE, ALD, MOCVD, and other new capabilities. This sector will serve a diverse community with interests in catalysis, oxide film growth, geochemistry, surface physics, nanoscience, tribology, electrochemistry, and so on.

Contact: hhong@aps.anl.gov

WORKSHOP ON DATA EVALUATION USING CONUSS AND PHOENIX • NOVEMBER 2-4 • The workshop was organized within the COMPRES infrastructure initiative to promote application of state-of-the-art nuclear resonant scattering (NRS) techniques for characterizing the properties of materials under high P-T conditions of planetary interiors. The workshop offered a basic introduction to two NRS techniques: synchrotron Mössbauer spectroscopy and nuclear resonant inelastic x-ray scattering; introduced CONUSS and PHOENIX software for data evaluation; provided hands-on training in the use of CONUSS and PHOENIX; addressed common issues that users confront; and discussed recently added features to the new version of the software.

DYNAMIC COMPRESSION SECTOR USER WORKSHOP • JANUARY 19-20 • The workshop focus was the identification of priority research directions afforded by the emerging integration of dynamic compression platforms and advanced x-ray capabilities at the APS, including specific plans for experiments and facilities. *Contact: shock@wsu.edu*



WORKSHOP ON TERAHERTZ SOURCES FOR TIME RESOLVED STUDIES OF MATTER • JULY 30-31 • The workshop was held to foster discussion of various ideas that could help to build tunable THz sources with pump pulses in the frequency range from 1 to 20 THz that are 1) narrow band and tunable with the relative bandwidth of the order of 1% and the peak electric field of the order 100 kV/cm; 2) broad band and near-half-cycle with the peak electric field larger than 1MV/cm. It is presumed that these sources should work in tandem with a free-electron laser or a storage ring-based synchrotron light source producing an x-ray probe pulse. *Contact: azholents@aps.anl.gov*

SMALL-ANGLE SCATTERING SHORT COURSE 2010: "BEYOND RG" • MARCH 17-21 • The objective of the course was to raise the capabilities of the small-angle scattering (SAS) community by providing an intermediate-level course for those in need of a better understanding of SAS theory and techniques utilized at the APS. The course offered an overview of SAS theory, capabilities, and data reduction and analysis tools to enable the community to submit highly effective beam-time proposals and to facilitate better utilization of the resources at the APS. The course included hands-on experiments at a selected APS small-angle x-ray scattering facility, and data reduction and evaluation. *Contact: ilavsky@aps.anl.gov*



LSXS 2012 - SCHOOL FOR LIQUID SURFACE X-RAY SCATTERING: THEORY AND EXPERIMENTAL METHODS • OCTOBER 17-19 • Aimed at graduate students and post-docs, the workshop offered a combination of classroom and experimental work to introduce participants to the range of phenomena and properties that can be studied with synchrotron-based liquid surface x-ray scattering. The program included three hands-on activities that highlighted the major techniques and introduced participants to the liquid scattering instruments at the APS.

Contacts: lin@cars.uchicago.edu, schloss@uic.edu, wangj@aps.anl.gov



Argonne Director Eric Isaacs (left), APS Director Brian Stephenson, and NPR journalist and User Meeting speaker Richard Harris in the audience for the meeting's opening session.

A record crowd of more than 600 attended all or part of the 2012 APS/CNM/EMC Users Meeting from May 7–10! Opening the meeting, Argonne Director **Eric Isaacs** emphasized the importance of national user facilities to the overall mission of the Lab, as well as to the national “knowledge enterprise.” Next, the Honorable **Judy Biggert** (IL-13) reiterated bipartisan congressional support for science but cautioned that full funding initiatives for science face serious challenges in today’s political climate. Keynote speaker and National Public Radio (NPR) award-winning journalist **Richard Harris** brought his insight on science and the news. Directors of the three Office of Science user facilities at Argonne, **Brian Stephenson** (APS); **Amanda Petford-Long** (CNM); and **Dean Miller** (Electron Microscopy Center) described recent scientific

accomplishments and future directions for their facilities. **Tony Lanzirotti**, Chair of the National User Facility Organization also spoke.

The APS Plenary Sessions featured a talk by **Alexis Templeton** (Univ. of Colorado Boulder), winner of the first APS Users Organization Rosalind Franklin Young Investigator Award in 2004, describing her work in the intervening years. **Damian Ekiert** (Univ. of California, San Francisco), the 2012 Franklin Award winner (see story below), described his award-winning project, followed by **Linda Young** (XSD Director), who presented on-going and future work with x-rays in the fourth dimension. **Mike Gillan** (Univ. College London, UK) described new insights about the molecular-scale energetics of water. **Ahmet Uysal** (Argonne), the invited student talk winner, explained how knowledge from biology could be used to create better nanomaterials. **George Srajer** (APS Upgrade Project Director) presented the three alternate scenarios for beamline locations as the APS moves forward with the APS Upgrade Project.

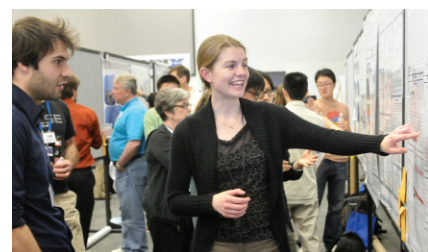
The meeting included 47 exhibitors, 3 cross-facility workshops, 7 facility-specific workshops, a poster session with 140 posters, and 4 CNM short courses. Abstracts of all talks as well as poster abstracts can be found at <http://usersmeeting2012.conference.anl.gov/>. **Contact: Susan Strasser, strasser@aps.anl.gov**



Alexis Templeton speaking at the APS Plenary Session of the 2012 User Meeting.



APS invited student talk winner Ahmet Uysal.



Anne March (XSD) discusses her work at the poster session.

2012 APSUO FRANKLIN AWARD TO EKIERT

The APS Users Organization (APSUO) named **Damian C. Ekiert** the winner of the 2012 Rosalind Franklin Young Investigator Award for his work on broadly neutralizing antibodies, which holds promise for structure-based design of a universal vaccine for influenza. The award was presented at the APS Users Meeting (see story above). Thanks to the work of Ekiert and others on broadly neutralizing antibodies, it may be possible for one vaccine to protect against most types of flu over a much longer term. Ekiert used x-

rays from the GM/CA-XSD facility at APS Sector 23 to determine the structure of two antibodies that neutralize many strains of influenza, in complex with their target antigen, hemagglutinin. The structural data pinpointed the region on the virus targeted by the antibody. Further studies showed that the structure of this region is unchanged across many strains of influenza. Ekiert is now a post-doctoral fellow at the Univ. of California, San Francisco, working on host-pathogen interactions in *M. tuberculosis*.

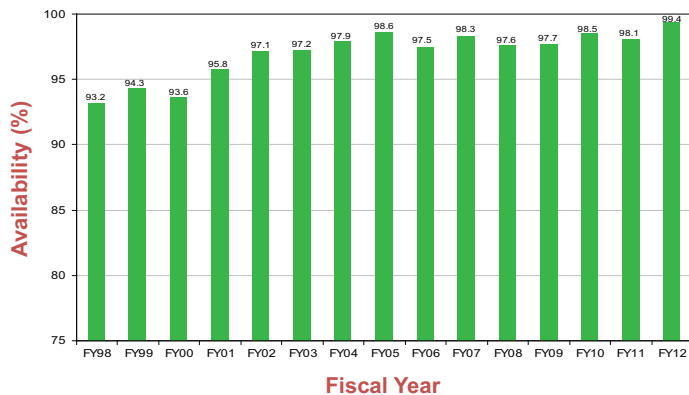


APS X-RAY SOURCE & USER DATA

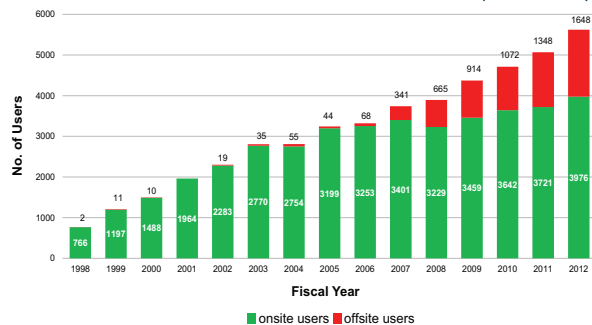
APS storage ring reliability (MTBF), FY98-FY12



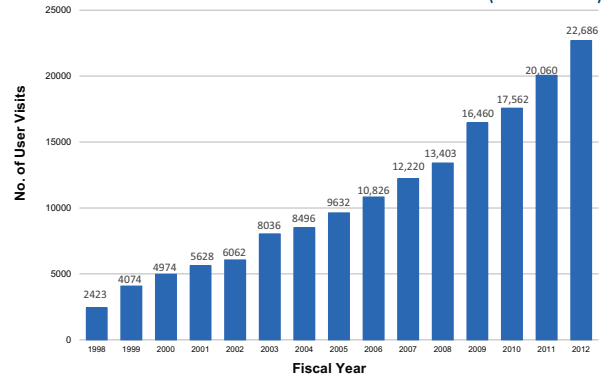
APS x-ray availability, FY98-FY12



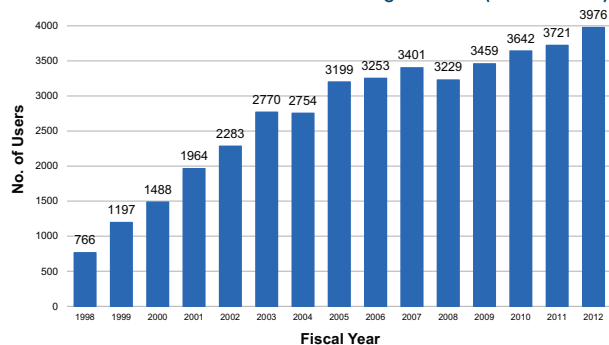
Number of on-site & off-site user visits to the APS (FY98-FY12)



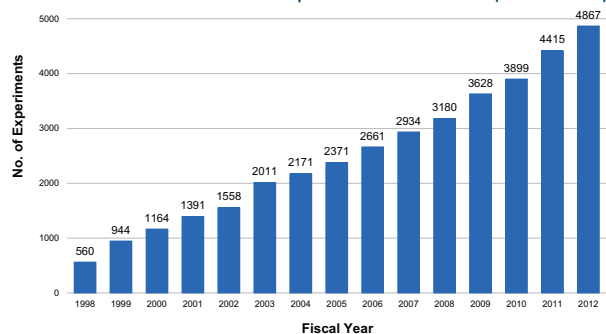
Number of user visits to the APS (FY98-FY12)



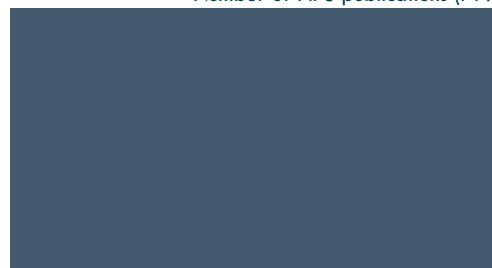
Number of APS on-site badged users (FY98-FY12)



Number of experiments at the APS (FY98-FY12)



Number of APS publications (FY98-FY12)



For lists of APS publications see <http://www.aps.anl.gov/Science/Publications/>

AVAILABILITY AND RELIABILITY

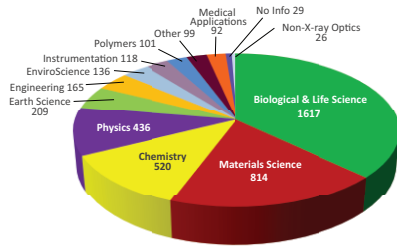
In fiscal year 2012* the APS x-ray source continued to function as a highly reliable delivery system for synchrotron x-ray beams for research. Several factors support the overall growth in both the APS user community and the number of experiments carried out by that community. But there is a direct correlation between the number of x-ray hours available to users; the success of the APS experiment program; and the physicists, engineers, and technicians responsible for achieving and maintaining optimum x-ray source performance. Below are definitions of important measures for the delivery of x-ray beam to users (shown graphically above).

Storage Ring Reliability: A measure of the mean time between beam losses (faults), or MTBF, calculated by taking the delivered beam and dividing by the total number of faults. The APS targets, and routinely exceeds, 70 h MTBF. A fault is defined as complete unavailability of beam either via beam loss or removal of shutter permit not related to weather. A fault also occurs when beam has decayed to the point where stability and orbit can no longer be considered reliable. At the APS, this threshold is 50 mA.

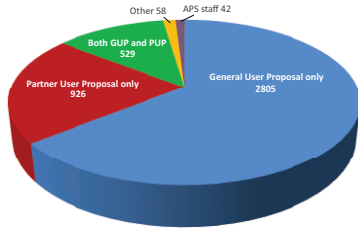
X-ray Availability: The number of hours that the beam is available to the users divided by the number of hours of scheduled beam delivery prior to the beginning of a run. The specific definition of available beam is that the APS Main Control Room has granted permission to the users to open their shutters, and there is more than 50-mA stored beam in the storage ring.

* While the highlights in, and title of, this report cover calendar year 2012 data on accelerator performance and user statistics are measured on the basis of fiscal years.

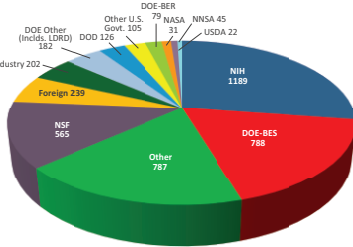
APS users by experiment subject (FY12)



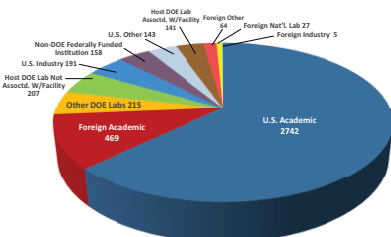
APS users by user type (FY12)



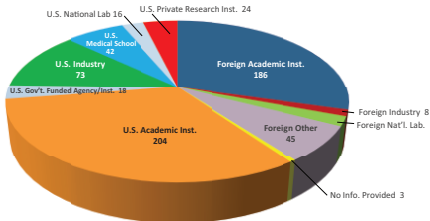
APS users by source of support (FY12)



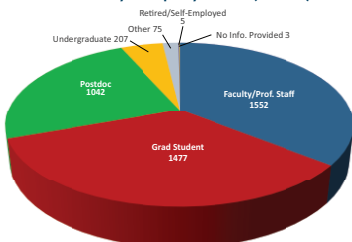
APS users by employer (FY12)



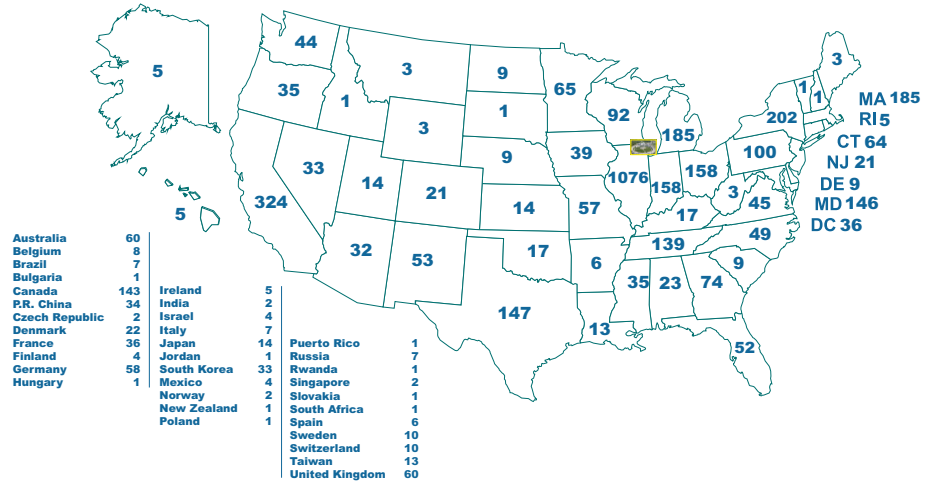
APS users by institution type (FY12)



APS users by employment (FY12)

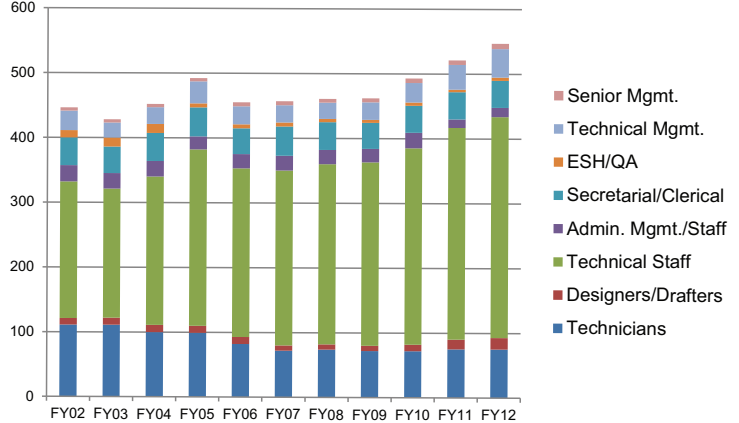


APS users by institutional geographic distribution (FY12)

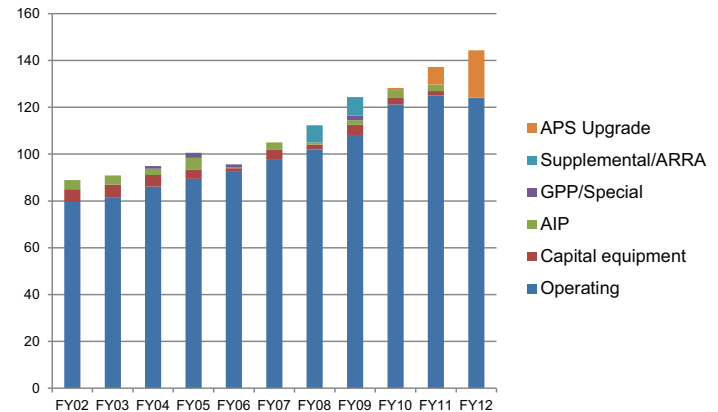


APS STAFFING AND FUNDING

APS staffing levels, FY02-FY12



APS funding levels, FY02-FY12



TYPICAL APS MACHINE PARAMETERS

LINAC

Output energy	375 MeV
Maximum energy	450 MeV
Output beam charge	1–3 nC
Normalized emittance	10–20 mm-mrad
Frequency	2.856 GHz
Modulator pulse rep rate	30 Hz
Gun rep rate (1–6 pulses, 33.3 ms apart every 0.5 s)	2–12 Hz
Beam pulse length	8–15 ns
Bunch length	1–10 ps FWHM

PARTICLE ACCUMULATOR RING

Nominal energy	325 MeV
Maximum energy	450 MeV
Circumference	30.66 m
Cycle time	500 ms
Fundamental radio frequency (RF1)	9.77 MHz
12th harmonic rf frequency (RF12)	117.3 MHz
RMS bunch length (after compression)	0.34 ns

INJECTOR SYNCHROTRON (BOOSTER)

Nominal extraction energy	7.0 GeV
Injection energy	325 MeV
Circumference	368.0 m
Lattice structure	10 FODO cells/ quadrant
Ramping rep rate	2 Hz
Natural emittance	69 nm-rad-92 nm-rad
Radio frequency	351.930 MHz

STORAGE RING SYSTEM

Nominal energy	7.0 GeV
Circumference	1104 m
Number of sectors	40
Length available for insertion device	5.0 m
Nominal circulating current, multibunch	100 mA
Natural emittance	2.5 nm-rad
RMS momentum spread	0.096%
Effective emittance	3.1 nm-rad
Vertical emittance	0.040 nm-rad
Coupling	1.5%
Revolution frequency	271.554 kHz
Radio frequency	351.930 MHz
Number of bunches	24 to 1296
Time between bunches	153 to 2.8 ns
RMS bunch length	25 ps to 40 ps
RMS bunch length of 16 mA in hybrid mode	50 ps

APS SOURCE PARAMETERS

UNDULATOR A (28 INSERTION DEVICES [IDs])

Period: 3.30 cm
Length: 2.1 m in sectors 16, 21, 23, 24, 34; 2.3 m in Sector 6; 2.4 m in others
Minimum gap: 10.5 mm
B_{\max}/K_{\max} : 0.892 T/2.75 (effective; at minimum gap)
Tuning range: 3.0–13.0 keV (1st harmonic) 3.0–45.0 keV (1st–5th harmonic)
On-axis brilliance at 7 keV (ph/s/mrad ² /mm ² /0.1%bw): 4.1 x 10 ¹⁹ (2.4 m), 4.0 x 10 ¹⁹ (2.3 m), 3.3 x 10 ¹⁹ (2.1 m)
Source size and divergence at 8 keV: Σ_x : 276 μm Σ_y : 11 μm Σ_x : 12.7 μrad (2.4 m), 12.8 μrad (2.3 m), 12.9 μrad (2.1 m) Σ_y : 6.7 μrad (2.4 m), 6.8 μrad (2.3 m), 7.1 μrad (2.1 m)

2.30-CM UNDULATOR (3 IDs IN SECTORS 1, 11, 14)

Period: 2.30 cm
Length: 2.4 m
Minimum gap: 10.5 mm
B_{\max}/K_{\max} : 0.558 T/1.20 (effective; at minimum gap)
Tuning range: 11.8–20.0 keV (1st harmonic) 11.8–70.0 keV (1st–5th harmonic, non-contiguous)
On-axis brilliance at 12 keV (ph/s/mrad ² /mm ² /0.1%bw): 6.9 x 10 ¹⁹
Source size and divergence at 12 keV: Σ_x : 276 μm Σ_y : 11 μm Σ_x : 12.3 μrad Σ_y : 5.9 μrad

2.70-CM UNDULATOR (4 IDs IN SECTORS 3, 12, 14)

Period: 2.70 cm
Length: 2.1 m in Sector 12; 2.4 m in others
Minimum gap: 10.5 mm
B_{\max}/K_{\max} : 0.698 T/1.76 (effective; at minimum gap)
Tuning range: 6.7–16.0 keV (1st harmonic) 6.7–60.0 keV (1st–5th harmonic, non-contiguous)
On-axis brilliance at 8.5 keV (ph/s/mrad ² /mm ² /0.1%bw): 5.7 x 10 ¹⁹ (2.4 m), 4.7 x 10 ¹⁹ (2.1 m)
Source size and divergence at 8 keV: Σ_x : 276 μm Σ_y : 11 μm Σ_x : 12.7 μrad (2.4 m), 12.9 μrad (2.1 m) Σ_y : 6.7 μrad (2.4 m), 7.1 μrad (2.1 m)

**3.00-CM UNDULATOR
(8 IDs IN SECTORS 12, 13, 16, 21, 23, 30, 34)**

Period: 3.00 cm
Length: 2.1 m in sectors 12, 13, 16, 21, 23, 34; 2.4 m in Sector 30
Minimum gap: 10.5 mm
B_{\max}/K_{\max} : 0.787 T/2.20 (effective; at minimum gap)
Tuning range: 4.6–14.5 keV (1st harmonic) 4.6–50.0 keV (1st–5th harmonic)
On-axis brilliance at 8 keV (ph/s/mrad ² /mm ² /0.1%bw): 4.8 x 10 ¹⁹ (2.4 m), 3.9 x 10 ¹⁹ (2.1 m)
Source size and divergence at 8 keV: Σ_x : 276 μm Σ_y : 11 μm Σ_x : 12.7 μrad (2.4 m), 12.9 μrad (2.1 m) Σ_y : 6.7 μrad (2.4 m), 7.1 μrad (2.1 m)

APS SOURCE PARAMETERS

3.50-CM SmCo UNDULATOR (SECTOR 4)

Period: 3.50 cm
 Length: 2.4 m
 Minimum gap: 9.75 mm
 B_{\max}/K_{\max} : 0.918 T/3.00 (effective; at minimum gap)
 Tuning range: 2.4–12.5 keV (1st harmonic)
 2.4–42.0 keV (1st–5th harmonic)
 On-axis brilliance at 7 keV (ph/s/mrad²/mm²/0.1%bw): 3.7×10^{19}
 Source size and divergence at 8 keV:
 Σ_x : 276 μm Σ_y : 11 μm
 $\Sigma_{x'}$: 12.7 μrad $\Sigma_{y'}$: 6.7 μrad

3.60-CM UNDULATOR (SECTOR 13)

Period: 3.60 cm
 Length: 2.1 m
 Minimum gap: 11.0 mm
 B_{\max}/K_{\max} : 0.936 T/3.15 (effective; at minimum gap)
 Tuning range: 2.2–11.8 keV (1st harmonic)
 2.2–40.0 keV (1st–5th harmonic)
 On-axis brilliance at 6.5 keV (ph/s/mrad²/mm²/0.1%bw): 2.8×10^{19}
 Source size and divergence at 8 keV:
 Σ_x : 276 μm Σ_y : 11 μm
 $\Sigma_{x'}$: 12.9 μrad $\Sigma_{y'}$: 7.1 μrad

5.50-CM UNDULATOR (SECTOR 2)

Period: 5.50 cm
 Length: 2.4 m
 Minimum gap: 14.0 mm
 B_{\max}/K_{\max} : 0.965 T/4.96 (effective; at minimum gap)
 Tuning range: 0.64–7.0 keV (1st harmonic)
 0.64–25.0 keV (1st–5th harmonic)
 On-axis brilliance at 4 keV (ph/s/mrad²/mm²/0.1%bw): 1.7×10^{19}
 Source size and divergence at 4 keV:
 Σ_x : 276 μm Σ_y : 11 μm
 $\Sigma_{x'}$: 13.9 μrad $\Sigma_{y'}$: 8.8 μrad

IEX 12.5-CM QUASI-PERIODIC POLARIZING UNDULATOR (SECTOR 29)

Period: 12.5 cm
 Length: 4.8 m
Circular polarization mode:
 Max. currents: horizontal coils 34.4 A, vertical coils 20.7 A
 K_{\max} : 2.73 (effective; at max. currents)
 B_{\max} : 0.27 T (peak; at max. currents)
 Tuning range: 0.44–3.5 keV (1st harmonic)
 On-axis brilliance at 1.8 keV (ph/s/mrad²/mm²/0.1%bw): 1.4×10^{19}
Linear horizontal polarization mode:
 Max. current: vertical coils 47.6 A
 K_{\max} : 5.39 (effective; at max. current)
 B_{\max} : 0.54 T (peak; at max. current)
 Tuning range: 0.24–3.5 keV (1st harmonic)
 0.24–11.0 keV (1st–5th harmonic)
 On-axis brilliance at 2.1 keV (ph/s/mrad²/mm²/0.1%bw): 1.1×10^{19}
Linear vertical polarization mode:
 Max. current: horizontal coils 50.3 A
 K_{\max} : 3.86 (effective; at max. current)
 B_{\max} : 0.37 T (peak; at max. current)
 Tuning range: 0.44–3.5 keV (1st harmonic)
 0.44–11.0 keV (1st–5th harmonic)
 On-axis brilliance at 2.1 keV (ph/s/mrad²/mm²/0.1%bw): 1.1×10^{19}
 Fast polarization switching not required
 Source size and divergence at 2 keV:
 Σ_x : 276 μm Σ_y : 13 μm
 $\Sigma_{x'}$: 13.9 μrad $\Sigma_{y'}$: 8.8 μrad

APS SOURCE PARAMETERS

12.8-CM CIRCULARLY POLARIZING UNDULATOR (SECTOR 4)

Period: 12.8 cm
 Length: 2.1 m
Circular polarization mode:
 Max. currents: horizontal coils 1.34 kA, vertical coils 0.40 kA
 K_{\max} : 2.85 (effective; at max. currents)
 B_{\max} : 0.30 T (peak; at max. currents)
 Tuning range: 0.4–3.0 keV (1st harmonic)
 On-axis brilliance at 1.8 keV (ph/s/mrad²/mm²/0.1%bw): 3.1×10^{18}
Linear horizontal polarization mode:
 Max. current: vertical coils 0.40 kA
 K_{\max} : 2.85 (effective; at max. current)
 B_{\max} : 0.30 T (peak; at max. current)
 Tuning range: 0.72–3.0 keV (1st harmonic)
 0.72–10.0 keV (1st–5th harmonic)
 On-axis brilliance at 2.1 keV (ph/s/mrad²/mm²/0.1%bw): 2.3×10^{18}
Linear vertical polarization mode:
 Max. current: horizontal coils 1.60 kA
 K_{\max} : 3.23 (effective; at max. current)
 B_{\max} : 0.34 T (peak; at max. current)
 Tuning range: 0.58–3.0 keV (1st harmonic)
 0.58–10.0 keV (1st–5th harmonic)
 On-axis brilliance at 2.1 keV (ph/s/mrad²/mm²/0.1%bw): 2.3×10^{18}
 Switching frequency (limited by storage ring operation): 0–0.5 Hz
 Switching rise time: 50 ms
 Source size and divergence at 2 keV:
 Σ_x : 276 μm Σ_y : 12 μm
 $\Sigma_{x'}$: 16.7 μrad $\Sigma_{y'}$: 12.7 μrad

SCUO SUPERCONDUCTING UNDULATOR (SECTOR 6)

Period: 1.60 cm
 Length: 0.34 m
 Gap: 9.5 mm (fixed)
 Max. current: 650 A
 B_{\max}/K_{\max} : 0.774 T/1.15 (effective; at maximum current)
 Tuning range: 17.5–26 keV (1st harmonic)
 17.5–100.0 keV (1st–5th harmonic, non-contiguous)
 On-axis brilliance at 87.5 keV (ph/s/mrad²/mm²/0.1%bw): 5.3×10^{17}
 Source size and divergence at 87.5 keV:
 Σ_x : 276 μm Σ_y : 11 μm
 $\Sigma_{x'}$: 12.3 μrad $\Sigma_{y'}$: 5.8 μrad

APS BENDING MAGNET

Critical energy: 19.51 keV
 Energy range: 1–100 keV
 On-axis brilliance at 16 keV (ph/s/mrad²/mm²/0.1%bw): 5.4×10^{15}
 On-axis angular flux density at 16 keV (ph/s/mrad²/0.1%bw): 9.6×10^{13}
 Horizontal angular flux density at 6 keV (ph/s/mradh/0.1%bw): 1.6×10^{13}
 Source size and divergence at the critical energy:
 Σ_x : 92 μm Σ_y : 31 μm
 $\Sigma_{x'}$: 6 μrad $\Sigma_{y'}$: 47 μrad



APS Science 2012 Editorial Board:

Cele Abad-Zapatero (University of Illinois at Chicago), Mark A. Beno (ANL-XSD), Rodney E. Gerig (ANL-PSC), Jonathan C. Lang (ANL-XSD), Dennis M. Mills, (ANL-PSC), William G. Ruzicka (ANL-AES), George Srajer (ANL-PSC), G. Brian Stephenson (ANL-PSC), Linda Young (ANL-XSD), Alexander A. (Sasha) Zholents (ANL-ASD)

The research highlights in this report were written by:

Mary Alexandra Agner

William Arthur Atkins (waarc@grics.net)

David Bradley (david@sciencebase.com)

Yvonne Carts-Powell (yvonne.cartspowell@gmail.com)

Vic Comello (ANL-CEP, vcomello@anl.gov)

Dana Desonie (desonie@cox.net)

Sandy Field (sfield@fieldscientific.com)

Karen Fox (kfox@nasw.org)

Emma Hitt (emma@hittmedicalwriting.com)

Philip Koth (philkoth@comcast.net)

Elise LeQuire (cygnete@mindspring.com)

David Lindley (dlindley@nasw.org)

Mona A. Mort (monasbox@gmail.com)

Nicola Parry (nicola@parrymedicalwriting.com)

Mark Wolverton (exetermw@earthlink.net)

Photography: Wes P. Agresta and George J. Joch (both ANL-CEP)

Aerial photograph of the APS: John Hill (Tigerhill Studio, <http://www.tigerhillstudio.com>)

Publications, contracts, rights and permissions, circulation: Jessie L. Skwarek (ANL-PSC)

Printing: Gary R. Weidner (ANL-CEP)

CD production: Linda M. Graf and Lorenza M. Salinas (both ANL-CEP)

Editorial and project coordination, design, photography: Richard B. Fenner (ANL-PSC)

Our thanks to the corresponding authors and others who assisted in the preparation of the research highlights, to the users and APS personnel who wrote articles for the report, and our apologies to anyone inadvertently left off this list. To all: your contributions are appreciated.